



University of
Nottingham
UK | CHINA | MALAYSIA



PQS-Dependent Quorum Sensing in
Pseudomonas aeruginosa
is Linked to
Protein Export via the Twin-Arginine
Translocation (Tat) System

Frances May Smith, MBIolSci, MRes.

Thesis submitted to the University of Nottingham

for the degree of Doctor of Philosophy

2021

Author's Declaration

Unless otherwise stated, all work presented in this thesis is entirely my own. The work was undertaken during my period of registration for a PhD at the University of Nottingham, and no part of it has been submitted for another degree at the University of Nottingham or any other institute of learning.

Abstract

Pseudomonas aeruginosa is a leading cause of nosocomial infection due to its inherent resistance to multiple classes of antibiotics and ability to readily form protective antibiotic-tolerant biofilms. *P. aeruginosa* has a vast number of regulatory systems as well as multiple interlinked hierarchical quorum sensing (QS) systems that allows tight control over its large genome. The PQS-dependent QS system utilises alkyl-quinolones (AQs) as autoinducers, including the *Pseudomonas* quinolone signal (PQS) and its immediate precursor, 2-heptyl-4-hydroxyquinoline (HHQ). PQS-dependent QS coordinates the production and release of virulence factors, secondary metabolites, rhamnolipids, microvesicles, and extracellular DNA, which are important for biofilm formation. The Twin-arginine transport (Tat) System translocates fully-folded proteins across the inner membrane and inhibition, mutation or deletion of the *tat* genes resulted in down-regulated PQS biosynthesis. The primary aim of this PhD was to understand why loss of the Tat system causes perturbation of *pqs* QS. This was studied in two ways, through a) transcriptome analysis and b) mutagenesis of each known Tat substrate to discover whether a single substrate could account for the phenotype.

Comparison of *tat* mutant transcriptome with wild-type PAO1-DK revealed highly up-regulated genes involved in anthranilate degradation. Anthranilate is degraded and fed into tri-carboxylic acid (TCA) cycle for energy generation but is also used in the first step of AQ biosynthesis. Up-regulated anthranilate degradation as seen in the transcriptome data may account for the perturbation of *pqs* QS in *tat* mutants as the two are reciprocally regulated. Expression from promoters of the first two operons in the anthranilate degradation pathway (*antABC* and *catBCA*) and their respective regulators (*antR* and *catR*) was confirmed to be up-regulated upon deletion or mutation of the *tat* system using bioluminescent transcriptional reporters.

Perturbed *pqs* QS and up-regulated anthranilate degradation may be due to failed translocation of one or more of the effectors translocated by the Tat system. Deletion mutants of 34 Tat system substrates were screened for reduced *pqsA* expression and up-regulated *antA* expression. Both were observed in a *petA* mutant, which encodes the Rieske subunit of the cytochrome *bc₁* complex. *cytB* and *cytC₁* mutants similarly exhibited reduced *pqsA* expression and AQ production. PA14 Δ *petA* mutants grew thin, flat, eDNA-deficient biofilms similar to PA14 Δ *tatABC*, and these were partially restored to a mature biofilm phenotype upon complementation. Results suggested that failure to translocate PetA caused the cell to shift from producing secondary metabolites, many of which are controlled by PQS quorum sensing, to primary metabolic processes such as degradation of aromatic amino acids in order to conserve energy.

The Tat pathway is an ideal target for novel antivirulence agents due to its involvement in export of virulence factors and of effectors involved in anaerobic respiration and osmotic stress response. Deletion of the *tat* system disrupts *pqs* QS and subsequently biofilm formation, which is often implicated in chronic or acute recurring *P. aeruginosa* infections. As such, the second aim of this PhD was to develop inhibitors of the Tat system. Analogues of the published small-molecule Tat inhibitor (2E)-3-[(4-methylphenyl)sulfonyl]acrylonitrile (also known as Bay 11-7082) were screened for their activity against *pqsA* expression and pyoverdine production, and structure-activity relationships (SAR) were investigated. Replacement of the nitrile group with an amide (CONH₂) functional group increased *pqsA*-inhibitory activity, but addition of an ethoxycarbonyl (COOEt) functional group had the opposite effect. By altering substituents on the phenyl ring, the combination 3-Cl, 4-F increased inhibitory activity for *pqsA* expression. All compounds exhibited some bacterial growth inhibition, except for those with an *N,N*-dimethylcarboxamide (CONMe₂) functional group which had very little effect

on growth. Investigation of eukaryotic cell viability following incubation with Bay 11-7082 and 4-Me-PhSACONH₂ showed the latter was less cytotoxic.

This work gives new insight into the effects of *tat* mutation upon the transcriptome of *P. aeruginosa* PAO1-DK, and shows that the slower growth, perturbed PQS-dependent quorum sensing, and thin, flat biofilm formation seen in *tat* mutants is likely due to failed export of the Rieske subunit of the cytochrome *bc*₁ complex, PetA. SAR analysis of analogues of a known Tat inhibitor, Bay 11-7082, should help advance knowledge for the development of inhibitors of *pqsA* expression and potentially also the Tat system.

Publications

Soh, E.Y.-C., Smith, F., Gimenez, M.R., Yang, L., Vejborg, R.M., Fletcher, M., *et al.* (2021) Disruption of the *Pseudomonas aeruginosa* Tat system perturbs PQS-dependent quorum sensing and biofilm maturation through lack of the Rieske cytochrome *bc*₁ sub-unit. *PLOS Pathog* **17**: e1009425.

See Appendix for full text.

Acknowledgements

I would firstly like to thank my PIs, Kim Hardie and Paul Williams, for their immense support throughout this PhD. Their guidance and encouragement has been so valuable, I really appreciated that their door was always open if I needed to talk through anything and because of them I have thoroughly enjoyed undertaking my PhD. I would also like to thank Kim and Paul for their encouragement to apply for grants and attend conferences all over the world, it was greatly appreciated and has made my time at Nottingham a very enjoyable one.

I must also thank my bench supervisor, Matt Fletcher who talked me through designing experiments (especially with cloning), trained me, provided technical support and showed me the best way to analyse data. I would like him to know how grateful I am for all his help, especially when I was just starting out and needed all the guidance I could get!

On the more technical side, I would like to thank Bérengère Ize and Maxime Gimenez at Laboratoire d'Ingénierie des Systèmes Macromoléculaires, Institut de Microbiologie de la Méditerranée, CNRS, Marseille for their generosity and eagerness to collaborate with me on the Tat substrate screening project. Thank you's also go to Alex Truman for synthesising the Bay 11-7082 analogues, and to Nigel Halliday, for his LC-MS/MS analysis. Danni Scales, I can't thank you enough for your help with my WGS bioinformatic analysis – I would have been lost without your guidance and skills. To my Master's students, especially Charles, it was a pleasure to supervise you and your enthusiasm towards lab research and refilling my tip boxes was greatly appreciated. I would also like to thank the Wellcome Trust for the funding of my DTP and making all this possible.

Thanks go out to the Hardie group, with special mention to Dean Walsh, Claire Laxton, Marina Serdar, Birte Hollmann, Mark Perkins, and SiYu Wu, our

fortnightly meetings were essential for troubleshooting problems and refuelling on cake before returning to the lab. You were all worthy opponents in the Great British Hardie group biscuit baking competition. Hardie group lake walks during the pandemic lockdowns were always something to look forward to and I am honoured to have been part of such a wonderful team of people.

My friends and office pals, you are all wonderful people who have kept me sane and laughing, and I consider you all life-long friends. I would like to give special mention to Carol, Danni, Will, Sam, Nikki, Eric, Bashir, and Chris. Our holidays to the Peak district, Lisbon and the Azores were such fun and you have all made my time in the lab so memorable.

To Dan, I cannot thank you enough for your unwavering support, endless cups of tea, late night study sessions, listening to me rant when experiments weren't going well and when writing was slow progress. You may not understand any of what is written in this thesis, but you have helped me enormously to get it done and get it written up.

Finally, to my family, you have encouraged me throughout my PhD to keep going, you took me in during the first lockdown when the world stopped, and kept me sane as I started to write this thesis. You made sure to take me on long walks around the Peak District and Cumbria when it was time for a much-needed break. We made it through 2020, and the Quaranteam Quizzers was a huge part of that, so thank you everyone for getting involved in our weekly quiz nights and stopping me from going mad.

I'm sure there are people that I have forgotten to mention here, so to everyone who has helped and supported me over the last 5 years, thank you for helping me realise a dream.

Table of Contents

Author's Declaration	1
Abstract	2
Publications	4
Acknowledgements	5
List of Tables	11
List of Figures	12
Abbreviations	18
Chapter 1: Introduction	22
1.1 The genus <i>Pseudomonas</i>	23
1.2 <i>Pseudomonas aeruginosa</i>	24
1.3 Clinical Relevance of <i>P. aeruginosa</i>	25
1.4 Antibiotic Resistance in <i>P. aeruginosa</i>	29
Innate.....	30
Adaptive....	31
Acquired....	33
1.5 <i>P. aeruginosa</i> Virulence.....	33
Motility.....	34
Pyocyanin.....	34
Elastase.....	35
Iron uptake.....	35
Rhamnolipids	37
Hydrogen cyanide.....	37
Biofilm formation	37
1.6 Global Gene Regulation via Quorum Sensing Systems	40
PQS-dependent quorum sensing.....	43
AQ biosynthesis.....	44
1.7 Protein Translocation via the Twin Arginine Translocation (Tat) Pathway	45
Overview of the Tat pathway.....	45
Tat system assembly and function	46
Tat signal peptides.....	48
Implications of <i>P. aeruginosa</i> Tat system in virulence.....	49
1.8 Aims of This Study	50

Chapter 2: Materials and Methods	52
2.1 Bacterial growth media and culture conditions	53
Storage of Bacterial Strains	53
2.2 Bacterial strains and plasmids	54
2.3 Molecular biology	63
Amplification of DNA fragments by Polymerase Chain Reaction	65
Plasmid Extraction	66
Restriction Digest	66
Gel Electrophoresis and DNA purification	66
Ligation of DNA fragments with vector backbone	66
Preparation of electrocompetent <i>E. coli</i> cells.....	67
Preparation of electrocompetent <i>P. aeruginosa</i>	67
Transformation of plasmids into electrocompetent cells	67
Conjugation into <i>P. aeruginosa</i>	68
Colony PCR	68
Genomic DNA extraction.....	69
Confirmation of DNA by sanger sequencing of DNA	69
2.4 Genetic modifications	69
Deletion of <i>antA</i> with pDM4 suicide vector	69
Creation of bioluminescent transcriptional reporters	72
2.5 Phenotypic assays	73
Pyocyanin.....	73
Supernatant induction of <i>pqsA</i> bioluminescent reporter	74
Liquid Chromatography-Tandem mass spectroscopy (LC-MS/MS) analysis ..	74
2.6 Microtiter Assays	75
Bioluminescence and optical density assay.....	75
Bay 11-7082 analogue IC ₅₀ /EC ₅₀ assays	75
Fluorescence and optical density assay	76
AlamarBlue cell viability assay.....	76
2.7 Microscopy.....	77
Biofilm formation.....	77
Visualisation of biofilm components.....	77
Confocal microscopy	77
2.8 Bioinformatics	78
Genomic analysis.....	78
Chapter 3: The metabolic balance between PQS biosynthesis and anthranilate degradation is disrupted upon deletion of the Tat system ..	80
3.1 Introduction	81
3.2 Results.....	85
3.2.1. PQS biosynthesis in the <i>tat</i> mutant of PAO1-DK and PA14	85
3.2.2. Pyocyanin production.....	90
3.2.3. Characterisation of the <i>tat</i> mutant transcriptome	92

3.2.4.	Comparison of <i>tat</i> mutant and $\Delta pqsA$ mutant transcriptomes ...	101
3.2.5.	Expression of the twin-arginine transport system	105
3.2.6.	Construction of bioluminescent transcriptional reporters to study expression of the anthranilate degradation pathway.....	109
3.2.7.	Anthranilate degradation is greater in <i>tat</i> pathway mutants	110
3.2.8.	Anthranilate degradation is up-regulated in a $\Delta pqsA$ mutant and <i>tatA</i> ::Tn5 $\Delta pqsA$ double mutant.....	116
3.2.9.	Determining response of <i>tat</i> mutation to exogenously added anthranilate	118
3.2.10.	Construction of $\Delta antA$ mutant in PAO1-DK, PAO1-DK $\Delta tatABC$ and PAO1-DK $\Delta pqsA$	125
3.2.11.	Genomic analysis of PAO1-DK, PAO1-DK $\Delta antA$, PAO1-DK $\Delta tatABC$ $\Delta antA$ and PAO1-DK $\Delta pqsA$ $\Delta antA$	125
3.2.12.	Effect of $\Delta antA$ deletion on growth in LB.....	127
3.2.13.	Deletion of <i>anta</i> , <i>tatABC</i> , or <i>pqsA</i> has no effect on <i>lux</i> -reporter light output.....	128
3.2.14.	Effect of $\Delta antA$ deletion on anthranilate degradation	129
3.2.15.	Expression of <i>pqsA</i> in $\Delta antA$ mutants	135
3.3	Discussion	138
Chapter 4: Identification of the Tat substrate primarily responsible for causing perturbation in PQS-dependent quorum sensing		148
4.1	Introduction	149
4.2	Results.....	153
4.2.1.	Screening of a deletion mutant library of Tat system substrates.....	153
4.2.1.1.	Expression of <i>pqsA</i> and <i>anta</i>	153
4.2.1.2.	Altered pyocyanin production.....	155
4.2.2.	The pleiotropic effects of <i>PA4431</i> deletion are similar to <i>tat</i> mutation 158	
4.2.2.1.	PQS biosynthesis is lower in the $\Delta petA$ mutant and partially restored upon genetic complementation	160
4.2.2.2.	Anthranilate production in a $\Delta petA$ mutant.....	165
4.2.2.3.	Expression of <i>rhIA</i> in a $\Delta petA$ mutant	166
4.2.2.4.	Tat system function with $\Delta petA$ deletion	168
4.2.2.5.	Cytochrome <i>b</i> and cytochrome <i>c</i> ₁ mutant phenotypes are the same as the <i>petA</i> mutant phenotype.....	170
4.2.3.	Biofilm formation by the $\Delta petA$ mutant in comparison with wild-type and $\Delta tatABC$ mutant	172
	<i>P. aeruginosa</i> PAO1-DK and $\Delta tatABC$ mutants have distinct biofilm morphologies	172
4.2.4.1.	PA14 $\Delta petA$ mutant biofilms.....	175
4.3	Discussion	180
Chapter 5: Screening analogues of the Bay 11-7082 compound for increased activity and structure-activity relationship		184

5.1. Introduction.....	185
5.2. Results.....	190
5.2.1. Screening of Bay 11-7082 analogues for increased activity	190
5.2.2. Growth is inhibited at high concentrations of TI1	200
5.2.3. Growth inhibition at high concentrations of Bay 11-7082 analogues TI1-TI14.....	201
5.2.4. Reduced growth inhibition is observed using Bay 11-7082 analogues bearing a CONMe ₂ functional group.....	204
5.2.5. Potency of TI1 was increased by 3-Cl, 4-F phenyl ring substituents and reduced by 3-Cl,4-Me or 4-AcNH substitutions	205
5.2.6. Evaluation of nitrile group variants and their effect on activity .	208
5.2.7. <i>pqsA</i> inhibitory activity of analogues TI17-TI30 at 20 μM and 40 μM.....	215
5.2.8. Upregulation of <i>antA</i> expression in response to TI1 and analogues.....	217
5.2.9. Exploiting pyoverdine (PVD) production as a screen for TI compound inhibitory activity	219
5.2.10 Jurkat T cell viability in the presence of TI1 and TI6.....	222
5.3. Discussion	224
Chapter 6: Conclusions and Outlook	228
Reference List.....	236
Appendix.....	254

List of Tables

Table 1.1. Antibiotics used to treat <i>P. aeruginosa</i> infections.	28
Table 1.2 Clinically relevant <i>P. aeruginosa</i> RND Efflux Pumps and their antibiotic substrates.	32
Table 2.1. List of bacterial strains used during this study.	62
Table 2.2. Plasmids used during this study.....	63
Table 2.3. List of primers used during this study.....	64
Table 2.4. DNA fragment sizes following PCR amplification of <i>antA</i> , <i>antR</i> , <i>catB</i> , <i>catR</i> and <i>hisI</i> promoters.	73
Table 3.1. Expression of genes involved in anthranilate degradation is up-regulated in the absence of a Tat protein export system.....	95
Table 3.2. List of DEG in a <i>pqsA</i> mutant and a <i>tat</i> mutant when compared to PAO1-DK wild-type.	105
Table 4.1. Substrates exported by the <i>P. aeruginosa</i> Tat secretion pathway....	151
Table 5.1. High-throughput screens for inhibitors of the Tat system found in the literature.	186
Table 5.2. Published Tat system inhibitors and the available structures.	187
Table 5.3. Structural Analogues of the Tat inhibitor compound TI1.....	194
Table 7.1. Up-regulated genes in PAO1-DK Δ <i>tatA</i> mutant.....	260
Table 7.2. Down-regulated genes in PAO1-DK Δ <i>tatA</i> mutant.....	266
Table 7.3. Quality assessment of genome assemblies.....	270

List of Figures

Figure 1.1. Stages of biofilm formation.....	40
Figure 1.2. Schematic overview of the three quorum sensing regulatory networks in <i>P. aeruginosa</i>	43
Figure 1.3. Cycling of Tat pathway assembly, translocation and disassembly.....	46
Figure 2.1. Construction of pDM4 $\Delta antA$ deletion plasmid (a) and confirmation of deletion mutants (b).	71
Figure 3.1. <i>tat</i> mutation affects biofilm formation..	83
Figure 3.2. Biosynthesis of PQS was downregulated upon <i>tat</i> mutation or deletion in both PAO1-DK and PA14.	86
Figure 3.3. LC-MS/MS quantification of secreted AQS in wild-type and $\Delta tatABC$ mutants.	87
Figure 3.4. HHQ, PQS and HQNO in culture supernatants following 16 h growth.	88
Figure 3.5. Induction of <i>pqsA</i> expression in PAO1-DK $\Delta pqsA$ by exogenous AQS produced by PAO1-DK, PA14 and their respective <i>tat</i> mutants.....	89
Figure 3.6. Pyocyanin extracted from wild-type and <i>tatABC</i> mutant culture supernatants.....	91
Figure 3.7. Volcano plot of differently expressed genes in PAO1-DK and a <i>tat</i> mutant.....	93
Figure 3.8. The anthranilate degradation pathway.	94
Figure 3.9. Anaerobic respiration pathway.	96
Figure 3.10. GO cellular compartments.....	98
Figure 3.11. GO biological processes of differentially expressed genes in PAO1-DK <i>tat</i> mutant compared with PAO1-DK wild-type.....	99
Figure 3.12. GO molecular functions of differentially expressed genes.	100
Figure 3.13. Differently expressed genes of PAO1-N WT vs <i>pqsA</i> mutant and PAO1-DK WT vs <i>tat</i> mutant.....	102

Figure 3.14. Operon containing genes encoding the twin-arginine transport system.....	105
Figure 3.15. Maximum expression of the <i>hisI-hisE-tatA-tatB-tatC-PA5071</i> operon was elevated in $\Delta pqsA$ and <i>tatA::Tn5</i> mutants but reduced in the double mutant and in PAO1-DK $\Delta tatABC$	106
Figure 3.16. Expression of the <i>tat</i> operon promoter (<i>hisI'</i>) remained elevated instead of exhibiting a transient peak when <i>tatA</i> was interrupted by a transposon irrespective of PQS deletion.....	107
Figure 3.17. Expression of <i>antA</i> , <i>antR</i> , <i>catB</i> and <i>catR</i> in wild-type PAO1-DK and a <i>tat</i> mutant.....	111
Figure 3.18. Expression of <i>antA</i> , <i>antR</i> , <i>catB</i> and <i>catR</i> in PA14 and PA14 $\Delta tatABC$	113
Figure 3.19. Growth of PAO1-DK and PA14 wild-type and <i>tat</i> mutants over 24 h.	114
Figure 3.20. LC-MS/MS quantification of anthranilate in culture supernatants..	115
Figure 3.21. Expression of the anthranilate degradation pathway in <i>tat</i> and <i>pqsA</i> mutants.	117
Figure 3.22. Inhibitory effects of high concentrations of anthranilate on the growth of PAO1-DK and PA14.....	119
Figure 3.23. Expression of <i>antA</i> is induced by exogenous anthranilate.....	120
Figure 3.24. Exogenously supplied anthranilate induces expression of genes involved in anthranilate degradation pathway.....	121
Figure 3.25. Exogenous anthranilate induces expression of <i>antA</i> , <i>antR</i> , <i>catB</i> and <i>catR</i> in PA14 and the isogenic $\Delta tatABC$ mutant.	122
Figure 3.26. Exogenous anthranilate represses expression of <i>pqsA</i> in PA14 and PA14 $\Delta tatABC$	123
Figure 3.27. Whole genome sequencing comparison of wild-type PAO1-DK, the $\Delta antA$ deletion mutant, PAO1-DK $\Delta tatABC \Delta antA$ and PAO1-DK $\Delta pqsA \Delta antA$	126

Figure 3.28. Deletion of <i>antA</i> restores growth in a <i>tatABC</i> mutant.....	128
Figure 3.29. Maximum expression from a constitutive <i>ptac</i> promoter in various mutants shows no change in luminescence.	129
Figure 3.30. LC-MS/MS semi-quantification of anthranilate extracted from culture supernatants.....	130
Figure 3.31. Expression of the anthranilate degradation pathway upon deletion of <i>antA</i> and <i>pqsA</i>	132
Figure 3.32. Expression of the anthranilate degradation pathway in PAO1-DK and various <i>antA</i> and <i>tatABC</i> mutants.	134
Figure 3.33. Expression of <i>antA</i> over 24 h in PAO1-DK $\Delta antA$, $\Delta tatABC$ and $\Delta pqsA$ single and double mutants.	135
Figure 3.34. Expression of <i>pqsA</i> in $\Delta antA$, $\Delta tatABC$ and $\Delta pqsA$ mutants.....	136
Figure 3.35. Total pyocyanin produced by PAO1-DK, $\Delta antA$, $\Delta tatABC$ and $\Delta pqsA$ mutants and various mutants.....	137
Figure 3.36. AQ biosynthesis pathway in <i>P. aeruginosa</i>	142
Figure 3.37. Model showing regulation of anthranilate metabolism genes (<i>antABC</i> , <i>catBCA</i>) and the AQ biosynthetic operon (<i>pqsABCDEphnAB</i>) by AntR, PqsR, RhlR, MpaR, and PrrF sRNAs.	143
Figure 3.38. Schematic to illustrate hypothesised regulatory changes to <i>antA</i> , <i>antR</i> and <i>pqsA</i> expression in wild-type, $\Delta pqsA$, <i>tat</i> , and $\Delta antA$ mutants.....	146
Figure 4.1. Expression of <i>pqsA</i> in PA14, PA14 $\Delta tatABC$, and deletion mutants of substrates exported via the Tat system.	154
Figure 4.2. Maximum expression of the <i>antA</i> promoter in PA14 and PA14 $\Delta tatABC$ compared with that in each of the 34 Tat substrate mutants.	155
Figure 4.3. Normalised pyocyanin in 8 h culture supernatants of Tat substrate deletion mutants.	156
Figure 4.4. Schematic diagram of the cytochrome <i>bc₁</i> complex unit.	159
Figure 4.5. Growth (a) and <i>pqsA</i> expression in (b) of PA14, a PA14 <i>tat</i> deletion mutant and a <i>petA</i> deletion mutant over 24 h.	161

Figure 4.6. AQs extracted from culture supernatants of PA14, PA14 Δ <i>tatABC</i> , PA14 Δ <i>petA</i> and PA14 Δ <i>petA-CTC::petA</i> at 8 h and semiquantified with LC-MS/MS.	162
Figure 4.7. LC-MS/MS semi-quantification of AQs in culture supernatants from PA14, PA14 Δ <i>tatABC</i> , PA14 Δ <i>petA</i> and PA14 Δ <i>petA-CTC::petA</i> following 16 h growth in LB.	163
Figure 4.8. Pyocyanin production by <i>P. aeruginosa</i> at 8 h in PA14, a Δ <i>tatABC</i> mutant, a Δ <i>petA</i> mutant and the <i>petA</i> complemented strain.....	164
Figure 4.9. Semi-quantification of anthranilate production by PA14, PA14 Δ <i>tatABC</i> , PA14 Δ <i>petA</i> , PA14 Δ <i>petA-CTX_petA</i> following 8 h and 16 h growth in LB.	165
Figure 4.10. Expression of <i>rhlA</i> and growth of PA14 in (a), PA14 Δ <i>tatABC</i> (b) and PA14 Δ <i>petA</i> (c).....	167
Figure 4.11. Constitutive <i>ptac</i> promoter expression in a Δ <i>tatABC</i> mutant and Δ <i>petA</i> mutant shows <i>lux</i> output is not affected by gene deletion.....	168
Figure 4.12. Mature pyoverdine production is abolished in a <i>tat</i> mutant but retained in <i>petA</i> mutant.....	169
Figure 4.13. Growth (a), <i>pqsA</i> expression (b), and semi-quantification of AQs (c) in PA14, Δ <i>tatABC</i> and Δ <i>petA</i> , Δ <i>petB</i> and Δ <i>petC</i> mutants.	171
Figure 4.14. Representative images of PAO1-DK and PAO1-DK Δ <i>tatABC</i> biofilms following 48 h static growth	174
Figure 4.15. Static biofilms of PA14, a <i>tatABC</i> mutant, <i>petA</i> mutant and complemented <i>petA</i> mutant following 48 h growth.....	176
Figure 4.16. Extracellular DNA quantified from planktonic cultures after (a) 8 h growth and (b) 16 h.....	178
Figure 5.1 Schematic showing design of fluorescent protein screen for inhibition of the Tat system.	191
Figure 5.2. Activity of Bay 11-7082 (T11) against <i>antA</i> (EC_{50} 20.46) and <i>pqsA</i> expression (IC_{50} =27.41).....	192

Figure 5.3. Inhibitors screened using <i>pqsA</i> expression to determine IC ₅₀ . Bay 11-7082 structure was modified either at positions 3 and/or 4 of the phenyl ring (within blue circle) or at the nitrile site (within pink circle).	193
Figure 5.4. Growth of PAO1-DK miniCTX:: <i>pqsA'</i> - <i>lux</i> in 17 μM, 39 μM, 88 μM, 198 μM, 444 μM and 1000 μM TI1.....	200
Figure 5.5. Growth of PAO1-DK miniCTX:: <i>pqsA'</i> - <i>lux</i> in a range of concentrations of a)TI1, b)TI2, c)TI3, d)TI4, e) TI5, and f) TI6.....	202
Figure 5.6. Growth of PAO1-DK miniCTX:: <i>pqsA'</i> - <i>lux</i> in a range of concentrations of a)TI7, b)TI8, c)TI9, d)TI10, e) TI11, and f) TI12, g)TI13 and h) TI14. .	203
Figure 5.7. Growth of PAO1-DK miniCTX:: <i>pqsA'</i> - <i>lux</i> is not severely reduced by Tat inhibitor 15 (a) and Tat inhibitor 16 (b).....	204
Figure 5.8. Dose response curves for TI1 and analogues TI2-5 and TI14 bearing different phenyl ring substituent groups.	206
Figure 5.9. Inhibition of <i>pqsA</i> expression is influenced by phenyl ring substituents.....	207
Figure 5.10. Comparison of IC ₅₀ for inhibition of <i>pqsA'</i> - <i>lux</i> expression by TI1-TI16.....	208
Figure 5.11. Dose-response curves of TI1 analogues TI6, TI10, TI12 and TI8 incorporating a CONH ₂ functional group together with different phenyl ring substituent groups.....	210
Figure 5.12. Replacement of the CN functionality with COOEt to generate analogues TI7, TI9, TI11 and TI13, increased IC ₅₀ concentrations for <i>pqsA</i> expression.....	211
Figure 5.13. Effect of TI9 on <i>pqsA</i> expression at concentrations ranging from 0.5 μM to 1000 μM.....	213
Figure 5.14. Peak expression of <i>pqsA</i> is unaltered when grown in the presence of TI15 and TI16, analogues with a CONMe ₂ functional group.	214
Figure 5.15. Dose-response curves for TI15 and TI16 which have a CONMe ₂ functional group.	215

Figure 5.16. Normalised <i>pqsA</i> expression for PAO1-DK miniCTX:: <i>pqsA'-lux</i> in response to analogues TI17-TI22 at 20 μ M or 40 μ M.....	216
Figure 5.17. Comparison of IC ₅₀ and EC ₅₀ concentrations for TI1-6, TI8-TI10, TI12 and TI14.	217
Figure 5.18. Dose response curve for activation of <i>antA</i> following growth in response to TI4 (a) and TI5 (b).....	218
Figure 5.19. PVD production in PAO1-DK, PAO1-DK Δ pqsA and PAO1-DK Δ tatABC mutant.....	220
Figure 5.20. Normalised PVD production of PAO1-DK grown in iron-limited M9 + succinate medium containing 20 μ M or 40 μ M and TI1, TI4, TI6, TI7, TI8, TI9, TI15 or TI16.....	221
Figure 5.21. Alamar blue cell viability assay with Jurkat T cells.....	223
Figure 6.1. Schematic diagram showing key changes within a <i>tat</i> mutant (b) compared to wild-type <i>P. aeruginosa</i> (a) uncovered during this PhD.	231
Figure 7.1. Example of cell harvest for RNAseq.....	267
Figure 7.2. Bioluminescent transcriptional reporter in <i>P. aeruginosa</i> carrying an <i>antA':lux</i> promoter fusion.....	268
Figure 7.3. Construction of transcriptional reporters to measure anthranilate degradation pathway expression.....	269
Figure 7.4. Predicted model and ligand-binding domain of PA14_57570.....	271
Figure 7.5. Flow chart showing process of mapping sequence conservation to 3D structure of PetA.	271
Figure 7.6. Conservation of residues within the PetA sequence as determined by Consurf.	271
Figure 7.7. 3D model of PetA (PA14_57570) visualised with PyMol.....	271

Abbreviations

°C	degrees Celsius
% (v/v)	percentage volume per total volume
% (w/v)	percentage weight per total volume
AHLs	<i>N</i> -acyl-homoserine lactones
AQs	2-alkyl-4-quinolones
BLI	β-lactamase inhibitor
bp	base pair
cAMP	Cyclic adenosinemonophosphate
c-di-GMP	Cyclic-dimeric-guanosine monophosphate
C4-HSL	<i>N</i> -butanoyl-L-homoserine lactone
CDC	Centre for Disease Control and Prevention
CF	cystic fibrosis
CFTR	CF transmembrane conductance regulator
CLSM	confocal laser scanning microscopy
CMDR	Cell mask deep red (membrane stain)
COOEt	ethoxycarbonyl
CONH ₂	amide
CONMe ₂	<i>N,N</i> -dimethylcarboxamide
COMe	acetyl
DEG	differently expressed genes
DNA	deoxyribonucleic acid
dH ₂ O	deionised H ₂ O
dNTP	deoxynucleoside triphosphate
EC ₅₀	Half maximal effective concentration of compound
eDNA	extracellular DNA
EPS	exopolymeric substance
g	gram
GO	Gene ontology
h	hour
HHQ	2-heptyl-4-quinolone

IC ₅₀	Half maximal inhibitory concentration of compound
IM	Inner membrane
indel	insertions and deletions
LB	Luria-Bertani broth
LC-MS/MS	Liquid chromatography-tandem mass spectrometry
µg	microgram
µl	microlitre
µM	micromolar
MDR	Multidrug resistant
4-Me-PhSAN	(2E)-3-[(4-Methylphenyl)sulfonyl]acrylonitrile
mg	milligram
min	minute
mL	millilitre
n.f.	Nuclease free (water)
OD	optical density
3-oxo-C12-HSL	<i>N</i> -(3-oxododecanoyl)-L-homoserine lactone
PA	<i>Pseudomonas aeruginosa</i>
PAPI-1, PAPI-2	<i>Pseudomonas aeruginosa</i> pathogenicity islands 1, 2
PCR	polymerase chain reaction
PBS	phosphate buffered saline
PBP	Penicillin binding protein
PDR	Pan-drug resistant
PMF	Proton motive force
PQS	pseudomonas quinolone signal, 2-heptyl-3-hydroxy-4-quinolone
PVC	polyvinylchloride
QS	quorum sensing
RLU	Relative light unit
RPMI-1640	Roswell park memorial institute medium 1640
SDS-PAGE	sodium dodecyl sulphate-polyacrylamide gel electrophoresis
TAE	Tris-acetate-EDTA buffer
Tat	Twin-arginine translocation

TCA	Tricarboxylic acid
TF	transcription factor
SNP	Single-nucleotide polymorphism
SOC	super optimal broth with catabolite repression
v/v	Volume per volume
WGS	Whole-genome sequencing
w/v	Weight per volume
XDR	Extensively-drug resistant

Chapter 1: Introduction

1.1 The genus *Pseudomonas*

Pseudomonas is found in the proteobacteria phylum and the γ -proteobacteria class. It is a Gram-negative, non-sporulating, rod-shaped bacterium. *Pseudomonas* spp. are non-fermentative and oxidase-positive with a size of 0.5-1 μm width and 1-5 μm in length. There are around 200 different species of *Pseudomonas* listed in the Approved Lists of Bacterial names (Özen and Ussery, 2012).

Such a diverse genus occupies a wide variety of environmental niches. *Pseudomonas* species can be found growing in soil, water, washing machines, even the international space station, and can cause disease in plants, insects, animals and humans (Kumar and Anand, 2006; Kim *et al.*, 2013). *Pseudomonas syringae*, a notable crop plant pathogen, is also found in non-agricultural niches and is actively involved in the water cycle. In fact, *P. syringae* has been found in snow, clouds, rain, and rivers and is currently hypothesised to act as an ice nucleus within clouds due to its well established ice-nucleation ability (Morris *et al.*, 2008). Other well-studied examples of *Pseudomonas* species include the soil-dwelling bacterium *Pseudomonas putida*; and *Pseudomonas aeruginosa*, a notorious pathogen capable of acute and chronic infections of wounds, eyes, burns, bloodstream, and the cystic fibrosis lung. *P. aeruginosa* will be expanded upon in the following section as it is the main focus of this thesis. The versatility of *Pseudomonas* spp. has resulted in them becoming a useful tool. For example, *P. putida* is the most widely used *Pseudomonas* species industrially, *P. medocina* is used in industrial processes, *P. alcaligenes* is used for bioremediation of pollutants, and *P. fluorescens* is used in biocontrol (Jaeger and Reetz, 1998).

Pseudomonas spp. exist in planktonic form but can also readily switch to a communal biofilm lifestyle. Biofilms are complex communities of cells attached to

a surface and contained in an extracellular polymeric matrix comprised of proteins, exopolysaccharides and DNA (Costaglioli *et al.*, 2012). *Pseudomonas aeruginosa* is a prolific biofilm producer and production of a protective biofilm allows the bacteria to persist in otherwise hostile environmental conditions.

1.2 *Pseudomonas aeruginosa*

Pseudomonas aeruginosa is an opportunistic pathogen capable of infecting a wide range of hosts including plants, insects, animals and humans (Farrow and Pesci, 2007a). *P. aeruginosa* is a versatile human pathogen, that infects the blood, gut, eyes, and ears of immunocompromised individuals. It also causes persistent chronic infections in wounds and burns, and the cystic fibrosis lung.

P. aeruginosa is ubiquitous in the environment, although it favours moist conditions, and is able to catabolise a variety of organic compounds. It grows well at temperatures up to 42°C. As a facultative anaerobe, *P. aeruginosa* has the ability to use nitrate and nitrite as alternate terminal electron acceptors when oxygen is limited. Because of this, it can grow under hypoxic conditions. *P. aeruginosa* cells are motile with a polar monotrichous flagellum (O'Toole and Kolter, 1998). Notable characteristics of *P. aeruginosa* are a grape-like odour due to aminoacetophenone production and a blue/green colour attributed to phenazine production.

P. aeruginosa PAO1 has a large genome size of ~6.3 Mbp and reportedly the highest proportion of regulatory genes for a bacterial genome (Stover *et al.*, 2000). Strict regulation of such a large and complex genome allows adaptation to diverse environmental niches and survival under changing conditions. PAO1 was the first *Pseudomonas* strain to have its genome sequenced, and has 5,570 open reading frames (ORFs) with a GC content of approximately 65%.

Different strains of *P. aeruginosa* have been isolated over the years and are now regularly cultured in the laboratory. PAO1 is one of the most commonly used strains in laboratory research, it is a chloramphenicol-resistant derivative of the PAO strain first isolated from a chronic wound in Australia in 1954. The PAO strain was supplied worldwide for use in research laboratories and over the years insertions and deletions (indels) and single-nucleotide polymorphisms (SNPs) have resulted in diversification of its genome (Klockgether *et al.*, 2010). Many sublines have now developed through microevolution of the strain which has led to the use of additional defining nomenclature such as PAO1-DK for the Denmark subline, or PAO1-N which originates from the University of Nottingham. *Pseudomonas aeruginosa* PA14 is another commonly used laboratory strain originally isolated from a burn wound and is far more virulent than PAO1, most likely due to two additional *Pseudomonas aeruginosa* pathogenicity islands and a *ladS* mutation (PAPI-1 and PAPI-2) carried on its genome (He *et al.*, 2004; Mathee, 2018).

1.3 Clinical Relevance of *P. aeruginosa*

The ability to form biofilms on medical surfaces such as catheters, replacement joints or surgical equipment, plus resistance to disinfectants and many commonly used antimicrobials makes *P. aeruginosa* a common cause of nosocomial infection. The Infectious Disease Society of America (IDSA) has named *P. aeruginosa* as one of six highly dangerous microbes, the global leading causes of nosocomial infection. The six form the acronym ESKAPE pathogens, due to their virulence and ability to “escape” conventional antibiotic action (Azam and Khan, 2019). It is considered a worldwide healthcare issue by the International Nosocomial Infection Control Consortium with the majority of infections occurring in healthcare settings. In 2017 *P. aeruginosa* was added to the WHO priority list

for research and development of new antibiotics (Azam and Khan, 2019). It causes deadly or life-threatening infections in immunocompromised and highly vulnerable individuals, for example those with AIDS, cancer, or receiving treatment in intensive care units (Kerr and Snelling, 2009; Moradali *et al.*, 2017; Schultz *et al.*, 2020).

Whilst *P. aeruginosa* is a notorious cause of nosocomial infections, it is also often associated with community-acquired infection of the cystic fibrosis (CF) lung. Chronic and recurring lung infections result in frequent hospital admissions and severely lower quality of life of people with cystic fibrosis. Mutations in the CF transmembrane conductance regulator gene (CFTR) gives rise to multisystem disease. The CFTR regulator is responsible for maintaining normal osmotic balance across epithelial cells by allowing the passage of electrolytes and chloride ions. In CF patients the mucus layer is abnormal and has a thick, dehydrated and sticky texture which is harder to clear from the lung. As a result, CF patients are highly susceptible to *P. aeruginosa* respiratory infections. Recurring *P. aeruginosa* lung infections are the main cause of morbidity and mortality in CF patients (Moradali *et al.*, 2017). Between the age of 1 and 3 years, 30 – 50% of CF patients contract acute *P. aeruginosa* infections (Da Silva Filho *et al.*, 2013). *P. aeruginosa* switches to a mucoid phenotype allowing it to persist in the lungs despite antibiotic treatment, causing chronic infections (Henry *et al.*, 1992; Govan and Deretic, 1996). These chronic infections are often reported between the ages of 3 and 16 years old (Da Silva Filho *et al.*, 2013). Around 70% of adults with cystic fibrosis carry debilitating persistent *P. aeruginosa* lung infections to the end of their lives (Moradali *et al.*, 2017).

There is no one course of treatment for *P. aeruginosa* infection, and efficacy depends upon many factors including stage of infection at which antibiotics are administered, route of administration, location of infection, antibiotic type, pharmacokinetics and metabolism of the antibiotic, dose, and whether antibiotic

action is time or concentration dependent (Langton Hewer and Smyth, 2017; Bassetti *et al.*, 2018; Cigana *et al.*, 2020). Eight categories of antibiotic are commonly used in a *P. aeruginosa* regimen, often in combination. These are covered in greater detail in **Table 1.1**.

Antibiotic category	Description	Reference
Aminoglycoside	<ul style="list-style-type: none"> • tobramycin, gentamicin, amikacin and netilmicin • bind 16s rRNA in A-site of prokaryotic ribosomal subunits • prevent mRNA and tRNA interactions • inhibit protein translation 	(Noller, 1991; Kotra <i>et al.</i> , 2000; Bassetti <i>et al.</i> , 2018).
β -Lactam: penicillins	<ul style="list-style-type: none"> • β-lactams bind penicillin binding proteins (PBPs), inhibit transpeptidation, arrest cell wall synthesis • ticercillin, piperacillin • administered with β-lactamase inhibitors (BLIs) clavulanic acid or tazobactam due to intrinsic and imported β-lactamase genes 	(Meyers <i>et al.</i> , 1980; Papp-Wallace <i>et al.</i> , 2011; Bassetti <i>et al.</i> , 2018)
β -Lactam: cephalosporins	<ul style="list-style-type: none"> • ceftazidime and cefepime • favoured as incidence of allergic reaction to cephalosporin is 1-3% in the general population and they can be used to treat patients with a penicillin allergy 	(Frère, 1977; Richmond, 1978; Chaudhry <i>et al.</i> , 2019; Yuson <i>et al.</i> , 2019)
β -Lactam: carbapenems	<ul style="list-style-type: none"> • imipenem and meropenem 	(Bassetti <i>et al.</i> , 2018)
Monobactam	<ul style="list-style-type: none"> • aztreonam • monocyclic β-lactam ring • prevents cell wall synthesis through inhibition of transpeptidation, resulting in cell lysis 	(Pechère and Köhler, 1999)
Fluoroquinolone	<ul style="list-style-type: none"> • Ciprofloxacin and levofloxacin • Binds DNA topoisomerase IV and DNA gyrase in complex with DNA 	(Blondeau, 2004)

	<ul style="list-style-type: none"> • DNA synthesis unable to proceed at the replication fork, DNA fragments resulting in cell death 	
Fosfomycin	<ul style="list-style-type: none"> • inactivates pyruvyl-transferase involved in bacterial cell wall synthesis • leads to peptidoglycan fragmentation and cell lysis 	Kahan <i>et al.</i> , 1979; Pachori <i>et al.</i> , 2019)
Polymixin	<ul style="list-style-type: none"> • Polymixin B, Polymixin E (colistin) • cationic antimicrobial polypeptides that insert into bacterial membranes • destabilising them and increasing permeability (Li <i>et al.</i>, 2005) 	

Table 1.1. Antibiotics used to treat *P. aeruginosa* infections. There are 8 categories described, used either in combination or monotherapy.

The development of drug-resistant, multi-drug resistant (MDR), extensively-drug resistant (XDR) and pan-drug resistant (PDR) strains has severely restricted treatment options. MDR is defined as resistance to one or more antibiotics in 3 or more classes, XDR is resistance to one or more antibiotic in all classes and PDR is resistance to all antibiotics (Bassetti *et al.*, 2018).

For successful eradication rapid administration of antibiotics is essential, and susceptibility testing is necessary to avoid unwanted selection (Bassetti *et al.*, 2018; Cigana *et al.*, 2020). However, those who present with infection often need prompt treatment, this combined with a lack of rapid tests for antibiotic resistance means that patients are given broad-spectrum antibiotics which kill the host's protective microbiome and allow *P. aeruginosa* to grow unimpeded by competition. Selection in favour of *P. aeruginosa* is due to its inherent multidrug resistance to commonly used antibiotics, as well as antibiotic tolerance through formation of persistent biofilms which reduce antibiotic susceptibility. Additional resistance to newer antibiotics can be acquired through horizontal gene transfer or mutation of specific genes (Martínez and Baquero, 2002; Niederman, 2006).

1.4 Antibiotic Resistance in *P. aeruginosa*

Antimicrobial resistance (AMR) is the permanent increase in minimum inhibitory concentration (MIC) of an antibiotic, due to genetic changes such as acquisition of mobile genetic elements or mutation. AMR can be innate, acquired, or adapted and is not the same as antibiotic tolerance, which can be defined as transient changes to a phenotypic state that allows bacteria to survive antibiotic attack (Olsen, 2015). Resistance strategies can be found throughout natural environments due to the abundance of naturally-produced antibiotics which are secondary metabolites exported and used to survive against competing bacteria (Sengupta *et al.*, 2013). Alexander Fleming, the discoverer of the first broad-spectrum antibiotic penicillin, predicted emergence of resistance to penicillin as early as 1945 (Fleming, 1945). Once challenged with antibiotics in a clinical setting, growth of resistant strains unimpeded by competition occurs as sensitive bacteria are killed off. The infection then progresses with the antibiotic resistant strain predominating.

In general, *P. aeruginosa* is inherently resistant to many commonly used antibiotics and employs all types of resistance mechanisms (Pechère and Köhler, 1999; Normark and Normark, 2002). AMR can be sub-divided into three categories: innate (also known as intrinsic) resistance, acquired resistance and adaptive resistance (Pechère and Köhler, 1999; Normark and Normark, 2002). Each category is outlined below.

Innate

Innate or intrinsic antimicrobial resistance is the natural resistance of the “wild-type” species, without genetic mutation. *P. aeruginosa* is intrinsically resistant to many commonly used antibiotics due to low membrane permeability, resistance-nodulation-division (RND) multidrug efflux (Mex) pumps, and a chromosomally-encoded β -lactamase AmpC (Langendonk *et al.*, 2021). AmpC provides a constitutive low level of resistance to β -lactamase antibiotics by hydrolysis of the β -lactam ring (Juan *et al.*, 2005). Expression of *ampC* can also be induced in response to cephalosporins and aminopenicillins, through disruption of a peptidoglycan recycling pathway or loss of PBP4 (Cavallari *et al.*, 2013).

The *P. aeruginosa* genome encodes 12 RND-type multidrug efflux pumps, which actively remove antibiotic agents from the cell preventing them from reaching their target (Stover *et al.*, 2000). MexAB-OprM is a constitutively active efflux pump in wild-type *P. aeruginosa* causing a basal level of resistance to lincomycin, novobiocin, chloramphenicol, carbapenems, fluoroquinolones, macrolides, penicillins, tetracyclines and most β -lactams (Langendonk *et al.*, 2021). It also extrudes triclosan, a widely-used biocide, and sodium dodecyl sulfate, a common surfactant (Chuanchuen *et al.*, 2003; Montaseri and Forbes, 2016). The MexAB-OprM efflux system can contribute to the development of multi-drug resistant strains (Goli *et al.*, 2016).

Low membrane permeability reduces antibiotic accumulation in the cell. There are relatively few porins in the outer membrane, the most common is OprF, and second most common, OprD (Trias *et al.*, 1989; Chevalier *et al.*, 2017). OprD allows entry of carbapenem antibiotics into *P. aeruginosa*, and its downregulation or mutation is implicated in adaptive and acquired resistance. Within biofilms copious packaging of outer-membrane vesicles with OprD occurs increasing tolerance to carbapenems. OMVs are formed through budding of the outer membrane and contain many periplasmic components (Langendonk *et al.*, 2021).

Creation of OMVs with highly abundant OprD porins has two functions, it significantly lowers the presence of OprD within the outer membrane, and it draws in carbapenems to the OMV preventing accumulation within the cell (Park *et al.*, 2015; Chevalier *et al.*, 2017).

Adaptive

Adaptive antibiotic resistance involves transient changes to gene expression in response to environmental circumstances, and often involves global regulatory networks and quorum sensing pathways to coordinate a subset of genes involved in response to antibiotic attack. Once the environmental circumstances have changed, resistance is reversed. Many two-component sensing systems are involved in alteration of gene expression, including *phoPQ*, *parRS*, *creCD*, *pmrAB*, and *cprRS* (Fernández *et al.*, 2012; Langendonk *et al.*, 2021). Other adaptive mechanisms of response include changes to motility, biofilm formation, overexpression of *ampC* and genes coding for Mex-type efflux pumps (Walters III *et al.*, 2003; Cavallari *et al.*, 2013; McElroy *et al.*, 2014; Sun *et al.*, 2018; Coleman *et al.*, 2020).

Overexpression of efflux pumps in response to external stressors is a common adaptive mechanism seen in resistant strains. There are four clinically relevant RND pumps outlined below in **Table 1.2**. MexAB-OprM was mentioned earlier, and the antibiotic substrates of MexXY-OprM are aminoglycosides, erythromycin, tetracycline and cefepime (Masuda *et al.*, 2000; Hocquet *et al.*, 2003). MexEF-OprN exports chloramphenicol, fluoroquinolones, tetracycline, imipenem and trimethoprim (Langendonk *et al.*, 2021). MexCD-OprJ extrudes chloramphenicol, fluoroquinolones, tetracycline and erythromycin (Masuda *et al.*, 2000). Loss of transcriptional repressors is often the cause of upregulation.

RND Efflux Pump	Antimicrobial Substrate	Expression
MexAB-OprM	lincomycin novobiocin chloramphenicol carbapenems fluoroquinolones macrolides penicillins tetracyclines most β -lactams triclosan SDS	Constitutive, <i>mexR</i> mutants have up-regulated expression
MexXY-OprM	aminoglycosides erythromycin tetracycline cefepime	Negative regulation by MexZ repressor, <i>mexZ</i> mutation leads to overproduction
MexEF-OprN	chloramphenicol fluoroquinolones tetracycline imipenem trimethoprim	Positive regulation of expression by MexT, which is often inactive in wild-type PA
MexCD-OprJ	chloramphenicol fluoroquinolones tetracycline erythromycin	Expressed in strains with mutations in the negative regulatory gene, <i>nfxB</i> .

Table 1.2 Clinically relevant *P. aeruginosa* RND Efflux Pumps and their antibiotic substrates. Expression of each pump is also described (Langendonk et al., 2021).

Acquired

Acquired antibiotic resistance occurs through advantageous mutations or horizontal transfer of antibiotic resistance genes on mobile genetic elements such as plasmids or transposons. In *P. aeruginosa*, enzymes for aminoglycoside alteration and novel β -lactamases are acquired through horizontal gene transfer, whereas decrease or modification of porins and antibiotic targets are due to chromosomal mutation, along with overexpression of efflux pumps and β -lactamases (Langendonk *et al.*, 2021). Mutations within DNA gyrase and Topoisomerase IV protect against fluoroquinolones, and methylation of 16S rRNA prevents aminoglycoside binding (Lee *et al.*, 2005; Doi and Arakawa, 2007; Moradali *et al.*, 2017).

1.5 *P. aeruginosa* Virulence

P. aeruginosa is able to survive and thrive in such diverse and adverse conditions due to its arsenal of responsive mechanisms that sense and regulate genes to respond to oxidative stress, antibiotic attack, iron depletion, starvation, heavy metals, salt, inflammatory cytokines, as well as changes in temperature, oxygen availability, and phosphate levels (Moradali *et al.*, 2017). *P. aeruginosa* produces a vast array of virulence factors that allow cells to colonise different sites in the host body by evading defences, disrupting immune responses, scavenging for iron and vital nutrients, and growing in low oxygen conditions. Virulence factors are either cell-associated, such as pili and flagella, or secreted, and there is a wide variety including pyocyanin, exoproteases, siderophores and rhamnolipids. In addition, *P. aeruginosa* forms protective biofilms made of cell aggregates surrounded by an exopolymeric substance (EPS) that slows diffusion of reactive

oxygen species and antibiotics. Biofilms are important in establishing persistent, chronic infections.

Motility

Motility contributes to virulence by allowing cells to travel to and colonise favourable environments. Individual *P. aeruginosa* cells swim in liquid, swarm on semi-solid surfaces and twitch, glide or slide on solid surfaces. Swimming through liquid is possible by rotational changes in the flagellum, whereas swarming involves both flagella and type IV pili as well as overproduction of rhamnolipid-rich surfactants (Köhler *et al.*, 2000; Kearns, 2010; Hook *et al.*, 2019). Swarming cells tend to be hyper-flagellated and move in a coordinated manner, genes involved in swarming are under the control of *las* and *rhl* quorum sensing systems (see **Section 1.6**) (Köhler *et al.*, 2000). Twitching, however, uses extension, attachment and withdrawal of type IV pili for coordinated cell movement (Skerker and Berg, 2001). Pili are vital for biofilm formation and *pilA* mutants were unable to form microcolonies instead producing only thin, flat, biofilms when grown on polyvinylchloride (PVC) plastic under static conditions (O'Toole and Kolter, 1998; Kühn *et al.*, 2021). Motility allows cells to be able to swim to a surface, colonise it, and form a mature biofilm.

Pyocyanin

Phenazines are redox-active secondary metabolites secreted into the extracellular milieu with a number of beneficial functions. Pyocyanin is a phenazine produced by *P. aeruginosa*. It gives a characteristic blue-green colour to stationary-phase cultures and colonies of *P. aeruginosa*. The virulence of pyocyanin-deficient mutants is much lower than wild-type (Recinos *et al.*, 2012).

Pyocyanin is a heterocyclic zwitterion that can permeate cell membranes easily, it is redox-active and cytotoxic to both prokaryotes and eukaryotes. After

diffusing into cells, pyocyanin produces intracellular superoxide through reaction with available NAD(P)H (Hassan and Fridovich, 1980; Reszka *et al.*, 2004; Rada *et al.*, 2008). Synthesis of pyocyanin with the phenazine biosynthetic pathway involves two almost identical operons *phzA1-G1* and *phzA2-G2* and the starting precursor chorismate (Recinos *et al.*, 2012). PhzM and PhzS are also required for pyocyanin biosynthesis. Regulation of these genes is through quorum sensing, as well as the two-component signalling system GacA/GacS (see **Section 1.6**)(Reimann *et al.*, 1997; Recinos *et al.*, 2012).

Elastase

The most abundant exoprotease in the proteome is elastase B, also referred to as LasB (Cigana *et al.*, 2021). A small (33 kDa) zinc metalloprotease, its expression is induced by cell-density dependent *las* quorum sensing through the response regulator LasR (Bever and Iglewski, 1988; Gambello and Iglewski, 1991). It is released via type II-dependent secretion, beginning with translocation across the inner membrane by the Sec system, then cleavage of its signal peptide in the periplasm. Eventually LasB is released to the extracellular milieu via the Xcp pathway (Galloway, 1991; Michel *et al.*, 2011; Cigana *et al.*, 2021). Elastase impairs host innate immunity and degrades elastin, fibronectin, mucins, and host cell barriers to aid infection (Saint-Criq *et al.*, 2018; Li *et al.*, 2019; Cigana *et al.*, 2021).

Iron uptake

Like most living cells *P. aeruginosa* requires iron for growth, it is an important transition metal commonly used in metalloproteins for oxidation-reduction reactions. Iron can exist in one of two oxidation states. Fe³⁺ is the most abundant form in oxygenated environments but presents a problem for bacteria as it has low water-solubility and therefore is difficult to take up. Conversely, Fe²⁺ is

far more soluble but predominantly found in anaerobic environments (Cornelis and Dingemans, 2013). Iron is required for life, but too much iron is toxic to the cell. As such, *P. aeruginosa* implements a number of different iron uptake strategies alongside regulatory networks of the genes involved in order to control the influx of iron.

Siderophores are secreted into the environment with the purpose of sequestering Fe³⁺. Pyoverdine and pyochelin are the two main siderophores in *P. aeruginosa*, pyoverdine is involved in iron scavenging and pyochelin is able to chelate additional transition metal ions such as Zn(II), Cu(II), Co(II), Mo(VI) and Ni(II) (Azam and Khan, 2019). Ferrisiderophores enter the cell using TonB-dependent receptors, such as the FpvA receptor which takes up pyoverdine, and FptA, pyochelin (Cornelis and Dingemans, 2013). In addition, *P. aeruginosa* can import exogenous siderophores (xenosiderophores) giving it a competitive edge.

Pyocyanin, along with its precursor phenazine-1-carboxylic acid (PCA), reduces host protein-bound Fe³⁺ to a more soluble Fe²⁺ oxidative state. Uptake of the reduced ions occurs via diffusion across the outer membrane and subsequent translocation of the inner membrane via the FeOABC system. PCA and pyocyanin can promote biofilm formation by reducing Fe³⁺ to the more bioavailable Fe²⁺ (Wang *et al.*, 2011; Cornelis and Dingemans, 2013).

Host iron is not freely available for uptake by invading pathogens, instead it is kept within a haem molecule or bound to transferrin or lactoferrin. *P. aeruginosa* is able to scavenge and uptake host haem from haem-containing proteins, with its Phu or Has systems. Haem is extremely hydrophobic and therefore is held within haemoproteins. The Phu TonB-dependent receptor directly extracts haem and transports it into the cell, whereas the Has receptor utilises an additional haemophore.

Rhamnolipids

Rhamnolipids are glycolipid biosurfactants of which there are three types active at the surface in *P. aeruginosa*: 3-(3 hydroxyalkanoyloxy) alcanoic acids (HAAs) which are produced by RhIA, mono-rhamnolipids, formed through addition of rhamnose to HAA by RhIB, and di-rhamnolipids, generated by RhIC by adding a sugar moiety to mono-rhamnolipids (Kim and Lee, 2016). Rhamnolipids are important for maintaining the channels within mature biofilms used for the exchange of essential gas and nutrients with waste products (Azam and Khan, 2019). Rhamnolipids are also required for proper swimming and twitching motility (Kim and Lee, 2016).

Hydrogen cyanide

P. aeruginosa produces the membrane-bound HcnABC enzyme which catalyses the formation of toxic hydrogen cyanide using CO₂ and glycine as substrates (Castric, 1975; Pessi and Haas, 2000). HCN is an inhibitor of cytochrome c oxidase, and its role in virulence has been demonstrated through transposon insertion within the *hcn* genes, which eliminated killing of *P. aeruginosa*-infected *C. elegans* (Gallagher and Manoil, 2001).

Biofilm formation

Biofilms are surface-attached communities of microbes living in and surrounded by a hydrated extracellular polymeric substance (EPS) also called a biofilm matrix (Li *et al.*, 2017). The *P. aeruginosa* matrix is a three dimensional scaffold in which cells are embedded, primarily in self-generated exopolysaccharides (alginate, Pel, Psl), extracellular DNA, proteins, and lipids (Hentzer *et al.*, 2001; Allesen-Holm *et al.*, 2006; Diggle *et al.*, 2006; Ryder *et al.*, 2007). Biofilm matrices can constitute 90% of the total biomass and hold

proportionally large amounts of water which protects bacteria from desiccation (Moradali *et al.*, 2017). In certain mature biofilms of *Pseudomonas aeruginosa*, such as those generated in a flow chamber, channels form to aid nutrients, gases and waste exchange (Kumar and Anand, 2006; Hall and Mah, 2017). The matrix fixes bacteria in positions very close to each other which allows for highly effective intercellular communication and generation of extracellular digestive systems by retaining secreted enzymes, metabolites and nutrients as a reservoir (Flemming and Wingender, 2010). Biofilms can be attached to biotic or abiotic surfaces and are associated with long-term chronic infections resistant to antibiotics, for example, the chronic infections of the cystic fibrosis (CF) lung (Moses *et al.*, 2000; Hall and Mah, 2017). Researchers at the Centre for Disease Control and Prevention (CDC) found that 80% of chronic infections are caused by clinical isolates that readily form biofilms in a 96-well plate, plus one study showed 60% of chronic wound specimens contained biofilms that could be seen with light microscopy and scanning electron microscopy (Li *et al.*, 2017).

In essence biofilms enable bacteria to survive harsher environments than their planktonic counterparts. Bacteria within biofilms switch to a less virulent, more dormant state allowing them to evade detection by the host immune system. Biofilms form a protective barrier to keep cells separate from the unfavourable surrounding milieu, creating a micro-environment that shelters from oxidative stress, chemical attack, and phagocytosis by macrophages. During infection the biofilm matrix binds secreted antibodies, and hydrogen peroxide is unable to fully penetrate the biofilm due to secreted catalases (Fux *et al.*, 2005; Moradali *et al.*, 2017). Growth within biofilms is slower which allows cells to persist despite nutrient limitation and build-up of metabolic waste, and during starvation eDNA can also be used as a nutrient source.

The most prominent difference between planktonic and sessile, biofilm-embedded, bacteria is the change in antibiotic susceptibility. *P. aeruginosa* is 1000-

fold more tolerant to some antibiotics when growing in a biofilm than planktonic culture (Fux *et al.*, 2005; Hengzhuang *et al.*, 2011). Restricted diffusion of exogenous compounds within the matrix is a major factor here. In addition, negatively charged elements of the matrix, such as alginate and extracellular DNA, slow the diffusion of positive antibiotics such as aminoglycosides by binding to them (Walters III *et al.*, 2003; Fux *et al.*, 2005; Mulcahy *et al.*, 2008). Unexpectedly, exposure to subinhibitory concentrations of some antibiotics actually induces the formation of thicker biofilms through alginate overproduction (Fux *et al.*, 2005).

The phenotypic switch from planktonic motile bacteria to sessile lifestyle involves expression changes of hundreds of genes and is coordinated by dynamic regulation at each level from transcription to post-translation. The motility to sessility switch is considered a response to environmental signals and is governed by many aspects including rising cellular cyclic-diGMP levels, phosphorylation by two-component regulatory systems, and quorum sensing signalling networks (Williams and Cámara, 2009; Mikkelsen *et al.*, 2011; Valentini and Filloux, 2016).

There are five stages to biofilm formation and development outlined in **Figure 1.1**. Firstly, bacteria reversibly attach to the surface using adhesins in response to numerous environmental signals. Then, when conditions are favourable this becomes irreversible attachment. During the third stage cells aggregate, grow, and create more EPS such as Pel and Psl, forming microcolonies. Next, microcolonies will join to form a macrocolony, the mature biofilm has a complex three-dimensional structure, often seen as a characteristic mushroom shape in *P. aeruginosa*. The final stage is dispersal, bacteria leave the mature biofilm to return to a planktonic lifestyle, then colonise elsewhere (Hall and Mah, 2017).

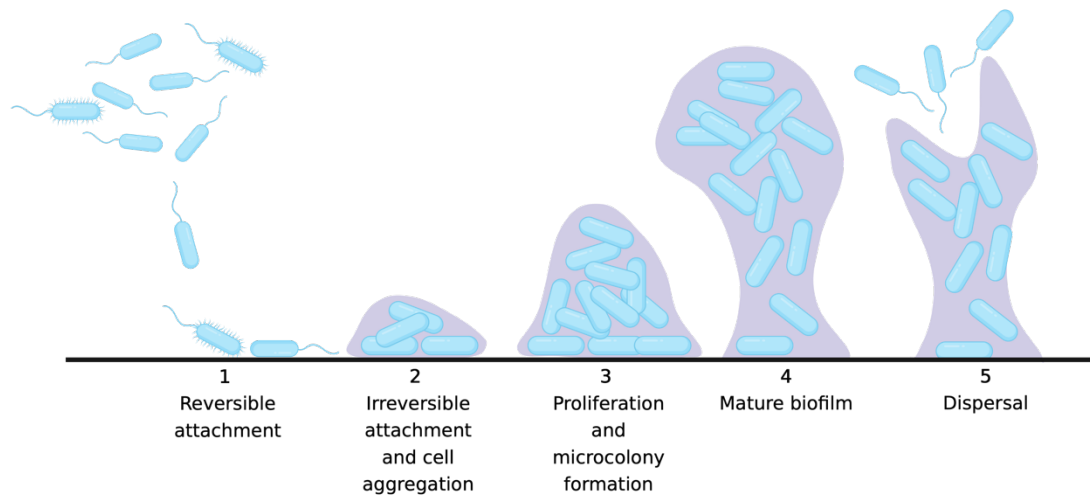


Figure 1.1. Stages of biofilm formation. Diagram shows attachment, cell-cell adhesion, growth and maturation of the biofilm. *P. aeruginosa* is coloured blue and the EPS is coloured purple. Created in biorender.com

Virulence factor production is often an energetically costly process that is more effective with community involvement, therefore biosynthesis of virulence factors and the motility-sessility switch is often under the control of quorum sensing systems (Moradali *et al.*, 2017).

1.6 Global Gene Regulation via Quorum Sensing Systems

P. aeruginosa has a relatively large genome size of 6.3 Mbp, in comparison, *E. coli* has a genome of 4.6 Mbp (Stover *et al.*, 2000). With such a large genome, *P. aeruginosa* must keep tight control over its gene expression to remain competitive. As such, there are many regulatory proteins that allow it to be so metabolically versatile and survive in such a wide range of different environmental niches (Pang *et al.*, 2019). Over 60 two-component regulatory systems are utilised by *P. aeruginosa* (Rodrigue *et al.*, 2000). These typically consist of a transmembrane sensor kinase able to respond to one, or more than one stimuli,

and a response regulator. The sensor kinase autophosphorylates in response to stimuli, the phosphoryl group is then transferred to the response regulator. The phosphorylated response regulator then activates expression of a number of genes required for the appropriate response to the stimulus. Two-component systems allow rapid adaptation to changes in the environment and are involved in many physiological processes including chemotaxis, iron acquisition, pili production, adhesion, rhamnolipid and virulence factor production (Rodrigue *et al.*, 2000). Over 20 transcription factors (TFs) have been identified that are involved in virulence alone, with 347 directly targeted genes and thousands of others whose expression changed following TF deletion (Huang *et al.*, 2019).

Quorum sensing is the term for cooperative behavioural patterns seen in bacterial communities. Quorum sensing is a chemical messaging system employed by bacteria for intercellular communication, enabling bacterial populations to collectively alter their gene regulation and subsequently their behaviour in a cell density-dependent manner and was first described in *P. aeruginosa* in 1995 (Latifi *et al.*, 1995; Winson *et al.*, 1995). Quorum sensing coordinates collective responses and is therefore beneficial for survival of the population.

Quorum sensing signalling molecules (QSSMs) are produced by dedicated synthases and those synthesised by *P. aeruginosa* diffuse freely into and out of bacterial cells (Lee and Zhang, 2014). As the bacterial population grows, QSSMs accumulate in the extracellular space, making an excellent indicator of cell density. Once the threshold concentration of QSSMs is reached, they bind to specific receptors and induce a conformational change. The receptors are regulators of transcription and the receptor-signal complex goes on to affect expression of quorum sensing-controlled genes. Over 10% of *P. aeruginosa* genes are directly regulated by quorum sensing as simultaneous expression changes of these genes within a community of bacteria is the most beneficial to survival (Lee and Zhang, 2014). For example, concerted production of virulence factors is metabolically

costly and should only occur when population is large enough to overcome the host. QS-controlled genes include those associated with stress response, altering the metabolic flux through various pathways, motility, lifestyle change to sessility, biofilm formation, production of virulence determinants and antibiotic resistance (Venturi, 2006; Williams and Cámara, 2009; Lee and Zhang, 2014).

P. aeruginosa utilises three hierarchical interlinked quorum sensing systems (*las*, *rhl* and *pqs*) for population-dependent coordination of an overlapping subset of genes (Latifi *et al.*, 1995; Ochsner and Reiser, 1995; Pesci *et al.*, 1999). The *las* and *rhl* systems are LuxI/LuxR type systems, where the LuxI-type enzyme synthesises *N*-acyl-homoserine lactones (AHLs) signal molecule and a LuxR-type transcription factor (LasR and RhlR in *P. aeruginosa*) binds to the autoinducer, enabling transcriptional activation of the autoinducer biosynthesis genes *lasI* and *rhlI* respectively (Fuqua *et al.*, 1994; Bassler, 1999). The elements of the third QS system, the *pqs* system, are described in the next sections. Each QS system produces its own autoinducer which binds to the regulatory factors LasR, RhlR and PqsR respectively to induce expression of their biosynthetic operon (Brint and Ohman, 1995; Ochsner and Reiser, 1995; Cao *et al.*, 2001; Huang *et al.*, 2019). The autoinducer for *las* QS is *N*-(3-oxododecanoyl)-L-homoserine lactone, commonly abbreviated as 3-oxo-C12-HSL (Pearson *et al.*, 1994). The RhlI synthase produces *N*-butanoyl-L-homoserine lactone (C4-HSL) (Winson *et al.*, 1995).

There is considerable interplay and crosstalk between the quorum sensing systems. PqsR can induce expression of *rhlI*, and the regulator LasR activates *pqsR* and *pqsH* whereas RhlR negatively effects *pqsR* and *pqsABCDE/phnAB* transcription as shown in **Figure 1.2** (McKnight *et al.*, 2000; Wade *et al.*, 2005; Dubern and Diggle, 2008). Antagonistic interplay of *pqsR* expression through LasR and RhlR is mediated by the ratio of their coinducers 3-oxo-C12-HSL and C4-HSL (Stanley *et al.*, 2001). Many virulence factors are often under the control of more than one of these QS systems, including pyocyanin and rhamnolipid biosynthesis, biofilm

formation, motility and elastase production (Pesci *et al.*, 1999; Köhler *et al.*, 2000; Diggle *et al.*, 2003; Diggle *et al.*, 2007).

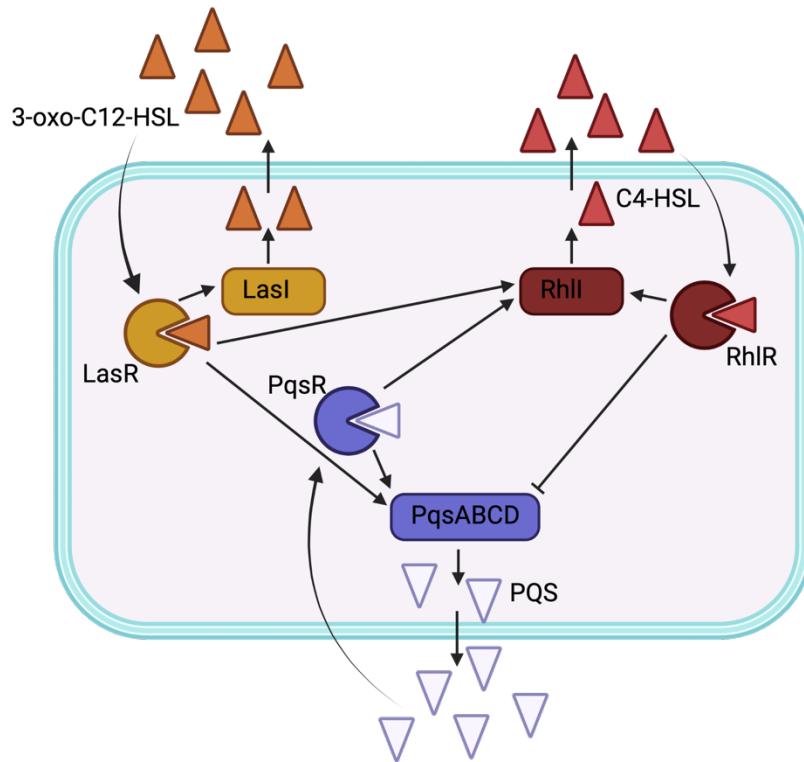


Figure 1.2. Schematic overview of the three quorum sensing regulatory networks in *P. aeruginosa*. The AHLs 3-oxo-C12-HSL and C4-HSL are synthesised by LasI and RhIR respectively. PQS is synthesised by the products of the *pqsABCD* operon and *pqsH*. Created in BioRender.com.

PQS-dependent quorum sensing

The *pqs* quorum sensing system relies upon 2-alkyl-4-quinolones (AQs) as the cognate QSSMs, of which over 56 are produced by the cell (Pesci *et al.*, 1999; Lépine *et al.*, 2004). The two major AQs used as autoinducers are the *Pseudomonas* quinolone signal (PQS), 2-heptyl-3-hydroxy-4-quinolone, and its precursor HHQ, 2-heptyl-4-hydroxyquinoline (Pesci *et al.*, 1999; Déziel *et al.*, 2004). Both PQS and HHQ are able to bind PqsR and induce expression of the *pqsABCDE/phnAB* operon, although HHQ is 100-fold less effective as a coinducer (Wade *et al.*, 2005; Xiao, Déziel, *et al.*, 2006).

PQS is solubilised using the rhamnolipid biosurfactants which increases PQS activity (Calfee *et al.*, 2005). Due to its low solubility in aqueous solution, it is generally considered that PQS is trafficked between cells while packaged in outer membrane vesicles (OMVs) (Florez *et al.*, 2017).

AQ biosynthesis

Anthranilate is used by the cell as the precursor for PQS biosynthesis and is one of two substrates for the first gene product in the PQS biosynthetic operon, PqsA. The products of the PQS biosynthetic operon *pqsABCD* along with PqsE synthesise HHQ, which is then used as a substrate for the monooxygenase PqsH to create PQS (Gallagher *et al.*, 2002; Dubern and Diggle, 2008; Soh *et al.*, 2021). Another monooxygenase, PqsL, is required to produce AQ *N*-oxides such as 2-hydroxy-2-heptylquinoline-*N*-oxide (HQNO) (Lépine *et al.*, 2004).

The PqsA substrate, anthranilate, is a core metabolite also used for tryptophan biosynthesis, and can be degraded and fed into the TCA cycle for energy production. Anthranilate is supplied via two pathways – the conversion of chorismate to anthranilate by anthranilate synthase and through tryptophan degradation within the kynurenine pathway (Farrow and Pesci, 2007a). There are two anthranilate synthases in *P. aeruginosa*, TrpEG and PhnAB (Essar, Eberly, Hadero, *et al.*, 1990). PqsR/PQS-regulated genes encoding the large and small subunits of anthranilate synthase are *phnA* and *phnB* respectively; they are located adjacent to *pqsABCDE* and are expressed together as an operon (Rampioni *et al.*, 2016). Their transcription is positively regulated by PqsR (Farrow and Pesci, 2007a). The KynA, KynB and KynU enzymes of the kynurenine pathway is used to supply anthranilate for PQS biosynthesis during growth in rich medium, and the *phnAB* genes are used in minimal medium (Farrow and Pesci, 2007a).

1.7 Protein Translocation via the Twin Arginine Translocation (Tat) Pathway

Overview of the Tat pathway

The Tat system can be found throughout the microbial community and in the thylakoid membranes of chloroplasts (Berks, 2015). There is a high degree of variability in its use (Lee *et al.*, 2006). The Tat pathway is so named because of the invariant arginine dipeptide found in the signal peptides required for targeting substrates to the Tat translocon. Signal peptides commonly have 3 domains, a positively charged N-terminal region, a core hydrophobic or H-region, and a polar C-terminal region. Signal peptides targeting the Tat system have the consensus sequence Ser/Thr-**Arg-Arg**-X-Phe-Leu-Lys (Palmer and Stansfeld, 2020). The Tat protein translocation pathway is the only system that transports fully folded proteins from the cytoplasm to the periplasm, providing a route out of the cell for proteins that require a ligand/ cofactor insertion or multiprotein assembly in the cytoplasm. In the case of heteromeric proteins only one subunit is required to carry a Tat signal peptide for translocation (Urs a Ochsner *et al.*, 2002). Tat translocation is not an essential process in *P. aeruginosa* (Soh *et al.*, 2021).

In *P. aeruginosa* there are three integral membrane proteins that make up the Tat system: TatA, TatB, and TatC. These are encoded on a 6-gene operon between the genes for two proteins involved in histidine biosynthesis (HisI and HisE) and a hypothetical protein (PA5071) which may be involved in rRNA processing (Stover *et al.*, 2000; Voulhoux *et al.*, 2001). There is an *E. coli* TatD gene homologue encoded elsewhere on the genome but this is not thought to be required for Tat activity (Voulhoux *et al.*, 2001).

Tat system assembly and function

The Tat system is composed of TatA family and TatC family proteins. TatA monomers embed into the cytoplasmic face of the inner membrane with a single helix at their N-terminus (Palmer and Stansfeld, 2020). In *P. aeruginosa* two functionally distinct TatA family proteins exist, TatA and TatB (Sargent *et al.*, 1999; Palmer and Stansfeld, 2020). Their transmembrane helix is considered short, it barely spans the width of the membrane (Rodriguez *et al.*, 2013; Zhang *et al.*, 2014). TatC, in comparison, comprises 6 transmembrane helices and a “cap” protruding out into the periplasm (Ramasamy *et al.*, 2013). Of the 6 helices, the final two are similar in length to that of TatA and TatB. Together they create a thinner membrane at this point (Rollauer *et al.*, 2012; Ramasamy *et al.*, 2013).

Many theories as to the mechanism of assembly have existed over the years, but the current model is assembly upon binding substrate signal peptide, followed by disassembly when no longer in use (Palmer and Stansfeld, 2020). The Tat pathway cycles from resting state, to initiation of transport, reorganisation of the receptor complex to form a mature complex, substrate translocation, and complex disassembly to return to resting state (**Figure 1.3**).

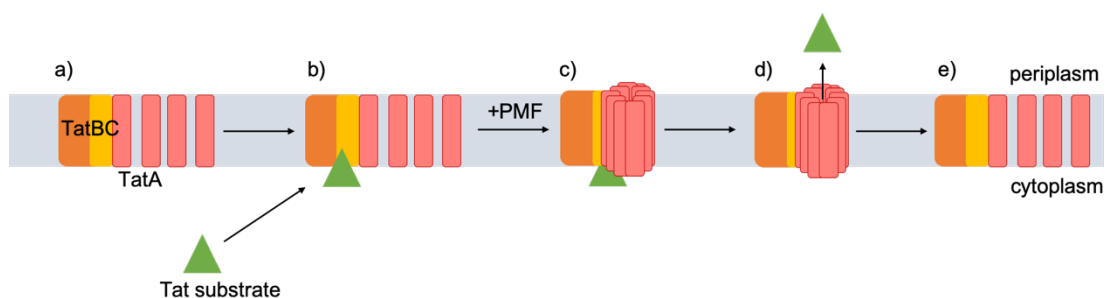


Figure 1.3. Cycling of Tat pathway assembly, translocation and disassembly. Each step is outlined in more detail below. Briefly, the components exist in a resting state as TatBCA and TatA pool (a), upon interaction with substrate PMF-dependent recruitment and assembly of TataA monomers begins (b,c). Following translocation to the periplasm the Tat system disassembles and returns to resting state (d,e).

In its resting state, the Tat system comprises of 3 to 4 copies each of TatA, TatB and TatC monomers in equal proportions (Alcock *et al.*, 2016; Palmer and Stansfeld, 2020). The initiation of transport primes the TatABC receptor complex for proton motive force (PMF)-dependent recruitment and oligomerisation of TatA from a TatA oligomer pool within the membrane (Berks, 2015). Binding of the Tat substrate signal peptide is thought to be the first step, and the twin arginine residues are recognised by a conserved region on TatC at the cytoplasmic face. Following initial binding, the signal peptide changes to a hairpin conformation to bind further into the complex (Hamsanathan *et al.*, 2017). The hydrophobic region of the signal peptide interacts with TatB, creating the hairpin conformation. This structural change stimulates a reorganisation and TatB is replaced by TatC, then TatA occupies the vacated binding site (Palmer and Stansfeld, 2020). TatB is thought to associate with TatC helix 6 in place of TatA, so effectively the two monomers have swapped their binding sites. In this activated state, PMF-dependent TatA recruitment begins (Berks, 2015).

Due to the lack of structural information, it is unclear if TatA oligomerisation forms a pore of fixed size, or if the size varies depending on the substrate. There are two hypotheses as to the mechanism of substrate translocation, either enough TatA monomers assemble to form a channel to fit the exact size of the substrate, or the influx of short transmembrane helices of TatA, TatB and TatC are able to weaken the bilayer for transient disruption that is enough to make it kinetically possible for a large 3D structure to cross in one direction to the periplasm (Palmer and Stansfeld, 2020). Following translocation, the signal peptide is cleaved and the pore dissociates and returns to resting state receptor complex.

Effectors translocated via the Tat pathway may remain in the periplasm, insert into the inner membrane or go on to be secreted by the type II secretion system (T2SS). Gram-negative bacteria have a number of different protein

secretion systems which export a variety of effector proteins of different functions into the extracellular milieu, or directly into eukaryotic and prokaryotic cells (Filloux, 2011). The major pathway for T2SS is the Xcp general secretory pathway encoded by an 11 gene cluster, *xcPQRSTUVWXYZ*, and *xcpA/pilD* found elsewhere on the genome (Bally *et al.*, 1991; Nunn and Lory, 1991; Stover *et al.*, 2000; Filloux, 2004). It is unclear how substrates are targeted to the Xcp/secretin module for export in *P. aeruginosa* (Filloux, 2011).

Tat signal peptides

Substrates targeted for export via the Tat pathway carry a tripartite Tat signal peptide which consists of a positively charged N-terminal region, an often helical hydrophobic centre consisting of at least 12 amino acids and a polar C-region (Gimenez *et al.*, 2018; Palmer and Stansfeld, 2020). The N-terminal region contains two conserved arginine residues which form part of a SRRxFLK motif, giving the name "twin-arginine" translocation pathway. Both arginine residues are considered essential for effective translocation, however the other residues in the motif are only semi-conserved and not essential for protein transport. The structure ends in a cleavage site for signal peptidases (Dalbey and Wickner, 1985; Lüke *et al.*, 2009). A basic amino acid is frequently found in the C-region and instead of aiding Tat recognition and transport, it is thought to function as a Sec-avoidance motif as the positive charge prevents recognition by the Sec machinery due to high similarity of both signal peptides (Bogsch *et al.*, 1997; Gimenez *et al.*, 2018).

Depending on the bacterium, different types/numbers of proteins are exported via the Tat system. Some only have a few exported by this route, whereas others rely upon the system far more (Ball *et al.*, 2016). There are 34 known substrates of the Tat system in *P. aeruginosa* (Ball *et al.*, 2016). Many of these are important virulence factors involved in biofilm formation, cell survival and adaptation (Lee *et al.*, 2006). For example, the Tat system is required for the export

of phospholipases, proteins involved in anaerobic respiration, motility, responding to osmotic stress, and pyoverdinin-mediated iron uptake (Ochsner *et al.*, 2002). The full list of Tat system substrates is covered in Chapter 4.

Implications of *P. aeruginosa* Tat system in virulence

A *P. aeruginosa* *tat* mutant was avirulent in a rat pulmonary infection model, and transposon insertion into *tat* genes resulted in reduced eDNA release, lower rhamnolipid and microvesicle production, perturbed PQS biosynthesis, and formation of thin, flat biofilms (Ochsner *et al.*, 2002; Soh *et al.*, 2021). This will be covered in extensive detail in Chapter 3 and Chapter 4.

In addition, the Tat pathway exports a number of virulence factors involved in anaerobic respiration, motility, response to osmotic stress, pyoverdinin-dependent iron acquisition and phospholipases. As such, the Tat system would be an excellent target for development of novel inhibitors for antivirulence therapies due to its role in virulence.

1.8 Aims of This Study

PQS-dependent quorum sensing is perturbed in *tat* system transposon mutants, expression of the biosynthesis operon is greatly down-regulated, and there are pleiotropic phenotypic changes including decreased eDNA release, flat biofilms, and decreased rhamnolipid and microvesicle production (Soh *et al.*, 2021). It is possible that one or more of the proteins transported by the Tat system could also be involved with PQS-dependent quorum sensing, thus providing a link between deletion of the Tat system and perturbation of PQS quorum sensing.

Aims:

- Study the effects of Tat deletion at a transcriptional level with RNAseq analysis and transcriptional bioreporters to identify expression changes that may cause perturbed PQS quorum sensing.
- Test proteins translocated by Tat system for their relation to *pqs* QS.
- Screen structural analogues of a known Tat inhibitor to determine structure-activity relationship and improve potency of Tat inhibition.

Chapter 2: Materials and Methods

2.1 Bacterial growth media and culture conditions

Unless indicated otherwise all strains were grown in liquid lysogeny broth (LB) or grown on LB agar plates at 37°C. Liquid cultures were shaken at 250 rpm. LB was composed of 10 g/L tryptone, 10 g/L NaCl and 5 g/L yeast extract. For growth on agar plates, bacteriological agar was added to the LB at a concentration of 15 g/L. When required, the following antibiotics were added: Nalidixic Acid (Nal) at 15 µg/mL; tetracycline (Tc) at 150 µg/mL for use with *P. aeruginosa*, 15 µg/mL for *E. coli*; and gentamicin (Gm) at 10 µg/mL.

M9 minimal medium was prepared so that 1 litre contained 200 mL M9 5X salt solution, 2 mL 1 M MgSO₄, 20 mL 1 M succinate, 100 µl of 1M CaCl₂, and 50 mL 10% casamino acids dissolved in dH₂O and the pH was adjusted to 7.2. Succinate was added immediately prior to inoculation, and casamino acids were not included in biofilm experiments.

Congo red plates were used to show colony morphology as described by Mayer-Hamblett *et al.* (2014). Briefly, 10 g agar, 1 g of yeast and 1 g of casamino acids were dissolved in 850 mL of distilled H₂O and autoclaved. Once cooled, 100 mL of 10X M63 salts, 2.5 mL 1 M MgCl₂, 1 mL of 0.1 M (NH₄)₂Fe(SO₄)₂·6H₂O, 1 mL 40 mg/mL Congo Red, 1 M CaCl₂, and 50 mL 1 M glucose. The final agar concentration is 1% (Mayer-Hamblett *et al.*, 2014).

Storage of Bacterial Strains

Following overnight growth in 5 mL LB broth containing any necessary selective antibiotics, 750 µl of culture was added to 750 µl 50% (v/v) glycerol in sterile cryotubes (Starstedt) and stored at -80°C.

2.2 Bacterial strains and plasmids

The following bacterial strains and plasmids were used during this study:

Strain	Description	Reference
<i>E. coli</i>		
<i>E. coli</i> S17-1 λ pir	Conjugative strain	(Simon <i>et al.</i> , 1983)
<i>E. coli</i> NEB [®] 5 α	For high-efficiency electrocompetent transformation. Derivative of DH5 α [™] . Catalog number C2989K. T1 phage resistant and <i>endA</i> deficient. <i>fhuA2</i> Δ (<i>argF-lacZ</i>)U169 <i>phoA</i> <i>glnV44</i> Φ 80 Δ (<i>lacZ</i>)M15 <i>gyrA96</i> <i>recA1</i> <i>relA1</i> <i>endA1</i> <i>thi-1</i> <i>hsdR17</i> .	New England Biolabs
<i>P. aeruginosa</i>		
PAO1-DK	Denmark subline	(Soh <i>et al.</i> , 2021)
PAO1-DK <i>tatA</i> ::Tn5	Tn5 transposon insertion in <i>tatA</i> gene	(Soh <i>et al.</i> , 2021)
PAO1-DK Δ <i>pqsA</i>	deleted <i>pqsA</i> gene, unable to synthesise AQs	(Soh <i>et al.</i> , 2021)
PAO1-DK Δ <i>pqsA</i> <i>tatA</i> ::Tn5	deleted <i>pqsA</i> gene and Tn5 transposon insertion in <i>tatA</i> gene	(Soh <i>et al.</i> , 2021)
PAO1-DK Δ <i>tatABC</i>	deleted <i>tatABC</i> genes	(Soh <i>et al.</i> , 2021)
PAO1-DK Δ <i>antA</i>	deleted <i>antA</i> gene, unable to degrade anthranilate	This study
PAO1-DK Δ <i>tatABC</i> Δ <i>antA</i>	deleted <i>tatABC</i> and <i>antA</i> genes	This study
PAO1-DK Δ <i>pqsA</i> Δ <i>antA</i>	deleted <i>pqsA</i> and <i>antA</i> gene	This study
PAO1-DK miniCTX:: <i>'antA-lux</i>	Denmark subline of PAO1 carrying transcriptional reporter for <i>antA</i>	This study
PAO1-DK miniCTX:: <i>'antR-lux</i>	Denmark subline of PAO1 carrying transcriptional reporter for <i>antR</i>	This study
PAO1-DK miniCTX:: <i>'catB-lux</i>	Denmark subline of PAO1 carrying transcriptional reporter for <i>catB</i>	This study
PAO1-DK miniCTX:: <i>'catR-lux</i>	Denmark subline of PAO1 carrying transcriptional reporter for <i>catR</i>	This study
PAO1-DK miniCTX:: <i>'pqsA-lux</i>	Denmark subline of PAO1 carrying transcriptional reporter for <i>pqsA</i>	This study
PAO1-DK miniCTX:: <i>'hisI-lux</i>	Denmark subline of PAO1 carrying transcriptional reporter for <i>hisI</i>	This study
PAO1-DK <i>tatA</i> ::Tn5 miniCTX:: <i>'antA-lux</i>	Tn5 transposon insertion in <i>tatA</i> gene, carrying transcriptional reporter for <i>antA</i>	This study
PAO1-DK <i>tatA</i> ::Tn5 miniCTX:: <i>'antR-lux</i>	Tn5 transposon insertion in <i>tatA</i> gene, carrying transcriptional reporter for <i>antR</i>	This study
PAO1-DK <i>tatA</i> ::Tn5 miniCTX:: <i>'catB-lux</i>	Tn5 transposon insertion in <i>tatA</i> gene, carrying transcriptional reporter for <i>catB</i>	This study

PAO1-DK <i>tatA</i> ::Tn5 miniCTX:: <i>catR-lux</i>	Tn5 transposon insertion in <i>tatA</i> gene, carrying transcriptional reporter for <i>catR</i>	This study
PAO1-DK <i>tatA</i> ::Tn5 miniCTX:: <i>pqsA-lux</i>	Tn5 transposon insertion in <i>tatA</i> gene, carrying transcriptional reporter for <i>pqsA</i>	This study
PAO1-DK <i>tatA</i> ::Tn5 miniCTX:: <i>hisI-lux</i>	Tn5 transposon insertion in <i>tatA</i> gene, carrying transcriptional reporter for <i>hisI</i>	This study
PAO1-DK $\Delta pqsA$ miniCTX:: <i>antA-lux</i>	deleted <i>pqsA</i> gene, unable to synthesise AQs, carrying transcriptional reporter for <i>antA</i>	This study
PAO1-DK $\Delta pqsA$ miniCTX:: <i>antR-lux</i>	deleted <i>pqsA</i> gene, unable to synthesise AQs, carrying transcriptional reporter for <i>antR</i>	This study
PAO1-DK $\Delta pqsA$ miniCTX:: <i>catB-lux</i>	deleted <i>pqsA</i> gene, unable to synthesise AQs, carrying transcriptional reporter for <i>catB</i>	This study
PAO1-DK $\Delta pqsA$ miniCTX:: <i>catR-lux</i>	deleted <i>pqsA</i> gene, unable to synthesise AQs, carrying transcriptional reporter for <i>catR</i>	This study
PAO1-DK $\Delta pqsA$ miniCTX:: <i>hisI-lux</i>	deleted <i>pqsA</i> gene, unable to synthesise AQs, carrying transcriptional reporter for <i>hisI</i>	This study
PAO1-DK $\Delta pqsA$ <i>tatA</i> ::Tn5 miniCTX:: <i>antA-lux</i>	deleted <i>pqsA</i> gene and Tn5 transposon insertion in <i>tatA</i> gene carrying transcriptional reporter for <i>antA</i>	This study
PAO1-DK $\Delta pqsA$ <i>tatA</i> ::Tn5 miniCTX:: <i>antR-lux</i>	deleted <i>pqsA</i> gene and Tn5 transposon insertion in <i>tatA</i> gene carrying transcriptional reporter for <i>antR</i>	This study
PAO1-DK $\Delta pqsA$ <i>tatA</i> ::Tn5 miniCTX:: <i>catB-lux</i>	deleted <i>pqsA</i> gene and Tn5 transposon insertion in <i>tatA</i> gene carrying transcriptional reporter for <i>catB</i>	This study
PAO1-DK $\Delta pqsA$ <i>tatA</i> ::Tn5 miniCTX:: <i>catR-lux</i>	deleted <i>pqsA</i> gene and Tn5 transposon insertion in <i>tatA</i> gene carrying transcriptional reporter for <i>catR</i>	This study
PAO1-DK $\Delta pqsA$ <i>tatA</i> ::Tn5 miniCTX:: <i>hisI-lux</i>	deleted <i>pqsA</i> gene and Tn5 transposon insertion in <i>tatA</i> gene carrying transcriptional reporter for <i>hisI</i>	This study
PAO1-DK $\Delta tatABC$ miniCTX:: <i>antA-lux</i>	deleted <i>tatABC</i> genes carrying transcriptional reporter for <i>antA</i>	This study
PAO1-DK $\Delta tatABC$ miniCTX:: <i>antR-lux</i>	deleted <i>tatABC</i> genes carrying transcriptional reporter for <i>antR</i>	This study
PAO1-DK $\Delta tatABC$ miniCTX:: <i>catB-lux</i>	deleted <i>tatABC</i> genes carrying transcriptional reporter for <i>catB</i>	This study
PAO1-DK $\Delta tatABC$ miniCTX:: <i>catR-lux</i>	deleted <i>tatABC</i> genes carrying transcriptional reporter for <i>catR</i>	This study
PAO1-DK $\Delta tatABC$ miniCTX:: <i>hisI-lux</i>	deleted <i>tatABC</i> genes carrying transcriptional reporter for <i>hisI</i>	This study
PAO1-DK $\Delta antA$ miniCTX:: <i>antA-lux</i>	deleted <i>antA</i> gene carrying transcriptional reporter for <i>antA</i>	This study

PAO1-DK $\Delta antA$ miniCTX:: <i>'antR-lux</i>	deleted <i>antA</i> gene carrying transcriptional reporter for <i>antR</i>	This study
PAO1-DK $\Delta antA$ miniCTX:: <i>'catB-lux</i>	deleted <i>antA</i> gene carrying transcriptional reporter for <i>catB</i>	This study
PAO1-DK $\Delta antA$ miniCTX:: <i>'catR-lux</i>	deleted <i>antA</i> gene carrying transcriptional reporter for <i>catR</i>	This study
PAO1-DK $\Delta antA$ miniCTX:: <i>'pqsA-lux</i>	deleted <i>antA</i> gene carrying transcriptional reporter for <i>pqsA</i>	This study
PAO1-DK $\Delta tatABC$ $\Delta antA$ miniCTX:: <i>'antA-lux</i>	deleted <i>antA</i> and <i>tatABC</i> genes carrying transcriptional reporter for <i>antA</i>	This study
PAO1-DK $\Delta tatABC$ $\Delta antA$ miniCTX:: <i>'antR-lux</i>	deleted <i>antA</i> and <i>tatABC</i> genes carrying transcriptional reporter for <i>antR</i>	This study
PAO1-DK $\Delta tatABC$ $\Delta antA$ miniCTX:: <i>'catB-lux</i>	deleted <i>antA</i> and <i>tatABC</i> genes carrying transcriptional reporter for <i>catB</i>	This study
PAO1-DK $\Delta tatABC$ $\Delta antA$ miniCTX:: <i>'catR-lux</i>	deleted <i>antA</i> and <i>tatABC</i> genes carrying transcriptional reporter for <i>catR</i>	This study
PAO1-DK $\Delta tatABC$ $\Delta antA$ miniCTX:: <i>'pqsA-lux</i>	deleted <i>antA</i> and <i>tatABC</i> genes carrying transcriptional reporter for <i>pqsA</i>	This study
PAO1-DK $\Delta pqsA$ $\Delta antA$ miniCTX:: <i>'antA-lux</i>	deleted <i>antA</i> and <i>pqsA</i> genes carrying transcriptional reporter for <i>antA</i>	This study
PAO1-DK $\Delta pqsA$ $\Delta antA$ miniCTX:: <i>'antR-lux</i>	deleted <i>antA</i> and <i>pqsA</i> genes carrying transcriptional reporter for <i>antR</i>	This study
PAO1-DK $\Delta pqsA$ $\Delta antA$ miniCTX:: <i>'catB-lux</i>	deleted <i>antA</i> and <i>pqsA</i> genes carrying transcriptional reporter for <i>catB</i>	This study
PAO1-DK $\Delta pqsA$ $\Delta antA$ miniCTX:: <i>'catR-lux</i>	deleted <i>antA</i> and <i>pqsA</i> genes carrying transcriptional reporter for <i>catR</i>	This study
PAO1-DK $\Delta pqsA$ $\Delta antA$ miniCTX:: <i>'pqsA-lux</i>	deleted <i>antA</i> and <i>pqsA</i> genes carrying transcriptional reporter for <i>pqsA</i>	This study
PAO1-W $\Delta phzA1-G1$ $\Delta phzA2-G2$	Deleted phenazine biosynthetic operons, unable to make pyocyanin	(Recinos <i>et al.</i> , 2012)
PAO1-N $\Delta pvdD$	Unable to make pyoverdine	Mark Perkins, University of Nottingham
PAO1-N $\Delta pchEF$	Unable to make pyochelin	Mark Perkins, University of Nottingham
PAO1-N $\Delta pvdD$ $\Delta pchEF$	Unable to make pyoverdine and pyochelin	Mark Perkins, University of Nottingham
PA14	Common laboratory strain	(Kukavica-Ibrulj <i>et al.</i> , 2008)
PA14 $\Delta tatABC$	Knockout of <i>tatABC</i> genes	Kindly donated by Berengere Ize (Ball <i>et al.</i> , 2016)
PA14 $\Delta PA0144$	Deletion mutant of a substrate of the Tat secretion system	(Gimenez <i>et al.</i> , 2018)

PA14 Δ PA4812	Deletion mutant of a substrate of the Tat secretion system	Gimenez <i>et al.</i> , 2018)
PA14 Δ PA4858	Deletion mutant of a substrate of the Tat secretion system	Gimenez <i>et al.</i> , 2018)
PA14 Δ PA5327	Deletion mutant of a substrate of the Tat secretion system	Gimenez <i>et al.</i> , 2018)
PA14 Δ PA5538	Deletion mutant of a substrate of the Tat secretion system	Gimenez <i>et al.</i> , 2018)
PA14 Δ PA14_48450	Deletion mutant of a substrate of the Tat secretion system	Gimenez <i>et al.</i> , 2018)
PA14 miniCTX:: <i>pqsA-lux</i>	PA14 wild-type strain carrying <i>pqsA</i> transcriptional reporter	This study
PA14 Δ tatABC miniCTX:: <i>pqsA-lux</i>	Deleted <i>tatABC</i> genes carrying <i>pqsA</i> transcriptional reporter	This study
PA14 Δ PA0144 miniCTX:: <i>pqsA-lux</i>	Deletion mutant of a substrate of the Tat secretion system carrying <i>pqsA</i> transcriptional reporter	This study
PA14 Δ PA0365 miniCTX:: <i>pqsA-lux</i>	Deletion mutant of a substrate of the Tat secretion system carrying <i>pqsA</i> transcriptional reporter	This study
PA14 Δ PA0735 miniCTX:: <i>pqsA-lux</i>	Deletion mutant of a substrate of the Tat secretion system carrying <i>pqsA</i> transcriptional reporter	This study
PA14 Δ PA0844 miniCTX:: <i>pqsA-lux</i>	Deletion mutant of a substrate of the Tat secretion system carrying <i>pqsA</i> transcriptional reporter	This study
PA14 Δ PA1174 miniCTX:: <i>pqsA-lux</i>	Deletion mutant of a substrate of the Tat secretion system carrying <i>pqsA</i> transcriptional reporter	This study
PA14 Δ PA1601 miniCTX:: <i>pqsA-lux</i>	Deletion mutant of a substrate of the Tat secretion system carrying <i>pqsA</i> transcriptional reporter	This study
PA14 Δ PA1880 miniCTX:: <i>pqsA-lux</i>	Deletion mutant of a substrate of the Tat secretion system carrying <i>pqsA</i> transcriptional reporter	This study
PA14 Δ PA2065 miniCTX:: <i>pqsA-lux</i>	Deletion mutant of a substrate of the Tat secretion system carrying <i>pqsA</i> transcriptional reporter	This study
PA14 Δ PA2124 miniCTX:: <i>pqsA-lux</i>	Deletion mutant of a substrate of the Tat secretion system carrying <i>pqsA</i> transcriptional reporter	This study
PA14 Δ PA2264 miniCTX:: <i>pqsA-lux</i>	Deletion mutant of a substrate of the Tat secretion system carrying <i>pqsA</i> transcriptional reporter	This study
PA14 Δ PA2328 miniCTX:: <i>pqsA-lux</i>	Deletion mutant of a substrate of the Tat secretion system carrying <i>pqsA</i> transcriptional reporter	This study
PA14 Δ PA2378 miniCTX:: <i>pqsA-lux</i>	Deletion mutant of a substrate of the Tat secretion system carrying <i>pqsA</i> transcriptional reporter	This study
PA14 Δ PA2389 miniCTX:: <i>pqsA-lux</i>	Deletion mutant of a substrate of the Tat secretion system carrying <i>pqsA</i> transcriptional reporter	This study
PA14 Δ PA2392 miniCTX:: <i>pqsA-lux</i>	Deletion mutant of a substrate of the Tat secretion system carrying <i>pqsA</i> transcriptional reporter	This study

PA14 Δ PA2394 miniCTX:: <i>pqsA-lux</i>	Deletion mutant of a substrate of the Tat secretion system carrying <i>pqsA</i> transcriptional reporter	This study
PA14 Δ PA2531 miniCTX:: <i>pqsA-lux</i>	Deletion mutant of a substrate of the Tat secretion system carrying <i>pqsA</i> transcriptional reporter	This study
PA14 Δ PA2635 miniCTX:: <i>pqsA-lux</i>	Deletion mutant of a substrate of the Tat secretion system carrying <i>pqsA</i> transcriptional reporter	This study
PA14 Δ PA2699 miniCTX:: <i>pqsA-lux</i>	Deletion mutant of a substrate of the Tat secretion system carrying <i>pqsA</i> transcriptional reporter	This study
PA14 Δ PA3222 miniCTX:: <i>pqsA-lux</i>	Deletion mutant of a substrate of the Tat secretion system carrying <i>pqsA</i> transcriptional reporter	This study
PA14 Δ PA3319 miniCTX:: <i>pqsA-lux</i>	Deletion mutant of a substrate of the Tat secretion system carrying <i>pqsA</i> transcriptional reporter	This study
PA14 Δ PA3392 miniCTX:: <i>pqsA-lux</i>	Deletion mutant of a substrate of the Tat secretion system carrying <i>pqsA</i> transcriptional reporter	This study
PA14 Δ PA3713 miniCTX:: <i>pqsA-lux</i>	Deletion mutant of a substrate of the Tat secretion system carrying <i>pqsA</i> transcriptional reporter	This study
PA14 Δ PA3768 miniCTX:: <i>pqsA-lux</i>	Deletion mutant of a substrate of the Tat secretion system carrying <i>pqsA</i> transcriptional reporter	This study
PA14 Δ PA3910 miniCTX:: <i>pqsA-lux</i>	Deletion mutant of a substrate of the Tat secretion system carrying <i>pqsA</i> transcriptional reporter	This study
PA14 Δ PA4140 miniCTX:: <i>pqsA-lux</i>	Deletion mutant of a substrate of the Tat secretion system carrying <i>pqsA</i> transcriptional reporter	This study
PA14 Δ PA4159 miniCTX:: <i>pqsA-lux</i>	Deletion mutant of a substrate of the Tat secretion system carrying <i>pqsA</i> transcriptional reporter	This study
PA14 Δ PA4431 miniCTX:: <i>pqsA-lux</i>	Deletion mutant of a substrate of the Tat secretion system carrying <i>pqsA</i> transcriptional reporter	This study
PA14 Δ PA4621 miniCTX:: <i>pqsA-lux</i>	Deletion mutant of a substrate of the Tat secretion system carrying <i>pqsA</i> transcriptional reporter	This study
PA14 Δ PA4692 miniCTX:: <i>pqsA-lux</i>	Deletion mutant of a substrate of the Tat secretion system carrying <i>pqsA</i> transcriptional reporter	This study
PA14 Δ PA4812 miniCTX:: <i>pqsA-lux</i>	Deletion mutant of a substrate of the Tat secretion system carrying <i>pqsA</i> transcriptional reporter	This study
PA14 Δ PA4858 miniCTX:: <i>pqsA-lux</i>	Deletion mutant of a substrate of the Tat secretion system carrying <i>pqsA</i> transcriptional reporter	This study
PA14 Δ PA5327 miniCTX:: <i>pqsA-lux</i>	Deletion mutant of a substrate of the Tat secretion system carrying <i>pqsA</i> transcriptional reporter	This study

PA14 Δ PA5538 miniCTX:: <i>pqsA-lux</i>	Deletion mutant of a substrate of the Tat secretion system carrying <i>pqsA</i> transcriptional reporter	This study
PA14 Δ PA14_48450 miniCTX:: <i>pqsA-lux</i>	Deletion mutant of a substrate of the Tat secretion system carrying <i>pqsA</i> transcriptional reporter	This study
PA14 miniCTX:: <i>antA-lux</i>	PA14 wild-type strain carrying <i>antA</i> transcriptional reporter	This study
PA14 miniCTX:: <i>antR-lux</i>	PA14 wild-type strain carrying <i>antR</i> transcriptional reporter	This study
PA14 miniCTX:: <i>catB-lux</i>	PA14 wild-type strain carrying <i>catB</i> transcriptional reporter	This study
PA14 miniCTX:: <i>catR-lux</i>	PA14 wild-type strain carrying <i>catR</i> transcriptional reporter	This study
PA14 miniCTX:: <i>pqsA-lux</i>	PA14 wild-type strain carrying <i>pqsA</i> transcriptional reporter	This study
PA14 Δ tatABC miniCTX:: <i>antA-lux</i>	Deleted <i>tatABC</i> genes carrying <i>antA</i> transcriptional reporter	This study
PA14 Δ tatABC miniCTX:: <i>antR-lux</i>	Deleted <i>tatABC</i> genes carrying <i>antR</i> transcriptional reporter	This study
PA14 Δ tatABC miniCTX:: <i>catB-lux</i>	Deleted <i>tatABC</i> genes carrying <i>catB</i> transcriptional reporter	This study
PA14 Δ tatABC miniCTX:: <i>catR-lux</i>	Deleted <i>tatABC</i> genes carrying <i>catR</i> transcriptional reporter	This study
PA14 Δ tatABC miniCTX:: <i>pqsA-lux</i>	Deleted <i>tatABC</i> genes carrying <i>pqsA</i> transcriptional reporter	This study
PA14 Δ PA0144 miniCTX:: <i>antA-lux</i>	Deletion mutant of a substrate of the Tat secretion system carrying <i>antA</i> transcriptional reporter	This study
PA14 Δ PA0365 miniCTX:: <i>antA-lux</i>	Deletion mutant of a substrate of the Tat secretion system carrying <i>antA</i> transcriptional reporter	This study
PA14 Δ PA0735 miniCTX:: <i>antA-lux</i>	Deletion mutant of a substrate of the Tat secretion system carrying <i>antA</i> transcriptional reporter	This study
PA14 Δ PA0844 miniCTX:: <i>antA-lux</i>	Deletion mutant of a substrate of the Tat secretion system carrying <i>antA</i> transcriptional reporter	This study
PA14 Δ PA1174 miniCTX:: <i>antA-lux</i>	Deletion mutant of a substrate of the Tat secretion system carrying <i>antA</i> transcriptional reporter	This study
PA14 Δ PA1601 miniCTX:: <i>antA-lux</i>	Deletion mutant of a substrate of the Tat secretion system carrying <i>antA</i> transcriptional reporter	This study
PA14 Δ PA1880 miniCTX:: <i>antA-lux</i>	Deletion mutant of a substrate of the Tat secretion system carrying <i>antA</i> transcriptional reporter	This study
PA14 Δ PA2065 miniCTX:: <i>antA-lux</i>	Deletion mutant of a substrate of the Tat secretion system carrying <i>antA</i> transcriptional reporter	This study
PA14 Δ PA2124 miniCTX:: <i>antA-lux</i>	Deletion mutant of a substrate of the Tat secretion system carrying <i>antA</i> transcriptional reporter	This study
PA14 Δ PA2264 miniCTX:: <i>antA-lux</i>	Deletion mutant of a substrate of the Tat secretion system carrying <i>antA</i> transcriptional reporter	This study

PA14 Δ PA2328 miniCTX:: <i>'antA-lux</i>	Deletion mutant of a substrate of the Tat secretion system carrying <i>antA</i> transcriptional reporter	This study
PA14 Δ PA2378 miniCTX:: <i>'antA-lux</i>	Deletion mutant of a substrate of the Tat secretion system carrying <i>antA</i> transcriptional reporter	This study
PA14 Δ PA2389 miniCTX:: <i>'antA-lux</i>	Deletion mutant of a substrate of the Tat secretion system carrying <i>antA</i> transcriptional reporter	This study
PA14 Δ PA2392 miniCTX:: <i>'antA-lux</i>	Deletion mutant of a substrate of the Tat secretion system carrying <i>antA</i> transcriptional reporter	This study
PA14 Δ PA2394 miniCTX:: <i>'antA-lux</i>	Deletion mutant of a substrate of the Tat secretion system carrying <i>antA</i> transcriptional reporter	This study
PA14 Δ PA2531 miniCTX:: <i>'antA-lux</i>	Deletion mutant of a substrate of the Tat secretion system carrying <i>antA</i> transcriptional reporter	This study
PA14 Δ PA2635 miniCTX:: <i>'antA-lux</i>	Deletion mutant of a substrate of the Tat secretion system carrying <i>antA</i> transcriptional reporter	This study
PA14 Δ PA2699 miniCTX:: <i>'antA-lux</i>	Deletion mutant of a substrate of the Tat secretion system carrying <i>antA</i> transcriptional reporter	This study
PA14 Δ PA3222 miniCTX:: <i>'antA-lux</i>	Deletion mutant of a substrate of the Tat secretion system carrying <i>antA</i> transcriptional reporter	This study
PA14 Δ PA3319 miniCTX:: <i>'antA-lux</i>	Deletion mutant of a substrate of the Tat secretion system carrying <i>antA</i> transcriptional reporter	This study
PA14 Δ PA3392 miniCTX:: <i>'antA-lux</i>	Deletion mutant of a substrate of the Tat secretion system carrying <i>antA</i> transcriptional reporter	This study
PA14 Δ PA3713 miniCTX:: <i>'antA-lux</i>	Deletion mutant of a substrate of the Tat secretion system carrying <i>antA</i> transcriptional reporter	This study
PA14 Δ PA3768 miniCTX:: <i>'antA-lux</i>	Deletion mutant of a substrate of the Tat secretion system carrying <i>antA</i> transcriptional reporter	This study
PA14 Δ PA3910 miniCTX:: <i>'antA-lux</i>	Deletion mutant of a substrate of the Tat secretion system carrying <i>antA</i> transcriptional reporter	This study
PA14 Δ PA4140 miniCTX:: <i>'antA-lux</i>	Deletion mutant of a substrate of the Tat secretion system carrying <i>antA</i> transcriptional reporter	This study
PA14 Δ PA4159 miniCTX:: <i>'antA-lux</i>	Deletion mutant of a substrate of the Tat secretion system carrying <i>antA</i> transcriptional reporter	This study
PA14 Δ PA4431 miniCTX:: <i>'antA-lux</i>	Deletion mutant of a substrate of the Tat secretion system carrying <i>antA</i> transcriptional reporter	This study
PA14 Δ PA4621 miniCTX:: <i>'antA-lux</i>	Deletion mutant of a substrate of the Tat secretion system carrying <i>antA</i> transcriptional reporter	This study

PA14 Δ PA4692 miniCTX:: <i>'antA-lux</i>	Deletion mutant of a substrate of the Tat secretion system carrying <i>antA</i> transcriptional reporter	This study
PA14 Δ PA4812 miniCTX:: <i>'antA-lux</i>	Deletion mutant of a substrate of the Tat secretion system carrying <i>antA</i> transcriptional reporter	This study
PA14 Δ PA4858 miniCTX:: <i>'antA-lux</i>	Deletion mutant of a substrate of the Tat secretion system carrying <i>antA</i> transcriptional reporter	This study
PA14 Δ PA5327 miniCTX:: <i>'antA-lux</i>	Deletion mutant of a substrate of the Tat secretion system carrying <i>antA</i> transcriptional reporter	This study
PA14 Δ PA5538 miniCTX:: <i>'antA-lux</i>	Deletion mutant of a substrate of the Tat secretion system carrying <i>antA</i> transcriptional reporter	This study
PA14 Δ PA14_48450 miniCTX:: <i>'antA-lux</i>	Deletion mutant of a substrate of the Tat secretion system carrying <i>antA</i> transcriptional reporter	This study
PA14 Δ PA4429	Clean deletion of PA4429	Kindly donated by Berengere Ize, C.N.R.S, Marseille
PA14 Δ PA4429 miniCTX:: <i>'pqsA-lux</i>	Clean deletion of PA4429 carrying <i>pqsA</i> transcriptional reporter	This study
PA14 Δ PA4430	Clean deletion of PA4430	Kindly donated by Berengere Ize, C.N.R.S, Marseille
PA14 Δ PA4430 miniCTX:: <i>'pqsA-lux</i>	Clean deletion of PA4430 carrying <i>pqsA</i> transcriptional reporter	This study
PA14 Δ petA- miniCTX:: <i>'petA</i>	Clean deletion of PA4431 (<i>petA</i>) complemented with <i>petA</i> on miniCTX vector	Kindly donated by Berengere Ize, C.N.R.S, Marseille

Table 2.1. List of bacterial strains used during this study.

All vectors used are listed in **Table 2.2**.

Plasmid	Features	Origin
pMiniCTX:: <i>lux</i>	Inserts at neutral CTX site on <i>pseudomonas</i> chromosome. Contains a <i>luxCDABE</i> operon for bioluminescence, Tc ^R	(Calvo <i>et al.</i> , 2000)
pMiniCTX:: <i>antA'-lux</i>	Contains a <i>luxCDABE</i> operon under the control of <i>antA</i> promoter, Tc ^R	This study
pMiniCTX:: <i>antR'-lux</i>	Contains a <i>luxCDABE</i> operon under the control of <i>antR</i> promoter, Tc ^R	This study
pMiniCTX:: <i>catB'-lux</i>	Contains a <i>luxCDABE</i> operon under the control of <i>catB</i> promoter, Tc ^R	This study
pMiniCTX:: <i>catR'-lux</i>	Contains a <i>luxCDABE</i> operon under the control of <i>catR</i> promoter, Tc ^R	This study
pMiniCTX:: <i>pqsA'-ux</i>	Contains a <i>luxCDABE</i> operon under the control of <i>pqsA</i> promoter, Tc ^R	(Soh <i>et al.</i> , 2021)
pMiniCTX:: <i>hisI'-lux</i>	Contains a <i>luxCDABE</i> operon under the control of <i>hisI</i> promoter, the promoter for the <i>tatABC</i> operon, Tc ^R	This study
pDM4	Suicide plasmid containing <i>sacBR</i> genes for sucrose sensitivity, Gm ^R	(Buscher <i>et al.</i> , 2005)
pDM4 Δ <i>antA</i>	pDM4 plasmid containing <i>antA</i> flanking regions and deleted <i>antA</i> gene. For clean deletion of <i>antA</i> gene in <i>Pseudomonas aeruginosa</i> , Gm ^R	This study
pSW002-Pc-TorA-mTurquoise2	For constitutive expression of Tat-secreted green-fluorescent protein mTurquoise2, Tc ^R	(Wilton <i>et al.</i> , 2018)
pminiCTX1:: <i>petA</i>	<i>petA</i> under the control of its own promoter in mini-CTX1	(Soh <i>et al.</i> , 2021)

Table 2.2. Plasmids used during this study.

2.3 Molecular biology

The following oligonucleotides were used during this study:

Oligonucleotide	Sequence (5' – 3')	Details	Restriction site
<i>antA</i> CTX UF	TATAAGCTTTGCACA TCGACTTCA	Forward primer for cloning <i>antA</i> promoter region	<i>HinDIII</i>
<i>antA</i> CTX DR	TATGGATCCCTGTTC GAGGCTTCT	Reverse primer for cloning <i>antA</i> promoter region	<i>BamHI</i>
<i>antR</i> CTX UF	TATAAGCTTTGTGCT GACGTGATA	Forward primer for cloning <i>antR</i> promoter region	<i>HinDIII</i>

<i>antR</i> CTX DR	TATGGATCCATGGGT CCTCATCAT	Reverse primer for cloning <i>antR</i> promoter region	<i>Bam</i> HI
<i>catB</i> CTX UF	TATAAGCTTTGTGCGC AGATGCTTT	Forward primer for cloning <i>catB</i> promoter region	<i>Hin</i> DIII
<i>catB</i> CTX DR	TATGGATCCTTTGGGA TCACGGCTT	Reverse primer for cloning <i>catB</i> promoter region	<i>Bam</i> HI
<i>catR</i> CTX UF	TATAAGCTTCGGCAT TCACGTTGT	Forward primer for cloning <i>catR</i> promoter region	<i>Hin</i> DIII
<i>catR</i> CTX DR	TATGGATCCAAGTAG CGCAGGTGA	Reverse primer for cloning <i>catR</i> promoter region	<i>Bam</i> HI
<i>hisI</i> CTX UF	TATAAGCTTCTGAAC ATCGAAGGC	Forward primer for cloning promoter of <i>hisI</i> <i>Etat</i> <i>ABCPA5071</i> operon	<i>Hin</i> DIII
<i>hisI</i> CTX DR	TATGGATCCGTTCCA GTGAATCTC	Reverse primer for cloning promoter of <i>hisI</i> <i>Etat</i> <i>ABCPA5071</i> operon	<i>Bam</i> HI
<i>antA</i> pDM4 +500 UF	TATTCTAGATGCAAC ATCTCCTCC	For creating an <i>antA</i> deletion	<i>Xba</i> I
<i>antA</i> pDM4 +500 DR	TATGAATTCCTGTTC GAGGCTTCT	For creating an <i>antA</i> deletion	<i>Eco</i> RI
<i>antA</i> pDM4 -500 UF	TATGAATTCGAGATC ACCCACGAA	For creating an <i>antA</i> deletion	<i>Eco</i> RI
<i>antA</i> pDM4 -500 DR	TATCTCGAGCAGGAA CAGGGTCTT	For creating an <i>antA</i> deletion	<i>Xho</i> I
pDM4 seq UF	ACAGGAACACTTAAC GGCTG	Forward primer for sequencing insert in pDM4	-
pDM4 seq DR	TGTCCCTCCTGTTCA GCTACT	Reverse primer for sequencing insert in pDM4	-
<i>antA</i> seq UF	CAGGATCAGTCCCTT GATCAG	Forward Chromosomal Sequencing Primer for <i>antA</i>	-
<i>antA</i> seq DR	GAGGCGAAGTCGAAG TAGAAG	Reverse Chromosomal Sequencing Primer for <i>antA</i>	-

Table 2.3. List of primers used during this study.

Amplification of DNA fragments by Polymerase Chain Reaction

Polymerase chain reaction (PCR) was used to amplify specific fragments of DNA from either a plasmid DNA or genomic DNA template. PCR was carried out using both GoTaq® G2 Green Master Mix (Promega) and Q5® High-fidelity 2X Master Mix (NEB). The upstream and downstream oligonucleotides were stored at 100 nM at -20°C, and a working stock was made from a 1/10 dilution in nuclease free (n.f.) water.

For a 50 µl reaction, 100 ng template DNA was added to 25 µl of master mix and 5 µl of each working stock of the upstream and downstream oligonucleotide. N.f. water was added for a total volume of 50 µl and the reaction mixed gently with a pipette. The PCR thermocycling conditions changed depending on the size of the DNA fragment and the melting temperature (T_m) of the two oligonucleotides. A brief guide is as follows:

Step		DNA polymerase	
		GoTaq®	Q5®
1	95°C	2 min	98°C 30 s
2	95°C	30 s	98°C 10 s
3	T _m -5°C	30 s	T _m -5°C 30 s
4	72°C	1 min/kb	72°C 30 s/kb
5	72°C	5 min	72°C 2 min

Reactions were then stored at 4°C if not used immediately.

Plasmid Extraction

Plasmids were extracted from overnight 5 mL cultures grown in LB broth containing the plasmid-selective antibiotic. The Sigma-Aldrich GenElute™ Plasmid Miniprep kit was used to isolate plasmids following the manufacturer's instructions and DNA was eluted into 50 µl n.f. water and stored at -20°C. A NanoDrop® spectrophotometer 1000 (Fisher Scientific) was used to measure the concentration and assess the purity of double-stranded DNA in the sample.

Restriction Digest

Approximately 1 µg DNA was digested with restriction endonucleases produced by either Promega or NEB as per the manufacturer's instructions.

Gel Electrophoresis and DNA purification

Agarose gel electrophoresis was used to separate DNA fragments by their mass. Typically a 1% agarose gel was used, so that 1 g of agarose was dissolved in a total volume of 100 mL Tris-acetate-EDTA (TAE) buffer (0.04 M Tris-acetate, pH 8 + 1 mM ethylenediaminetetraacetic acid (EDTA)) and then 0.1 µl/mL Invitrogen™ Sybr™ Safe (Thermo Fischer Scientific) DNA stain was added. 10-50 µl DNA was loaded into each well and was run through the gel in TAE buffer at 90 V 1 h.

Ligation of DNA fragments with vector backbone

A 20 µl reaction was made from 0.5 µl T4 DNA ligase (Promega), 2 µl 10X ligase buffer (Promega), the insert and vector DNA at a molar ratio of 5:1, and n.f. water for the remaining volume. Ligation was carried out over 16 h at 16°C in PCR thermocycler. Following ligation samples were dialysed 1 h using 0.025 µm nitrocellulose membrane filters (Merck Millipore Ltd.) floating on dH₂O before electroporation into electrocompetent cells.

Preparation of electrocompetent *E. coli* cells

Overnight culture of *E. coli* S17-1 λ pir was added to 100 mL fresh LB at an OD₆₀₀ of 0.05, this was then incubated for 6 h at 37°C, 200 rpm. The culture was split into 5 and cells were harvested by centrifugation at 5000 xg , 4°C for 20 min. Once the supernatant was discarded each pellet was resuspended gently in 20 mL 10% (v/v) glycerol. This centrifugation-resuspension step was repeated thrice, each time resuspending the pellet in lower volumes of 10% (v/v) glycerol: 20 mL, 5 mL, then 250 μ l. Finally, 50 μ l aliquots were prepared from the final resuspension and these were stored at -80°C.

Preparation of electrocompetent *P. aeruginosa*

The *P. aeruginosa* strain to be transformed was grown as a standard overnight 5 mL culture at 42°C, 200 rpm. Cells were harvested by centrifugation at 5000 xg for 10 min at 4°C then washed in sterile dH₂O three times before resuspending in a volume of 100 μ l sterile dH₂O.

Transformation of plasmids into electrocompetent cells

Solutions containing plasmid DNA were dialysed to remove salt on 0.025 nm pore filter membrane (Millipore) floating on dH₂O for 1 h immediately prior to transformation into bacterial cells.

All aliquots of electrocompetent cells were thawed and kept on ice before electroporation. For transformation of electrocompetent *E. coli* and *P. aeruginosa*, 4-10 μ l of plasmid DNA was added to a 50 μ l aliquot of electrocompetent cells, mixed gently and electroporated in a 2 mm electroporation cuvette (Bio-rad) using a Bio-rad Micropulser at 12.5 kV/cm. Next, 950 μ l pre-warmed LB or SOC outgrowth medium (NEB) was added and the cuvette incubated 1 h at 37°C, static. Finally, 50 μ l was spread on a selective LB agar plate, the remaining cells pelleted and resuspended in 50 μ l LB broth before spreading on a second plate. Transformed cells were selected for by antibiotic resistance encoded in the plasmid.

Conjugation into *P. aeruginosa*

5 mL LB overnight cultures of recipient *P. aeruginosa* strains were grown at 42°C to inactivate the restriction enzyme system which degrades foreign DNA. At the same time, donor *E. coli* S17-1 λ pir strains were grown at 37°C shaking 250 rpm. 500 μ l of donor and recipient cultures were mixed and then washed in 1 mL fresh LB. Controls for individual strains were not mixed but prepared in the same manner. After 5 min of centrifugation at 6,000 xg samples were resuspended in 50 μ l LB and spotted onto dry LB plates. The plates were dried 15 min under a flame then incubated 30°C 6 h. After 6 h spots were resuspended in 1 mL LB and then 50 μ l of each was spread on an LB plate containing the nalidixic acid 15 μ g/mL and the correct selective antibiotic for isolation of *Pseudomonas* strains carrying the intended plasmid. pDM4 carries a gentamicin resistance cassette and miniCTX::*lux* confers tetracycline resistance.

Colony PCR

Clones growing on a selective agar plate following transformation or conjugation were patch-plated onto a numbered grid on a fresh selective agar plate. Following overnight incubation at 37°C, small sections of each clone were transferred to a PCR tube containing 12.5 μ l GoTaq® G2 Green Master Mix (Promega), 5 μ l of each oligonucleotide from 10 nM working stocks, and 2.5 μ l nuclease free water. PCR thermocycling conditions are as follows:

Step	Temperature	Time	Return to step	N° of repeats
1	95°C	10 min		
2	95°C	30 s		
3	58°C	30 s		
4	72°C	1 min/kb	2	30
5	72°C	10 min		

Genomic DNA extraction

Genomic DNA was extracted with the GenElute™ Bacterial Genomic DNA extraction kit (Sigma Aldrich) according to the manufacturer's protocol, the DNA was eluted in nuclease free water and stored at -20°C.

Confirmation of DNA by sanger sequencing of DNA

The concentration of DNA and purity of the sample was assessed with the NanoDrop® Spectrophotometer 1000 (Fisher Scientific). Sanger sequencing was carried out by Source Bioscience and the results analysed using Benchling (<https://www.benchling.com>).

2.4 Genetic modifications

Deletion of *antA* with pDM4 suicide vector

Knockout of *antA* was carried out using homologous recombination and the sucrose-sensitive suicide plasmid pDM4 (**Figure 2.1a**). in-frame deletion between bases 27 and 1,284 of the *antA* ORF was made using the suicide vector deletion system described by Buscher et. al. (2005)(Buscher *et al.*, 2005). The oligonucleotides "*antA* pDM4 +500 UF" and "*antA* pDM4 +500 DR" (**Table 2.3**) were used to amplify the 783 bp upstream region, and "*antA* pDM4 -500 UF" and "*antA* pDM4 -500 DR", the 665 bp downstream region. Homology arms were chosen to start just within the start and end of the open reading frame and extend out either side of the gene. These were cloned using specific primers which introduce a restriction endonuclease site on the end of each DNA fragment. Once digested and purified the DNA fragments were ligated together and into pDM4 in one step and the plasmid transformed into *E. coli* S17-1 λ *pir*. Successful transformation was selected for using gentamicin resistance. Plasmids were extracted from each clone and the insertion of both homologous regions was

detected with PCR using the primers "pDM4 seq UF" and "pDM4 seq DR" which flank the multiple cloning site on the vector. A plasmid containing both inserts was confirmed with sanger sequencing.

Conjugation of the pDM4 Δ *antA* deletion plasmid into *P. aeruginosa* was carried out as described earlier. Clones growing on PIA agar containing gentamicin at 10 μ g/mL were transferred to a numbered grid and grown overnight on LB Gm 10 μ g/mL plates. These contain a single-crossover insertion of the pDM4 Δ *antA* plasmid at one of the homology regions on the bacterial chromosome. Double-crossover homologous recombination events between duplicated sequences in the heterozygote were selected for by growth in LB 5% sucrose using the *sacB* gene. Each clone was used to inoculate overnight cultures of LB sucrose 5% (w/v) broth, after growth at 37°C 200 rpm a 1×10^6 dilution was plated onto LB sucrose 5% (w/v) agar and this sucrose selection process was carried out three times.

Clones growing on LB sucrose 5% (w/v) agar were transferred to identical grid positions, first on LB agar then LB Gm 10 μ g/mL agar and those that grew only on the former had undergone a double-crossover homologous recombination event and no longer contained the pDM4 vector backbone (**Figure 2.1a**). Sucrose selection of double-crossover events produces strains which carry either the wild-type gene or in-frame deletion on the bacterial chromosome. Specific chromosomal oligonucleotides "*antA* seq UF" and "*antA* seq DR" were used to PCR amplify this region (**Figure 2.1b**). Those that carried the in-frame deletion produced a DNA fragment far shorter than the wild-type fragment. Creation of isogenic mutants was confirmed with whole genome sequencing in addition to PCR amplification of the *antA* region.

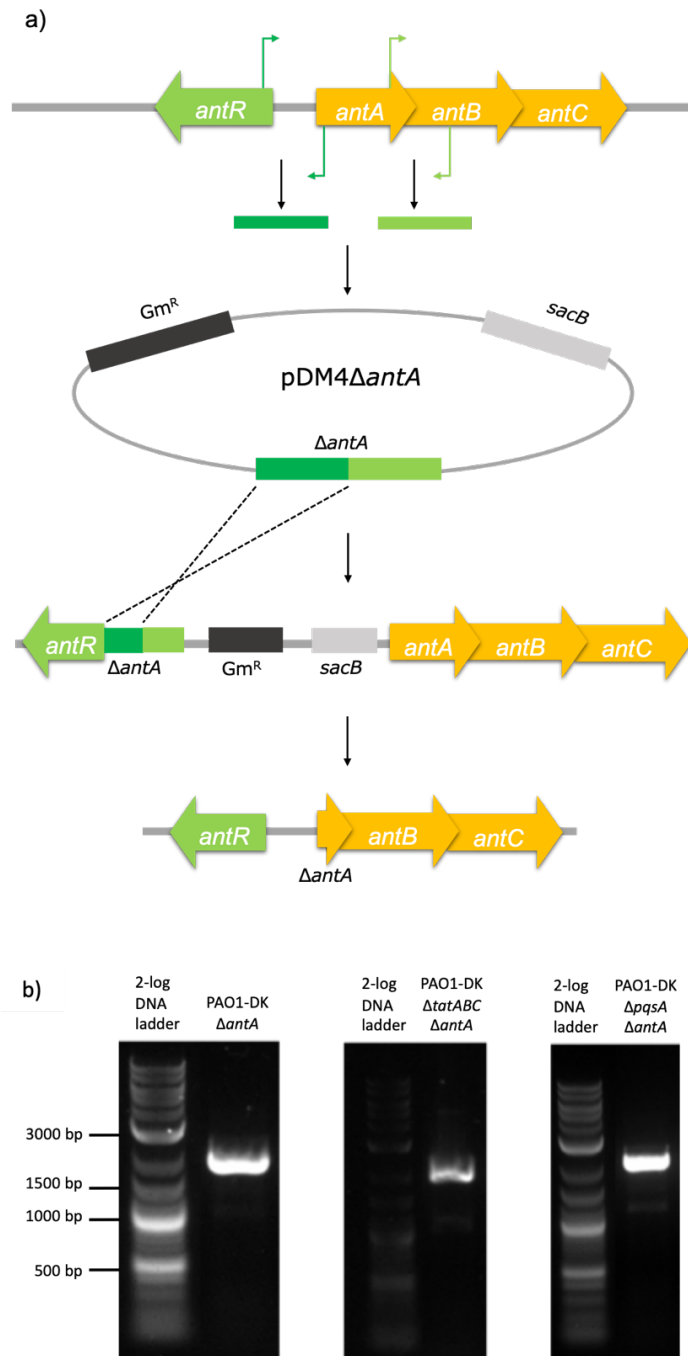


Figure 2.1. Construction of pDM4 $\Delta antA$ deletion plasmid (a) and confirmation of deletion mutants (b). a) Oligonucleotides (green arrows) were used to amplify upstream and downstream regions of *antA* by PCR (green bands). These were ligated together on a gentamicin-resistant pDM4 suicide vector carrying a *sacB* gene. pDM4 $\Delta antA$ was sequenced then conjugated into PAO1, PAO1 $\Delta tatABC$ and PAO1 $\Delta pqsA$. Newly-acquired gentamycin resistance allows isolation of clones following single homologous recombination with the bacterial chromosome. Double homologous recombination events were selected for with the *sacB* gene, whose expression causes cell death upon growth in sucrose. Lastly, the chromosomal $\Delta antA$ deletion is shown. b) Confirmation of mutants by PCR amplification of the chromosomal *antA* gene using the primers “*antA* seq UF” and “*antA* seq DR”. DNA fragment is 3,119 bp for wild-type gene and 1,868 bp for $\Delta antA$.

Creation of bioluminescent transcriptional reporters

Transcriptional fusions were made between promoter regions of *antA*, *antR*, *catB*, *catR* and *hisI* and the *luxCDABE* operon and inserted into the bacterial chromosome at a neutral location with a miniCTX::*lux* plasmid vector as described by Diggle *et al.* (Diggle *et al.*, 2007). Bioluminescence and cell density was measured in an automated luminometer-spectrophotometer as described by Fletcher *et al.* (Fletcher *et al.*, 2007).

Briefly, pminiCTX::*lux* vectors were amplified, extracted and purified from *E. coli* S17-1 λ pir using Sigma Aldrich miniprep kits. The plasmid was then digested with *HinDIII* and *BamHI* (Promega), and the cut and uncut DNA fragments were resolved on a 1% agarose gel. For digestion of 1 μ g plasmid DNA: 2 μ l 10X Buffer E (Promega) was mixed with the DNA and 0.5 μ l of each restriction endonuclease, then a total volume of 20 μ l was reached with nuclease free water. Reactions were left at 37°C 3 h. The DNA fragment corresponding to cut vector was extracted and purified using Qiagen QIAEXII gel extraction kit and stored at -20°C.

The promoter regions of the genes of interest were PCR amplified using Q5 2X master mix (NEB), and the primers found in **Table 2.3**. For a 50 μ l reaction, 25 μ l of Q5 2X Master mix was added to 23 μ l nuclease free water, 1 μ l PAO1 gDNA and 0.5 μ l of each primer at 100 nM. The PCR thermocycling conditions are the same as above. DNA fragments corresponding to the promoter regions were extracted following resolution on a 1% agarose gel (Qiagen QIAEXII gel extraction kit), then digested with *HinDIII* and *BamHI*. Digested plasmid and insert DNA were ligated together with T4 DNA ligase (Promega) as above, using the ratio of 5:1 insert:vector. Following a 1 h dialysis the samples were electroporated into *E. coli* S17-1 λ pir and grown on LB tetracycline 10 μ g/mL agar plates.

Individual colonies were patch-plated onto new antibiotic-selective agar plates, and the plasmids from each were extracted. Plasmids were digested with *HinDIII* and *BamHI*, and following resolution on a 1% agarose gel, DNA fragments

matching the predicted size (see **Table 2.4**) confirmed the presence of new bioluminescent transcriptional reporters.

Promoter	Length of PCR product (bp)
<i>antA</i>	518
<i>antR</i>	1,006
<i>catB</i>	412
<i>catR</i>	455
<i>hisI</i>	538

Table 2.4. DNA fragment sizes following PCR amplification of *antA*, *antR*, *catB*, *catR* and *hisI* promoters.

2.5 Phenotypic assays

Pyocyanin

Pyocyanin was quantified using an assay first described by Essar *et al.* (Essar, Eberly, Hadero, *et al.*, 1990). *P. aeruginosa* cultures were grown overnight in 5 mL LB broth, then 1 mL was washed in fresh LB and used to inoculate 25 mL LB at an OD₆₀₀ of 0.05. Cultures were grown in 250 mL conical flasks, 37°C, shaking 200 rpm, for 8 h. In triplicate, 3 mL chloroform was added to 5 mL filter-sterilised culture supernatant, mixed, and after formation the blue layer of chloroform was transferred to a fresh tube containing 1 mL of 0.2 M HCl. Each sample was vortex mixed and the subsequent pink layer containing 0.2 M HCl was transferred to a cuvette. Absorption at 520 nm was quantified and pyocyanin concentration in µg/mL was determined by multiplying results by the mass extinction coefficient, 17.072.

Supernatant induction of *pqsA* bioluminescent reporter

5 mL LB cultures of PAO1-DK miniCTX::*pqsA'*-*lux* and PAO1-DK Δ *pqsA* miniCTX::*pqsA'*-*lux* were grown 16 h, then 1 mL of each culture was pelleted, the supernatant was discarded and the pellet was resuspended in 1 mL LB. At the same time 5 mL LB cultures of PAO1-DK, PAO1-DK Δ *tatABC*, PA14 and PA14 Δ *tatABC* were grown 16 h overnight. These were centrifuged to pellet the cells and the supernatant was filter-sterilised with 0.22 μ m pore filters to remove debris and sterilise the supernatant. Supernatants from each strain were then mixed with LB to a ratio of 1:2 LB:supernatant and inoculated to an OD₆₀₀ of 0.01 with PAO1-DK Δ *pqsA* miniCTX::*pqsA'*-*lux* prepared earlier. 200 μ l of each condition was added to a 96-well flat-bottom microtiter plate in triplicate and the plate was incubated in an automated spectrophotometer at 37°C, static. The cell growth (OD₆₀₀) and luminescence (RLU) was recorded every 30 min for 24 h. Data were analysed with Microsoft Excel and Graphpad Prism 8.

Liquid Chromatography-Tandem mass spectroscopy (LC-MS/MS) analysis

Extraction of 2-alkyl-4-quinolone (AQ) and anthranilic acid from supernatants and LC-MS/MS was carried out by Nigel Halliday, School of Life Sciences, Centre for Biomolecular Sciences, University of Nottingham. Briefly, 100 μ l of each supernatant was diluted with 398 μ l fresh LB and 2 μ l internal standard (d4-PQS) for a 1:5 dilution. 500 μ l acidified (0.1% acetic acid) ethyl acetate was added to each sample and the mixture vortex mixed for 2-3 min, then the organic phase was removed to a 2 mL microcentrifuge tube. This acidified ethyl acetate extraction step was repeated twice more, each time the organic phases were transferred to the same tube. Samples were stored at -20°C, then dried and resuspended in 100 μ l methanol before analysis by LC-MS/MS.

2.6 Microtiter Assays

Bioluminescence and optical density assay

5 mL LB cultures of *P. aeruginosa* strains carrying the miniCTX::*promoter-of-interest-lux* transcriptional reporters were grown overnight for 16 h. 1 mL of culture was pelleted in a microcentrifuge 13,000 xg 1 min, the supernatant discarded and the pellet resuspended in 1 mL LB. This was used to inoculate 1 mL LB to an OD₆₀₀ of 0.01. Each well of a 96-well flat-bottom microtitre plate (black with transparent flat-bottom, GreinerOne) was filled with 200 µl of inoculated LB. Each strain or condition was measured in triplicate to give three technical repeats.

For assays comparing gene expression in the presence and absence of anthranilic acid, overnight cultures washed in 1 mL LB were also used to inoculate 1 mL LB containing 6 mM anthranilic acid (PAO1 strains) or 3 mM anthranilic acid (PA14 strains) in addition to 1 mL LB only.

Microtitre plates were incubated in an automated luminometer-spectrophotometer (TECAN infinite® F2000Pro) at 37°C, static, and the cell growth (OD₆₀₀) and luminescence (relative light units, RLU) was recorded at 30 min intervals for 24 h. Data were analysed with Microsoft Excel® and Graphpad Prism 8 software.

Bay 11-7082 analogue IC50/EC₅₀ assays

Bay 11-7082 synthesised by Alex Truman (University of Nottingham) is referred to as TI1 throughout and subsequent analogues synthesised by Alex Truman are labelled TI2-TI30. For each assay, Bay 11-7082 analogues were dissolved in 10 µl DMSO at a range of concentrations between 1 mM and 0.45 µM. 5 mL LB culture of PAO1-DK miniCTX::*pqsA'-lux* or PAO1-DK miniCTX::*antA'-lux* was grown at 37°C, 200 rpm for 16 h. 1 mL of overnight culture was washed in 1 mL LB then used to inoculate fresh LB at OD₆₀₀=0.05, of which 990 µl was then

added to 10 μ l tat inhibitor. 200 μ l cultures were grown in triplicate on a 96-well microtiter plate and an automated luminometer-spectrophotometer was used to measure cell growth (OD₆₀₀) and luminescence (RLU) every 30 min for 24 h. Controls included were PAO1-DK Δ tatABC miniCTX::*pqsA'-lux* or PAO1-DK Δ tatABC miniCTX::*antA'-lux*, a DMSO-only control, and sterile LB. Data were analysed with Microsoft Excel and Graphpad Prism 8.

Fluorescence and optical density assay

5 mL overnight cultures of PAO1-DK, PAO1-DK Δ tatABC, and PAO1-DK Δ pqsA were grown in LB broth at 37°C, 200 rpm. 1 mL of each culture was washed then used to inoculate fresh M9 minimal medium supplemented with 20 mM succinate at an OD₆₀₀ of 0.05. Bay 11-7082 analogues were added to 1 mL PAO1-inoculated media at concentrations of 40 μ M and 20 μ M, then 200 μ l was added in triplicate to the 96-well plate. Fluorescence (RFU) and growth (OD₆₀₀) was measured every 30 min over 24 h. For pyoverdine, fluorescence was measured with an excitation wavelength of 405 nm and an emission wavelength of 460 nm.

AlamarBlue cell viability assay

AlamarBlue cell viability reagent (ThermoFisher Scientific) is a non-toxic indigo-coloured compound that undergoes a colour change to red due to the reducing environment of metabolically active cells. The reduced form is also highly fluorescent (ex. 560/ em. 590).

Jurkat cells with >95% cell viability were diluted to 100,000 cells/mL in fresh media and 100 μ l was added to each well of a 96 well tissue culture plate (flat bottom, clear) containing a range of concentrations of TI1 (4-Me-PhSAN) and TI6 (4-Me-PhSACONH₂) in triplicate. The plate was incubated overnight at 37°C, 5% CO₂. After overnight growth 10% alamarBlue was added to complete media and incubated overnight at 37°C, 5% CO₂. Fluorescence of reduced alamarBlue was

measured in an automated plate reader (ex. 560/ em. 590) and used to quantify cell viability. The experiment was carried out three times.

2.7 Microscopy

Biofilm formation

P. aeruginosa strains were grown overnight in LB then 1 mL was harvested at 1000 x *g* for 1 min. Pellets were washed in 1 mL phosphate buffered saline (PBS), then harvested and resuspended in 1 mL M9 succinate minimal medium. Cells were used to inoculate fresh M9 succinate at an OD₆₀₀ of 0.05 and 300 µl was added to each well of an 8-well glass bottom chamber (Ibidi). The chamber was placed in a box and incubated at 37°C, static for 48 h.

Visualisation of biofilm components

For visualisation of cell biomass and eDNA, spent media was carefully removed without disturbing the biofilm formed on the bottom of the slide, and replaced with fresh M9 medium containing 2.5 µg/mL CellMask™ Deep Red plasma membrane stain (ThermoFisher Scientific) and 40 µM YOYO-1, an eDNA stain (ThermoFisher Scientific). Biofilms were imaged after 30 min incubation.

Confocal microscopy

Biofilms were imaged with a Zeiss inverted confocal laser scanning fluorescent microscope (Zeiss LSM70) and appropriate excitation/emission wavelengths for each channel (CMDR: 649 nm/666 nm, YOYO-1: 491 nm/509 nm, PI: 493 nm/636 nm, SYTO-9: 483 nm/503 nm). Images were processed with Zen imaging software (Carl Zeiss) and biomass, surface area and maximum biofilm

thickness for each channel was determined with Image J and Comstat 2 software (Heydorn *et al.*, 2000).

2.8 Bioinformatics

Genomic analysis

Genomic DNA was extracted from overnight cultures of PAO1-DK, PAO1-DK $\Delta antA$, PAO1-DK $\Delta tatABC \Delta antA$, and PAO1-DK $\Delta pqsA \Delta antA$ using GenElute Bacterial Genomic DNA kit (Sigma-Aldrich) according to the manufacturer's protocol. Concentration and purity was assessed with the Nanodrop ND-1000 (Nanodrop Technologies). DNA was sent to MicrobesNG for whole genome sequencing (WGS).

Libraries were prepared and quantified with the Kapa Biosystems Library Quantification Kit for Illumina on a Roche light cycler 96 qPCR machine. Libraries were sequenced on an Illumina instrument using a 250 bp paired end protocol. Reads were trimmed using Trimmomatic 0.30 with a sliding window quality cutoff of Q15 and their quality was assessed using in-house scripts and Samtools, BedTools, bwa-mem (Bolger *et al.*, 2014). Contigs were aligned to PAO1-W reference genome using ABACAS version 1.3.1 (<http://abacas.sourceforge.net/index.html>) to create a pseudogenome (Stover *et al.*, 2000). These were visualised using BLAST ring image generator (BRIG) version 0.95 and gene deletions were labelled (Alikhan *et al.*, 2011).

**Chapter 3: The metabolic balance
between PQS biosynthesis and
anthranilate degradation is disrupted
upon deletion of the Tat system**

3.1 Introduction

Mature *Pseudomonas aeruginosa* biofilm consists of clusters of growing cells contained within an extracellular polymeric matrix. The matrix is made up of exopolysaccharides (EPS), proteins, alginate, outer membrane vesicles, and extracellular DNA (eDNA), the latter of which is found at 5-fold greater concentrations than protein in PAO1 biofilms, and is 15-20-fold more abundant than carbohydrates (Matsukawa and Greenberg, 2004). eDNA is essential for biofilm function, structure, and migration by twitching motility (Turnbull *et al.*, 2016). *P. aeruginosa* forms mushroom-like microcolony structures when grown in a microfluidic-flow chamber in which eDNA acts as a cell-cell interconnecting matrix component key to structural integrity. In mature biofilms, eDNA is concentrated at the stalk, and addition of DNase I abolishes formation of large structures (Chiang *et al.*, 2013; Tolker-Nielsen, 2015). The release of eDNA is thought to be through lysis of a subpopulation of cells, or in the case of human infections, can be incorporated into biofilms from lysed eukaryotic cells such as polymorphonuclear leukocytes (Chiang *et al.*, 2013). Aside from its structural function, eDNA also acts to shield cells from aminoglycosides by chelating them with opposite charges on the DNA strand, increasing the resistance to tobramycin 1000-fold (Chiang *et al.*, 2013).

It was established that PQS signalling controls eDNA release in *P. aeruginosa* (Allesen-Holm *et al.* 2006, Yang *et al.* 2007). To further understand the regulatory mechanisms behind this and identify additional factors, a transposon screen for mutants defective in eDNA release was carried out by Tim Tolker-Nielsen and his colleagues (University of Copenhagen). Insertion mutants within genes of the *pqs* QS system had reduced eDNA release, and unexpectedly so did mutants of the Twin-arginine translocation (Tat) pathway.

The Tat protein export pathway is one of two type II secretion systems and is responsible for the export of at least 34 different substrates (Gimenez *et al.*, 2018). The *tatABC* operon is located in a 6 gene cluster (*hisI-hisE-tatA-tatB-tatC-PA5071*) that begins with *hisI* and *hisE*, the latter of which is just 26 bp upstream of *tatA*, and ends with PA5071, a hypothetical protein (Voulhoux *et al.*, 2001; Gimenez *et al.*, 2018). The Tat system is the only secretion system to transport fully-folded and multimeric proteins into the periplasm. Often these must assemble in the cytoplasm where conditions are favourable, and insertion of a cofactor or metal ion is needed before translocation. The Tat system consists of three gene products, TatB and TatC form a membrane spanning complex that binds the signal peptide on substrates, and TatA oligomerises at this site to form a pore specific for the substrate crossing the membrane. Different substrates require different numbers of TatA due to variations in their size, shape and charge (Palmer and Berks, 2012).

Biofilms of wild-type PAO1-DK and a *tatA::Tn5* mutant were analysed by confocal laser scanning microscopy (CLSM). Wild-type growth formed microcolonies with characteristic mushroom-like structures, but *tat* mutant biofilms were thin, flat, and contained very little eDNA, similar to *las* mutant or PQS-signalling disrupted biofilms (Soh *et al.*, 2021). See **Figure 3.1**.

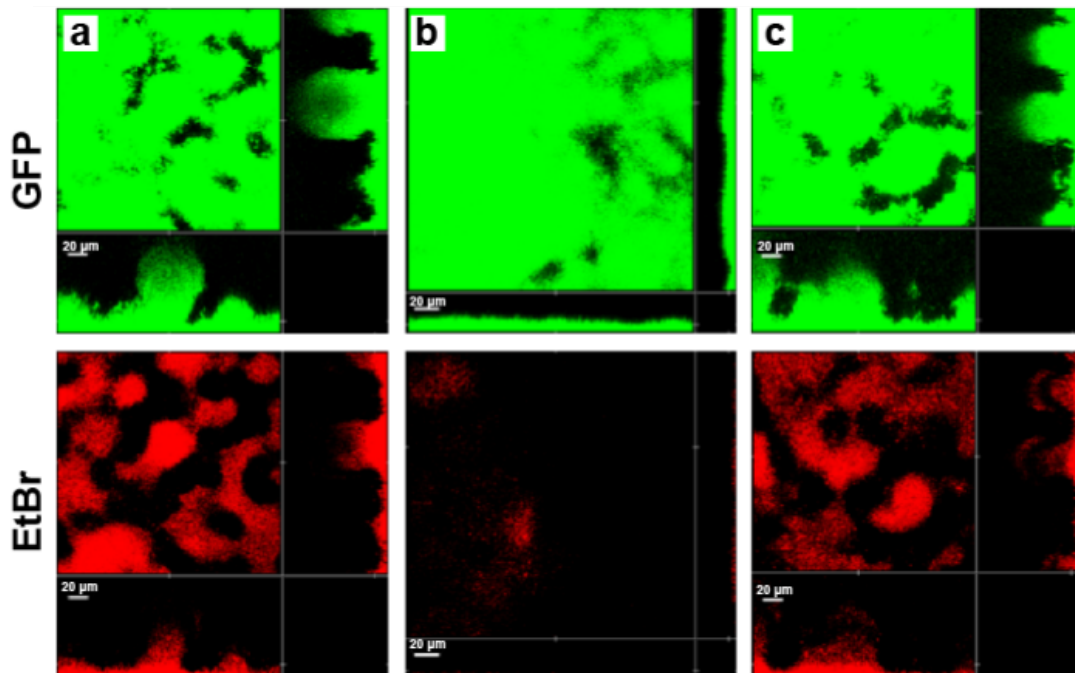


Figure 3.1. *tat* mutation affects biofilm formation. Biofilms of GFP-tagged a) PAO1 wild-type, b) a *tatA::Tn5* mutant, and c) a *tatA::Tn5/ptatA* complement strain were grown over 4 days in a flow chamber with FAB medium. Biofilms were stained with ethidium bromide and confocal laser scanning microscopy (CLSM) was used to visualise live cells (green fluorescence) and extracellular DNA (red fluorescence). Each picture shows a horizontal biofilm section as the main square, and a vertical cross-section to the right and below.

PQS-dependent quorum sensing in the *tat* mutant was investigated further. The *tatA::Tn5* mutant has decreased pyocyanin, rhamnolipid, and outer membrane vesicle production, all of which are dependent upon *pqs* quorum sensing (Soh *et al.*, 2021). Expression of *pqsA* is reduced by approximately 3-fold, and there is a ~50% reduction of the alkyl-quinolones (AQs) PQS and HHQ following 8 h planktonic growth. Expression of *pqsA* cannot be induced by addition of exogenous PQS and HHQ, as it can in a $\Delta pqsA$ mutant. This is hypothesised to be due to impaired access of AQs to PqsR, reducing its activity. Administration of an inhibitor of the Tat system, Bay 11-7082, at concentrations of 20 μ M and 40 μ M also lowered *pqsA* expression (Soh *et al.*, 2021).

Similarly, pyocyanin production is dependent on proper function of *pqs* QS. PqsR, along with the inducers PQS and HHQ, mediates expression of the pyocyanin biosynthetic operons *phzA1-G1* and *phzA2-G2*. The effector PqsE also induces expression of the pyocyanin biosynthetic operons. Secreted pyocyanin was decreased by ~3.5 fold in a *tatA::Tn5* mutant, and ~7.2 fold in a Δ *tatABC* mutant. This was correlated with lower expression from both *phzA1-G1* and *phzA2-G2* operons in both strains. The production of pyocyanin in PAO1-DK Δ *pqsA* is completely abolished, and could be restored by addition of exogenous PQS or HHQ. However, addition of PQS or HHQ to a PAO1-DK *tat* mutant did not return pyocyanin production to wild-type levels.

Together these data suggest that PQS biosynthesis is modulated upon mutation or deletion of the Tat system, and this in turn has pleiotropic effects including reduced eDNA release and defective biofilms. Therefore, further understanding of the link between PQS signalling and the Tat system is needed. This study aims to look closer at the transcriptomic changes of a *tat* mutant as regulatory changes may point towards a mechanism for reduced PQS biosynthesis. First, work was carried out to establish that disruption to PQS-dependent quorum sensing is not unique to the PAO1-DK strain.

3.2 Results

It was important to establish that modulation of PQS-dependent quorum sensing by the Tat system is not just a specific to the PAO1-DK strain. Therefore, the effects of mutation or deletion of the Tat pathway on PQS biosynthesis and pyocyanin production were studied in PAO1-DK in parallel with PA14. Originally isolated from a wound, PAO1 has long been used in the laboratory. PA14 is a more recent research strain which was originally isolated from a burn wound patient. While both are capable of causing disease, PA14 has increased virulence and a broader host range (Kukavica-Ibrulj *et al.*, 2008). Together they represent two main phylogenetic groups of *P. aeruginosa* (Muthukumarasamy *et al.*, 2020).

3.2.1. PQS biosynthesis in the *tat* mutant of PAO1-DK and PA14

It has previously been shown that PQS biosynthesis is perturbed upon mutation of the Tat system in PAO1-DK by using a bioluminescent transcriptional reporter carrying a promoter fusion of *pqsA* and the *luxCDABE* operon (Soh *et al.*, 2021). PQS export and OMV biogenesis is greater in PA14 than PAO1 when grown in LB media, and PA14 is considered a more virulent strain largely due to the presence of two pathogenicity islands PAPI-1 and PAPI-2, and a *ladS* mutation (He *et al.*, 2004; Kukavica-Ibrulj *et al.*, 2008; Florez *et al.*, 2017). If perturbation of PQS biosynthesis as a result of mutation or deletion of the Tat system is shared among *P. aeruginosa* strains then it may prove an ideal target for novel antivirulence agents. The expression of *pqsA* was measured in PAO1-DK and PAO1-DK Δ *tatABC* concurrently in order to confirm the published results and establish that the method was reproducible.

The miniCTX::*pqsA'-lux* vector was conjugated into PAO1-DK, PAO1-DK Δ *tatABC*, PA14, and PA14 Δ *tatABC* and the expression of *pqsA* was measured across 24 h growth in LB in an automated plate reader. As shown in **Figure 3.2**,

pqsA expression was reduced upon deletion of the Tat system in PA14 as well as in PAO1-DK. The maximum *pqsA* expression in PA14 Δ *tatABC* is ~40% of wild-type.

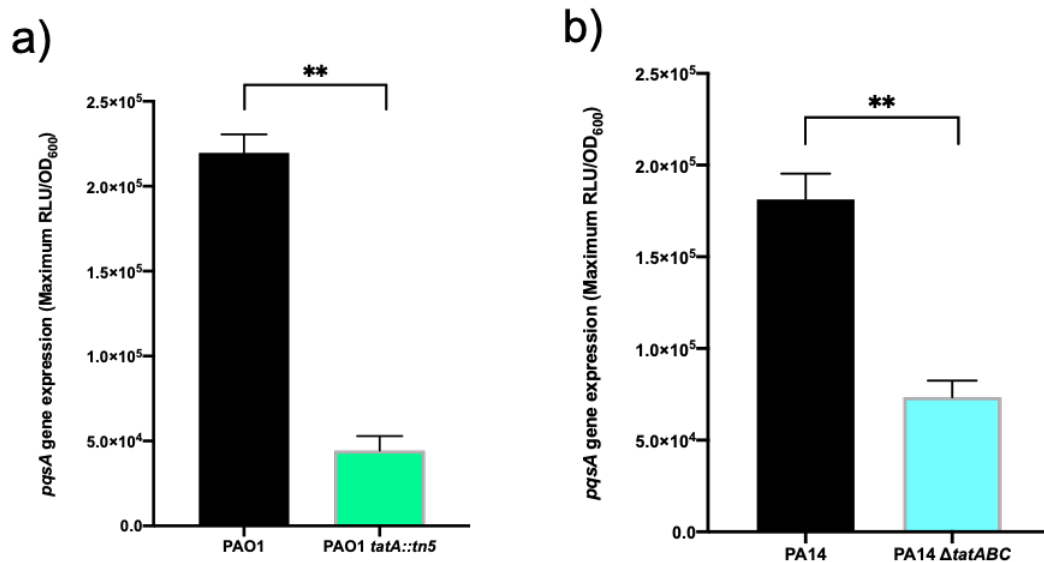


Figure 3.2. Biosynthesis of PQS was down-reguated upon *tat* mutation or deletion in both PAO1 and PA14. Expression of *pqsA*, the first gene in the PQS biosynthetic operon was significantly reduced in a) PAO1 Δ *tatABC* and b) PA14 Δ *tatABC* when compared to wild-type level. Experiments were repeated in triplicate, t-tests were performed to show statistical significance. $P \leq 0.01$.

The biosynthesis of the two main *pqs* QS signal molecules, HHQ and PQS, and the AQ *N*-oxide HQNO, is catalysed by the products of *pqsABCDE*, *pqsH* and *pqsL* (Rampioni *et al.*, 2016). As expression of the *pqsABCDE* operon is reduced upon mutation or deletion of the Tat system, the concentration of alkyl-quinolones (AQs) should also be affected. To investigate this, HHQ, PQS, and HQNO were extracted and purified from the supernatants of cell cultures following 8 h and 16 h growth in LB and semi-quantified by LC-MS/MS.

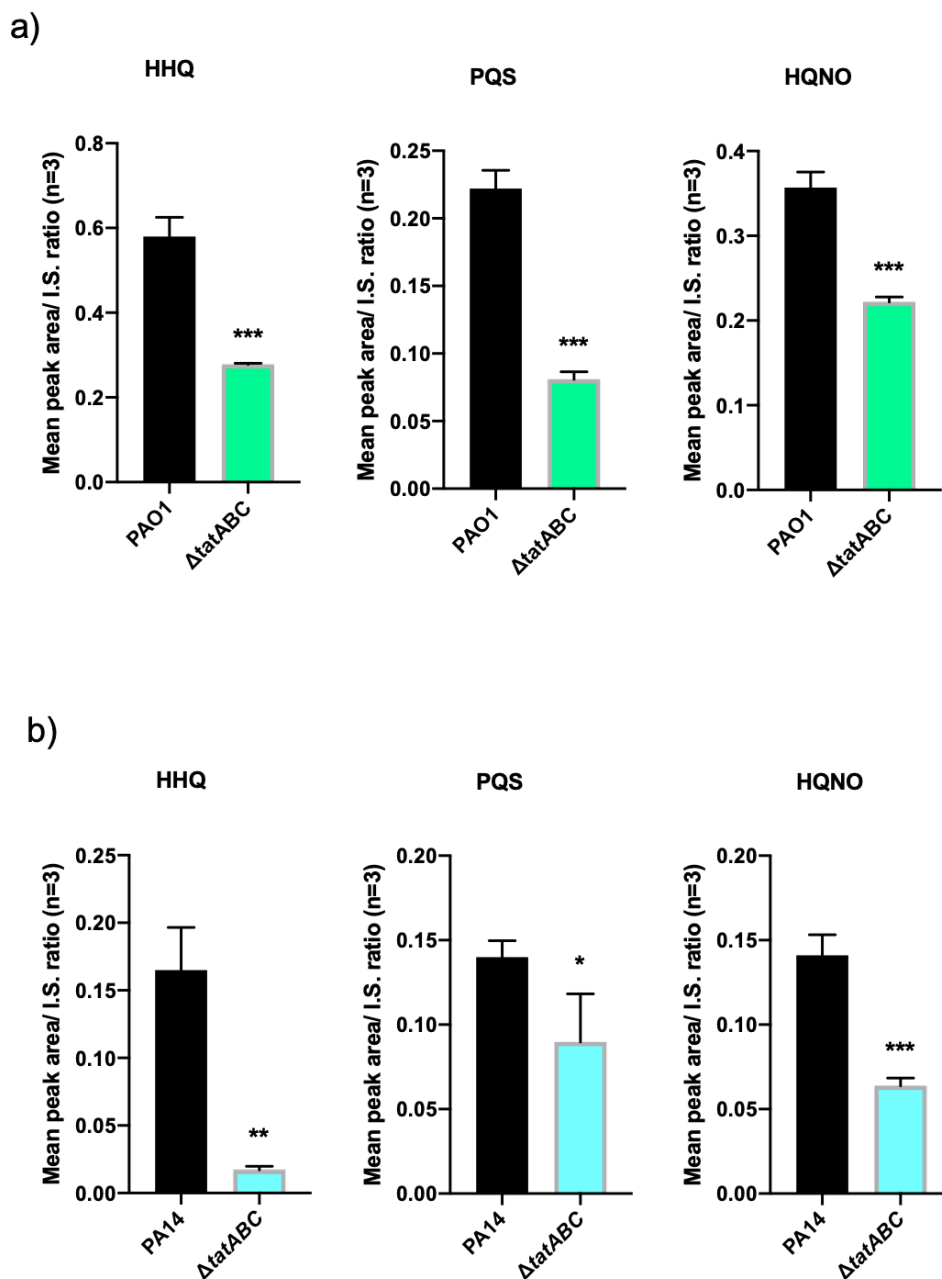


Figure 3.3. LC-MS/MS quantification of AQs in wild-type and $\Delta tatABC$ mutants. Supernatants were collected after 8 h growth and AQ compounds were extracted from a) wild-type PAO1 and PAO1 $\Delta tatABC$ and b) wild-type PA14 and PA14 $\Delta tatABC$, then semi-quantified by LC-MS/MS. Experiments were carried out in triplicate and t-tests were performed to show statistical significance.

PQS, its precursor HHQ and the AQ *N*-oxide, HQNO are all present in significantly lower concentrations than wild-type following 8 h growth of the PAO1-DK and PA14 *tat* mutants in LB (**Figure 3.3**).

After 16 h growth HHQ, PQS and HQNO production remained lower in the *tat* mutants of PAO1-DK and PA14 (**Figure 3.4**).

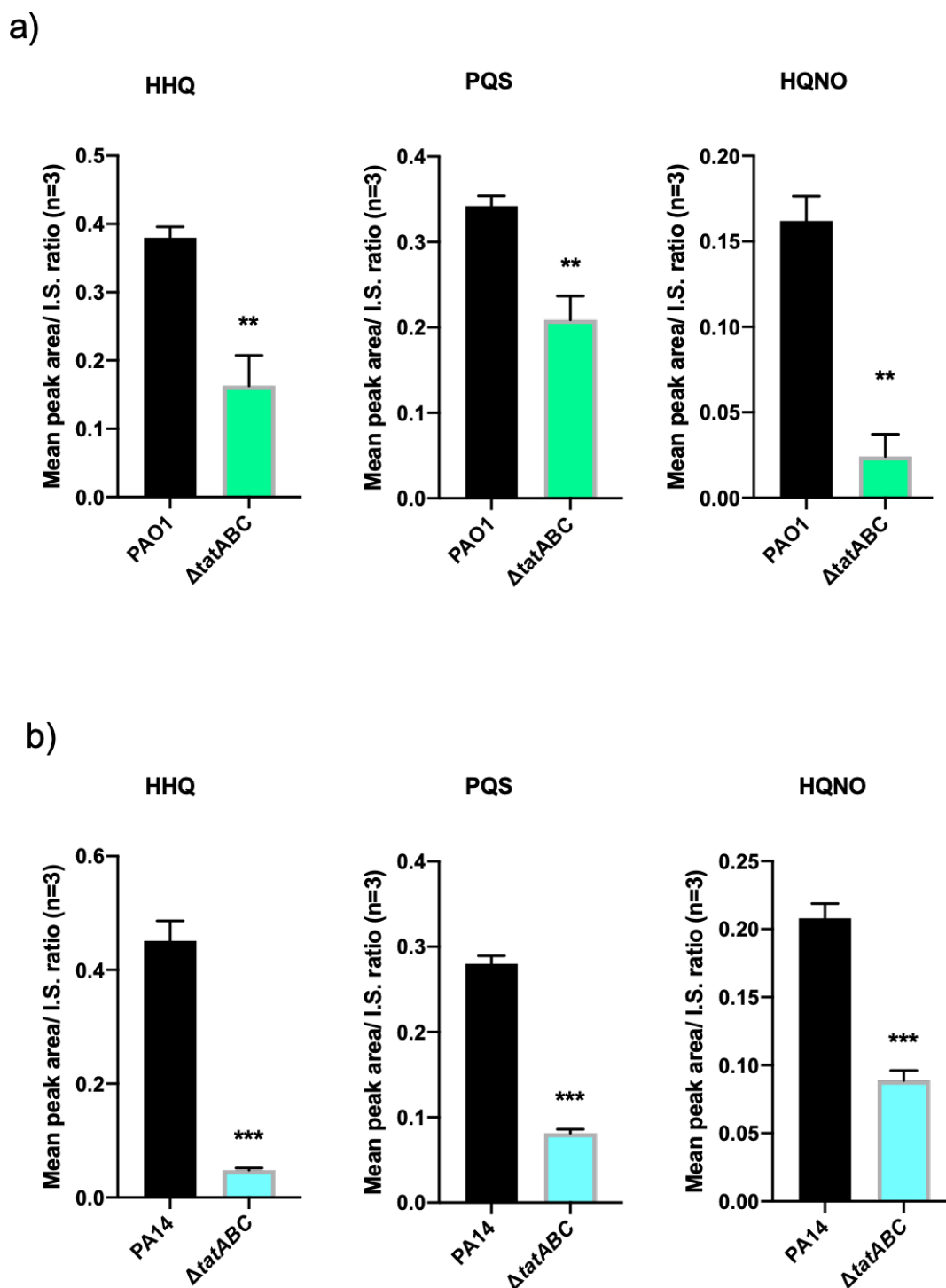


Figure 3.4. HHQ, PQS and HQNO in culture supernatants following 16 h growth. Alkyl-quinolones extracted and semi-quantified with LC-MS/MS from a) PAO1 and PAO1 Δ *tatABC* and b) PA14 and PA14 Δ *tatABC*. Experiments were carried out in triplicate and statistical significance was determined by t-tests.

In addition to LC-MS/MS analysis, secreted AQs in culture supernatants were detected using a biosensor. The biosensor consists of the strain PAO1-DK $\Delta pqsA$, which is unable to synthesise its own AQs, and the promoter fusion $miniCTX::pqsA'-lux$ inserted onto the chromosome. This acts as a bioluminescent reporter for exogenous AQs including HHQ and PQS, but not for AQ *N*-oxides such as HQNO. Exogenous AQs bind the regulator PqsR, increasing PqsR binding affinity, and *pqsA* expression is induced resulting in bioluminescence (Wade *et al.*, 2005; Xiao, He, *et al.*, 2006).

The culture supernatants of PAO1-DK, PA14 and their respective *tat* mutants were filter sterilised following 16 h growth to remove all cell debris. After mixing with fresh LB at a ratio of 1:2 (supernatant:LB) they were then inoculated with the biosensor strain and *pqsA* expression was measured over 24 h. **Figure 3.5** shows the maximum *pqsA* expression was greater when the biosensor was grown in LB mixed with the wild-type supernatants of both PAO1-DK and PA14 than their respective *tat* mutants. This suggests higher wild-type HHQ and PQS concentrations.

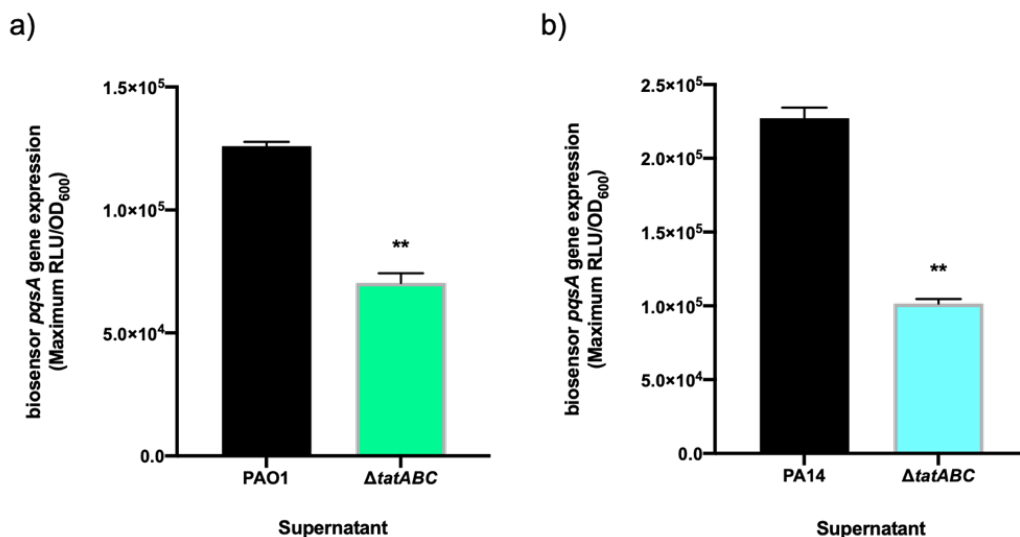


Figure 3.5. Induction of *pqsA* expression in PAO1 $\Delta pqsA$ by exogenous AQs produced by PAO1, PA14 and their respective *tat* mutants. Maximum gene expression over 24 h is plotted for a) PAO1 and PAO1 $\Delta tatABC$ supernatants mixed with fresh LB and b) PA14 and PA14 $\Delta tatABC$ supernatants mixed with fresh LB. t-tests were performed to show statistical significance.

3.2.2. Pyocyanin production

It has been demonstrated that *pqs* QS signal molecule biosynthesis is perturbed upon mutation or deletion of the Tat system (Soh et al, 2021). Downregulation of the biosynthetic operon is matched with lower production and secretion of the AQS. The PQS regulon is wide-reaching, deletion of *pqsA* from *P. aeruginosa* PAO1-N affects the transcription of 158 genes and addition of PQS significantly alters expression of 182 genes (Rampioni et al., 2010; Rampioni et al., 2016). Two nearly-identical operons *phzA1-G1* and *phzA2-G2* are responsible for the biosynthesis of the virulence factor pyocyanin. Addition of PQS increases pyocyanin, and mutation in the *pqs* biosynthesis genes causes a reduction in pyocyanin production (Diggle et al., 2003). To investigate the regulatory effects of disruption to *pqs* QS by deletion of the *tat* system in PA14, pyocyanin was extracted and quantified from culture supernatants. PAO1-W $\Delta phzA1-G1 \Delta phzA2-G2$ was used as a negative control as it does not produce pyocyanin. As such, values for PAO1-W $\Delta phzA1-G1 \Delta phzA2-G2$ were subtracted from the wild-type and $\Delta tatABC$ mutants to remove background noise.

Figure 3.6 shows a significant reduction in pyocyanin in PAO1-DK $\Delta tatABC$ and PA14 $\Delta tatABC$ compared to wild-type concentrations. There is an ~75% reduction in pyocyanin in PAO1-DK $\Delta tatABC$ and ~25% reduction in PA14 $\Delta tatABC$. PA14 produces ~5 fold more pyocyanin than PAO1-DK, as is well-established in the literature. Despite strain differences there was a significant reduction in pyocyanin production in a $\Delta tatABC$ mutant.

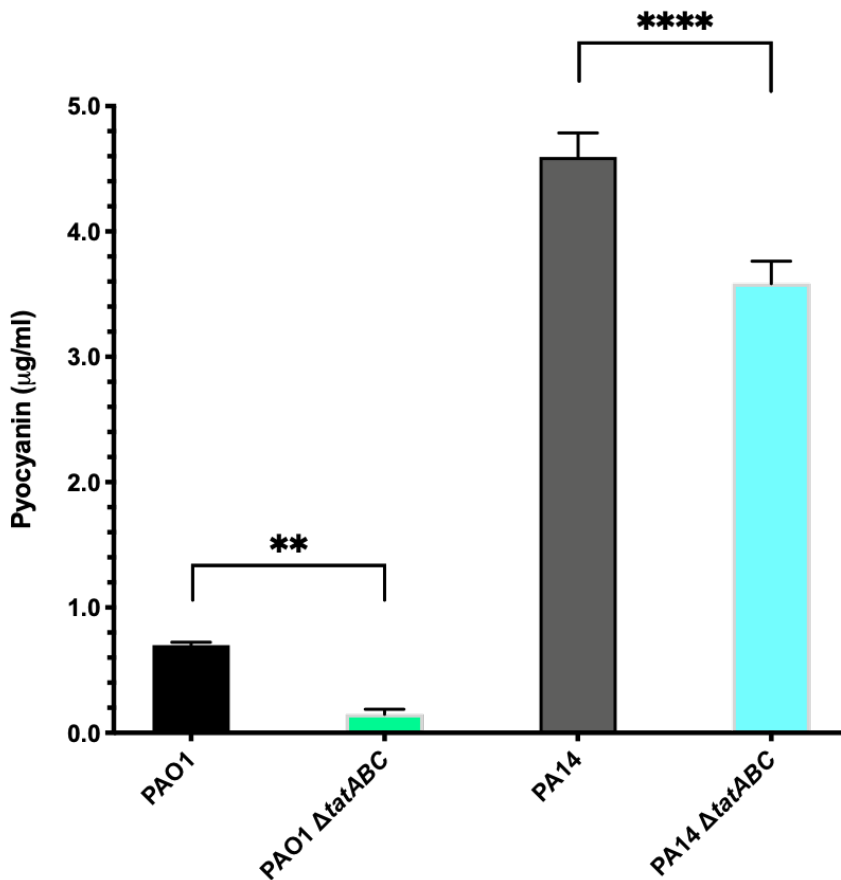


Figure 3.6. Pyocyanin extracted from wild-type and Δ tatABC mutant culture supernatants. Pyocyanin production in wild-type and mutant strains after growth for 8 h in LB at 37°C, shaking 200 rpm. PAO1 Δ phzA1-G1 Δ phzA2-G2 is unable to produce pyocyanin and was used as a negative control. Experiments were repeated in triplicate and t-tests were performed to show statistical significance. Mean values and SD are plotted.

Section Summary

These studies have provided clear evidence that PQS signalling is disrupted in a *tat* mutant and is the likely reason for reduced eDNA release, OMV production, rhamnolipid production and biofilms with deformed architecture (Soh et al, 2021). As this occurs in two common laboratory strains, each isolated from clinical samples, it may also hold true for clinical strains.

3.2.3. Characterisation of the *tat* mutant transcriptome

Differences in the transcriptomic profiles of PAO1-DK and a *tatA* mutant unable to produce the Tat system may point to a possible mechanism by which mutation of the Tat system disrupts PQS signalling as well as highlight additional phenotypes affected. RNAseq was performed by Liang Yang and colleagues (Singapore Centre for Environmental Life Sciences Engineering) and the data was kindly given for analysis with the hope that it would give in-depth insight into the regulatory effects of *tat* mutation. Briefly, PAO1-DK and PAO1-DK *tatA::Tn5* were grown in 24-well plates, 37°C shaking and cells were harvested at early stationary phase for RNA extraction (Appendix, **Figure 7.1**).

There were 355 differentially expressed genes (DEG) in the *tat* mutant, whose difference in expression between wild-type and *tat* mutant was greater than $\log_2(1)$ with a p value < 0.05. These make up 6.37% of the *P. aeruginosa* PAO1-DK genome. Of the 355 genes, 166 were down-regulated and 189 genes were up-regulated in the *tat* mutant. The full table of DEG can be found in the appendix, in **Table 7.1** and **Table 7.2**.

Differentially expressed genes with a magnitude of change greater than 2-fold and an adjusted p value of ≤ 0.05 were considered statistically valid and are shown on the volcano plot in **Figure 3.7**. The most up-regulated genes are towards the right, the most down-regulated are towards the left, and the most statistically significant DEG are towards the top of the graph. The p value was adjusted to eliminate false discovery rate and is shown by a dotted line at $-\log_{10}(\text{Adjusted P-value}) = 1.3$. Only statistically significant changes to gene expression above the threshold value are shown.

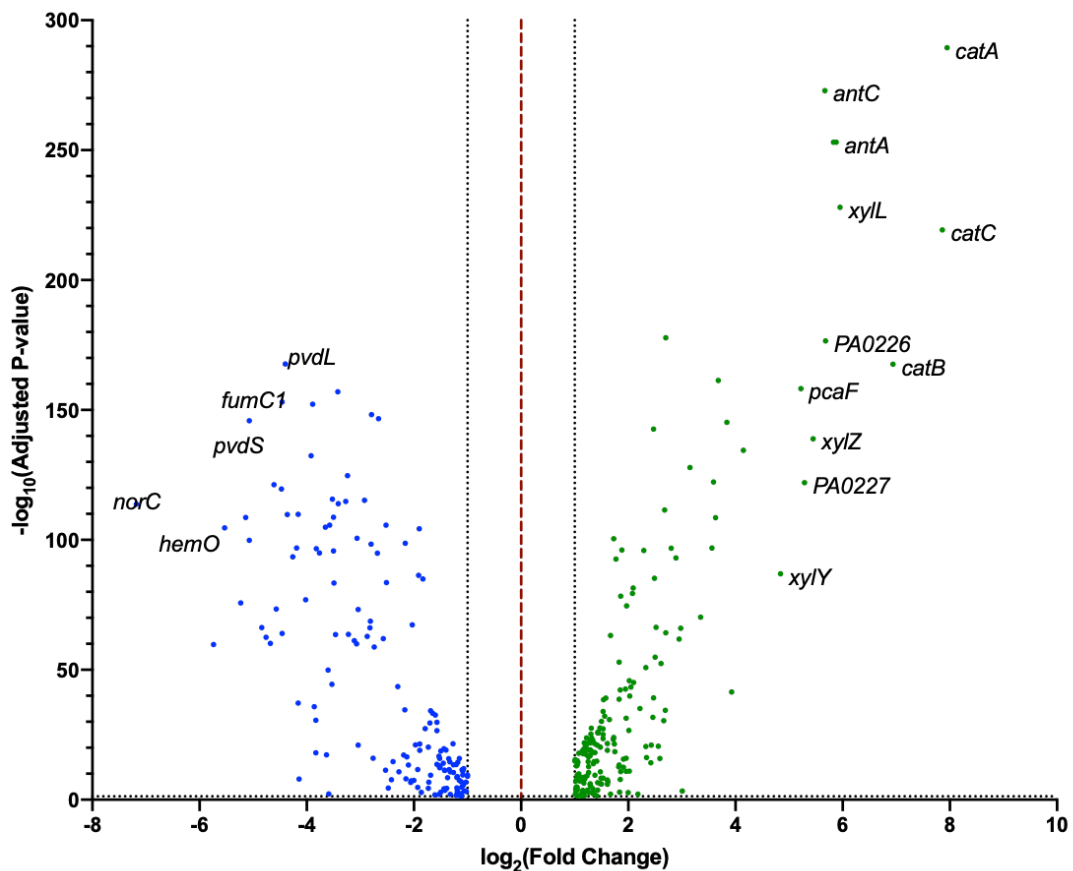


Figure 3.7. Volcano plot of differentially expressed genes in PAO1-DK and a *tat* mutant. The X-axis shows changes to expression ($\log_2(\text{Fold Change})$). The Y-axis shows statistical significance of the difference ($-\log_{10}(\text{Adjusted P-value})$). Green dots represent up-regulated genes and blue dots show down-regulated genes. Differentially expressed genes that are not significantly different ($p > 0.05$) are not shown. Gene expression change smaller than the threshold of $\log_2(\text{fold change}) = (1, -1)$ are not displayed.

Up-regulated Genes

The pathways with the greatest upregulation are carbon utilisation and aromatic ring catabolism. The gene products of *antA*, *antB*, *antC*, *catA*, *catB*, *catC*, *pcaI*, *pcaJ* and *pcaF* are sequentially used in the same catabolic process. This greatly enriched pathway degrades the aromatic compound anthranilate, a key central metabolite used as a precursor for both tryptophan biosynthesis and PQS biosynthesis (Costaglioli *et al.*, 2012). The pathway is outlined in **Figure 3.8**.

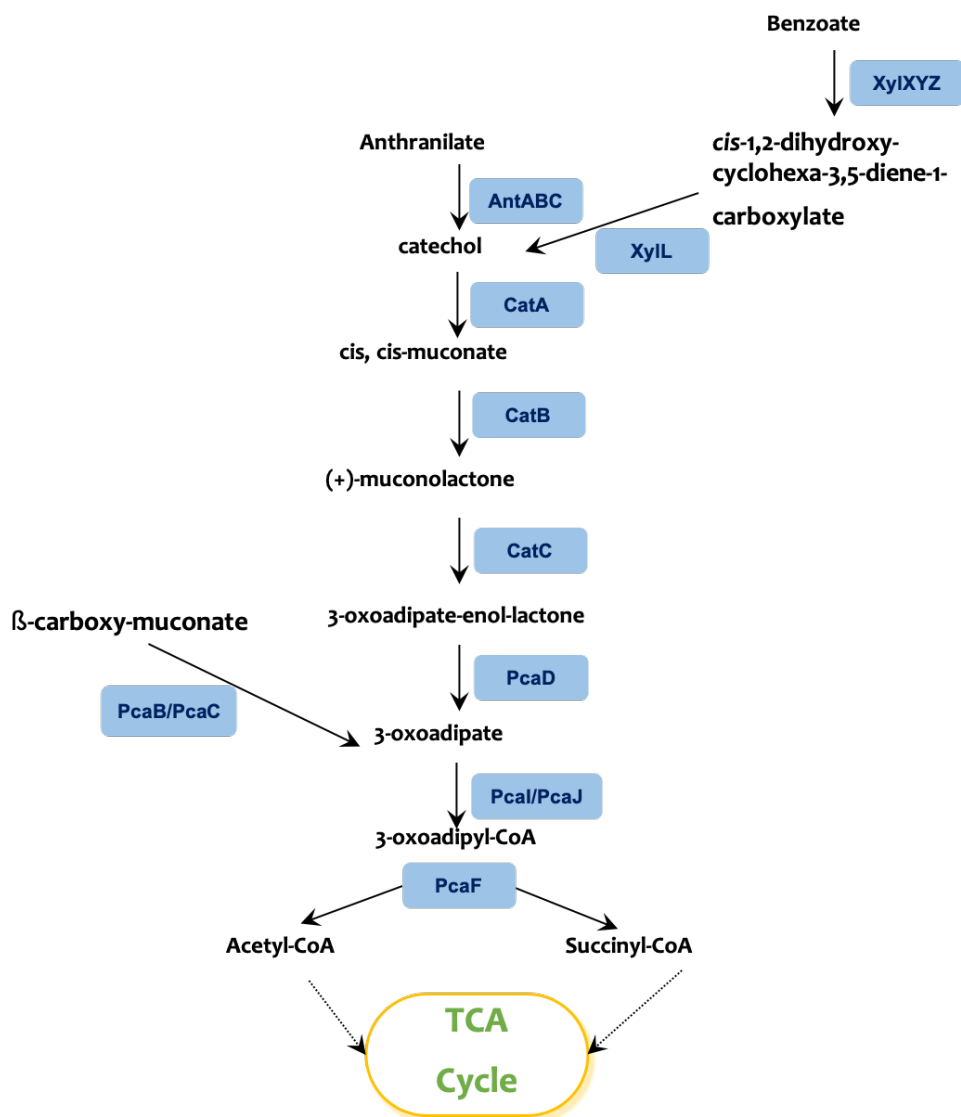


Figure 3.8. The anthranilate degradation pathway. Anthranilate is an aromatic compound degraded to succinyl-CoA or Acetyl-CoA then fed into the TCA cycle for energy production. The enzymes directly involved in this pathway are AntABC, CatA, CatB and CatC, PcaD, PcaI, PcaJ, and PcaF. Figure based off Costaglioli *et al.* 2012.

Figure 3.7 shows the two operons with the highest upregulation are *antABC*, encoding anthranilate dioxygenase and anthranilate dioxygenase reductase, and *catBCA* which encode muconate cycloisomerase I, muconate delta-isomerase, and catechol 1,2-dioxygenase. This pathway converts anthranilate to succinyl-CoA which is then fed into the TCA cycle for energy production as shown in **Figure 3.8** (Costaglioli *et al.*, 2012). There is a minimum 50-fold upregulation

of *antA*, *antB* and *antC* (**Table 3.1**). The gene products of *antR* and *catR* are the positive transcriptional regulators AntR and CatR. AntR utilises anthranilate as a coinducer for the expression of both *antABC* and *catBCA* operons, whereas CatR up-regulates expression of *catBCA* when *cis*, *cis*-muconate is bound (Parsek *et al.*, 1992; Kim *et al.*, 2012).

Feature	Annotation	Database Identifier	Fold Change In Tat Mutant
<i>antA</i>	anthranilate dioxygenase large subunit	PA2512	58.99
<i>antB</i>	anthranilate dioxygenase small subunit	PA2513	56.85
<i>antC</i>	anthranilate dioxygenase reductase	PA2514	50.74
<i>antR</i>	transcriptional regulator	PA2511	12.79
<i>catA</i>	catechol 1,2-dioxygenase	PA2507	247.89
<i>catB</i>	muconate cycloisomerase I	PA2509	122.95
<i>catC</i>	muconolactone delta-isomerase	PA2508	231.89
<i>catR</i>	transcriptional regulator	PA2510	5.50
<i>pcaC</i>	i-carboxymuconolactone decarboxylase	PA0232	8.85
<i>pcaD</i>	b-ketoadipate enol-lactone hydrolase	PA0231	7.73
<i>pcaB</i>	3-carboxy- <i>cis,cis</i> -muconate cycloisomerase	PA0230	7.87
<i>pcaT</i>	dicarboxylic acid transporter	PA0229	11.77
<i>pcaF</i>	beta-ketoadipyl CoA thiolase	PA0228	37.34
<i>pcaJ</i>	probable CoA transferase, subunit B	PA0227	39.15
<i>pcaI</i>	probable CoA transferase, subunit A	PA0226	51.36

Table 3.1. Expression of genes involved in anthranilate degradation is up-regulated in the absence of a Tat protein export system.

The highly up-regulated genes *xylL*, *xylZ*, *xylY*, *xylX*, and *xylS* are also involved in aromatic ring catabolism (**Figure 3.8**). Located on the opposite strand, they are adjacent to *antC* on the *P. aeruginosa* chromosome. KEGG (Kyoto encyclopedia of genes and genomes) pathway analysis revealed that these genes are part of the xylene degradation KEGG pathway and the benzoate degradation KEGG pathway (Kanehisa *et al.*, 2008). The gene products of *xylZ*, *xylY*, *xylX*, and *xylL* catalyse the reaction of methylbenzoate to 3-methylcatechol and

4-methylcatechol, the latter of which is a substrate of the overexpressed *catA* (**Figure 3.8**). Among the most enriched pathways are the *pca* genes, also involved in the degradation of aromatic compounds and carbon utilisation. Another significantly enriched pathway were genes involved in type III secretion (all *psc* genes, *pop* genes, *exs* genes, and *pcr* genes).

Down-regulated Genes

Enzymes involved in anaerobic respiration are among the most enriched down-regulated genes in a *tat* mutant. Nitric oxide (NO) reductase (NOR) and Nitrite reductase (NIR) are encoded by *norCBD* and *nirSMCFDLGHJEN* genes respectively and are located together in the genome (Arai, 2011). Nitrite reductase catalyses the reduction of nitrite to NO (**Figure 3.9**). *nirS* (structural gene) and *nirC* (a monoheme cytochrome *c*) are down-regulated by a fold change of -3.22 and -2.89 respectively but there is no change in expression of the genes for the regulators Anr and Dnr. NOR consists of NorB, a cytochrome *b* subunit, and NorC, a cytochrome *c* subunit (Arai, 2011). NorD is a possible denitrification protein, it is needed for creation of the active enzyme. Transcripts of *norB*, *norC*, and *norD* have a fold change of -16.19, -145.07 and -2.62 respectively. Both NIR and NOR accept electrons from the cytochrome *bc1* complex via cytochrome *c* during anaerobic respiration (Arai, 2011).

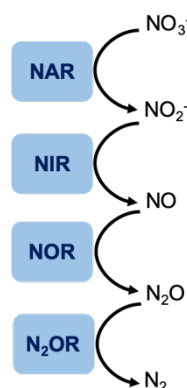


Figure 3.9. Anaerobic respiration pathway. During anaerobic respiration nitrogen oxides are used to accept electrons. NAR (nitrate reductase), NIR (nitrite reductase), NOR (nitric oxide reductase) and N_2OR (nitrous oxide reductase).

Down-regulated genes also include those involved in oxidative processes and oxidative stress (*sodM*, *hemO*), general stress response (*dnaK*) (Hare *et al.*, 2011). The *mexGHI* operon, the products of which form an RND efflux transporter, is highly expressed in the wild-type but down-regulated ~3-fold upon *tat* mutation.

Genes involved in iron chelation and response to low iron levels are significantly lower in a *tat* mutant. The biosynthetic pathways for the siderophores pyoverdinin and pyochelin (*pvd* genes and *pch* genes respectively), ferric-pyoverdinin import and iron dissociation (*fpv* genes), iron starvation (*PA4469*, *fumc1*, *fagA*), cell-surface signalling and import of heterologous siderophores (*femI*, *femR*, *femA*) are all repressed in a *tat* mutant (Llamas *et al.*, 2008; Schalk and Guillon, 2013; Ganne *et al.*, 2017).

Interestingly, the transcription of two small regulatory RNAs *prfF1* and *prfF2* is down-regulated. PrrF1 and PrrF2 repress *antR* and *antABC* expression under iron-depleted conditions. They also repress transcription of bacteroferritin *bfrB*, and probable bacteroferritin *PA4880* in low iron states, both of which have significantly lower expression in PAO1-DK Δ *tatABC*. (Oglesby *et al.*, 2008).

DEG can be characterised using the gene function classification system based on gene ontology (GO). This can be found at www.geneontology.org, and covers 3 areas: biological process, cellular compartment (location) and molecular function. Significantly enriched terms can be seen in **Figure 3.10**, **Figure 3.11** and **Figure 3.12**. **Figure 3.10** shows that DEG were found for proteins covering all cellular compartments, from cytoplasm all the way across the cell envelope to extracellular locations.

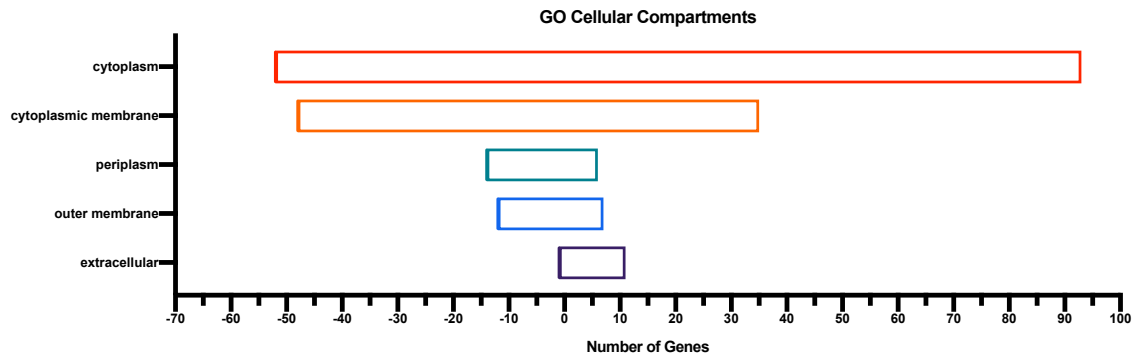


Figure 3.10. GO cellular compartments. Gene product locations of differentially expressed genes throughout the *P. aeruginosa* cell. Cytoplasm, 145 DEG; cytoplasmic membrane, 83 DEG; periplasm, 20 DEG; outer membrane, 19 DEG; extracellular space, 12 DEG.

Overall there were 254 biological processes listed, of which 117 were down-regulated and 136 were up-regulated (**Figure 3.11**). The most overexpressed GO biological processes were the genes involved in type III secretion, pathogenesis, oxidation-reduction and carbon utilisation through cellular catabolic processes. Genes involved in iron scavenging were mostly down-regulated. For example, biosynthesis of siderophores pyoverdine and pyochelin, siderophore transport, iron acquisition, and regulation of iron transport all show a reduction in gene expression.

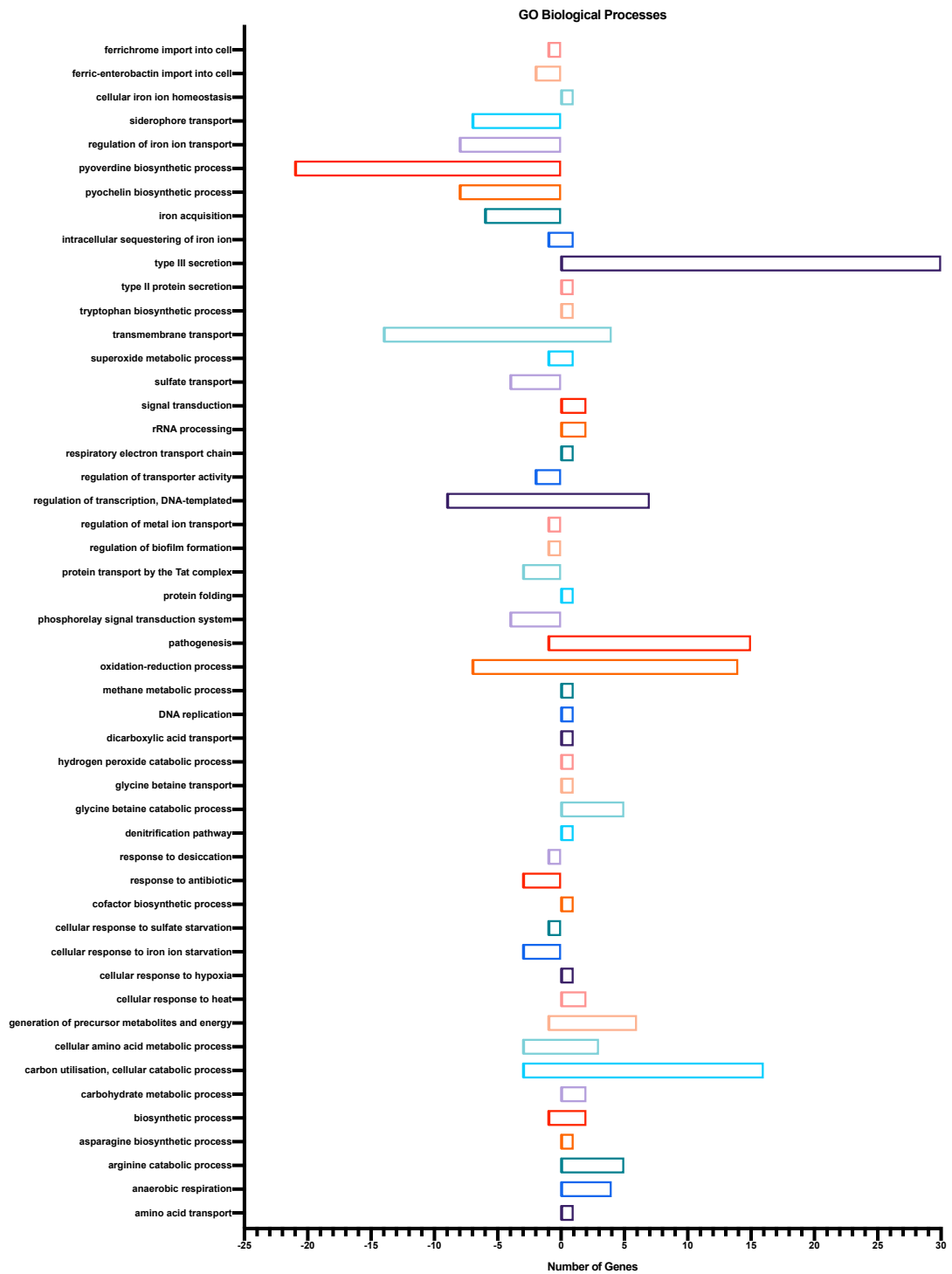


Figure 3.11. GO biological processes of differentially expressed genes in PAO1 *tat* mutant compared with PAO1 wild-type. The x-axis shows number of genes, positive numbers are up-regulated genes, down-regulated genes are negative numbers. The y-axis shows GO biological processes.

Of the 355 genes that were differentially expressed, only 52 GO molecular functions were assigned. Of these, 18 were down-regulated and 34 were up-regulated (**Figure 3.12**).

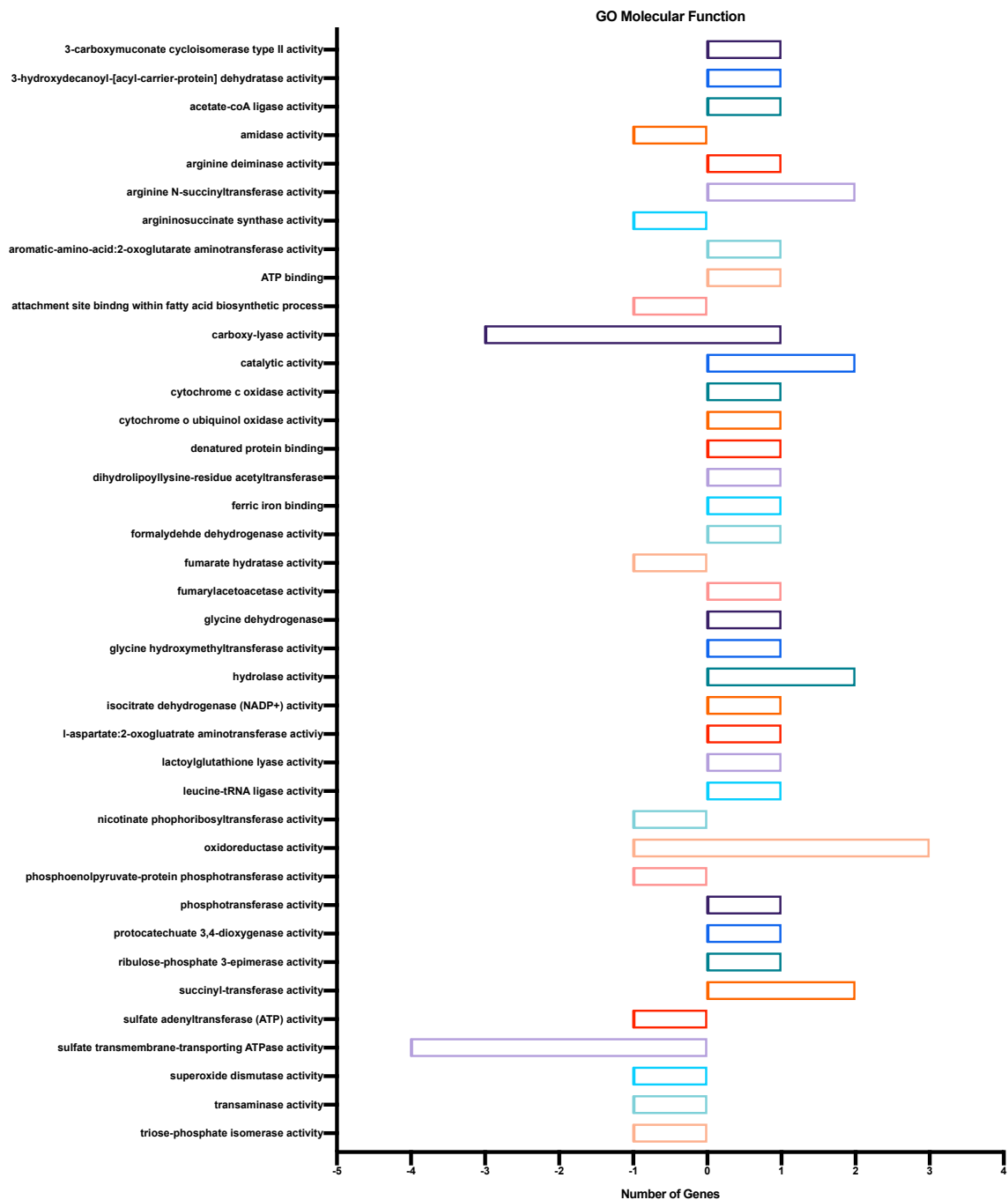


Figure 3.12. GO molecular functions of differentially expressed genes. The y-axis lists 39 GO terms and the x-axis shows the number of genes for each term that are expressed differentially in a PAO1 *tat* mutant compared to PAO1 wild-type.

Sulfate-transmembrane transporting ATPase activity and carboxy-lyase activity are among the most down-regulated GO molecular functions. Oxidoreductase activity, hydrolase activity, succinyl-transferase activity, N-arginine succinyl-transferase activity, catalytic activity occur in 2 or more up-regulated genes.

There are 34 different proteins known to be exported by the Tat system in *P. aeruginosa* (Gimenez *et al.*, 2018). Of these, 10 had altered expression in the *tat* mutant. The gene *fdnG*, the major subunit of formate dehydrogenase-O, was up-regulated and the genes *oprH*, *PA2328*, *pvdR*, *pvdP*, *pvdN*, *PA2531*, *nosZ*, *PA3768*, and *PA4159* were all down-regulated. The PVD biosynthesis genes and *nosZ*, which is involved in denitrification, are likely down-regulated due to disruption to *pqs* QS (Rampioni *et al.*, 2016).

3.2.4. Comparison of *tat* mutant and $\Delta pqsA$ mutant transcriptomes

There are 355 differently expressed genes upon mutation of the *tat* operon. Many of these are regulated by PQS-dependent quorum sensing. Changes to gene expression in an isogenic *pqsA* mutant unable to synthesise AQS were compared with the modulated transcriptome of a *tat* mutant using published transcriptomic data of PAO1-N $\Delta pqsA$ vs wild-type PAO1-N (Rampioni *et al.*, 2010; Rampioni *et al.*, 2016). Deletion of *pqsA* in PAO1-N alters expression of 158 genes, 2.8% of the *Pseudomonas* genome. Of these 54 are up-regulated and 104 are down-regulated, as seen in **Figure 3.13a** (Rampioni *et al.*, 2010).

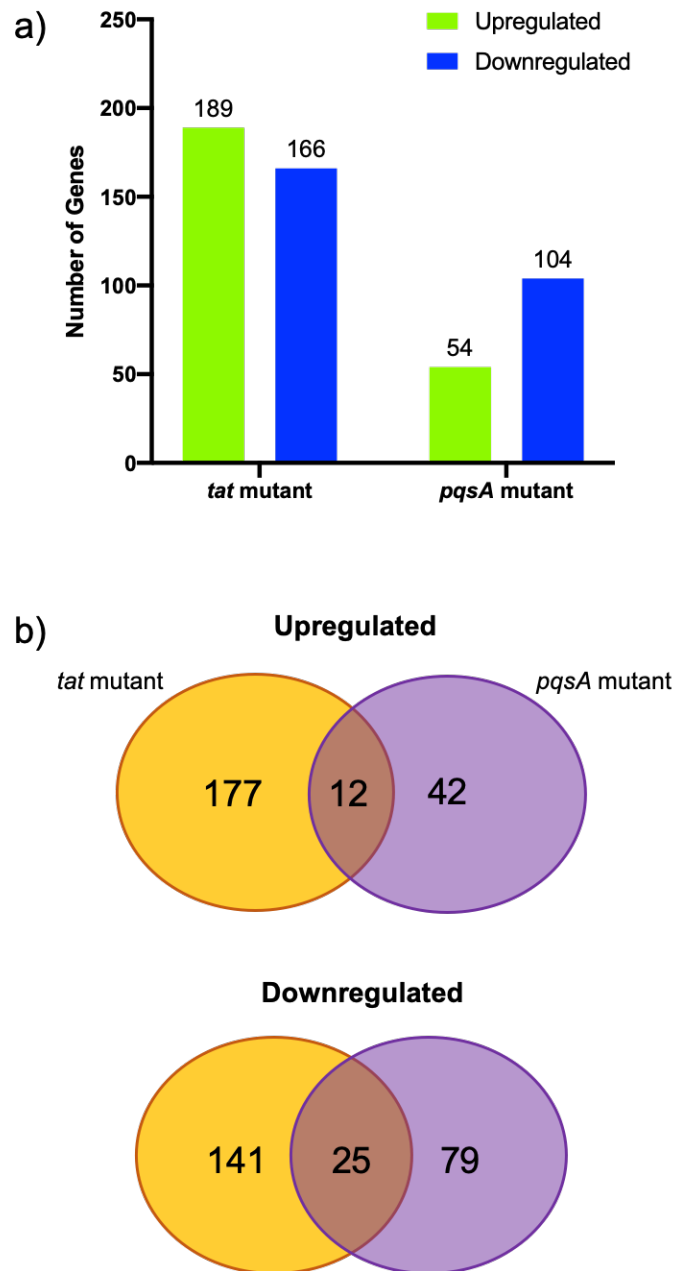


Figure 3.13. Differently expressed genes of PAO1 WT vs *pqsA* mutant and PAO1 WT vs *taf* mutant. Proportions of up-regulated and down-regulated genes (a) and venn diagram showing the number of genes with shared changes to expression (b).

Figure 3.13b demonstrates the number of genes with shared altered expression upon mutation of either *taf* or *pqsA* in PAO1. Overall 6.34% of the genes up-regulated in the *taf* mutant are also up-regulated in a *pqsA* mutant, this

increases to 15% of down-regulated genes. The *tat* mutant shares modulated expression of 37 genes with the *pqsA* mutant, all of which are listed in **Table 3.2**.

Among the down-regulated genes in a *pqsA* and *tatA* mutant are those involved in pyochelin biosynthesis, its regulation and uptake (*pchI*, *pchF*, *pchE*, *pchR*, *pchD*, *pchC*, *pchB*, *pchA*), pyoverdine biosynthesis (*PA2412*, *pvdH*), antibiotic resistance (*mexG*, *mexH*, *mexI*, *opmD*, *ampP*) and iron starvation (*PA4469*, *fumC1*, *fagA*). The *mexGHI* operon is under the control of PqsE (Rampioni *et al.*, 2016). A putative flavin-dependent monooxygenase, *PA2274*, and a protein involved in alkaline protease secretion, *aprX* are similarly down-regulated in both mutants (Rampioni *et al.*, 2010).

The genes *catABC*, *PA0226*, *pcaF*, are all up-regulated in an isogenic *pqsA* mutant and *tatA* mutant. These are involved in carbon utilisation through catabolism of catechols. The transcriptional regulator *xyIS* is also up-regulated. Transcription of *xyIS* occurs from two start sites, Ps1 and Ps2. Ps2 is a constitutive promoter, however Ps1 is regulated and responds to the intracellular XylS concentration (Zwick *et al.*, 2013). Similarly increased expression is seen in *dctA*, a C4-dicarboxylate transport protein, and *ddaR* a transcriptional regulator controlling methylarginine hydrolysis (Valentini *et al.*, 2011; Lundgren *et al.*, 2017). Interestingly, *PA5071*, the last gene in the operon containing the *tatABC* genes is up-regulated in both mutants. A BLASTN search revealed this gene sequence is unique to *Pseudomonas aeruginosa* however *PA5071* is predicted to have ribosomal RNA methyltransferase activity. The rRNA processing gene *ybiN* is also up-regulated.

Some genes have induced expression in a *tat* mutant which is reduced in a *pqsA* mutant. These include *PA1218*, a hypothetical protein, and subunits of the terminal electron acceptor cytochrome *o* ubiquinol oxidase, *cyoA* and *cyoC*.

Database Identifier	Gene name	Product name	Fold Change vs PA01	
			<i>pqsA</i> mutant	<i>tat</i> mutant
PA0212	<i>mdcE</i>	malonate decarboxylase gamma subunit	3.288	-3.25
PA0226	-	probable CoA transferase, subunit A	7.437	51.36
PA0228	<i>pcaF</i>	beta-ketoadipyl CoA thiolase	3.241	37.34
PA1183	<i>dctA</i>	C4-dicarboxylate transport protein	2.986	2.04
PA1196	<i>ddaR</i>	Probabile transcriptional regulator	1.516	2.60
PA1218	-	hypothetical protein	-2.458	2.45
PA1245	<i>aprX</i>	hypothetical protein	-1.515	-2.61
PA1317	<i>cyoA</i>	cytochrome o ubiquinol oxidase subunit II	-2.258	2.12
PA1319	<i>cyoC</i>	cytochrome o ubiquinol oxidase subunit III	-2.604	2.45
PA1429	-	probable cation-transporting P-type ATPase	1.702	2.90
PA1837	-	hypothetical protein	-1.862	-2.50
PA2033	-	hypothetical protein	-1.707	-17.90
PA2169	-	hypothetical protein	-1.747	2.03
PA2274	-	hypothetical protein	-17.122	-5.71
PA2412	-	conserved hypothetical protein	-1.786	-28.57
PA2413	<i>pvdH</i>	L-2,4-diaminobutyrate:2-ketoglutarate 4-aminotransferase	-1.674	-7.06
PA2506	-	hypothetical protein	2.349	15.28
PA2507	<i>catA</i>	catechol 1,2-dioxygenase	3.125	247.89
PA2508	<i>catC</i>	muconolactone delta-isomerase	2.544	231.89
PA2509	<i>catB</i>	muconate cycloisomerase I	3.597	122.95
PA2519	<i>xylS</i>	transcriptional regulator XylS	2.077	12.06
PA3718	-	probable MFS transporter	-2.242	-2.28
PA3840	<i>ybiN</i>	conserved hypothetical protein	1.71	3.55
PA4205	<i>mexG</i>	hypothetical protein	-2.944	-3.73
PA4206	<i>mexH</i>	RND, efflux membrane fusion protein precursor	-5.338	-3.14
PA4207	<i>mexI</i>	RND, efflux transporter	-7.925	-3.21
PA4208	<i>opmD</i>	probable outer membrane protein precursor	-20.813	-3.02
PA4218	<i>ampP</i>	probable transporter	-4.928	-7.54
PA4221	<i>fptA</i>	Fe(III)-pyochelin outer membrane receptor precursor	-7.076	-11.86
PA4222	<i>pchI</i>	probable ATP-binding component of ABC transporter	-7.157	-9.45
PA4225	<i>pchF</i>	pyochelin synthetase	-71.483	-11.95
PA4226	<i>pchE</i>	dihydroaeruginic acid synthetase	-139.217	-15.94

PA4227	<i>pchR</i>	Transcriptional regulator PchR	-8.728	-6.39
PA4228	<i>pchD</i>	pyochelin biosynthesis protein PchD	-21.066	-14.81
PA4229	<i>pchC</i>	pyochelin biosynthetic protein PchC	-1.611	-11.28
PA4230	<i>pchB</i>	salicylate biosynthesis protein PchB	-27.171	-10.63
PA4231	<i>pchA</i>	salicylate biosynthesis isochorismate synthase	-32.538	-9.26
PA4469	-	hypothetical protein	-1.512	-35.32
PA4470	<i>fumC1</i>	fumarate hydratase	-1.657	-22.00
PA4471	<i>fagA</i>	hypothetical protein	-1.598	-27.09
PA4513	<i>piuB</i>	probable oxidoreductase	-2.34	-2.04
PA5071	-	conserved hypothetical protein	1.873	10.19

Table 3.2. List of DEG in a *pqsA* mutant and a *tat* mutant when compared with PAO1 wild-type.

3.2.5. Expression of the twin-arginine transport system

The *P. aeruginosa* Tat system is encoded on a 6 gene operon under the control of the *hisI* promoter shown in **Figure 3.14**. The gene products of *hisIE* are histidine biosynthesis enzymes phosphoribosyl-AMP cyclohydrolase and phosphoribosyl-ATP pyrophosphohydrolase respectively. These are followed by the three genes encoding the Tat system, *tatABC*. The final gene in the operon is *PA5071*, a conserved hypothetical protein predicted to be rRNA small subunit methyltransferase.



Figure 3.14. Operon containing genes encoding the twin-arginine transport system. Gene products located in the cytoplasm are coloured green, those located in the cytoplasmic membrane are coloured yellow.

Transcriptome analysis with RNAseq of a *tat* mutant showed no change in *hisIE* expression. However, it is possible that mutation or deletion of the Tat system may have regulatory effects on its own expression. A bioluminescent transcriptional reporter for the promoter of the *tatABC* operon was constructed for further investigation. The reporter was then inserted onto the bacterial chromosome of PAO1-DK, PAO1-DK *tatA*::Tn5, and PAO1-DK Δ *tatABC* as well as the Δ *pqsA* mutant and Δ *pqsA* *tatA*::Tn5 double mutant. Expression from the promoter was measured across 24 h and the maximum expression for each strain can be seen in **Figure 3.15**.

Overexpression of *hisI* was seen in the *tatA*::Tn5 mutant, which confirms the increase in PA5071 transcription seen from RNAseq analysis. Expression of the *tat* genes was also up-regulated upon deletion of *pqsA*. Surprisingly, *hisI* was slightly down-regulated in a Δ *tatABC* mutant, and even further down-regulated in a Δ *pqsA* *tatA*::Tn5 double mutant despite being up-regulated in Δ *pqsA* and *tatA*::Tn5 single mutants.

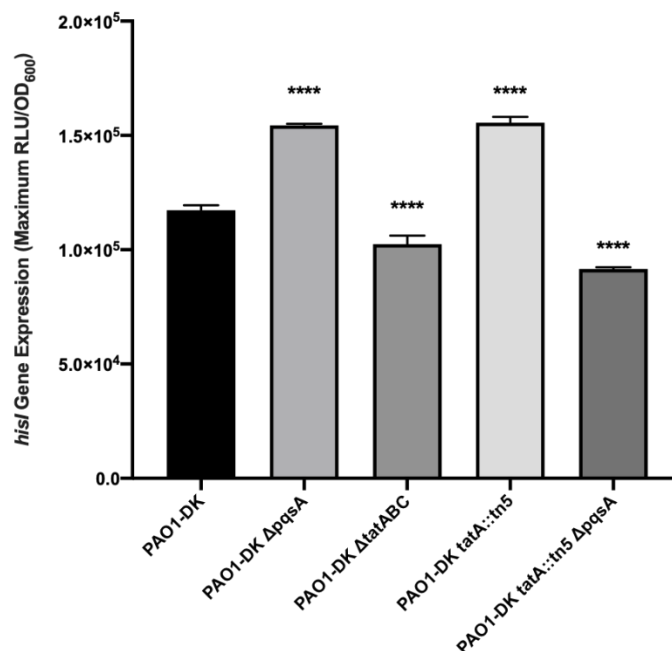


Figure 3.15. Maximum expression of the *hisI-hisE-tatA-tatB-tatC-PA5071* operon was elevated in Δ *pqsA* and *tatA*::Tn5 mutants but reduced in the double mutant and in PAO1 Δ *tatABC*. Strains were grown over 24 h in 200 μ l cultures at 37°C. Expression was measured with a chromosomally-inserted miniCTX::*hisI-lux* promoter fusion. One-way ANOVA determined statistical significance.

Each mutant exhibited a modulated expression profile across 24 h growth (Figure 3.16). PAO1-DK $\Delta pqsA$ and PAO1-DK $\Delta tatABC$ had the most similar expression profile to wild-type, as they both peaked at ~ 7 hours. The expression of *hisI* in PAO1-DK *tatA::Tn5* and PAO1-DK *tatA::Tn5* $\Delta pqsA$ did not have a clear, short, peak and once reached, it remained high for the rest of the sampling time. It appears that using a *tatA* transposon insertion affected expression of the *tatABC* operon to a greater extent than a deletion.

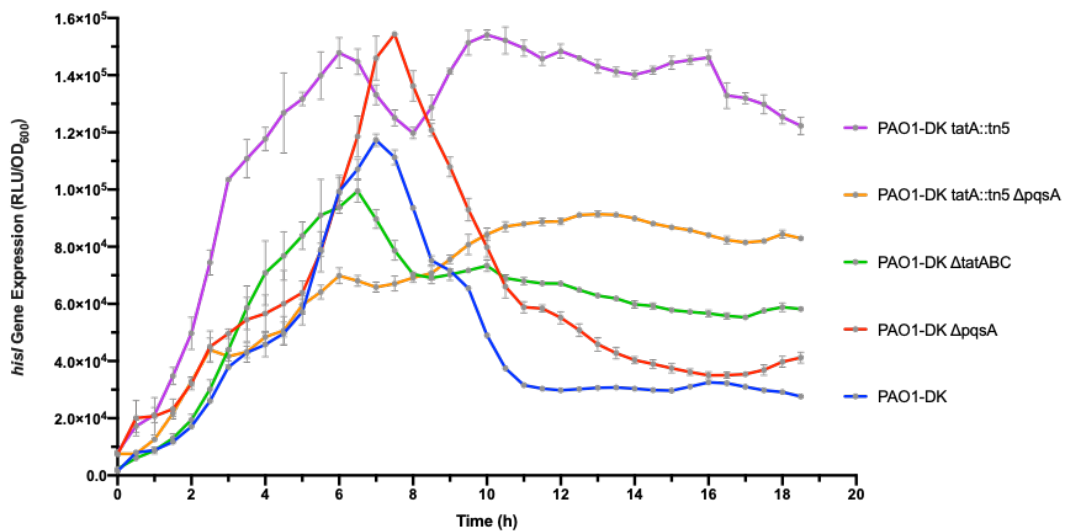


Figure 3.16. Expression of the *tat* operon promoter (*hisI'*) remained elevated instead of exhibiting a transient peak when *tatA* was interrupted by a transposon irrespective of PQS deletion. Expression in wild-type PAO1, a $\Delta pqsA$ mutant, $\Delta tatABC$ deletion mutant and *tat* transposon mutant was measured by following luminescence and OD₆₀₀ every 30 min across 24 h growth in 96-well plates. Mean and SD are plotted for each timepoint.

Section Summary

Genes involved in anthranilate degradation are up-regulated in a *tat* mutant to a greater degree than any other pathway. Many down-regulated genes, such as those involved in iron acquisition, are under the control of PQS QS regulation. PqsA, the first enzyme in the *pqsABCD/phnAB* operon is an anthranilate-CoA ligase (Coleman *et al.*, 2008). The up-regulated enzymes in the anthranilate degradation pathway consist of nearly the entire pathway, and follow the degradation of anthranilate up to the creation of succinyl-CoA which is fed directly into the Tri-carboxylic acid (TCA) cycle. This suggests that the reduction in PQS by the Tat mutant could be due to upregulation in precursor degradation. The genes involved in anthranilate degradation that are up-regulated in the PAO1-DK *tat* mutant can be found clustered together on the chromosome.

3.2.6. Construction of bioluminescent transcriptional reporters to study expression of the anthranilate degradation pathway

RNAseq data strongly suggested that when the Tat system is inactivated, genes within the anthranilate degradation pathway are up-regulated. In order to confirm these findings and further understand the expression of the anthranilate degradation pathway, bioreporters were created for real-time measurement of expression. A transcriptional fusion was created between each promoter region of the first two operons in the pathway (*antABC* and *catBCA*) and the *luxCDBAE* operon on a miniCTX vector. This vector inserts into a neutral location (CTX site) on the *P. aeruginosa* chromosome, and the *lux* operon is under the control of the promoter of interest (Appendix, **Figure 7.2**) (Michael K. Winson *et al.*, 1998; Calvo *et al.*, 2000).

LuxCDE, a fatty acid reductase, synthesises tetradecanal, a substrate of the luciferase LuxAB and together with readily available reduced flavin mononucleotide and molecular oxygen luciferase catalyses the reaction that emits light at 490 nm wavelength (Meighen, 1991). As a result, the level of gene expression is measurable through bioluminescence and this method provides a simple, comparable assay for transcriptional regulation and expression.

In addition to the *antA* and *catB* promoters, the promoters of their transcriptional regulators *antR* and *catR* were also cloned into the *miniCTX::lux* vectors (Appendix, **Figure 7.3**). *In silico* analysis of the upstream regions for each gene was carried out using Softberry BPROM s70 promoter tool to predict the start site and promoter sequence. Promoters for *antA* and *antR* have been published after they were determined experimentally (Kim *et al.*, 2012).

3.2.7. Anthranilate degradation is greater in *tat* pathway mutants

To determine the effect of a *tat* mutation on the expression of the first two operons in the anthranilate degradation pathway (*antABC* and *catBCA*) and of their corresponding regulators (*antR* and *catR*), bioluminescent transcriptional reporters were inserted into the bacterial chromosomes and bioluminescence was measured over a period of 24 h. The expression of the anthranilate degradation pathway was studied in PAO1-DK and PA14, and Tat system mutants of each strain.

PAO1-DK *antA* and *antR* expression was up-regulated ~3 fold in the *tatA* transposon mutant (**Figure 3.17**) and all genes of interest exhibited a modulated expression profile upon *tat* mutation. There was a delay in reaching the maximum gene expression for *antA*, *antR*, and *catB* which occurred at 10 h, 12 h, and 6 h in PAO1-DK, and 13 h, 18 h and 11 h in a *tat* mutant. Induced expression of *catB* occurred earlier than *antA* despite it being further down the anthranilate degradation pathway.

The greatest expression was seen in the genes associated with the anthranilate degradation pathway, with *antA* expressed more than *catB* (**Figure 3.17**). There was a ~2 fold increase in expression of *catB* upon mutation of the Tat system. The expression of *catR* was decreased slightly in the Tat mutant and there was no delay in expression.

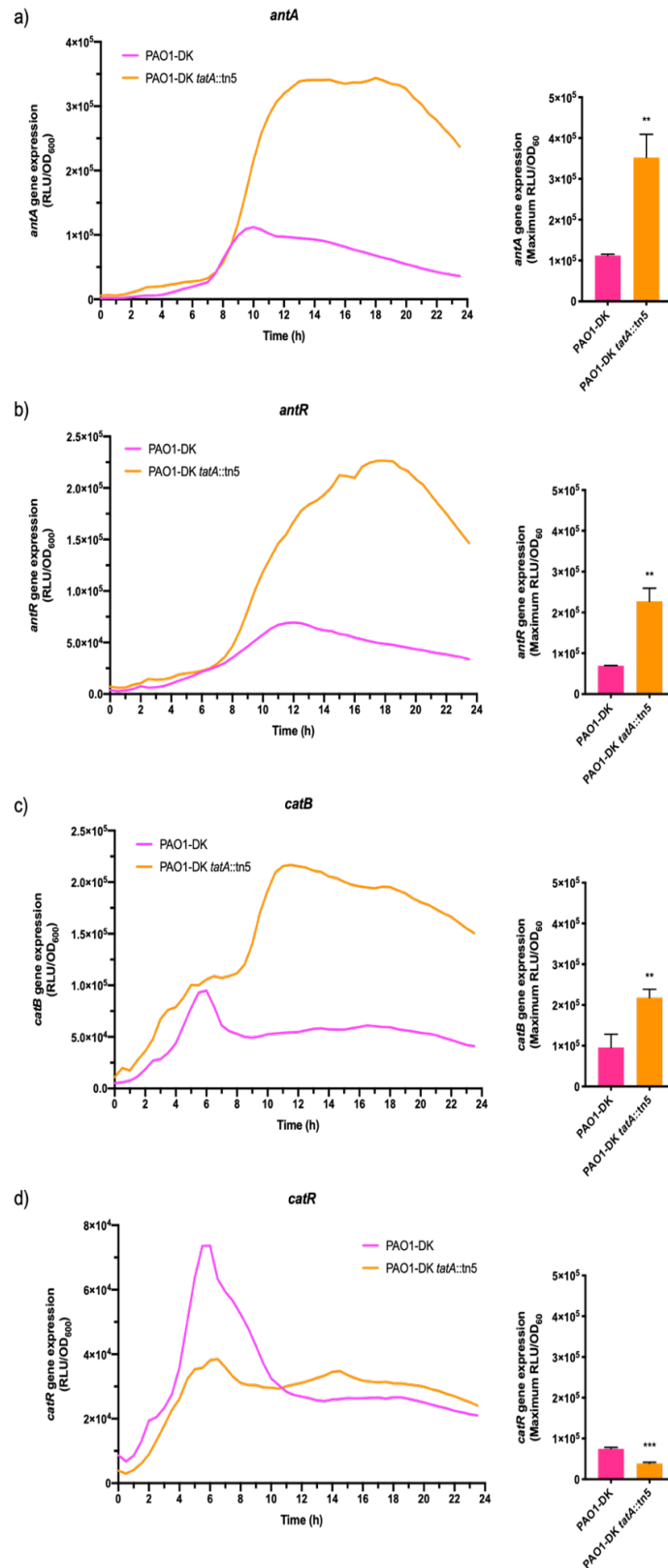


Figure 3.17. Expression of *antA*, *antR*, *catB* and *catR* in wild-type PAO1 and a *tat* mutant. Activity of the miniCTX::*lux* promoter fusions was standardised over growth (OD₆₀₀) of each strain. Expression (RLU/OD₆₀₀) was measured every 30 min over a 24 h period of growth in 96-well plates, 37°C. Maximum gene expression is shown on the right of each graph. Mean and SD are shown, as is statistical significance determined by t-tests. Experiment was repeated three times and in triplicate.

Expression of the anthranilate degradation pathway over 24 h was very different in PA14 (**Figure 3.18**). Wild-type PA14 exhibited a steady increase in expression of *antA* and *antR* over 20 h before reaching its maximum expression. The maximum expression of *catB* occurred at around 15 h and *catR* maximum expression was at 18 h. Upon deletion of the *tatABC* operon there was a characteristic delay in expression, and the expression from each promoter continued to rise over 24 h, and may continue to rise past that.

PA14 Δ *tatABC* also exhibited upregulation from the *antA* and *catB* promoters (**Figure 3.18**). The increase in expression was not as great as that seen in PAO1-DK but was nonetheless significantly different, as established using a t-test. Expression of *antR* and *catR* was reduced upon deletion of the Tat system.

It is worth noting that expression of the *antABC* operon was higher in PAO1-DK than in PA14 and this difference was reversed for the *catBCA* operon, where expression was lower in PAO1-DK. This was likely due to natural variance between strains and their regulation of the genes being studied. The expression level of *antR* and *catR* is similar between both strains.

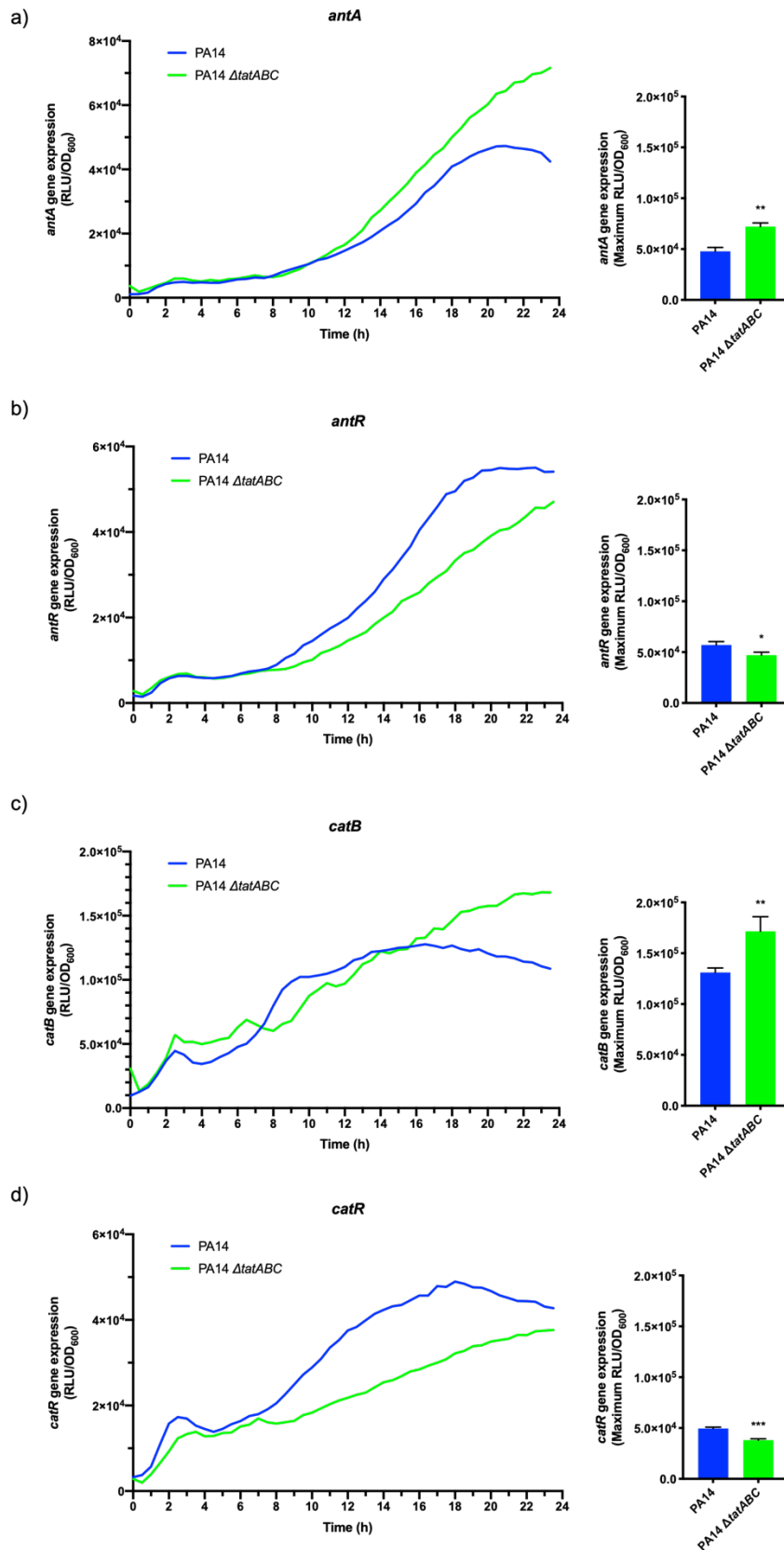


Figure 3.18. Expression of *antA*, *antR*, *catB* and *catR* in PA14 and PA14 Δ tatABC. Activity of the miniCTX::*lux* promoter fusions was standardised over growth (OD₆₀₀) of each strain. Experiments were repeated in triplicate and t-tests determined statistical significance.

Growth of *tat* mutants over 24 h was slower compared to wild-type PAO1-DK, and cultures did not reach the same final cell density in PA14 (**Figure 3.19**). They exhibited a characteristic growth defect. Differences between wild-type and *tat* mutant maximum growth reached after 24 h was found to be statistically significant by t-test ($p=0.003$).

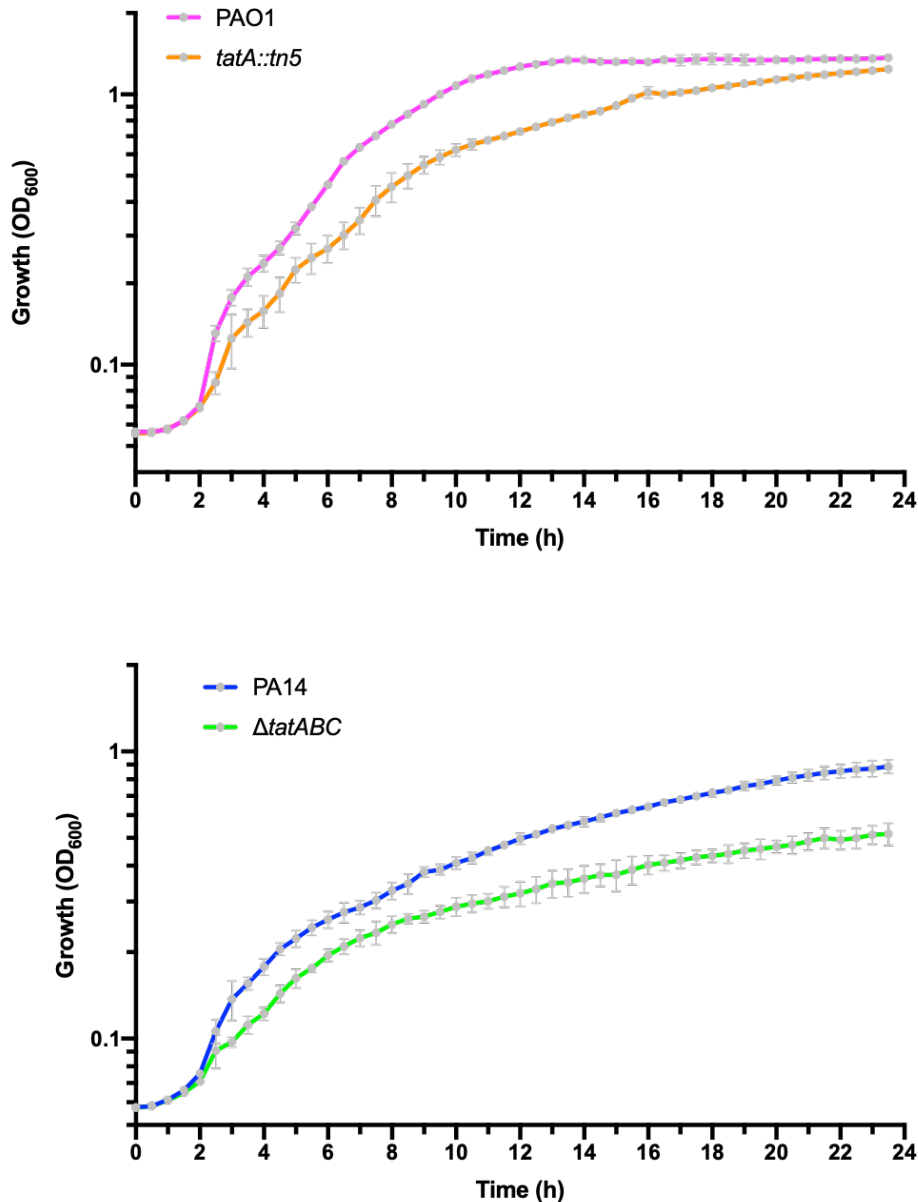


Figure 3.19. Growth of PAO1 and PA14 wild-type and *tat* mutants over 24 h. Cultures were grown in LB in a 96-well plate and incubated 37°C. Growth (OD₆₀₀) was measured every 30 min. Mean and SD are plotted in grey.

There are two anthranilate synthases in *P. aeruginosa*, TrpEG, which synthesises anthranilate as part of the tryptophan biosynthesis pathway, and PhnAB which synthesises anthranilate for PQS production. Anthranilate is also made through degradation of tryptophan by the products of *kynABU* (Palmer *et al.*, 2013). Anthranilate acts as a coinducer for *antA* expression (Kim *et al.*, 2012). To determine anthranilate production in wild-type and *tat* mutants, Nigel Halliday (University of Nottingham) kindly used LC-MS/MS to semi-quantify the anthranilate extracted from culture supernatants. PAO1-DK cultures contained ~ 4 fold more anthranilate at 16 h growth compared with 8 h growth. In PA14 there was a ~ 5 fold increase in anthranilate from 8 h to 16 h (**Figure 3.20**).

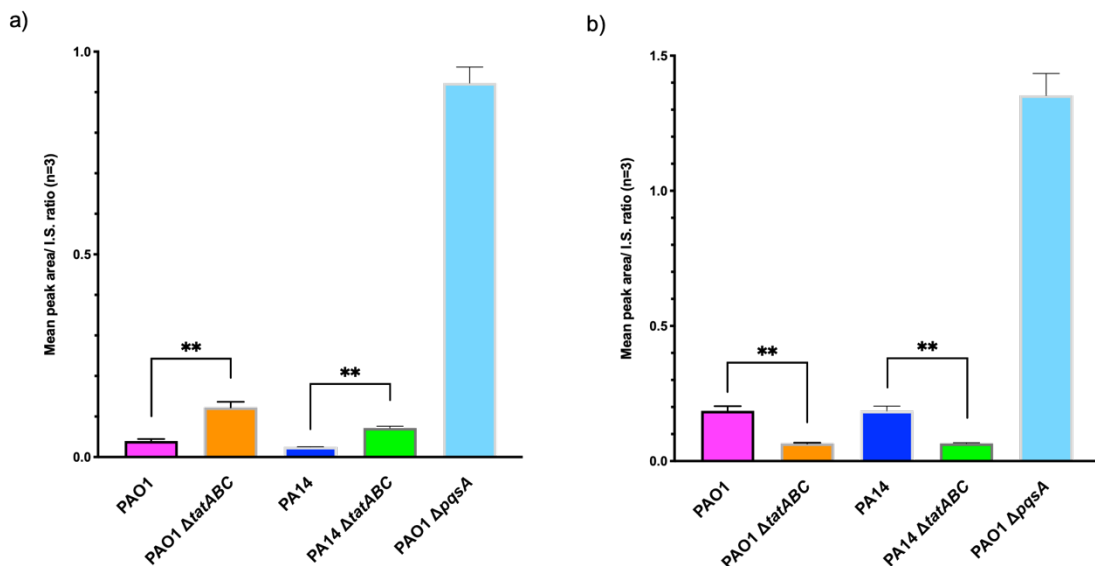


Figure 3.20. LC-MS/MS quantification of anthranilate in culture supernatants. PAO1, PAO1 Δ tatABC, PA14, PA14 Δ tatABC, and the positive control PAO1 Δ pqsA were grown for a) 8 h and b) 16 h in LB, 37°C, shaking 200 rpm. Cells were harvested and anthranilate extracted from culture supernatants. Experiments were carried out in triplicate and mean \pm SD is shown for each. t-tests show significant differences between wild-type and *tat* mutants for each timepoint. PAO1 Δ pqsA was found to be significantly different to PAO1 at both timepoints ($p \leq 0.01$).

A PAO1-DK Δ tatABC deletion mutant produced a ~ 3 fold higher concentration of anthranilate than wild-type PAO1-DK after 8 h growth (**Figure 3.20a**). A similar difference was seen in PA14, which was ~ 2.5 fold greater in the

Δ *tatABC* mutant vs wild-type. Following 16 h growth, bacterial cultures were at stationary-phase (**Figure 3.19**) and *antA* expression was greatly up-regulated at 16 h in the *tat* mutants of PAO1-DK and PA14 (**Figure 3.17, Figure 3.18**). **Figure 3.20b** shows there was more anthranilate in wild-type culture supernatants compared with *tat* mutant after 16 h. Perhaps new anthranilate made in *tat* mutants is used or degraded immediately, so does not accumulate and is not released to the supernatant.

3.2.8. Anthranilate degradation is up-regulated in a Δ *pqsA* mutant and *tatA*::Tn5 Δ *pqsA* double mutant

Transcriptomic analysis showed that *catA*, *catB*, and *catC* were up-regulated in a PAO1-DK Δ *pqsA* mutant, as displayed in **Table 3.2** (Rampioni et al., 2010). It was hypothesised that PAO1-DK Δ *pqsA* and PAO1-DK *tatA*::Tn5 Δ *pqsA* mutants would exhibit modulated expression similar to that seen in a *tat* mutant as PQS biosynthesis is perturbed in a *tat* mutant. Deletion of *pqsA* resulted in increased expression of *antA* by ~5 fold, *antR* by ~4 fold and *catB* by ~3 fold (**Figure 3.21**). Upregulation was greater compared with the *tat* mutant, which could be due to a greater accumulation of anthranilate due to completely abolished PQS biosynthesis. Deletion of *pqsA* resulted in slight downregulation of the *catR* promoter, which also occurs in the *tat* mutant.

The expression of the anthranilate degradation pathway was measured in a *tatA*::Tn5 Δ *pqsA* double mutant to investigate if the previously seen upregulation in the single mutants is cumulative. The *tatA*::Tn5 Δ *pqsA* double mutant had significantly increased expression of *antA*, *antR* and *catB* when compared with wild-type expression levels (**Figure 3.21a,b,c**). The increase in expression was not cumulative, upregulation in the double mutant was less than the upregulation seen in either the *pqsA* or *tatA*::Tn5 mutant. However, as with the single mutants, *antA*

expression is the greatest, followed by *catB* and *antR* expression, then *catR* has the lowest expression. Perhaps less anthranilate was produced in the $\Delta pqsA$ *tatA::Tn5* double mutant compared with PAO1-DK $\Delta pqsA$ due to slower growth, and therefore expression of anthranilate degradation was slightly lower.

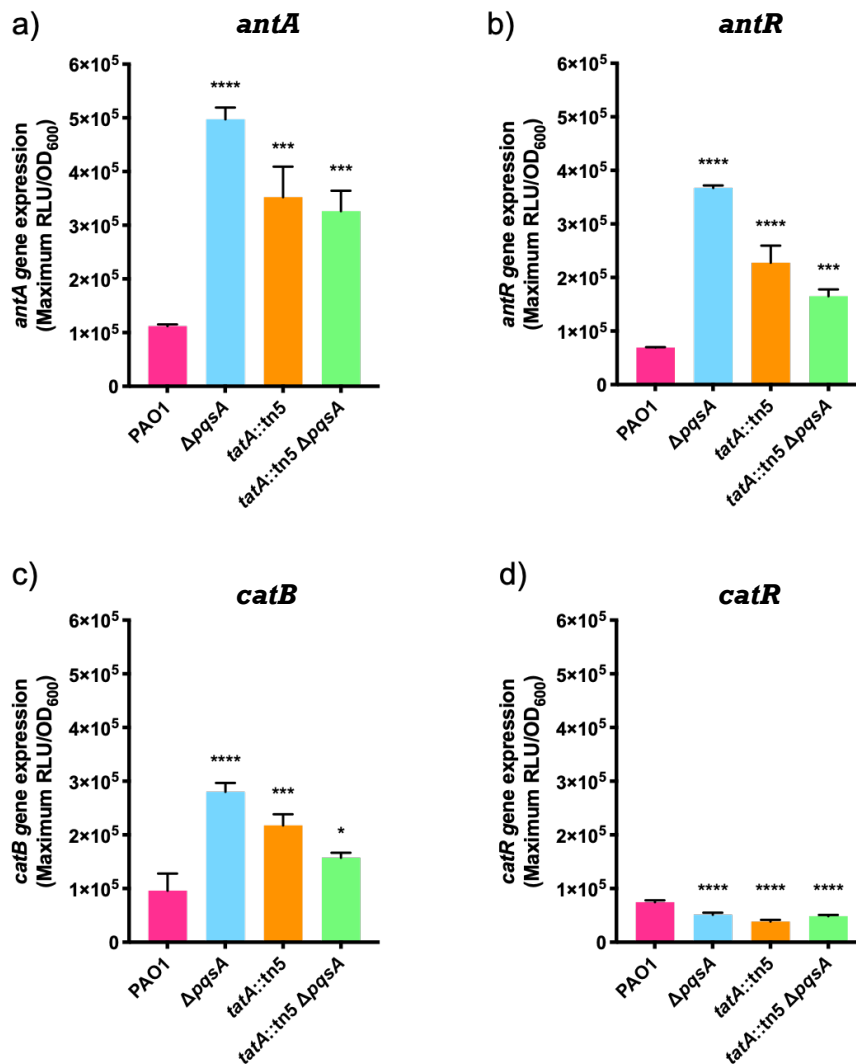


Figure 3.21. Expression of the anthranilate degradation pathway in *tat* and *pqsA* mutants. Expression was measured in triplicate over 24 h growth in LB in 96-well plates, at 37°C. Luminescence was standardised by dividing by growth (OD₆₀₀) and average maximum expression values are shown \pm SD.

3.2.9. Determining response of *tat* mutation to exogenously added anthranilate

It was hypothesised that the differential expression of genes involved in anthranilate catabolism and PQS biosynthesis is due to altered intracellular anthranilate. We have seen that there is more anthranilate produced by a *tat* mutant after 8 h of growth (**Figure 3.20**). Anthranilate is a co-inducer of genes involved in anthranilate catabolism (Oglesby *et al.*, 2008). Once bound to the transcriptional regulator AntR, expression from the *antA* promoter is increased while simultaneously inhibiting the activity of PqsR, an inducer of the *pqsABCDE* and *phnAB* operons and repressor of *antA* (Oglesby *et al.*, 2008; Hammond *et al.*, 2015; Maura *et al.*, 2016). Anthranilate is considered membrane permeable and exogenous anthranilate has been used to alter expression of *antA* previously (Farrow and Pesci, 2007b; Oglesby *et al.*, 2008; Choi *et al.*, 2011). Knowing this, expression of *antA*, *antR*, *catB* and *catR* of the *tat* mutant and *tatA::Tn5 ΔpqsA* double mutant in response to exogenous anthranilate was investigated and compared with the wild-type. If a *tat* mutant is able to respond in the same manner as the isogenic PAO1-DK wild-type strain, then this will support the theory that increased *antA* expression and reduced *pqsA* expression is due to increased endogenous anthranilate.

Firstly, a suitable concentration of anthranilate was determined by testing for strong induction of the anthranilate degradation pathway in PAO1-DK and PA14 without inhibiting cell growth. Strains were cultured in LB broth containing anthranilate at a range of concentrations (0-8 mM) and gene expression was measured using a chromosomally integrated *antA'-lux* promoter fusion (**Figure 3.22**). Concentrations of anthranilate above 6 mM had inhibitory effects on growth of PAO1-DK (**Figure 3.22**) and all concentrations tested against PA14 exhibited some level of growth inhibition. The maximum population density achieved declined from 0-6 mM, and at 8 mM of anthranilate, growth was completely inhibited.

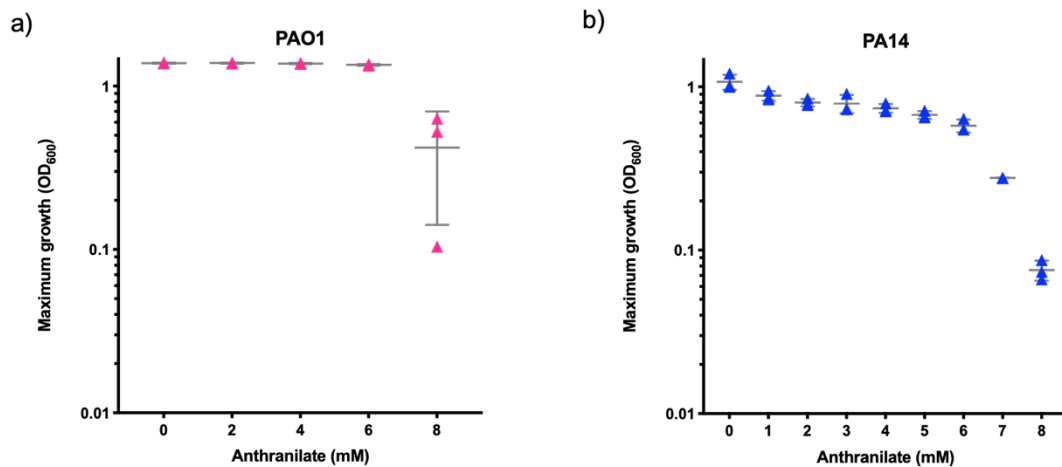


Figure 3.22. Inhibitory effects of high concentrations of anthranilate on the growth of PAO1 and PA14. PAO1 (a) and PA14 (b) were grown in LB containing anthranilate at concentrations ranging from 0-8 mM and growth (OD₆₀₀) was recorded. Experiments were carried out in triplicate and mean maximum growth \pm SD is plotted. Individual values are shown as a) pink triangles and b) blue triangles.

Figure 3.23 shows addition of anthranilate induced *antA* gene expression to a greater extent in PAO1-DK compared to PA14. PAO1-DK *antA* expression increased in a concentration-dependent manner until 6 mM exogenous anthranilate was reached. In PA14 expression was higher than the no-anthranilate control until 6 mM, but the greatest expression was at 1 mM which then declined between 1 mM and 6 mM. The concentration chosen for future assays was 6 mM for PAO1-DK and 3 mM for PA14. A concentration of 6 mM was chosen for PAO1-DK as it gave the highest value of *antA* maximum gene expression (**Figure 3.23**) without affecting the growth (**Figure 3.22**). PA14 required a compromise, so 3 mM anthranilate was chosen as it induced a large upregulation of *antA* without severely inhibiting the growth.

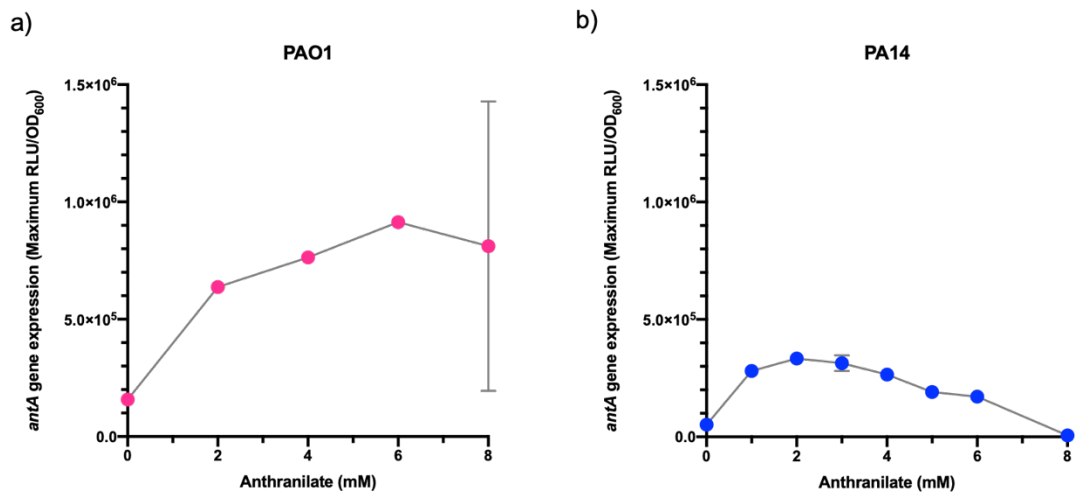


Figure 3.23. Expression of *antA* is induced by exogenous anthranilate. PAO1 (a) and PA14 (b) carrying an *antA::lux* promoter fusion were grown in LB + anthranilate (0-8 mM) in triplicate over 24 h. Expression was measured with an automated plate reader and standardised by dividing by cell growth (OD₆₀₀). Maximum gene expression at each concentration of anthranilate is plotted along with standard deviation.

As such, PAO1-DK and PA14 wild-type and Δ *tatABC* deletion mutants, as well as PAO1-DK Δ *pqsA* and PAO1-DK *tatA::Tn5* Δ *pqsA*, were cultured in LB + anthranilate at 6 mM and 3 mM respectively, and the expression of *antA*, *antR*, *catB* and *catR* measured using bioluminescent transcriptional reporters. The results show that *antA*, *antR* and *catB* were strongly up-regulated by exogenous addition of anthranilate in a *tatA::Tn5* mutant, Δ *pqsA* mutant and *tatA::Tn5* Δ *pqsA* double mutant (**Figure 3.24**).

The greatest increase in expression of *antA*, *antR* and *catB* occurred in PAO1-DK Δ *pqsA*, likely because accumulation of too much anthranilate is toxic (Aedekerck *et al.*, 2005). These genes were also overexpressed in a *tatA::Tn5* mutant. Surprisingly, the increase in expression of *antA*, *antR* and *catB* in response to increased intracellular anthranilate was less in PAO1-DK *tatA::Tn5* Δ *pqsA* than in the single mutants. As it stands, *tat* mutants do not export a number of virulence factors and other proteins, and have a significant growth defect, so the difference

in expression of *antA*, *antR* and *catB* upon *tat* mutation compared with *pqsA* mutation is likely due to this. This can be investigated further by screening mutants of substrates of the Tat system for similar phenotypes.

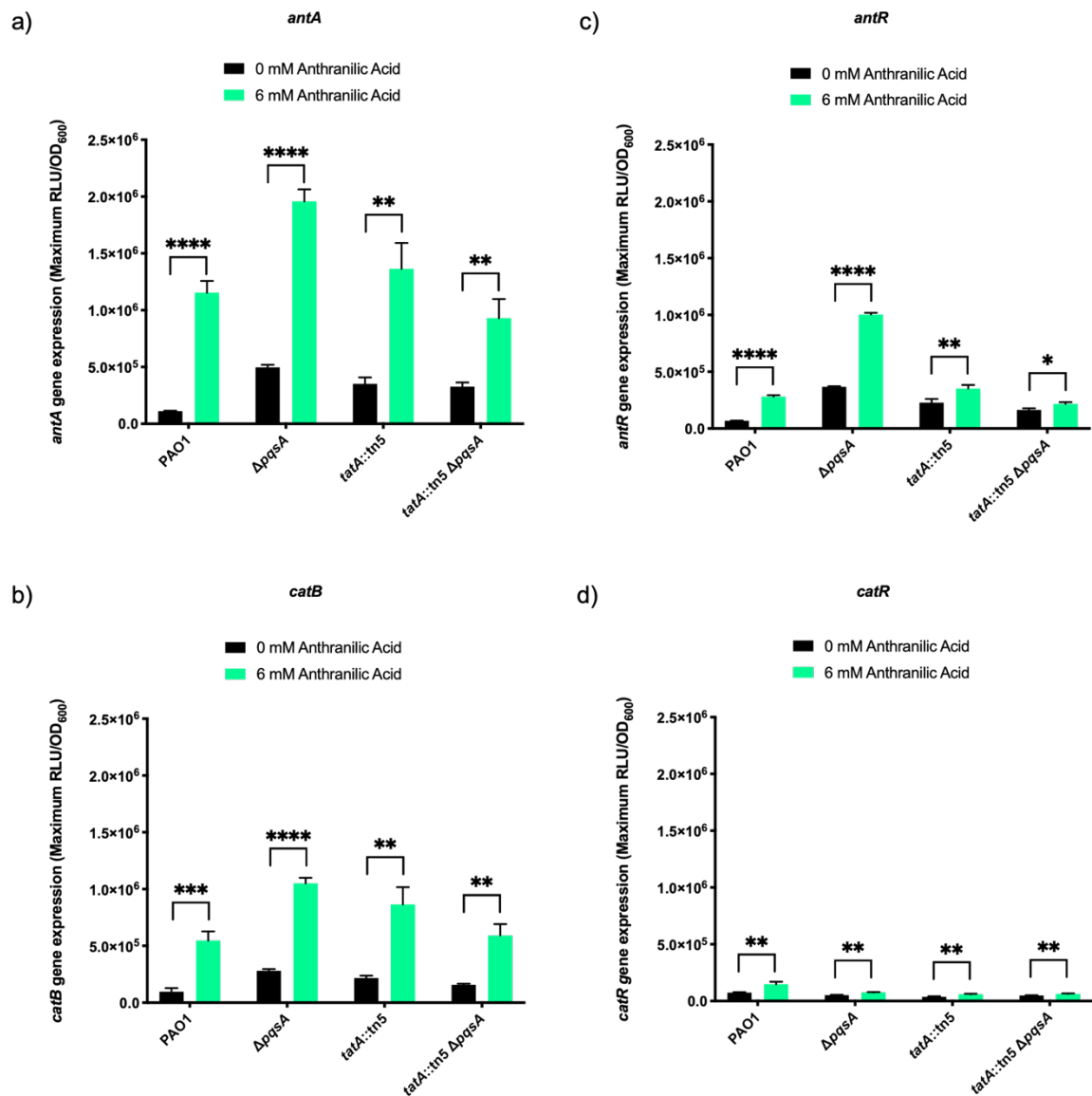


Figure 3.24. Exogenously supplied anthranilate induces expression of genes involved in anthranilate degradation pathway. Exogenous anthranilate causes an upregulation of a) *antA*, b) *antR*, c) *catB*, and d) *catR*, in all PAO1 strains. Experiment was carried out in triplicate and mean and SD are shown. Significant difference in maximum expression was determined by a t-test.

PA14 and PA14 Δ *tatABC* mutants containing *antA*, *antR* and *catB* promoter fusions were also investigated for their response to anthranilate. When both strains were grown in 3 mM anthranilate, *antA*, *antR* and *catB* were all up-regulated (Figure 3.25a,b,c).

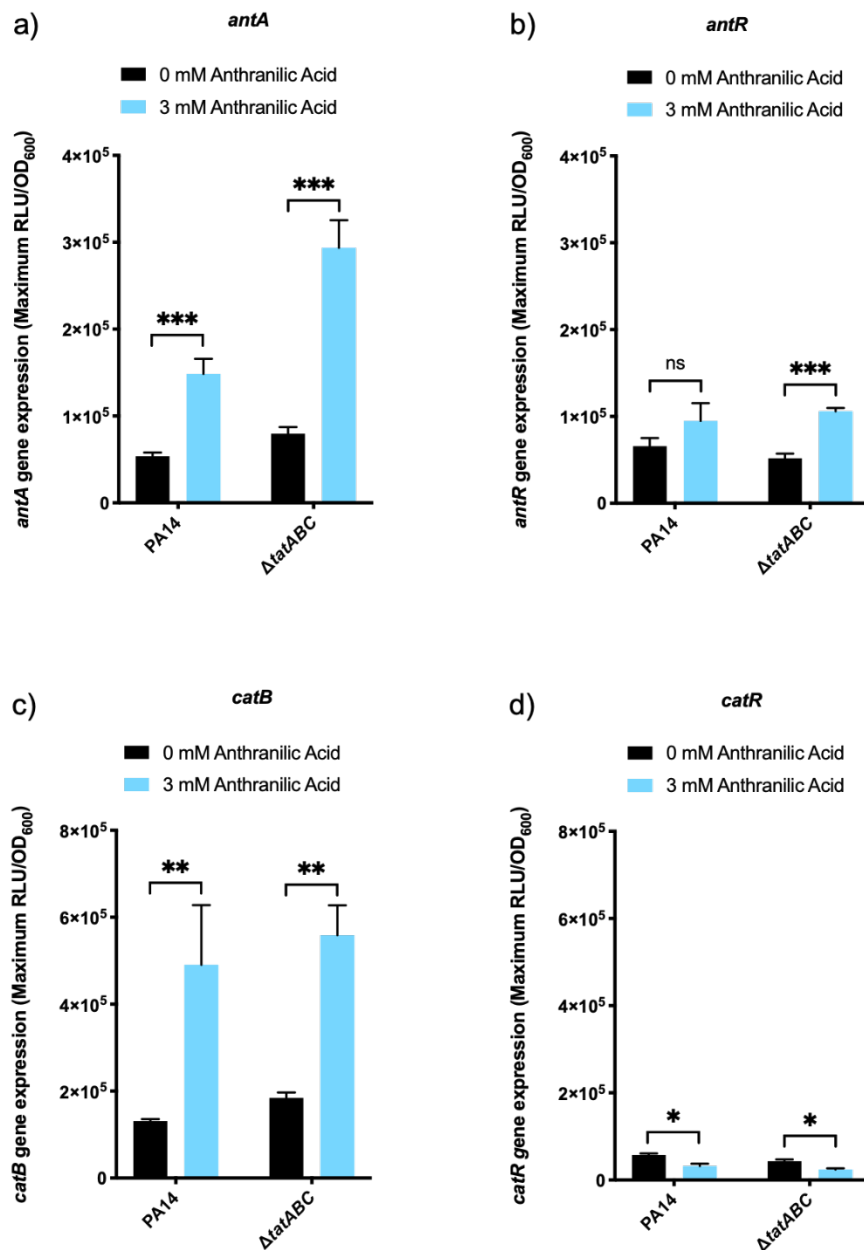


Figure 3.25. Exogenous anthranilate induces expression of *antA*, *antR*, *catB* and *catR* in PA14 and the isogenic Δ *tatABC* mutant. Wild-type PA14 and a Δ *tatABC* deletion mutant carrying promoter fusions of *antA*::*lux*, *antR*::*lux*, *catB*::*lux* and *catR*::*lux* were grown in LB and LB + anthranilate 3 mM over 24 h at 37°C. Gene expression was measured every 30 minutes in an automated plate reader. Strains were grown in triplicate and average maximum gene expression \pm SD is shown.

PA14 $\Delta tatABC$ exhibited a greater increase in *antA* expression in response to 3 mM anthranilate when compared with wild-type PA14. Addition of anthranilate decreased expression of *catR* in the $\Delta tatABC$ mutant and the isogenic wild-type strain but this is not biologically significant (**Figure 3.25**). Lastly, the response of *pqsA* to a high concentration of anthranilate was investigated in PA14 and PA14 $\Delta tatABC$. **Figure 3.26** shows there was a decrease of *pqsA* expression in both wild-type and $\Delta tatABC$ mutant.

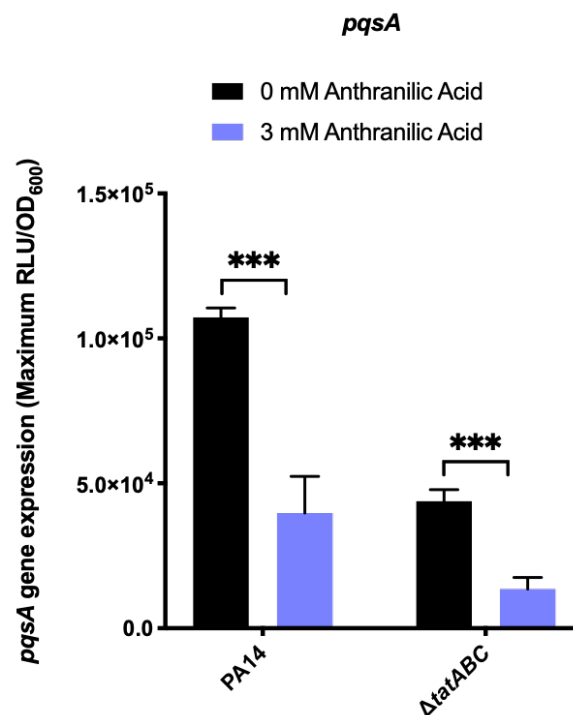


Figure 3.26. Exogenous anthranilate represses expression of *pqsA* in PA14 and PA14 $\Delta tatABC$. Wild-type PA14 and a $\Delta tatABC$ deletion mutant carrying a chromosomally integrated *pqsA::lux* promoter fusion were grown in LB and LB + anthranilate 3 mM. Gene expression was measured and average maximum expression in plotted with SD. Statistical significance was determined by t-tests.

Section Summary

The complex QS-dependent and independent regulatory network governing *antA* and *pqsA* transcription is well-studied in the literature, and anthranilate is a key intermediate at a metabolic branch point between the TCA cycle, tryptophan biosynthesis, and PQS biosynthesis (Oglesby *et al.*, 2008; Chugani and Greenberg, 2010; Choi *et al.*, 2011; Kim *et al.*, 2012; Wang *et al.*, 2020). Here we show that mutation or deletion of the twin-arginine transport system in PAO1-DK and PA14 induced expression of the first two operons in the anthranilate degradation pathway, *antA* and *catB*, along with their regulators *antR* and *catR*. This was also seen in a $\Delta pqsA$ mutant, and it was hypothesised that disruption of *pqs* QS in a *tat* mutant is the reason for reduced eDNA release and biofilm formation. However, anthranilate quantification in spent media revealed a difference between *tat* and *pqsA* mutant. Disrupted PQS biosynthesis gives characteristically high levels of extracellular anthranilate, yet the *tat* mutant culture supernatant contained less anthranilate than wild-type during stationary phase. This could be because *pqsA* expression still occurs in a *tat* mutant so anthranilate is used by the PQS biosynthetic machinery, in addition to the products of the highly up-regulated *antABC catBCA* operons. Anthranilate degradation genes were highly up-regulated in *tat*, *pqsA* and *tat pqsA* mutants at this point.

Exogenous anthranilate may increase the intracellular concentration by diffusion into the cell, this would positively regulate expression of the *antA*, *antR* and *catB* genes in wild-type, *tat*, *pqsA* and *tat pqsA* mutants. Increase in anthranilate also causes downregulation of *pqsA* the first gene in the PQS biosynthetic operon. Additional investigation of the intracellular concentration of anthranilate with LC-MS/MS is needed before confirming this theory.

3.2.10. Construction of $\Delta antA$ mutant in PAO1-DK, PAO1-DK $\Delta tatABC$ and PAO1-DK $\Delta pqsA$

Anthranilate is a key metabolite used for PQS biosynthesis, tryptophan biosynthesis and energy production via the TCA cycle. As such, regulation of these pathways is under strict control for immediate response to changing environmental conditions and growth phases. To investigate the role of *antA* in relation to PQS-dependent quorum sensing and biofilm formation an in-frame deletion between bases 27 and 1,284 of the *antA* ORF was made using the suicide vector deletion system (Buscher *et al.*, 2005). Full details of the gene deletion are in Chapter 2.

3.2.11. Genomic analysis of PAO1-DK, PAO1-DK $\Delta antA$, PAO1-DK $\Delta tatABC \Delta antA$ and PAO1-DK $\Delta pqsA \Delta antA$

Next-generation whole genome sequencing (WGS) was carried out on wild-type PAO1-DK and subsequent $\Delta antA$ mutants in order to confirm specific, clean deletion of the *tatABC*, *pqsA* and *antA* genes (Appendix, **Table 7.3**). **Figure 3.27** shows a visual comparison of each genome assembly created using blast ring image generator (BRIG). Blank regions indicate a gene deletion as the assembly had no BLAST match to the reference genome. Each genome was identical to the PAO1-DK wild-type genome except for their individual *tatABC*, *pqsA* and *antA* deletion mutations. Any additional mutations shown were SNPs that are characteristic of the PAO1-DK subtype and different from the reference genome PAO1-W. They were seen in all of the WGS genomes. WGS confirms the clean deletion of the *antA*, *tatABC* and *pqsA* genes and any phenotypic changes associated with the strain are not from secondary mutations.

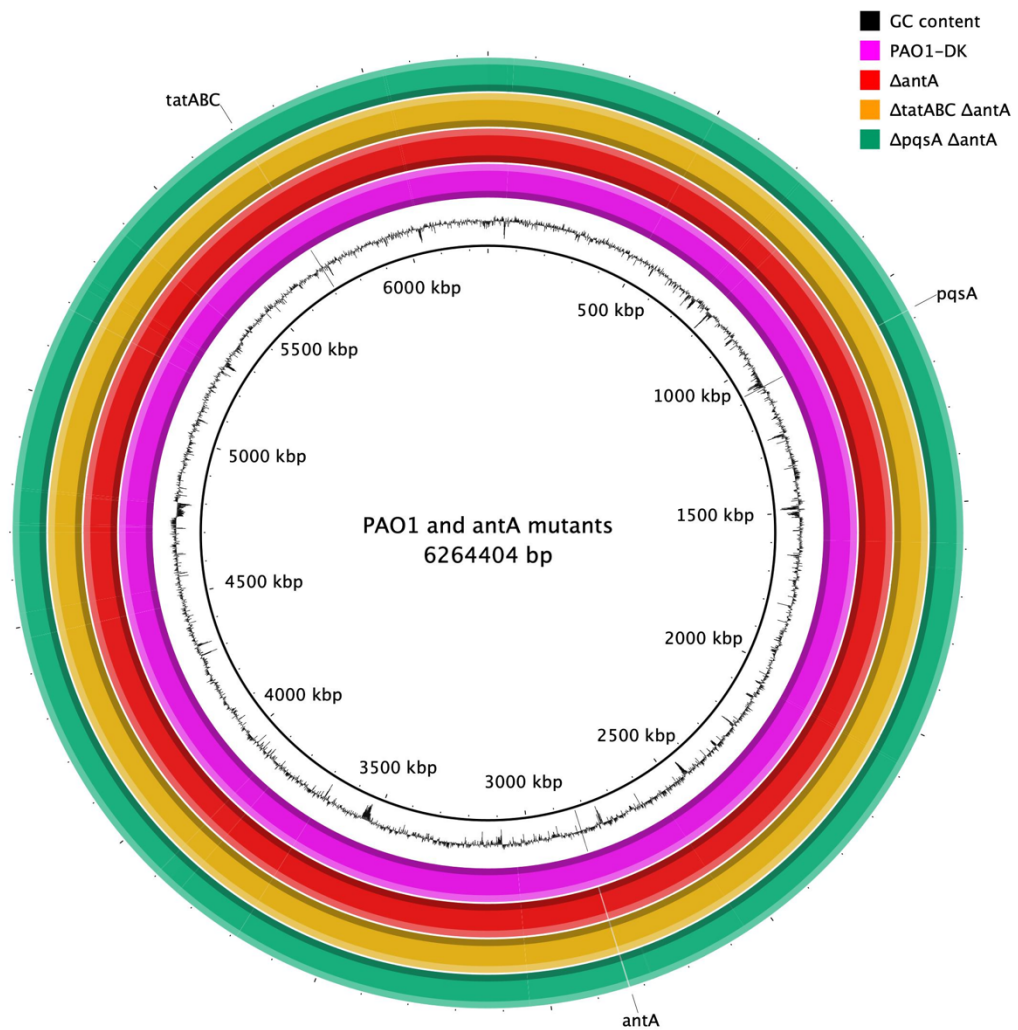


Figure 3.27. Whole genome sequencing comparison of wild-type PAO1-DK, the $\Delta antA$ deletion mutant, PAO1-DK $\Delta tatABC \Delta antA$ and PAO1-DK $\Delta pqsA \Delta antA$. PAO1-W was used as a reference genome and is indicated by the central thin black line. PAO1 GC content is visualised in the next ring, followed by the genomes sequenced by WGS. Deletions within the genome can be seen as a blank space as they do not have a BLAST match. The genes *antA*, *tatABC* and *pqsA* are labelled at their corresponding positions on the genome.

Trimmed reads were also assembled into contigs and genome assemblies by MicrobesNG and the quality of the data was assessed. There were no mismatches, and 75% coverage was achieved by 7 contigs for PAO1-DK, PAO1-DK $\Delta antA$ and PAO1-DK $\Delta tatABC \Delta antA$, and 9 contigs for PAO1-DK $\Delta pqsA \Delta antA$.

3.2.12. Effect of $\Delta antA$ deletion on growth in LB

Anthranilate, as previously mentioned, is degraded and fed into the citric acid cycle to be used as an energy source and the genes responsible are up-regulated during stationary/late-stationary phase through AntR- and RhIR-dependent activation of transcription (Choi *et al.*, 2011; Kim *et al.*, 2012). Therefore, it was hypothesised that deletion of *antA* may affect planktonic growth of the bacteria. To test this, wild-type PAO1-DK and isogenic $\Delta antA$, $\Delta tatABC$, $\Delta pqsA$ mutants as well as $\Delta pqsA \Delta antA$, and $\Delta tatABC \Delta antA$ double mutant strains were grown in LB for 24 h and OD₆₀₀ was measured every half hour.

Figure 3.28 shows that deletion of *antA* had no effect on growth of the strain in LB, there was no visible lag before reaching the same optical density. Deletion of $\Delta pqsA$ did not affect cell growth (Hazan *et al.*, 2016) and PAO1-DK $\Delta pqsA \Delta antA$ also had the same cell growth phenotype as wild-type. As seen earlier in the study, the $\Delta tatABC$ strain exhibited slower growth past 5 h which never fully reached wild-type OD₆₀₀. Interestingly, this is almost completely abolished in the $\Delta tatABC \Delta antA$ double mutant, which did not have a growth defect (**Figure 3.28**).

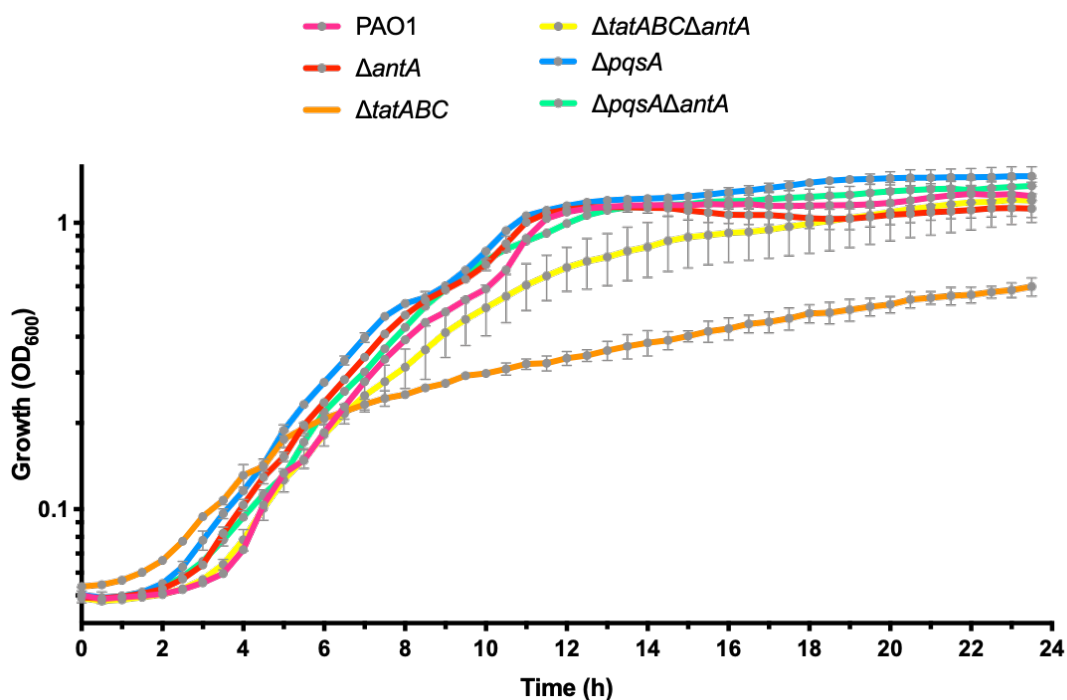


Figure 3.28. Deletion of *antA* restores growth in a *tatABC* mutant. Growth of 200 μ l cultures at 37°C in a 96-well plate. Cell density (OD_{600}) was measured at 30 min intervals. Three biological and three technical repeats were carried out. Mean \pm SD is plotted.

3.2.13. Deletion of *antA*, *tatABC*, or *pqsA* has no effect on *lux*-reporter light output

To be sure that changes to luminescence are due to regulatory changes, and not lower activity of the *luxCDABE* gene products, transcriptional reporters carrying the *lux* genes fused to a *ptac* constitutive promoter were introduced to the genome of PAO1-DK, PAO1-DK $\Delta antA$, PAO1-DK $\Delta tatABC$, PAO1-DK $\Delta pqsA$, PAO1-DK $\Delta tatABC \Delta antA$ and PAO1-DK $\Delta tatABC \Delta antA$. Maximal light output as a function of growth (RLU/ OD_{600}) can be seen in **Figure 3.29** and is largely unaffected by *antA*, *pqsA* or *tatABC* deletion.

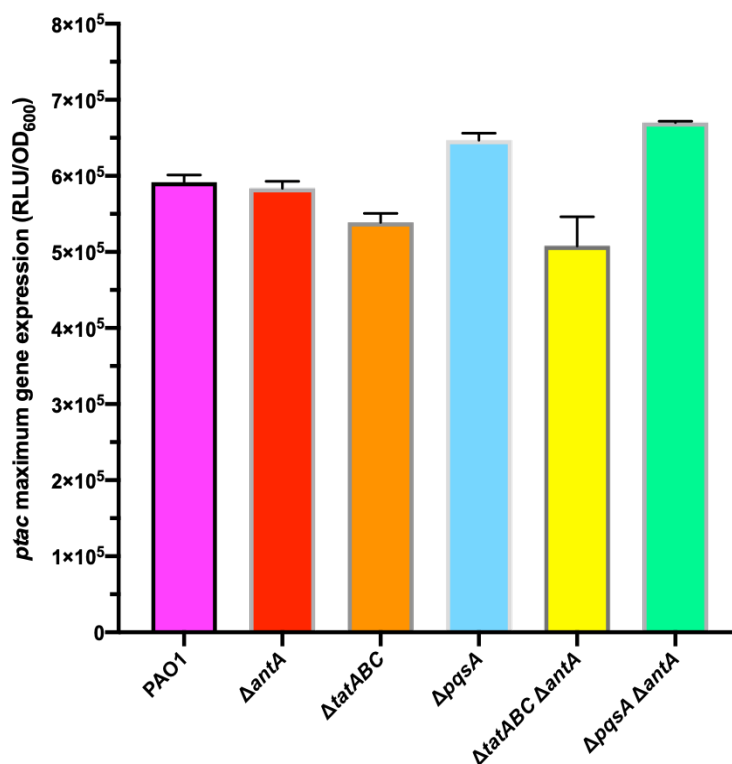


Figure 3.29. Maximum expression from a constitutive *ptac* promoter in various mutants shows no change in luminescence. miniCTX::*ptac'-lux* vectors were integrated into the chromosome of each mutant and luminescence was recorded over 24 h growth in LB. Experiment was carried out in triplicate and average maximum gene expression \pm SD is plotted.

3.2.14. Effect of $\Delta antA$ deletion on anthranilate degradation

To determine how the biosynthesis and accumulation of anthranilate is affected by deletion of *antA*, anthranilate was extracted from culture supernatants at 8 h and 16 h timepoints. **Figure 3.30** shows relative quantities of anthranilate for each $\Delta antA$, $\Delta tatABC$ and $\Delta pqsA$ mutant semi-quantified by LC-MS/MS.

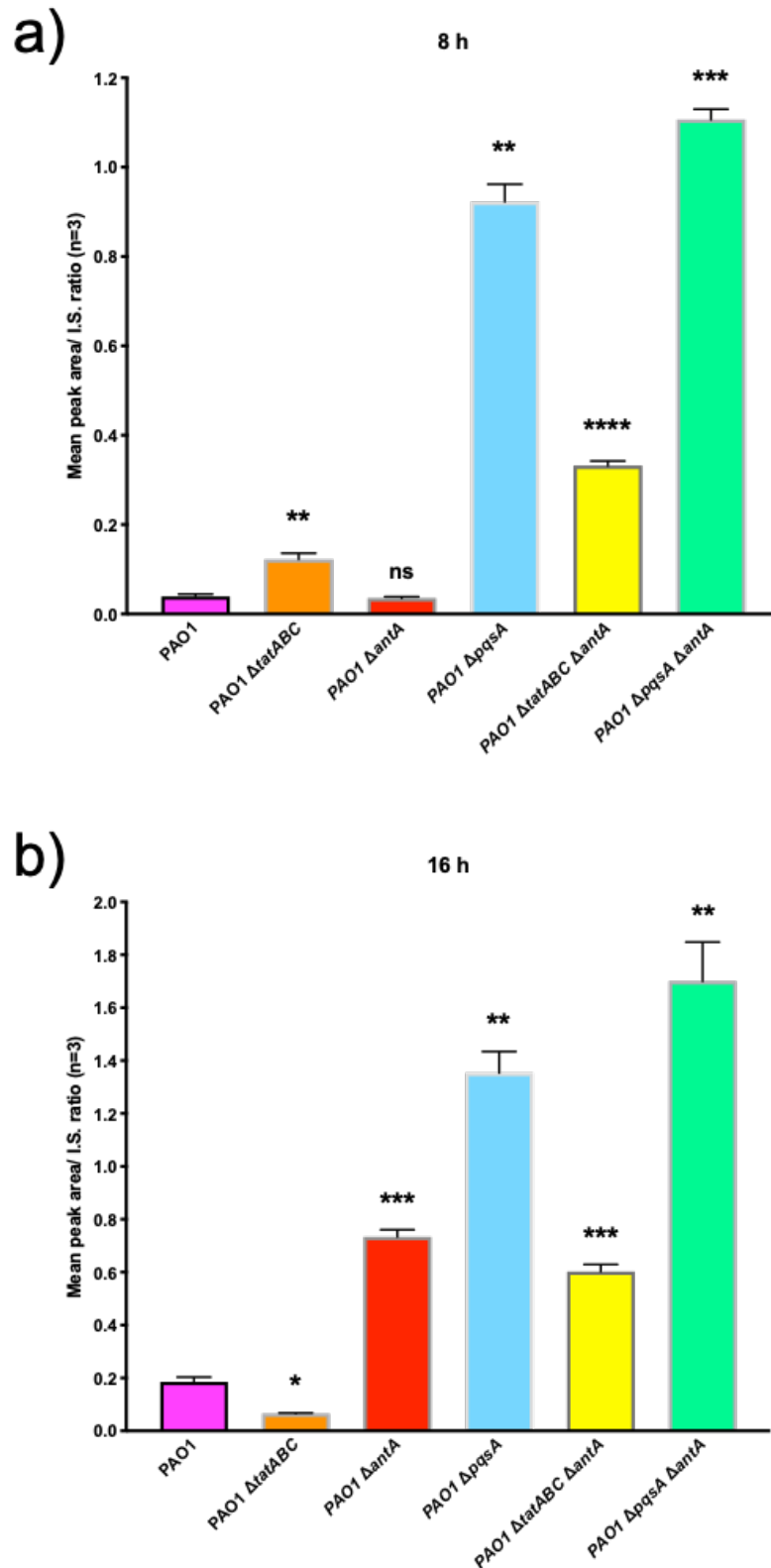


Figure 3.30. LC-MS/MS semi-quantification of anthranilate extracted from culture supernatants. Top panel: LC-MS/MS semi-quantification of anthranilate extracted from culture supernatants after 8 h growth. Bottom panel: Anthranilate in culture supernatants of Δ antA, Δ tatABC and Δ pqsA mutants after 16 h growth semi-quantified by LC-MS/MS. Experiments were repeated in triplicate, mean and SD are shown.

Figure 3.30 shows following 8 h growth, the concentration of anthranilate present in the $\Delta antA$ mutant spent media was no different to wild-type. However, there were significant increases in the $\Delta tatABC$ mutant and $\Delta tatABC \Delta antA$ double mutant. Anthranilate levels in the $\Delta pqsA$ mutant supernatant were ~ 22 fold greater than PAO1-DK wild-type, and ~ 30 fold higher than wild-type in the $\Delta pqsA \Delta antA$ double mutant. This shows that mutation of either *pqsA* or *tatABC* resulted in increased anthranilate levels in cell free culture supernatants.

After 16 h, the concentration of anthranilate in culture supernatants was higher than wild-type in all mutants bar the $\Delta tatABC$ mutant (**Figure 3.30b**). PAO1-DK $\Delta antA$ and the $\Delta tatABC \Delta antA$ double mutant both had ~ 4 fold increase in anthranilate, so it is likely the increase in the double mutant was due to *antA* deletion. Again, the highest concentration of anthranilate was found in culture supernatants of the $\Delta pqsA$ mutant and $\Delta pqsA \Delta antA$ double mutants, with slightly more in the double mutant.

An $\Delta antA$ mutant strain should be unable to degrade anthranilate, but still able to synthesise PQS and tryptophan. By introducing bioreporters the expression of the anthranilate degradation pathway and PQS biosynthesis was measured in PAO1-DK wild-type, $\Delta antA$, $\Delta pqsA$, $\Delta tatABC$ and the $\Delta pqsA \Delta antA$, $\Delta tatABC \Delta antA$ double mutants.

Figure 3.31a shows that deletion of *antA* up-regulated expression from the *antA* promoter by around 2.5 fold, likely as a response to increased intracellular anthranilate concentration. As seen previously, expression of *antA* was increased in a $\Delta pqsA$ mutant. When both *antA* and *pqsA* were deleted from the chromosome, expression from the *antA* promoter was ~ 4 fold greater.

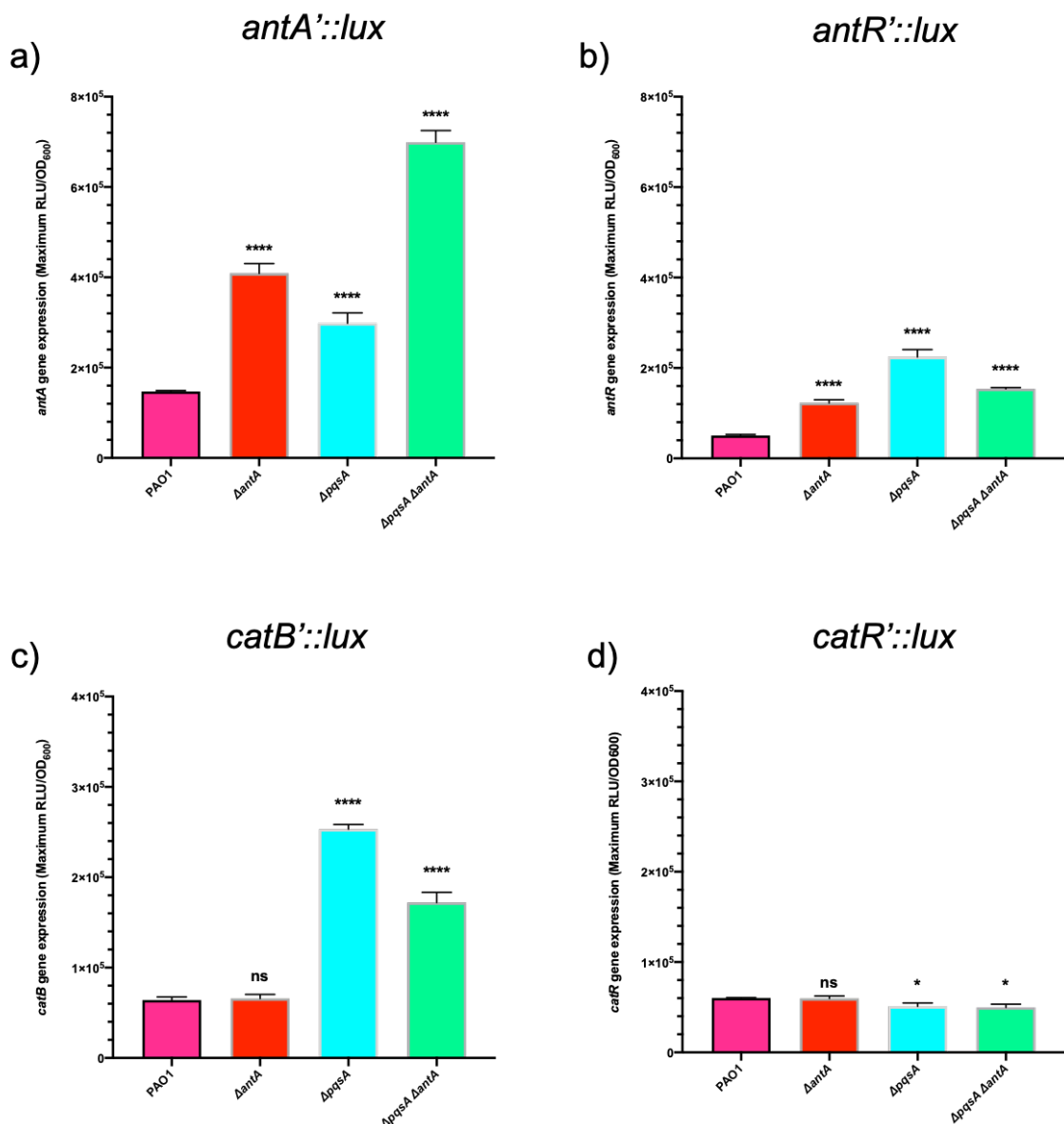


Figure 3.31. Expression of the anthranilate degradation pathway upon deletion of *antA* and *pqsA*. Chromosomally integrated *antA*::*lux*, *antR*::*lux*, *catB*::*lux*, and *catR*::*lux* promoter fusions were introduced to PAO1 and isogenic mutants PAO1 Δ*antA*, PAO1 Δ*pqsA*, and PAO1 Δ*pqsA* Δ*antA*. Expression was measured every 30 min over 24 h in an automated plate reader and standardised by dividing luminescence with cell growth (OD₆₀₀). Maximum expression reached by each strain is shown. Experiments were carried out three times in triplicate, mean ± SD is plotted. t-tests determined statistical significance.

Upregulation of *antR* is significantly increased in an $\Delta antA$, a $\Delta pqsA$, and an $\Delta antA \Delta pqsA$ double mutant, probably due to increased intracellular anthranilate binding to AntR and upregulating its own expression. PAO1-DK $\Delta pqsA$ had the greatest increase in *antR* expression, ~ 5 fold higher than wild-type (**Figure 3.31b**). The promoters for *catB* and *catR* were not expressed differentially in the $\Delta antA$ mutant, upregulation was observed only when *pqsA* was deleted in the wild-type and $\Delta antA$ mutants (**Figure 3.31c,d**).

Changes to expression of *antA*, *antR*, *catB* and *catR* when *antA* and *tatABC* were deleted can be seen in **Figure 3.32** and **Figure 3.33**. Again, there was a ~ 2.5 fold increase in expression of *antA* for PAO1-DK $\Delta antA$, and even greater upregulation in the $\Delta tatABC$ mutant, and a further increase in the $\Delta tatABC \Delta antA$ mutant to ~ 4 fold greater than wild-type expression levels (**Figure 3.32a**). **Figure 3.32b** shows this greater upregulation was also seen at the *antR* promoter. Upregulation of the *catB* promoter occurred in a $\Delta tatABC$ mutant, there was no change in the $\Delta antA$ mutant. The *catR* promoter has statistically significant changes to expression but these were most likely not biologically significant (**Figure 3.32c,d**).

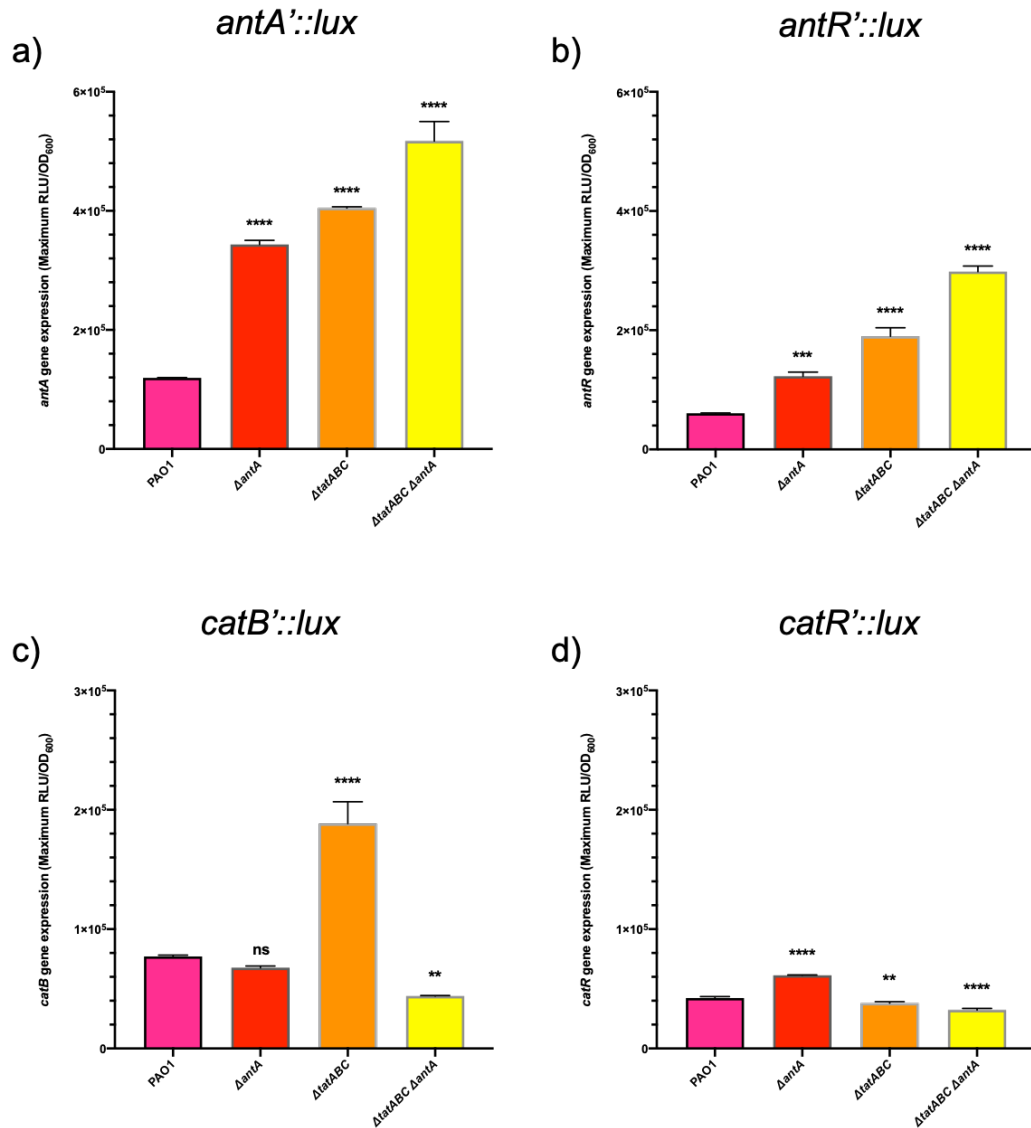


Figure 3.32. Expression of the anthranilate degradation pathway in PAO1 and various *antA* and *tatABC* mutants. MiniCTX::*lux* promoter fusions containing *antA*, *antR*, *catB* and *catR* promoters transcriptionally fused to the *luxCDABE* operon were introduced to PAO1, an $\Delta antA$ mutant, a $\Delta tatABC$ mutant and a $\Delta tatABC \Delta antA$ double mutant. Expression was measured by dividing luminescence by growth (OD₆₀₀). Mean maximum expression is plotted with SD and statistical significance determined by t-tests. Each figure is representative of three technical repeats.

Expression of *antA* over 24 h can be seen in **Figure 3.33**. Expression increased after ~ 7 h growth of PAO1-DK $\Delta pqsA$ and after ~8 h growth for wild-type and the remaining mutants. Peak expression was reached at different times, PAO1-DK maximum expression was at 10 h, PAO1-DK $\Delta pqsA$ had a sustained peak

in expression from 8 h to 14 h, and deletion of *antA* caused a delay in peak *antA* expression in all strains. Growth of these mutants is shown in **Figure 3.28**.

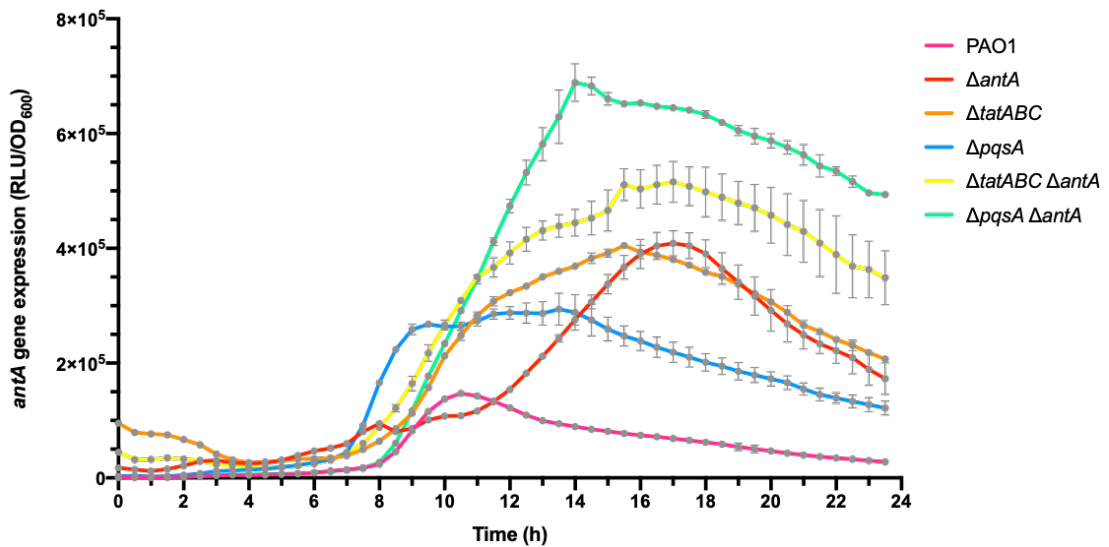


Figure 3.33. Expression of *antA* over 24 h in PAO1 $\Delta antA$, $\Delta tatABC$ and $\Delta pqsA$ single and double mutants. Growth (OD_{600}) and expression (RLU) was measured every 30 min and standardised by dividing luminescence by growth (OD_{600}). Each strain was grown in triplicate and the experiment was repeated three times. Mean and SD is plotted. Expression of *antA* in each strain is shown as follows: PAO1 (pink), PAO1 $\Delta antA$ (red), PAO1 $\Delta tatABC$ (orange), PAO1 $\Delta pqsA$ (blue), PAO1 $\Delta tatABC \Delta antA$ (yellow), and PAO1 $\Delta pqsA \Delta antA$ (green).

3.2.15. Expression of *pqsA* in $\Delta antA$ mutants

It is clear from these results that deletion of $\Delta antA$ resulted in upregulation of the *antA* promoter. As AntA and PqsA both utilise anthranilate, expression of the *pqsA* operon was measured in the $\Delta antA$ mutants. It was hypothesised that *pqsA* expression would increase upon deletion of *antA* as more is available for AQ biosynthesis. Surprisingly, this was not the case. **Figure 3.34** shows the maximum expression of *pqsA* over 24 h growth in LB, 37°C, measured by a *pqsA'-lux* bioluminescent transcriptional reporter. There was a ~2 fold downregulation of *pqsA* in the $\Delta antA$ mutant. As seen previously the expression of *pqsA* in a $\Delta tatABC$ mutant was ~4 fold lower than wild-type. Reduction in expression in a $\Delta tatABC$ and

$\Delta antA$ deletion mutant was further reduced in the double mutant; PAO1-DK $\Delta tatABC \Delta antA$ has ~8 fold lower expression than wild-type.

There was no significant difference between PAO1-DK $\Delta pqsA$, PAO1-DK $\Delta tatABC \Delta antA$ and PAO1-DK $\Delta pqsA \Delta antA$ with respect to the expression of *pqsA*. This suggests that PQS biosynthesis is almost completely abolished in the $\Delta tatABC \Delta antA$ double mutant. This could be confirmed with LC-MS/MS quantification of AQs in culture supernatants, as well as with the PAO1-DK $\Delta pqsA$ miniCTX::*pqsA'*-*lux* bioreporter.

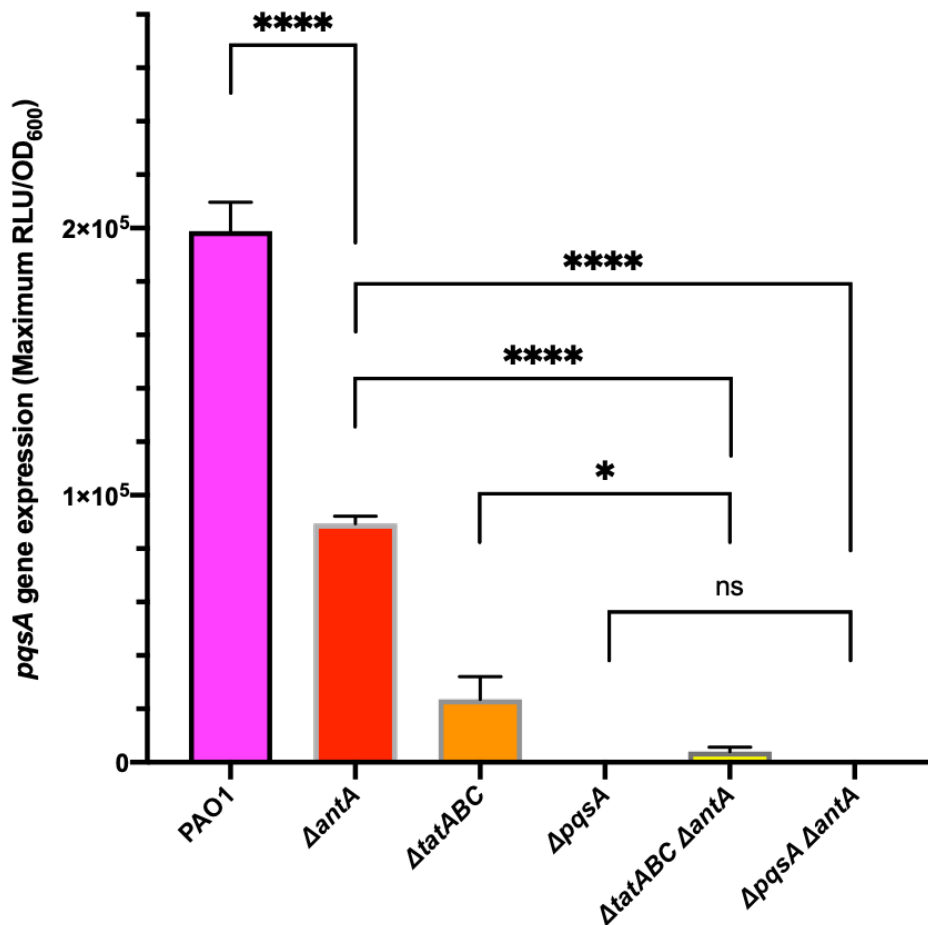


Figure 3.34. Expression of *pqsA* in $\Delta antA$, $\Delta tatABC$ and $\Delta pqsA$ mutants. A *pqsA*::*lux* bioreporter was introduced to PAO1, and the PAO1 mutants $\Delta antA$ (red), $\Delta tatABC$ mutant (orange), $\Delta tatABC \Delta antA$ (yellow), $\Delta pqsA$ and $\Delta pqsA \Delta antA$. Maximum expression over 24 h growth is plotted. Experiment was carried out in triplicate and mean and SD are plotted. Statistical significance was determined by one-way ANOVA test.

Lastly, pyocyanin production was assessed as an indicator of *pqs* QS activity as mutants of PQS biosynthetic operon *pqsABCDE* or *pqsR* exhibit significantly reduced pyocyanin production (Gallagher *et al.*, 2002; Diggle *et al.*, 2003). **Figure 3.35** shows total pyocyanin in cell culture supernatants following 8 h growth. As noted previously, deletion of the *tat* genes reduced pyocyanin production by ~3 fold. PAO1-DK $\Delta pqsA$ also had decreased pyocyanin production. Deletion of *antA* has no effect on pyocyanin production after 8 h, possibly because despite reduced *pqsA* expression, levels of PQS are sufficient to induce pyocyanin biosynthesis.

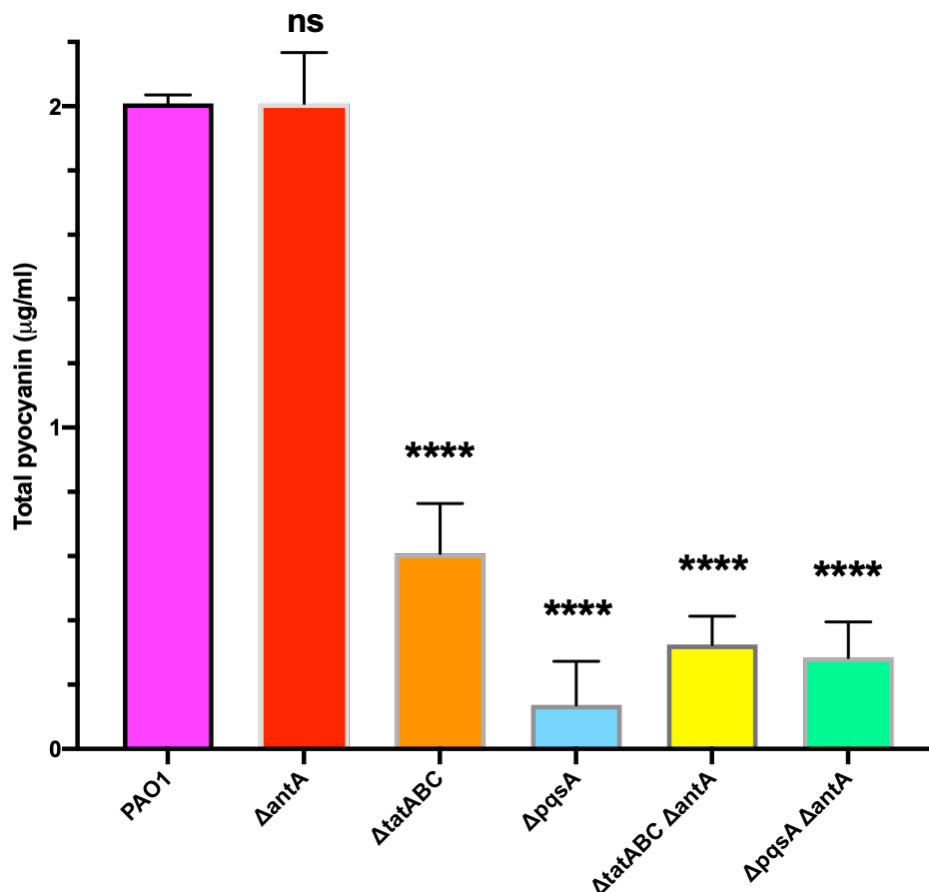


Figure 3.35. Total pyocyanin produced by PAO1, $\Delta antA$, $\Delta tatABC$ and $\Delta pqsA$ mutants and various mutants. PAO1 (pink), the PAO1 mutants $\Delta antA$ (red), $\Delta tatABC$ (orange), $\Delta pqsA$ (blue), $\Delta tatABC \Delta antA$ (yellow), and $\Delta pqsA \Delta antA$ (green) were grown for 8 h, 37°C, shaking 200 rpm. Cells were harvested and spent media was filter-sterilised. Pyocyanin was extracted and measured for each strain. Three biological repeats were analysed in parallel, mean and SD are plotted. One-way ANOVA was used to determine statistical significance relative to the wild-type.

3.3 Discussion

The disruption to PQS-dependent quorum sensing in mutants of the Tat secretion pathway was explored in depth by genome-wide transcriptional analysis through RNAseq and the results were validated with real-time expression of the modulated genes in the a *tatA*::Tn5 mutant. In addition, the effects of *tat* mutation was compared in both PAO1-DK and PA14, another common *P. aeruginosa* strain. Transcriptional studies were followed by deletion of the greatly up-regulated *antA* gene from PAO1-DK Δ *tatABC* as well as from wild-type PAO1-DK and a Δ *pqsA* mutant. The effect of these deletions was assessed through analysis of gene expression and of the biosynthesis of the quorum sensing signal molecule PQS.

Soh *et al.* showed that the pleiotropic effects of a *tat* mutation in PAO1-DK were due to perturbed PQS biosynthesis (Soh *et al.*, 2021). Dysregulation of *pqsA*, the first gene in the PQS biosynthetic operon, can be seen by a \sim 3 fold reduction of gene expression in PAO1-DK *tat* mutant. As a result pathways controlled by *pqs* QS, such as AQ biosynthesis, pyocyanin production, OMV release, and rhamnolipid production are all greatly reduced. PA14 Δ *tatABC* *pqsA* gene expression was significantly reduced, establishing that this is also a property associated with other *P. aeruginosa* strains. Reduced *pqsA* expression accounts for the lower levels of secreted PQS, HHQ and HQNO, and lower induction of *pqsA* in the bioreporter PAO1-DK Δ *pqsA* miniCTX::*pqsA'*-*lux* by culture supernatants. Similarly pyocyanin production, which is decreased upon deletion of genes within the *pqs* biosynthetic operon, is significantly lower in both PAO1-DK Δ *tatABC* and PA14 Δ *tatABC* (Gallagher *et al.*, 2002).

Transcriptomic analysis revealed mutation of the *tat* pathway has wide-reaching effects on *P. aeruginosa* gene expression. The PAO1-DK *tat* mutant had

355 differentially regulated genes involved in a variety of biological processes, of which 189 were up-regulated and 166 down-regulated.

RNAseq revealed upregulation of 30 Type III Secretion System (T3SS) genes including the *psc*, *pop*, *exs*, and *pcr* operons. T3SS genes *pcrV*, *pcrH*, *popB*, *popD*, *exsC*, *exsE*, *exsB*, and *pscE* are induced by PQS, yet were up-regulated in a *tat* mutant despite severely reduced *pqs* quorum sensing (Rampioni *et al.*, 2016). Transcription of T3SS genes is also controlled by ExsA, from the AraC/XylS-type transcriptional regulator family, and expression of *exsA* was up-regulated by 2.68 fold in a *tat* mutant which may explain overexpression (Hauser, 2009). The T3SS is also regulated at the initiation of secretion level, by the proteins ExsC, ExsD and ExsE, all of which were induced upon *tat* mutation suggesting increased Type III Secretion. Induction of T3SS regulon expression by ExsA can be brought on through increase of intracellular cyclic AMP (cAMP) concentration by the inner membrane-bound adenylate cyclase CyaB. cAMP is sensed by the global regulator Vfr and together with ExsA and cAMP transcription is up-regulated. Expression of the T3SS is also controlled by the global regulatory network of RetS, LadS and the GacA/GacS two component system. The RetS/GacS signalling cascade up-regulates transcription of the sRNAs RsmY and RsmZ, and together with RsmA, a post transcriptional regulator, T3SS is positively regulated (Moscoso *et al.*, 2011). However, these were not up-regulated in a *tat* mutant and are not exported via the Tat system so are unlikely to cause T3SS upregulation in a *tat* mutant (Hauser, 2009; Gimenez *et al.*, 2018).

Initiation of the T3SS regulon is also induced by depleted Ca²⁺ concentration, which also requires the presence of glutamate (Hauser, 2009). Intracellular calcium is maintained at 0.1-0.2 µM even in the face of high extracellular concentrations by blocking the uptake of and pumping out calcium ions. Ion channels, F-type and P-type ATPases, and ion gradient-driven transporters are all used to maintain ion homeostasis. One such P-type ATPase,

PA1429, was identified as a probable Ca²⁺ export pump by Guragain *et al.* and was up-regulated in a *tat* mutant by 2.9 fold (Guragain *et al.*, 2013). This may have caused lowering of intracellular [Ca²⁺] and together with glutamate could have triggered overexpression of the T3SS regulon in a *tat* mutant.

The most down-regulated genes in a *tat* mutant were predominantly involved in anaerobic respiration (*nir* and *nor* genes), oxidative stress (*sodM*, *hemO*) and general stress (*dnaK*). *P. aeruginosa* prefers aerobic growth but is able to grow anaerobically using nitrogenous oxides as a terminal electron acceptor (Levy-Booth *et al.*, 2014). The denitrification pathway proceeds through four reductase reactions, as outlined in **Figure 3.9**. Together they catalyse the process converting nitrous oxide to nitrogen (Levy-Booth *et al.*, 2014). A PAO1 Δ *tatC* mutant was previously shown to have a growth defect under anaerobic conditions (Urs a Ochsner *et al.*, 2002). NapA and NosZ are directly exported via the Tat system, also, *nir*, *nor*, *nar* and *nos* genes are reciprocally regulated by *pqs* QS which may contribute to the growth defect (Rampioni *et al.*, 2016; Gimenez *et al.*, 2018).

There was significant overlap between differentially expressed genes in a Δ *pqsA* mutant and a *tat* mutant. Both repressed pyoverdine and pyochelin biosynthesis, ferric-pyoverdine import (*fpv* genes), iron starvation (*PA4469*, *fumc1*, *fagA*), and PQS-regulated *mexGHI* transporter expression. PQS itself is an iron chelator and regulates various genes via iron-dependent and iron-independent pathways, as well as PqsR-independent pathways (Rampioni *et al.*, 2016). There was significant disruption to the expression of genes involved in heterologous siderophore import. PQS-dependent quorum sensing is interlinked with the cellular response to iron, as PQS chelates iron within the environment. Repression of PQS biosynthesis upon *tat* mutation must therefore affect mechanisms controlling iron homeostasis (Diggle *et al.*, 2007).

Not all of the genes within the *pqs* QS regulon had altered expression in a *tat* mutant, only 37 of a possible 158 genes had similar changes in expression. This was likely due to compensatory changes in the regulation of other PQS-controlled genes, plus, only one growth condition was used for transcriptomic analysis.

The greatest upregulation of genes was of those involved in carbon utilization and aromatic ring catabolism, focusing on the core metabolite anthranilate. Anthranilate degradation proceeds through sequential reactions catalysed by the gene products of *antABC*, *catBCA*, and *pcaCDBTFJI* as shown in **Figure 3.8** (Costaglioli *et al.*, 2012). Genes in the *antABC* operon were enriched by ~55 fold and the *catBCA* operon, between ~120 and ~250 fold. Their regulators *antR* and *catR* were also up-regulated in a *tat* mutant, as were the *pca* genes and *xyI* genes. The gene products of *xyIZ*, *xyIY*, *xyIX* and *xyIL* were up-regulated between ~12 and ~60 fold, together they transform methyl-benzoate into 3-methylcatechol and 4-methylcatechol (**Figure 3.8**).

Anthranilate is generated from chorismate by two different anthranilate synthases encoded on the genome, TrpEG and PhnAB, and by degradation of tryptophan via the kynurenine pathway with the products of the *kynABU* operon (Costaglioli *et al.*, 2012). TrpEG is thought to produce anthranilate for tryptophan biosynthesis and PhnAB, for PQS biosynthesis, due to differing peak expression (Essar, Eberly, Han, *et al.*, 1990). The *trpEG* genes are predominantly expressed during early stages of growth where there is low cell density, and repressed at high-cell density (Essar, Eberly, Hadero, *et al.*, 1990). LasR positively regulates *kynU*, *kynB* and *phnAB* during log phase, and PhnAB production is also induced by the autoinducer PQS, as well as by the effector protein PqsE, as *phnAB* is part of the *pqsABCDE/phnAB* operon (Rampioni *et al.*, 2010; Palmer *et al.*, 2013; Rampioni *et al.*, 2016). However, none of the genes involved in anthranilate production were differentially regulated in the RNAseq data.

Despite a large increase in transcription of genes that break down anthranilate and methyl-benzoate to make substrates of the citric acid cycle, there was very little change within expression of genes within the citric acid cycle and central carbon metabolism. The peripheral pathway gene *ascA*, which encodes acetyl-coA synthase was up-regulated 3.31 fold upon *tat* mutation, and within the TCA cycle, fumarate hydratase *fumC1* was actually down-regulated ~22 fold. However, the other two genes *fumA* and *fumC2* were not differentially expressed (Dolan *et al.*, 2019). This may be because wild-type levels of each TCA cycle enzyme are able to cope with increased substrate concentration. Published RNAseq data showed that deletion of *pqsA* also results in upregulation of the *catBCA* genes, highlighting the reciprocal relationship of PQS biosynthesis and anthranilate degradation (Rampioni *et al.*, 2010). PqsA catalyses the head-to-head condensation of anthranilate with β -keto-dodecanoate to create a precursor for PQS and up to 50 other AQs, see **Figure 3.36** (Fletcher *et al.*, 2007).

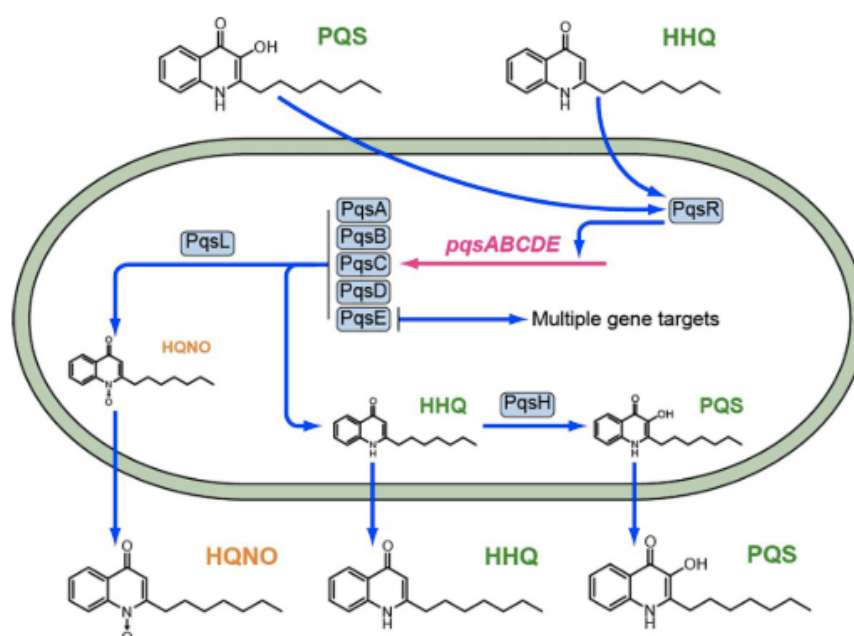


Figure 3.36. AQ biosynthesis pathway in *P. aeruginosa*. PqsABCDE proteins synthesise HHQ, and together with PqsL, HQNO. HHQ is converted to PQS by PqsH. PqsE acts as a thioesterase for AQ biosynthesis but also acts as an AQ-independent effector protein with multiple gene targets including pyocyanin and rhamnolipid production. HHQ and PQS bind PqsR and cause autoinduction of the *pqsABCDE* operon. Figure taken from Soh *et al.* 2021.

Expression of *antR* and *antA* is tightly controlled by many different regulators and interwoven with quorum sensing systems due to the shared substrate with PQS biosynthesis. This is outlined in **Figure 3.37**. AntR directly activates *antABC* expression, with anthranilate as a coinducer that increases affinity for the *antABC* promoter (Oglesby *et al.*, 2008). AntR also positively regulates *catBCA* expression (Oglesby *et al.*, 2008; Djapgne *et al.*, 2018). PqsR represses genes for anthranilate metabolism, preventing degradation of the substrate required for PQS biosynthesis. AntR and PqsR, the orange and blue regulators in **Figure 3.37**, work against each other for tight control of the *antA* and *pqsA* promoters.

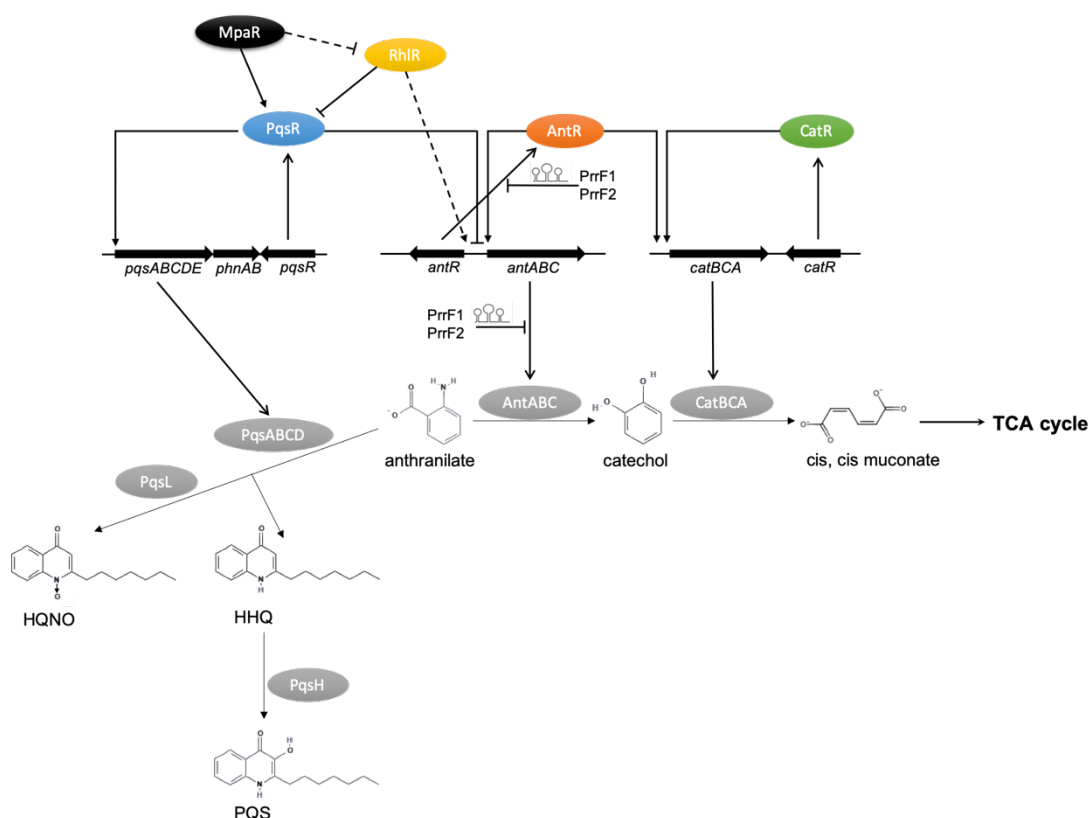


Figure 3.37. Model showing regulation of anthranilate metabolism genes (*antABC*, *catBCA*) and the AQ biosynthetic operon (*pqsABCDEphnAB*) by AntR, PqsR, RhIR, MpaR, and PrrF sRNAs.

MpaR regulates anthranilate degradation indirectly through induction of PqsR and repression of RhIR transcription. PqsR represses AntR expression, and AntR positively regulates its own expression in addition to *antABC* and *catBCA*. PrrF1 and PrrF2 sRNAs promote AQ production under iron-deplete conditions by regulating *antA* and *antR* mRNA translation. T-bars indicate inhibition, arrows indicate positive regulation. Solid lines and dashed lines show direct regulation and indirect regulation respectively. The structure of PrrFs was taken from Djapgne *et al.* 2018. Chemical structures are from pubchem.com.

PrrF1 and PrrF2 are two small regulatory RNAs with 95% sequence similarity. They promote AQ production by redundantly inhibiting *antABC* and *antR* translation through binding to the 5' untranslated region overlapping the translation start site of each mRNA (Djapgne *et al.*, 2018). Both PrrFs were down-regulated in a *tat* mutant (*prrF1* was repressed 4.87 fold, and *prrF2*, 17.62 fold) which may be a contributing factor to increased *antA* and *antR* expression.

MpaR is a regulator from the GntR-type family, these regulators are often involved in critical metabolic processes (Wang *et al.*, 2020). In this case, MpaR regulates PQS production and anthranilate metabolism. This is achieved through direct activation of *pqsR* expression as well as repression of *rhIR* as outlined in **Figure 3.37**, and deletion mutants have exhibited increased *antABC* transcription, biofilm formation and lower pyocyanin levels (Wang *et al.*, 2020).

Expression of *antA* is under complex hierarchical control by other QS regulators and is growth-phase dependent (**Figure 3.37**). During log phase of the growth cycle *antA* is repressed, and in late-stationary phase is activated by RhIR (Chugani and Greenberg, 2010; Kim *et al.*, 2012). This antagonistic interplay between *las* and *rhl* QS is mediated by the transcriptional regulator AntR, which directly induces transcription, and PqsR, which directly represses *antA* transcription and is outlined in more detail in **Figure 3.38** (Choi *et al.*, 2011).

Figure 3.38 shows a schematic model for the control of the *pqsABCDE/phnAB* promoter by its direct regulator, PqsR, and the *antABC* and *antR* promoters by their direct regulators, AntR and PqsR. Hypothesised regulation of each set of genes in wild-type *P. aeruginosa*, a $\Delta pqsA$ mutant and a *tat* mutant and a $\Delta antA$ mutant is shown for comparison. Only mutation or deletion of *tat* resulted in a growth defect, and this is likely due to failed export of one or more of the Tat pathway substrates.

The *pqsA-E* operon is co-regulated by QscR, RhIR, LasR, PqsR (MvfR), AmrZ, ExsA, GacA, GbdR, LasR, MexT, PchR, PhoB, and RsaL and altered activity or expression of these may have affected expression of *pqs* biosynthesis genes in the *tat* mutant, which in turn caused upregulation in anthranilate degradation (Huang *et al.*, 2019).

As *antA* and *pqsA* are both directly regulated by PqsR, the simplest explanation is that PqsR activity is reduced in a *tat* mutant, which prevents *antA* repression and *pqsA* expression during log phase (**Figure 3.38**). Soh *et al.* showed that addition of HHQ and PQS as PqsR co-inducers were unable to restore *pqsA* expression in a $\Delta pqsA$ *tatA::Tn5* mutant (Soh *et al.*, 2021). Neither expression of *pqsR* nor its localisation is affected by *tat* mutation, which suggests that access of, or response to, Aqs by PqsR requires a functional *tat* pathway (Soh *et al.*, 2021; Ye-Chen Soh, Thesis, University of Nottingham).

As less anthranilate is used for AQ biosynthesis upon *tat* mutation it may accumulate within the cell, increasing the binding of AntR to the *antA/antR* promoter region and further inducing expression of anthranilate degradation genes. **Figure 3.24** shows addition of anthranilate up-regulated *antA*, *antR* and *catB* and therefore increased endogenous anthranilate is likely to do the same. Further work should include LC-MS/MS quantification of intracellular anthranilate in PAO1-DK, a *tat* mutant, $\Delta pqsA$ mutant and $\Delta antA$ mutants, and their respective double mutants.

Due to the wide range of differentially expressed genes discovered by RNAseq, and complex regulatory networks that govern *pqsA* expression, it is impossible to say which regulator(s) are responsible for changes to PqsR-mediated *antA* repression in a *tat* mutant. Continuation of this project could delete various regulatory genes of PqsR in a *tat* mutant, such as QscR, MpaT, and RhIR to see if *pqsA* expression is restored.

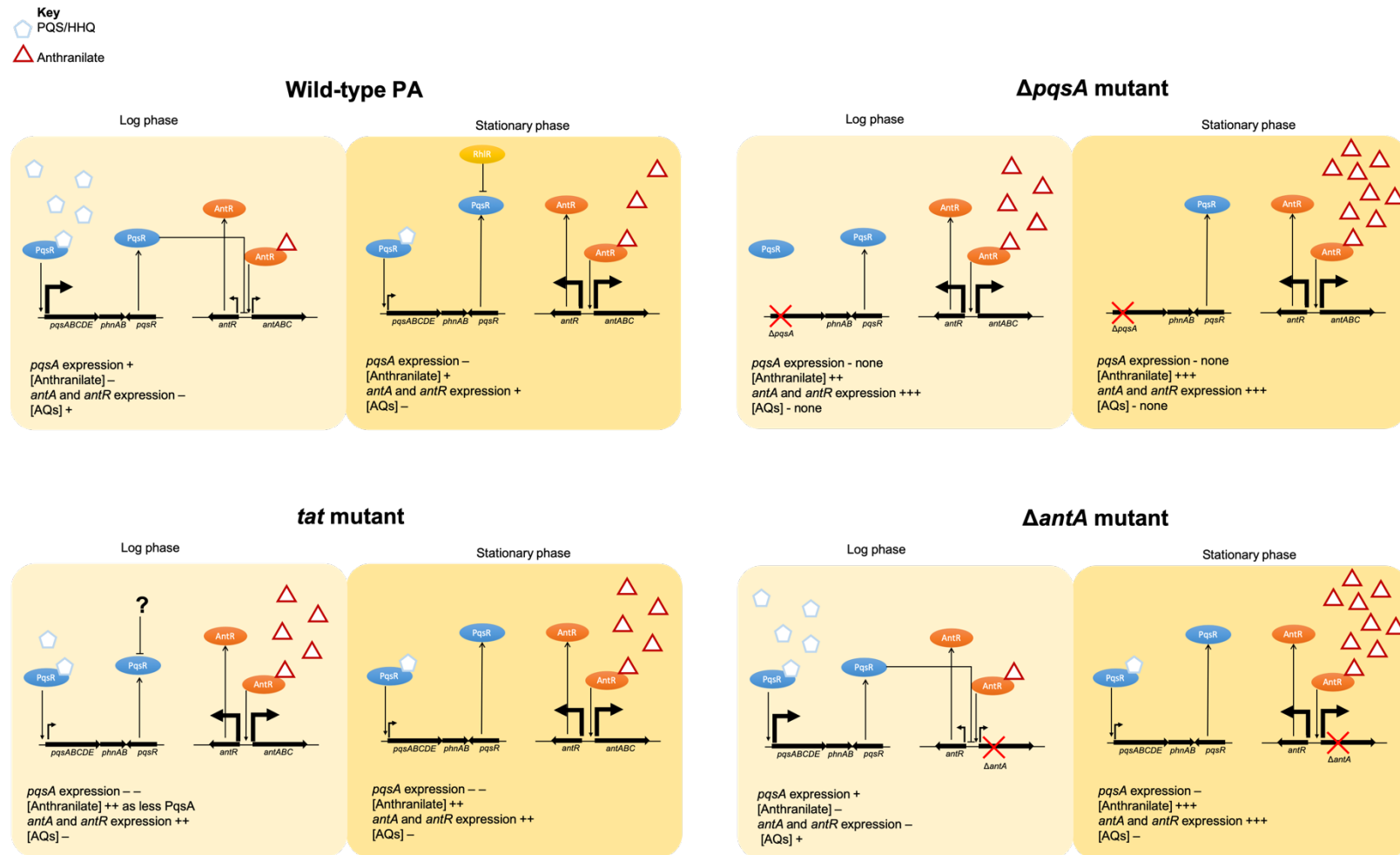


Figure 3.38. Schematic to illustrate hypothesised regulatory changes to *antA*, *antR* and *pqsA* expression in wild-type, $\Delta pqsA$, *tat*, and $\Delta antA$ mutants. Regulation of *antABC* by PqsR appears to be a key factor in the altered expression of *antA* and *pqsA* in the *tat* mutant as it is the only regulator to directly bind to both promoters. Therefore, in a *tat* mutant PqsR activity is impacted, this may be due to inhibition of *pqsA* by other regulators, or reduced access to PqsR by cognate autoinducers as a result of failed export of one of the Tat substrates, or due to the growth defect. Deletion of *pqsA* resulted in upregulation of anthranilate degradation genes most likely in response to the overproduction of anthranilate, which cannot be used for AQ biosynthesis. PAO1 $\Delta antA$ produced anthranilate levels similar to wild-type during log phase, and *antA* expression was no different. After 16 h growth anthranilate was increased in culture supernatants which suggests increased intracellular concentration, and with it, up-regulated expression at the *antA* and *antR* promoters despite *antA* deletion. Concentration is indicated by square brackets "[]", AQs PQS and HHQ as blue pentagons, and anthranilate a red triangle.

Mutation or deletion of the *tat* pathway resulted in an obvious growth defect (**Figure 3.19**) which may be the cause of delayed peak *antA* and *catB* expression. Deletion of $\Delta antA$ did not affect growth, but nearly abolished the growth defect seen in the $\Delta tatABC$ mutant. Tryptophan is essential for growth, so perhaps there is a reduction in tryptophan due to upregulation of anthranilate degradation upon *tat* mutation. This hypothesis could easily be tested by extraction of tryptophan within cells and quantification with LC-MS/MS or by adding tryptophan to $\Delta tatABC$ culture to see if growth is restored (Sadok *et al.*, 2017). Alternatively, deletion of *antA* in a $\Delta tatABC$ mutant prevents accumulation of toxic cis, cis muconate.

Conclusion

Tight control of the metabolite anthranilate is needed for the *P. aeruginosa* cell to respond to changing environmental conditions. Mutation or deletion of the *tat* pathway perturbs *pqs* QS as well as a number of other genes and prevents export of at least 34 known effectors. As a result, mutants of the Tat secretion system have slower growth, do not release eDNA or form mature biofilms, and have reduced microvesicles, rhamnolipids and PQS-controlled secondary metabolites such as pyocyanin (Soh *et al.*, 2021). Deletion of *antA* from a $\Delta tatABC$ mutant exacerbates the loss of PQS-dependent quorum sensing likely because it results in further accumulation of the co-inducer anthranilate. Although the work here has demonstrated the wide-reaching transcriptional changes due to *tat* mutation, there is no obvious mechanistic link to PQS-dependent quorum sensing. The Tat system exports 34 different effectors, with final locations in the inner membrane, periplasmic space and extracellular milieu (Soh *et al.*, 2021). Therefore, failed export of one or more of these proteins could be the link between *tat* mutation and perturbed *pqs* QS and additional work is needed to investigate this further.

**Chapter 4: Identification of the Tat
substrate primarily responsible for
causing perturbation in
PQS-dependent quorum sensing**

4.1 Introduction

A fully-functioning Tat system is vital for adaptation to environmental changes and effective virulence in *P. aeruginosa* (Ball *et al.*, 2016; Gimenez *et al.*, 2018). Deletion of the Tat system has a significant impact on the exoproteome as well as gene expression (Ball *et al.*, 2016). Ball *et al.* found no difference in the exoproteome of PAO1 under nutrient rich conditions, instead Tat substrates were primarily exported under phosphate starvation, a condition known to stimulate virulence factor production (Ball *et al.*, 2016).

The genome of *Pseudomonas aeruginosa* has been screened several times *in silico* for potential Tat substrates and between 18 and 57 have been identified depending on the method used. Ball *et al.* experimentally identified 36 proteins as having direct or indirect dependence on a functional Tat system by comparing the extracellular proteome of wild-type PAO1 and Δtat mutant. Recently, Gimenez *et al.* have built upon this to create a library of 34 validated Tat substrates in the strain *P. aeruginosa* PA14 (Gimenez *et al.*, 2018). Tat substrates were discovered through stringent *in silico* screening and utilisation of a novel *E. coli*-based amidase assay for *in vivo* validation. Briefly, signal peptides of Tat-transported AmiA and AmiC, two amidases, were deleted from *E. coli*. This mutant was unable to grow in SDS and readily form chains of cells. Putative *P. aeruginosa* Tat-signal peptides were fused to a mature AmiA coding sequence in lieu of the AmiA signal peptide, and then produced *in trans* the $\Delta amiAC$ mutant to see if wild-type phenotype could be restored. Single cells formed and were able to grow in SDS-containing media when the chimeric protein was exported via the Tat system, as cell wall biosynthesis is restored (Gimenez *et al.*, 2018).

The majority of PA Tat substrates are involved in adaptation to changing environments, virulence and pathogenicity. Secreted virulence factors, proteins

involved in iron acquisition, and proteins involved in energy metabolism make up 13 of the 36 Tat substrates. The remaining substrates are primarily involved in an oxidation-reduction process. There are 6 exported proteins whose predicted biological process and predicted function are unknown. Each substrate is listed in **Table 4.1** along with the function and database identifier.

Transcriptome analysis with RNAseq and bioluminescent transcriptional reporter assays showed that deletion or mutation of the *tatABC* operon altered expression of genes whose protein product utilises anthranilate as a substrate. Due to the reciprocal relationship between anthranilate degradation and PQS biosynthesis, *antABC* was induced upon *tat* mutation and the *pqsABCDE/phnAB* operon was significantly down-regulated by approximately 3 fold in PA14 and 4 fold in PAO1-DK (Soh *et al.*, 2021). In a Tat mutant cell growth was slowed, eDNA release was reduced, the PQS regulon was disrupted, and biofilm formation was almost completely abolished (Soh *et al.*, 2021).

The pleiotropic effects of the *tat* mutation were seen in both PAO1-DK and PA14, two commonly used laboratory strains that represent two main phylogenetic *P. aeruginosa* groups (Muthukumarasamy *et al.*, 2020). This study has shown that PAO1-DK and PA14 can be used interchangeably when measuring effects of *tatABC* deletion on PQS quorum sensing and anthranilate degradation. The aim of this study was to ascertain why (i) PQS signalling is perturbed, and (ii) why the anthranilate degradation pathway is induced in a *tat* mutant.

Mutant Number	PA Number	PA14 Number	Name and Function
1	PA0144	PA14_01780	Nucleoside 2-deoxyribosyltransferase
2	PA0365	PA14_04790	Hypothetical protein
3	PA0735	PA14_54770	Hypothetical protein
4	PA0844	PA14_53360	Hemolytic phospholipase C (PlcH)
5	PA1174	PA14_49250	Nitrate reductase catalytic subunit (NapA)
6	PA1601	PA14_43790	Aldehyde dehydrogenase
7	PA1880	PA14_40200	Oxidoreductase
8	PA2065	PA14_37790	Copper resistance protein (CopA)
9	PA2124	PA14_37100	Dehydrogenase
10	PA2264	PA14_35300	Putative sugar dehydrogenase
11	PA2328	PA14_34510	Hypothetical protein
12	PA2378	PA14_33900	Aldehyde dehydrogenase
13	PA2389	PA14_33770	Hypothetical protein (PvdR)
14	PA2392	PA14_33740	Tyrosinase (PvdP)
15	PA2394	PA14_33720	Aminotransferase (PvdN)
16	PA2531	PA14_31820	Aminotransferase
17	PA2635	PA14_30040	Hypothetical protein
18	PA2699	PA14_29230	Hydrolase
19	PA3222	PA14_22560	Permease
20	PA3319	PA14_21110	Non-hemolytic phospholipase C (PlcN)
21	PA3392	PA14_20200	Nitrous-oxide reductase (NosZ)
22	PA3713	PA14_16360	Spermidine dehydrogenase (SpdH)
23	PA3768	PA14_15670	Metallo-oxidoreductase
24	PA3910	PA14_13330	Phosphodiesterase/alkaline phosphatase (EddA)
25	PA4140	PA14_10370	Cholesterol oxidase (ChoA)
26	PA4159	PA14_10170	Iron-enterobactin transporter periplasmic binding protein (FepB)
27	PA4431	PA14_57570	Cytochrome <i>bc</i> ₁ Rieske subunit (PetA)
28	PA4621	PA14_61150	Oxidoreductase
29	PA4692	PA14_62110	Sulphite oxidase subunit (YedY)
30	PA4812	PA14_63605	Formate dehydrogenase-O, major subunit (FdnG)
31	PA4858	PA14_64270	Hypothetical protein
32	PA5327	PA14_70330	Oxidoreductase (SphC)
33	PA5538	PA14_73040	N-acetylmuramoyl-L-alanine amidase AmiC
34	Not conserved	PA14_48450	Peptidyl-arginine deiminase (Agu2A)*

Table 4.1. Substrates exported by the *P. aeruginosa* Tat secretion pathway. Each substrate has been deleted in PA14 and the clean deletion mutants are numbered 1 to 34.*There is no ortholog of PA14_48450 in PAO1 so the PA14 annotation is retained. Dr. Bérengère Ize, CNRS, Marseille donated the strains, which were created by Maxime Gimenez (Ball *et al.*, 2016; Gimenez *et al.*, 2018; Soh *et al.*, 2021).

Disruption of the Tat system can compromise cell membrane integrity, and mutation of Tat in *E. coli* resulted in an unstable outer membrane, periplasmic leakage, sensitivity to detergents, and formation of chains of up to 10 cells long (Stanley *et al.*, 2001). However, mutation of *tat* in *P. aeruginosa* does not result in a chain-forming phenotype (Ball *et al.*, 2016). Nevertheless, it is possible that mutation of *tat* may result in more subtle changes in the cell envelope.

It is also possible that one or more of the effectors transported by the Tat system is required for PQS-dependent quorum sensing. Transcriptomic analysis of differently regulated genes outlined in Chapter 3 revealed that expression of 10 of the Tat substrate genes were expressed differently in a *tat* mutant (Appendix, **Table 7.1** and **Table 7.2**). None of them were obvious candidates that might link Tat to PQS-dependent quorum sensing. With this knowledge, the work in this chapter aimed to screen the 34 *P. aeruginosa* Tat substrate deletion mutants (**Table 4.1**) for their impact on PQS biosynthesis and anthranilate degradation, as well as biofilm formation, virulence and resistance to antibiotics.

4.2 Results

4.2.1. Screening of a deletion mutant library of Tat system substrates

It was hypothesised that failure of *P. aeruginosa* cells to export a specific Tat substrate and its subsequent mislocalisation causes perturbation of PQS-dependent QS. The Tat protein export pathway has a wide variety of substrates which differ in expression, final destination, and function. An initial delve into the literature did not reveal any obvious candidates linked to PQS biosynthesis or anthranilate degradation, so a subgroup could not be singled out for further analysis. As such, each of the 34 PA14 Tat substrate mutants were tested for PQS signalling-perturbed phenotypes.

4.2.1.1. Expression of *pqsA* and *antA*

Expression of *pqsA* and *antA* were measured across the substrate mutant library in order to narrow down the group of Tat system substrate mutants to a reduced number of lead substrates. The miniCTX::*pqsA*'-lux and miniCTX::*antA*'-lux transcriptional reporters were integrated into each Tat system substrate mutant chromosome via conjugation and selection with tetracycline, and gene expression was measured over 24 h.

Figure 4.1 shows that only 3 of the 34 mutants had significantly altered expression of *pqsA*, and of these only one (the PA4431 mutant) was significantly lower than wild-type PA14. Tat substrate mutants 1 and 21 exhibited increased *pqsA* expression when compared with wild-type. The mutations were in *PA0144*, a nucleoside deoxyribosyltransferase, and *PA3392* which corresponds to *nosZ*, a nitrous oxide reductase. In the PA4431 mutant, number 27, *pqsA* expression was down-regulated to approximately one third of wild-type, which was similar to that

observed for the $\Delta tatABC$ mutant. The gene PA4431 encodes the Rieske iron-sulphur subunit of cytochrome bc_1 , PetA),

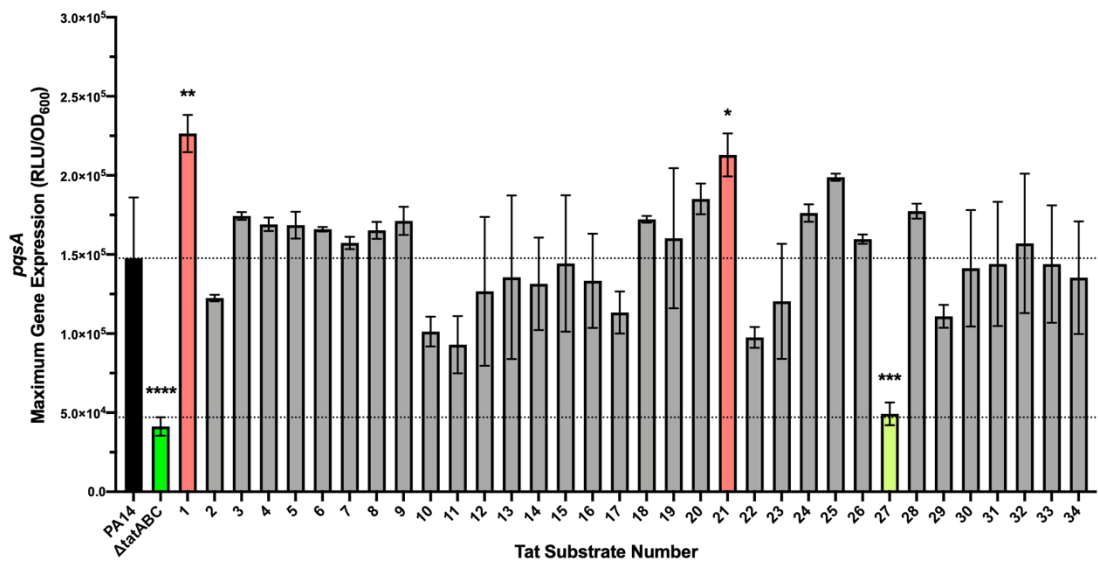


Figure 4.1. Expression of *pqsA* in PA14, PA14 $\Delta tatABC$, and deletion mutants of substrates exported via the Tat system. A miniCTX::*pqsA*-lux vector was introduced to the chromosome of each mutant and expression over 24 h was measured. Maximum expression was taken for each technical repeat and the mean \pm SD is plotted. The experiment was repeated 3 times. One-way ANOVA determined which strains had a statistically significant difference in expression compared to wild-type PA14. Mutants with significantly lower *pqsA* expression are shown in green and those with significantly higher *pqsA* expression are shown in red.

Figure 4.2 shows 8 of the 34 Tat substrate mutants had significantly higher *antA* expression compared with wild-type PA14. Mutants of Tat substrates 2 and 27 had the greatest upregulation of *antA*, with RLU values of around 5×10^4 . These are PA0365, a hypothetical membrane protein, and the previously mentioned PA4431 (*petA*). Both had ~ 2 fold increase in expression compared with wild-type PA14 and the difference was statistically significant with a *p* value of < 0.0001 . Tat substrate 4 is PA0844, or *plcH*, the gene for haemolytic phospholipase C. The remaining Tat substrate mutants with increased expression were 20, 21, 22, 24 and 25. In order, these are deletion mutants of PA3319 (non-haemolytic phospholipase C, *plcN*), PA3392 the nitrous-oxide reductase *nosZ*, PA3713 (spermidine

dehydrogenase, *spdH*), PA3910 (phosphodiesterase, *eddA*), and PA4140 (cholesterol oxidase, *choA*).

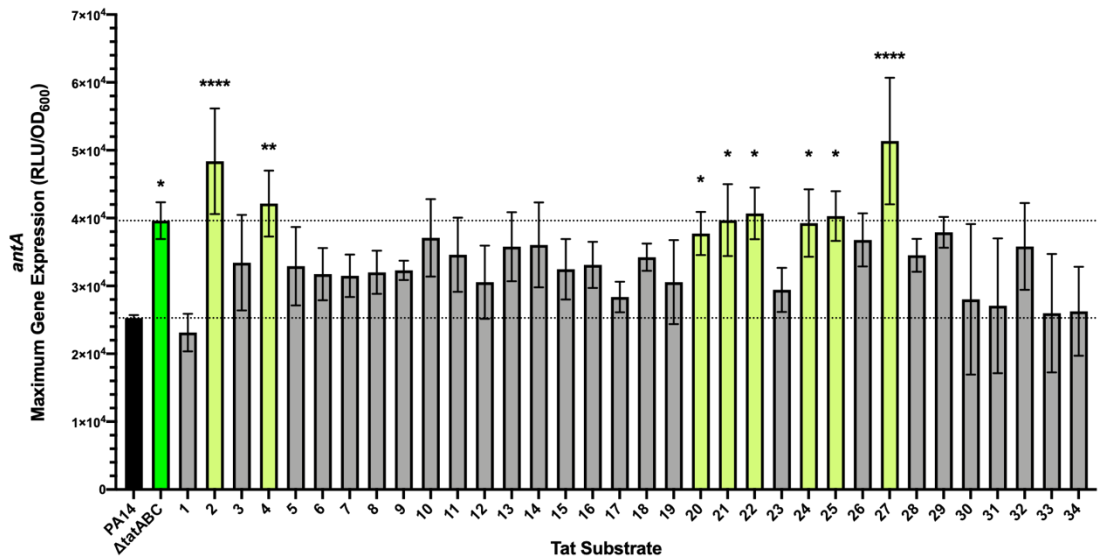


Figure 4.2. Maximum expression of the *antA* promoter in PA14 and PA14 Δ *tatABC* compared with that in each of the 34 Tat substrate mutants. A miniCTX::*antA*-lux vector was introduced to the chromosome of each mutant and expression over 24 h was measured. Maximum expression was taken for each technical repeat and the mean \pm SD is plotted. The experiment was repeated 3 times. One-way ANOVA determined which strains had a statistically significant difference in expression compared with wild-type PA14, these are shown in green.

4.2.1.2. Altered pyocyanin production

Production of the virulence factor pyocyanin is regulated by *rhl* and *pqs* quorum sensing systems. Biosynthesis is carried out by the products of two redundant seven-gene operons: *phzA1-G1* and *phzA2-G2* as well as the genes *phzH*, *phzM* and *phzS* (Mavrodi *et al.*, 2001). Although the genes in each operon share 98% identity, their upstream regions differ and the regulation of their expression responds to contrasting environmental cues (Chugani *et al.*, 2001; Higgins *et al.*, 2018). This differential regulation becomes obvious when looking at lifestyle, as *phzA1-G1* is up-regulated in planktonic growth and *phzA2-G2* in colony biofilms (Recinos *et al.*, 2012).

Pyocyanin production via the *phzA1-G1* operon is strongly up-regulated by *pqs* QS as cells transitioned to stationary phase (Déziel *et al.*, 2005). Expression of *phzA1-G1* was shown to be significantly reduced in a PAO1-DK *tat* mutant (Soh *et al.*, 2021). As such, one assay for indication of normal PQS quorum signalling is to measure the concentration of pyocyanin in culture supernatants at 8 h growth. Using the method previously published, pyocyanin concentration was measured in wild-type and PA14 Δ *tatABC* culture supernatants to establish a significant difference in pyocyanin concentration (Essar, Eberly, Hadero, *et al.*, 1990). Next, pyocyanin in all 34 Tat system substrate mutants was also measured both in biological and technical triplicates and the results can be seen in **Figure 4.3**. A phenazine mutant incapable of pyocyanin production was used as a control.

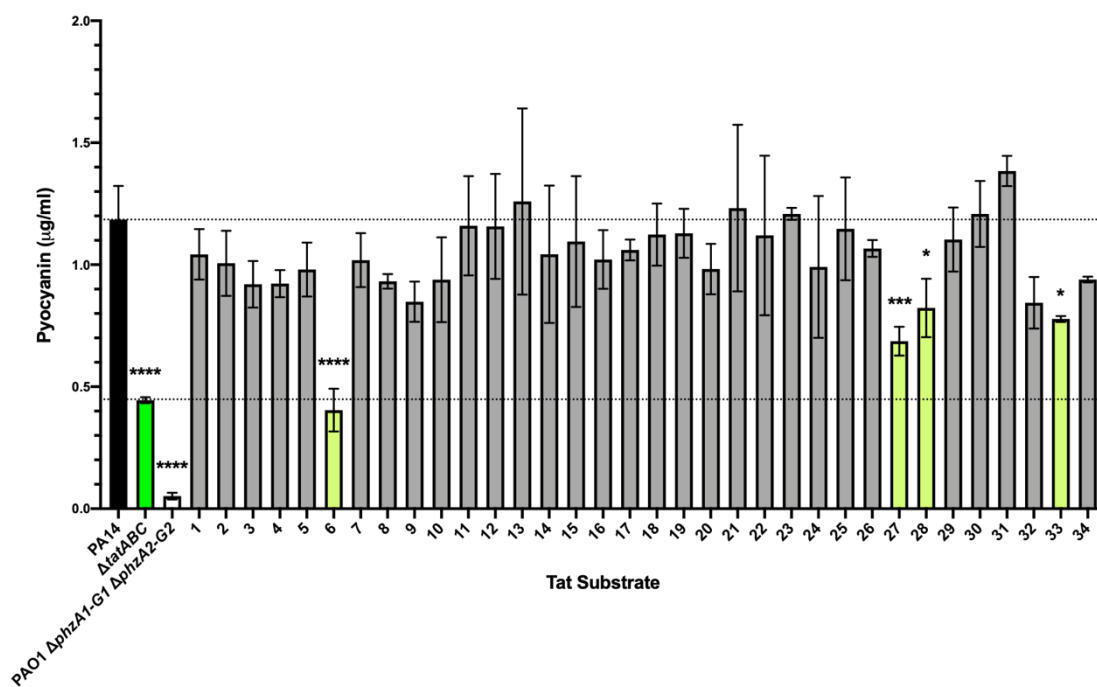


Figure 4.3. Normalised pyocyanin in 8 h culture supernatants of Tat substrate deletion mutants. Pyocyanin extracted from wild-type PA14, PA14 Δ *tatABC* and a phenazine-deficient strain was quantified and compared with pyocyanin production in each Tat substrate deletion mutant (1-34). One-way ANOVA test determined significant difference to PA14 (****= $P \leq 0.0001$, ***= $P \leq 0.001$, **= $P \leq 0.01$, *= $P \leq 0.05$) and mutants with statistically lower pyocyanin are highlighted in green.

Pyocyanin was reduced to approximately one third of the wild-type concentration upon deletion of *tatABC*. The deletion mutant of Tat substrate 6, which corresponds to the aldehyde dehydrogenase gene *PA1601*, had the lowest level of pyocyanin with ~ 0.4 $\mu\text{g}/\text{mL}$. Mutants of Tat substrates 27, 28 and 33 were also found to have significantly lower concentrations compared with wild-type levels. These are deletion mutants of genes *PA4431* (*petA*), *PA4621* (oxidoreductase) and *PA5538* (*amiC*) respectively. The rest of the Tat substrate deletion mutants made concentrations of pyocyanin that were not significantly different from wild type PA14.

Section Summary

Expression studies using a chromosomally integrated *pqsA* transcriptional reporter showed that only deletion *PA4431* (*petA*) gave significantly reduced *pqsA* expression. The severity of *pqsA* downregulation seen in *petA* was almost identical to that of the $\Delta\textit{tatABC}$ mutant. Similarly, pyocyanin production was significantly reduced in a *petA* mutant. All other strains with decreased pyocyanin production were eliminated as candidates in the *pqsA* screen, which showed no difference in expression of the PQS biosynthetic operon. In addition, expression measured with *miniCTX::antA'-lux* showed that *petA* was up-regulated, as observed in PA14 $\Delta\textit{tatABC}$. Cross examination using three different screens showed that the best candidate for a link between deletion of the Tat system and perturbed PQS biosynthesis was *petA*.

4.2.2. The pleiotropic effects of *PA4431* deletion are similar to *tat* mutation

As demonstrated earlier, deletion of *petA* resulted in the only Tat substrate mutant with repressed PQS biosynthesis, pyocyanin production, and up-regulated anthranilate degradation compared with the isogenic wild-type PA14. The gene *petA* encodes the Rieske subunit of the cytochrome *bc*₁ complex, an integral part of the electron transfer chain. Cyt *bc*₁ is also known as ubiquinol cytochrome *c* oxidase, or complex III (Xia *et al.*, 2013). It is found in various organisms, located in the inner membrane of mitochondria and cytoplasmic membrane of prokaryotes. In addition to its core contribution to cellular electrochemical potential, it is a key part of photosynthetic apparatus in purple bacteria. In *P. aeruginosa* the complex consists of three redox subunits: cytochrome *b*, which contains two hemes, cytochrome *c*, with one haem, and the Rieske subunit, also known as the iron-sulphur protein (ISP) that co-ordinates a 2Fe-2S cluster, as shown in **Figure 4.4** (Xia *et al.*, 2013). They are encoded by *petB* (*PA4430*), *petC* (*PA4429*), and *petA* (*PA4431*) respectively. *PetA* was chosen as the lead candidate for further study and complementation of Δ *petA* was assessed to see if the wild-type phenotype could be restored.

Cyt *bc*₁ is involved in aerobic respiration as well as respiration under anaerobic conditions in the presence of nitrite (Hasegawa *et al.*, 2003). It is needed to transfer electrons from the low-potential membrane quinone pool to high-potential cytochrome *c* when in aerobic conditions and to nitrite reductase during anaerobic respiration. During this process, protons are translocated across the membrane, adding to the proton motive force (Xia *et al.*, 2013).

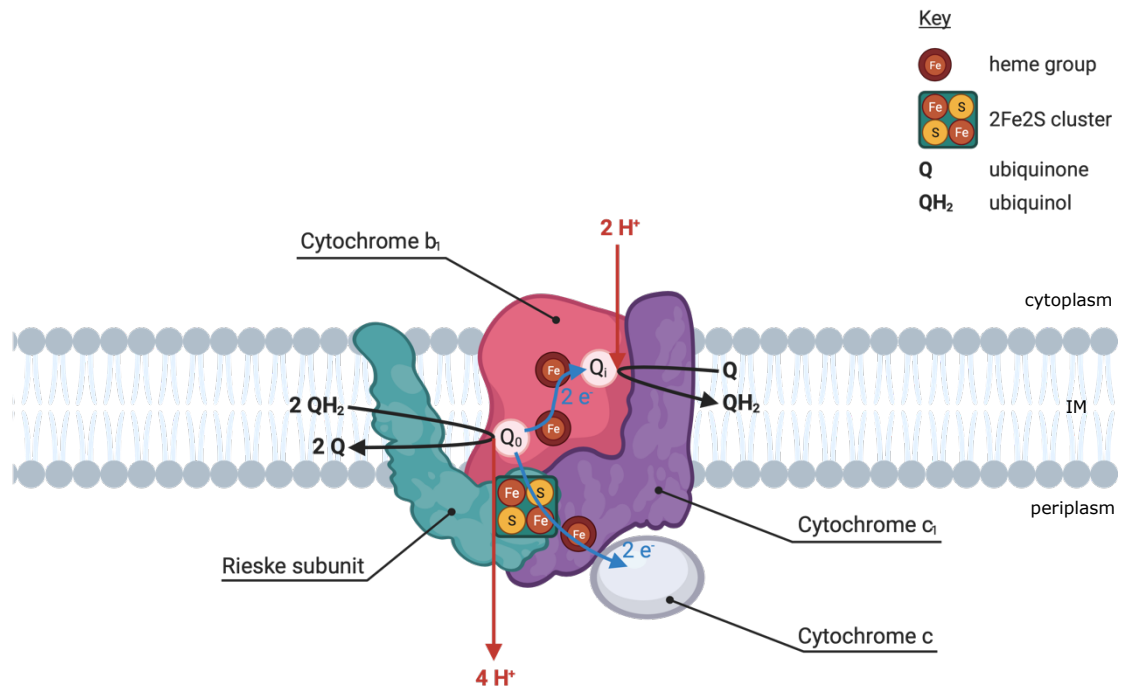


Figure 4.4. Schematic diagram of the cytochrome bc_1 complex unit. Membrane-spanning cytochrome b (pink), cytochrome c_1 (purple) and the Rieske subunit (blue) make up the cytochrome bc_1 complex of the electron transport chain. Protons are removed from the cytoplasm through reduction of ubiquinone at the Q_i site. Electrons are transferred from the ubiquinol pool to cytochrome c during aerobic conditions and protons are transported to the periplasm contributing to the proton-motive force. Created using BioRender.com

The Rieske subunit is a well-known example of a Tat substrate that retains its signal peptide as a membrane anchor following export in *P. aeruginosa*. The iron-sulphur cluster is coordinated by 2 histidine and 2 cysteine residues in other organisms, and is used to transfer electrons from cyt b to cyt c_1 as demonstrated in **Figure 4.4** (Ferraro *et al.*, 2005). The extracellular domain is connected to the membrane spanning region by a flexible linker region which aids movement between the two cytochrome subunits and subsequent transfer of electrons (Xia *et al.*, 2013).

Cytochrome bc_1 is ubiquitous and well-studied, there are high-resolution atomic structures from a range of organisms capturing various intermediate states of the reaction. Despite this, there are no structures based on x-ray crystallography for the *P. aeruginosa* cytochrome bc_1 complex. There is no current published link between the Rieske subunit of the cytochrome bc_1 complex and PQS-dependent quorum sensing so the phenotype of the $\Delta petA$ mutant was further investigated. *In silico* structure, function, and conservation prediction of PA14_57570 (PetA of PA14) is covered in the Appendix, **Figure 7.4**, **Figure 7.5**, **Figure 7.6**, and **Figure 7.7**.

4.2.2.1. PQS biosynthesis is lower in the $\Delta petA$ mutant and partially restored upon genetic complementation

As previously shown, *pqsA* expression was reduced in PA14 $\Delta petA$ and the maximum expression reached was very similar to that seen in PA14 $\Delta tatABC$ (**Figure 4.1**). The growth and *pqsA* expression over 24 h is shown in **Figure 4.5**. The *tat* mutant had a clear growth defect, as did *petA* (**Figure 4.5a**). Despite growth in rich media cells did not reach the same optical density as wild-type PA14. Similarly, wild-type *pqsA* expression increased rapidly from 4 h to 9 h, during exponential phase, before falling at a slower rate. PA14 $\Delta tatABC$ and PA14 $\Delta petA$ exhibited a similar *pqsA* expression profile, which had a much slower increase in *pqsA* expression compared with wild-type, between 4 h and 24 h. At the 4 h timepoint the growth rate slowed severely.

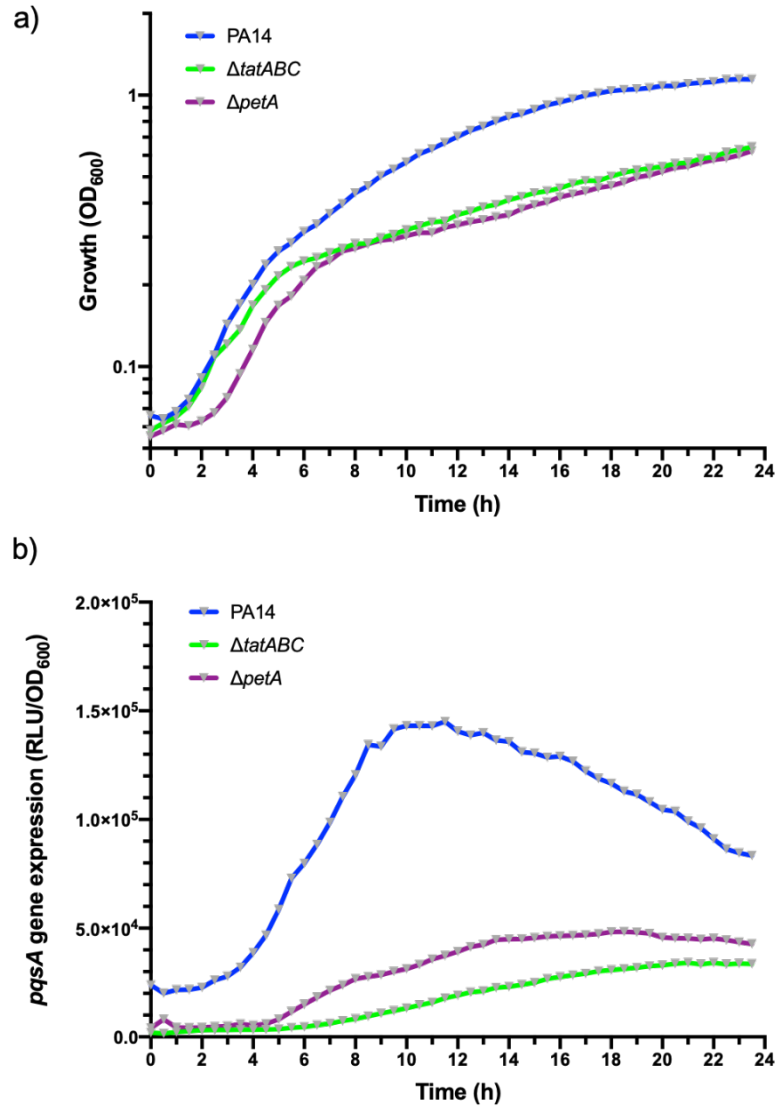


Figure 4.5. Growth (a) and *pqsA* expression in (b) of PA14, a PA14 *tat* deletion mutant and a *petA* deletion mutant over 24 h. Cultures were grown in triplicate over 24 h, OD₆₀₀ and luminescence (RLU) were measured every 30 min. Expression of *pqsA* was standardised to the growth (RLU/OD₆₀₀). Three independent experiments were carried out with similar results.

As maximal *pqsA* expression was ~3 fold lower in the $\Delta petA$ mutant compared with the wild-type, production of AQ signalling molecules was also investigated. Cultures were grown in LB broth at 37°C with good aeration. Samples were collected at two timepoints, 8 h and 16 h, which were chosen to cover late exponential and late stationary phase. The Aqs HHQ, PQS and HQNO were extracted and semi-quantified by LC-MS/MS.

Figure 4.6 shows a clear difference in AQ production between wild-type and both mutants after 8 h. HHQ is the precursor to PQS, and was ~8 fold lower in both $\Delta tatABC$ and $\Delta petA$ mutants. Following complementation of the $\Delta petA$ mutation, HHQ production increased to ~5 fold lower than wild-type but was not fully restored. Wild-type levels of PQS were ~3 fold higher than the $\Delta petA$ mutant and ~1.5 fold higher than PA14 $\Delta petA-CTX::petA$. However the PQS levels produced by the $\Delta tatABC$ mutant strain were not statistically lower than wild-type PA14 due to a broad spread of values. HQNO production was ~2 fold lower upon deletion of $\Delta tatABC$ and ~3 fold lower in the $\Delta petA$ mutant strain. Complementation of the $petA$ mutant raised HQNO levels to ~1.5 fold lower than wild-type, partially restoring the phenotype.

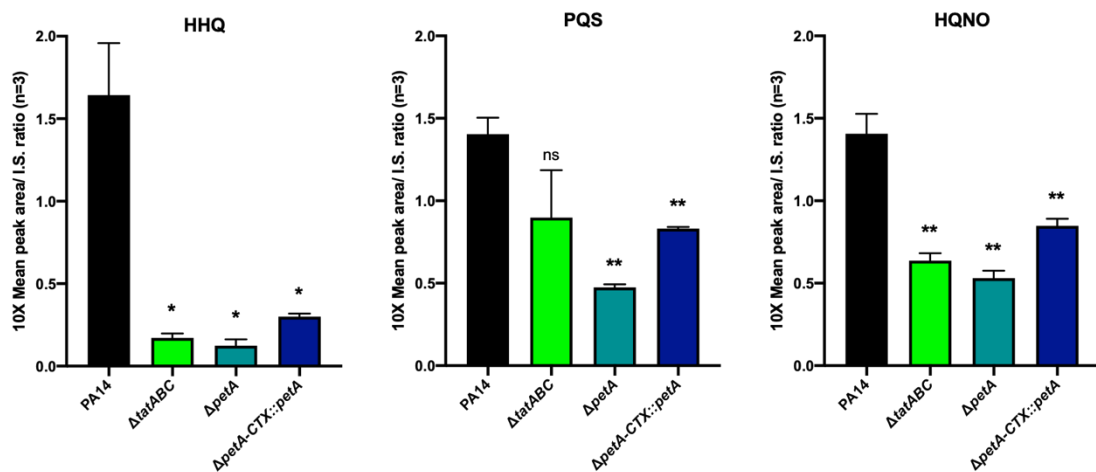


Figure 4.6. Aqs extracted from culture supernatants of PA14, PA14 $\Delta tatABC$, PA14 $\Delta petA$ and PA14 $\Delta petA-CTX::petA$ at 8 h and semiquantified with LC-MS/MS. PQS, its precursor HHQ, and HQNO extracted from 8 h culture supernatants of PA14 (black), PA14 $\Delta tatABC$ (green), PA14 $\Delta petA$ (teal) and the $petA$ complemented strain (blue). t-tests determined statistically significant differences compared to wild-type PA14. Data represent mean values \pm SD. $p \geq 0.05$ (ns), $p \leq 0.05$ (*), $p \leq 0.01$ (**), $p \leq 0.001$ (***)

Following 16 h growth the difference between AQ production in wild-type and mutant strains became more pronounced, as seen in **Figure 4.7**.

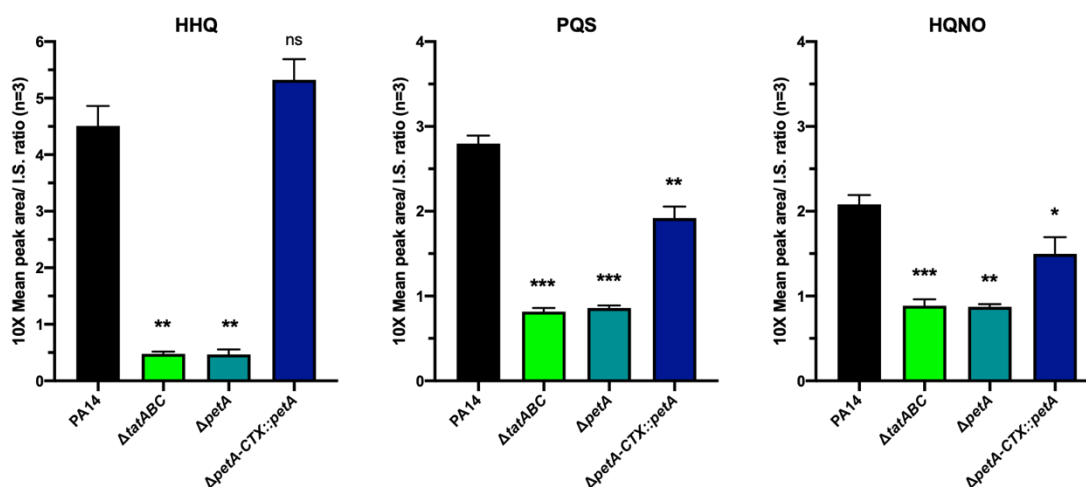


Figure 4.7. LC-MS/MS semi-quantification of AQs in culture supernatants from PA14, PA14 $\Delta tatABC$, PA14 $\Delta petA$ and PA14 $\Delta petA-CTX::petA$ following 16 h growth in LB. t-tests were used to show significant differences between wild-type PA14 levels and $\Delta tatABC$ mutant (green), $\Delta petA$ mutant (teal) and $petA$ complement (blue). Data represent mean values \pm SD. $P \geq 0.05$ (ns), $p \leq 0.05$ (*), $p \leq 0.01$ (**), $p \leq 0.001$ (***)

Higher levels of AQs were produced at the 16 h timepoint than at 8 h. HHQ production was reduced ~ 9 -fold in both the $\Delta tatABC$ and $\Delta petA$ mutants. This significant decrease in HHQ production was fully restored to wild-type level when $petA$ was complemented back in the PA14 $\Delta petA-CTX::petA$ strain. PQS was ~ 3 fold lower than wild-type in the $\Delta tatABC$ and $\Delta petA$ mutant strains and again was almost fully restored in the $petA$ complemented strain. **Figure 4.7** shows HQNO production was ~ 2 fold lower than wild-type in the $\Delta tatABC$ and $\Delta petA$ mutants and once again was almost fully restored in the $\Delta petA$ mutant upon complementation with miniCTX- $petA$. There was no difference in production of all three AQs when $\Delta tatABC$ mutant and the $\Delta petA$ mutant are compared.

PQS-dependent quorum sensing has regulatory control over pyocyanin production by upregulating expression of the *phzA1-G1* operon (Recinos *et al.*, 2012; Higgins *et al.*, 2018). As noted, *tat* mutation and *petA* deletion causes a

decrease in pyocyanin. The *petA* mutation was complemented with a miniCTX vector and pyocyanin was extracted and quantified from culture supernatants to determine whether complementation restored pyocyanin to wild-type levels. **Figure 4.8** shows a partial restoration after 8 h growth, as there appeared to be more pyocyanin in the *petA* complement than in the $\Delta petA$ strain. Statistical analysis with t-tests determined that PA14 and PA14 $\Delta petA$ -CTX::*petA* were significantly different at this timepoint ($p < 0.05$).

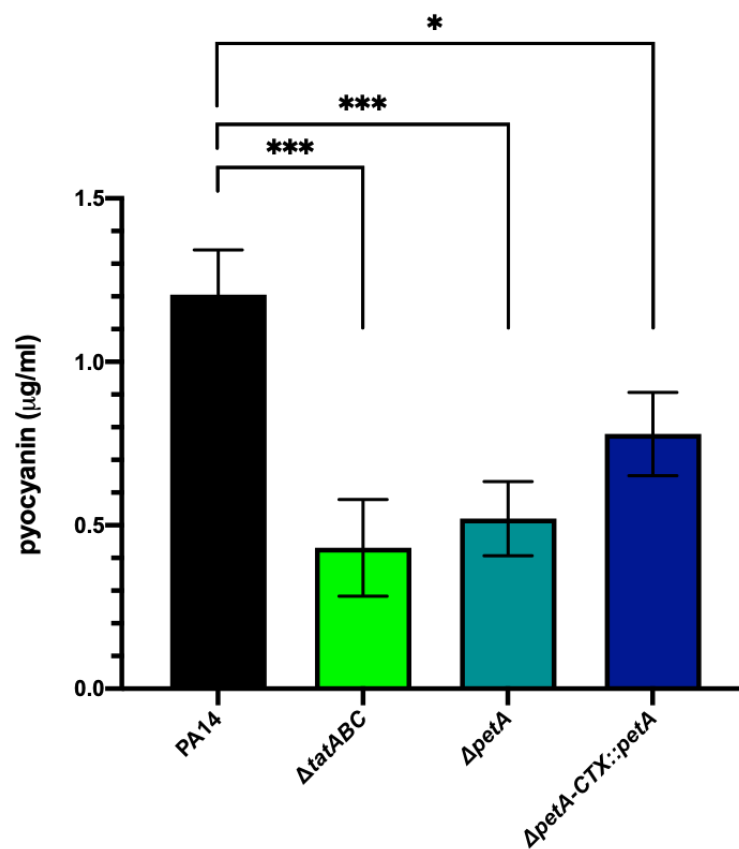


Figure 4.8. Pyocyanin production by *P. aeruginosa* at 8 h in PA14, a $\Delta tatABC$ mutant, a $\Delta petA$ mutant and the *petA* complemented strain. Experiment was carried out with biological and technical triplicates and graph shows the mean \pm SD.

4.2.2.2. Anthranilate production in a $\Delta petA$ mutant

LC-MS/MS was used to detect and semi-quantify anthranilate in culture supernatants following 8 h and 16 h growth (**Figure 4.9**). As seen previously, deletion of the *tatABC* operon in PAO1-DK resulted in an increase in anthranilate after 8 h planktonic growth but after 16 h growth there was significantly less than wild-type. In PA14 we see the same pattern – anthranilate production by PA14 $\Delta tatABC$ was ~ 2 fold greater during late exponential phase but ~ 3 fold less than wild-type PA14 during stationary phase. A *petA* deletion caused a ~ 2 fold increase in anthranilate after 8 h growth compared with wild-type PA14. This increase was less than the *tatABC* mutant however. There was almost no anthranilate in 16 h culture supernatants of PA14 $\Delta petA$, significantly less than what was found in PA14 $\Delta tatABC$. Complementation of *petA* deletion did not appear to restore the wild-type phenotype at 8 h growth, but anthranilate levels were not significantly different from wild-type after 16 h planktonic growth, so it appears there is a time delay on full complementation which was also observed for AQ production.

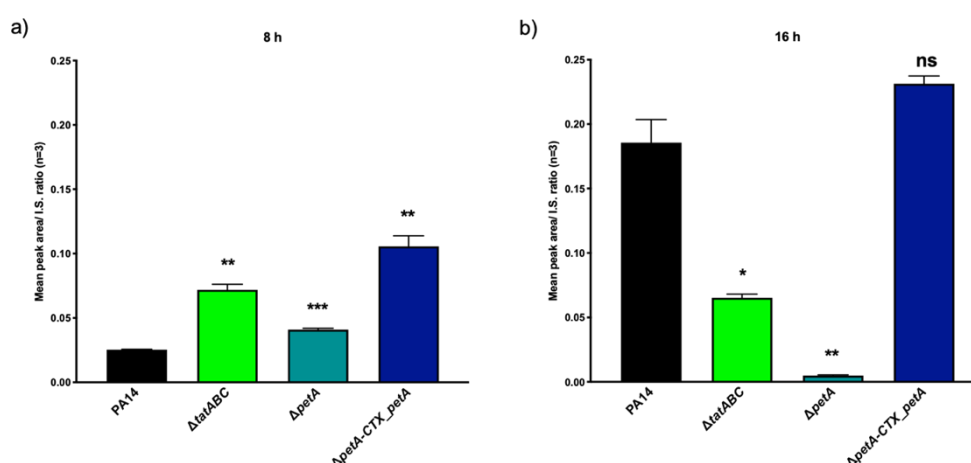


Figure 4.9. Semi-quantification of anthranilate production by PA14, PA14 $\Delta tatABC$, PA14 $\Delta petA$, PA14 $\Delta petA-CTX_petA$ following 8 h and 16 h growth in LB. Test was carried out with biological triplicates three times. Mean and SD are plotted. t-tests determined statistical significance from wild-type PA14 value.

4.2.2.3. Expression of *rhIA* in a $\Delta petA$ mutant

Rhamnolipids are biosurfactants found in the EPS matrix of *P. aeruginosa* biofilms and play a role in initialisation of biofilm microcolony formation, surface-associated migration, and biofilm dispersal (Flemming and Wingender, 2010). Their biosynthesis depends on the RhlAB proteins which can also be induced by PQS (Diggle *et al.*, 2003). Soh *et al.* has shown that *rhIAB* expression was reduced in PAO1-DK *tatA* and PAO1-DK $\Delta tatABC$ mutants and consequently, the levels of rhamnolipids produced were lower (Soh *et al.*, 2021).

Here, expression of *rhIAB* was quantified in the $\Delta petA$ mutant to determine whether this is also affected by mislocalisation of the Rieske subunit. To achieve this, miniCTX::*rhIA'-lux* was integrated into the chromosome of PA14, PA14 $\Delta tatABC$ and PA14 $\Delta petA$, and *rhIA* expression measured across 24 h growth. Changes to expression in response to different concentrations of exogenous PQS was also investigated.

Figure 4.10 shows that with no additional PQS, maximum *rhIA* expression was ~ 3 fold lower in both mutants. In addition, the response to 60 μM exogenous PQS was greater in wild-type PA14. Addition of PQS did not affect growth in all strains, yet the expression of *rhIA* was induced to varying degrees. Indeed, *rhIA* was up-regulated in wild-type to an RLU/OD₆₀₀ of $\sim 3 \times 10^5$, starting at around 8 h as cells entered stationary phase. PA14 $\Delta tatABC$ *rhIA* expression did not respond to PQS as readily as the wild-type and steadily increased in a linear fashion to $\sim 1 \times 10^5$ (RLU/OD₆₀₀). Expression of *rhIA* in the $\Delta petA$ mutant was similar to that observed in the *tat* mutant, once again suggesting that mislocalisation of this Tat substrate is responsible for the pleiotropic effects of *tat* mutation on PQS signalling.

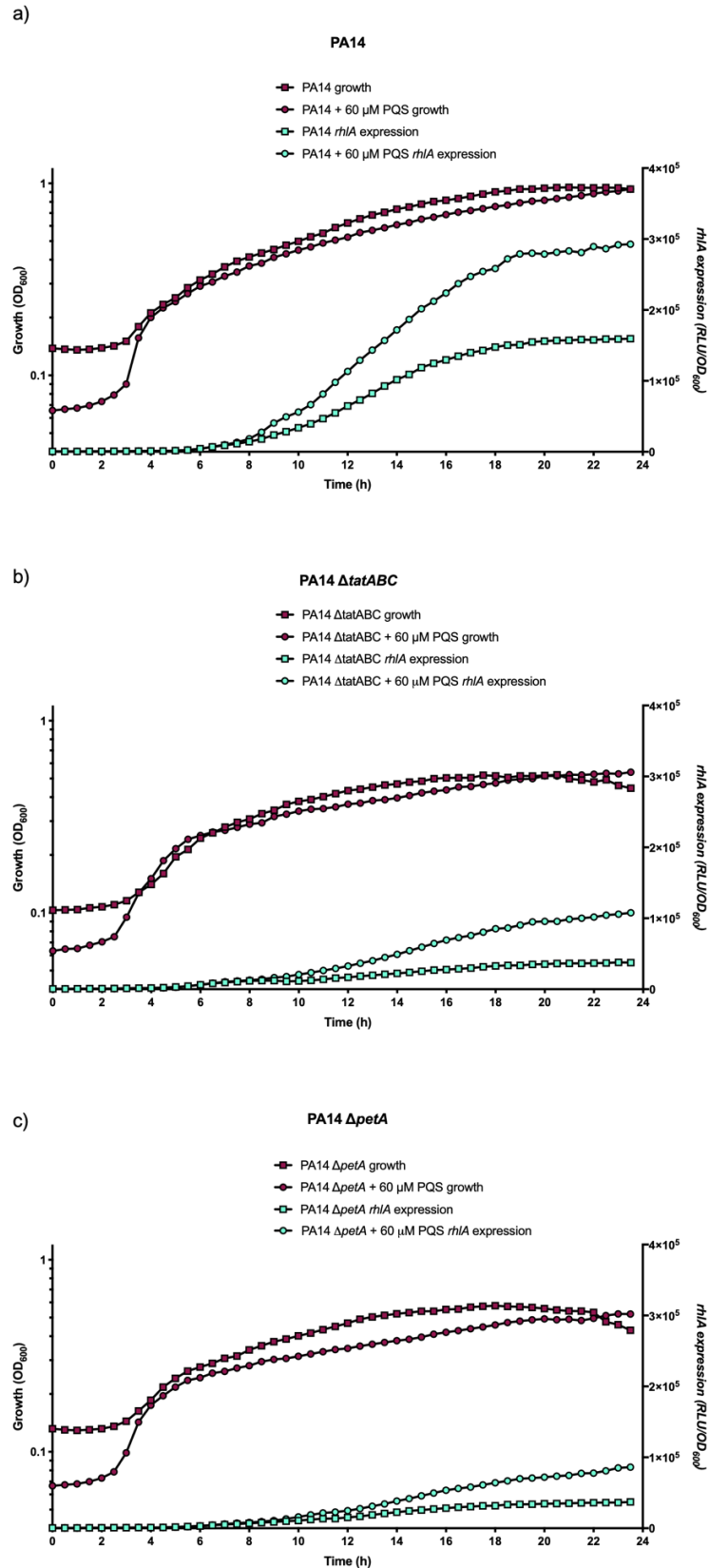


Figure 4.10. Expression of *rhIA* and growth of PA14 in (a), PA14 Δ tatABC (b) and PA14 Δ petA (c). Expression over 24 h was measured by bioluminescence from a chromosomally-inserted miniCTX::*rhIA*-*lux* transcriptional reporter. The experiment was performed in triplicate.

To be sure that light output was not affected by deletion of $\Delta petA$, a miniCTX-lux vector containing a constitutive *ptac* promoter transcriptionally fused to the *luxCDABE* operon was introduced to the chromosome of PA14, PA14 $\Delta tatABC$ and PA14 $\Delta petA$. Maximum gene expression across 24 h growth is shown in **Figure 4.11**. The measurement of constitutive expression was unchanged by *petA* mutation, therefore differences in luminescence seen in *pqsA* and *antA* transcriptional reporter assays is due to changes in the promoter regulation and not a consequence of disruption of luminescence.

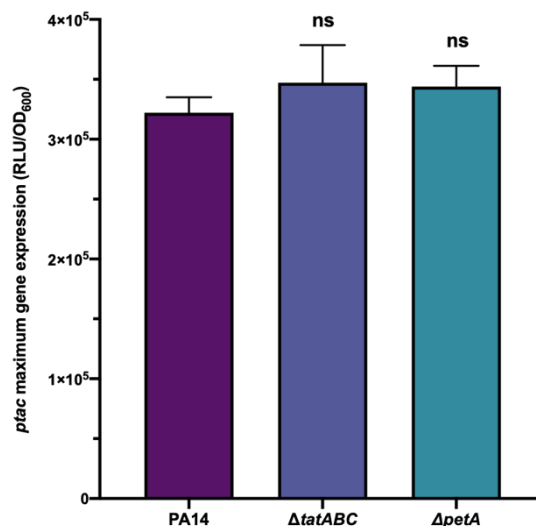


Figure 4.11. Constitutive *ptac* promoter expression in a $\Delta tatABC$ mutant and $\Delta petA$ mutant shows *lux* output is not affected by gene deletion. Assay was carried out in triplicate and mean with SD is displayed. miniCTX::*ptac*'-lux was introduced to each strain and grown over 24 h in LB. Bioluminescence was measured every 30 min and the maximum gene expression (RLU/OD₆₀₀) is plotted above.

4.2.2.4. Tat system function with $\Delta petA$ deletion

Pyoverdine (PVD) is a fluorescent siderophore used in iron acquisition and although there is variation between strains, the overriding structure comprises of three parts: a fluorescent dihydroquinoline-type chromophore, a peptide chain between 6-12 residues long, and a side chain bound to the chromophore that is often derived from the Krebs cycle (Schalk and Guillon, 2013). PVD biosynthesis

begins in the cytoplasm, close to the inner membrane, with creation of a non-fluorescent precursor. This is then transported across the IM to the periplasm where a fatty-acid membrane anchor is cleaved off. Finally, the fluorescent chromophore is formed by condensation of two residues, catalysed by PvdO, PvdN and PvdP. PvdP and PvdN are exported to the periplasm via the Tat system, and as a result a strain carrying $\Delta tatABC$ deletion does not produce the fluorescent chromophore (**Figure 4.12**). Mature pyoverdine fluoresces with an excitation wavelength of 405 nm and emission wavelength 460 nm in its iron-free state and as a result fluorescence can be used to assess Tat function in iron-depleted media.

The Tat system requires a PMF in order to oligomerise TatA subunits for translocation, but deletion of the Rieske subunit may cause a drop in PMF as the cytochrome bc_1 complex is a central part of the electron transport chain (Liang *et al.*, 2020). Diminishing respiratory flux was reported in *E. coli* upon deletion of cytochrome bd (Beebout *et al.*, 2021). As such, pyoverdine fluorescence was used to determine whether the Tat system remains functional in the PA14 $\Delta petA$ mutant (**Figure 4.12**).

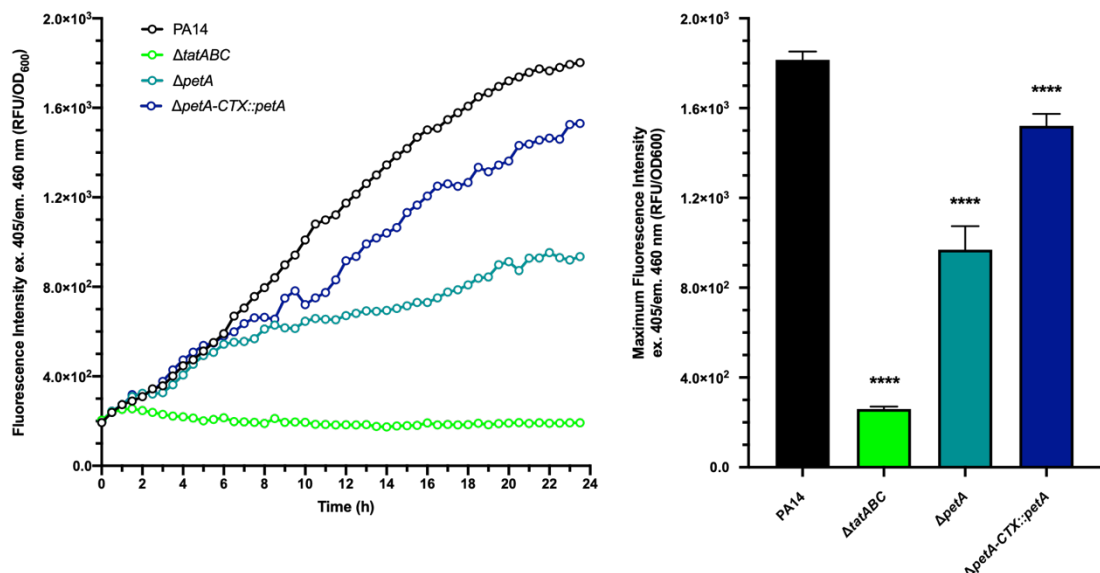


Figure 4.12. Mature pyoverdine production is abolished in a *tat* mutant but retained in *petA* mutant. Each strain was grown over 24 h in RPMI medium and fluorescence (excitation λ 405nm/emission λ 460 nm) was measured at 30 min intervals. Fluorescence intensity was normalised to cell growth by dividing relative fluorescence by OD₆₀₀. Experiment was carried out in triplicate.

Pyoverdine fluorescence was measured over 24 h growth in RPMI medium. There was a clear difference between all the strains. PA14 $\Delta tatABC$ did not fluoresce more than the basal level ~ 200 RFU/OD₆₀₀. In contrast, wild-type PAO1-DK produced a maximum fluorescence of 1.8×10^3 RFU/OD₆₀₀ due to mature PVD production. Fluorescence in PA14 $\Delta petA$ was reduced to 50% of wild-type PA14, suggesting that the Tat system is still functional as pyoverdine is produced. Lower levels of pyoverdine could be due to the energy/growth deficit in the cell, which is restored in the complemented mutant, in addition PVD production is under the control of *pqs* QS. Complementation of the $\Delta petA$ mutation with *petA in trans* increased pyoverdine fluorescence to near wild-type levels. t-tests showed that the pyoverdine phenotypes of each strain was statistically different to PA14.

4.2.2.5. Cytochrome *b* and cytochrome *c*₁ mutant phenotypes are the same as the *petA* mutant phenotype.

The Rieske subunit, PetA, is one of three subunits comprising the cytochrome *bc*₁ complex, but it is the only subunit translocated via the Tat export pathway. Cytochrome *b* ($\Delta petB$) and cytochrome *c*₁ ($\Delta petC$) deletion mutants were compared with a *petA* mutant to determine whether the pleiotropic effects of mutating *tat* were solely down to mislocalisation of the Rieske subunit, or whether the same disruption can be reproduced by deletion of other cytochrome *bc*₁ complex subunits.

Figure 4.13 shows that *petB* and *petC* deletion resulted in growth reduction, similar to that of the $\Delta tatABC$ and $\Delta petA$ mutants. In addition, *pqsA* expression was reduced to $\sim 50\%$ of wild-type levels, and LC-MS/MS semi-quantification of 8 h culture supernatant AQS revealed major reductions in HHQ, PQS and HQNO production.

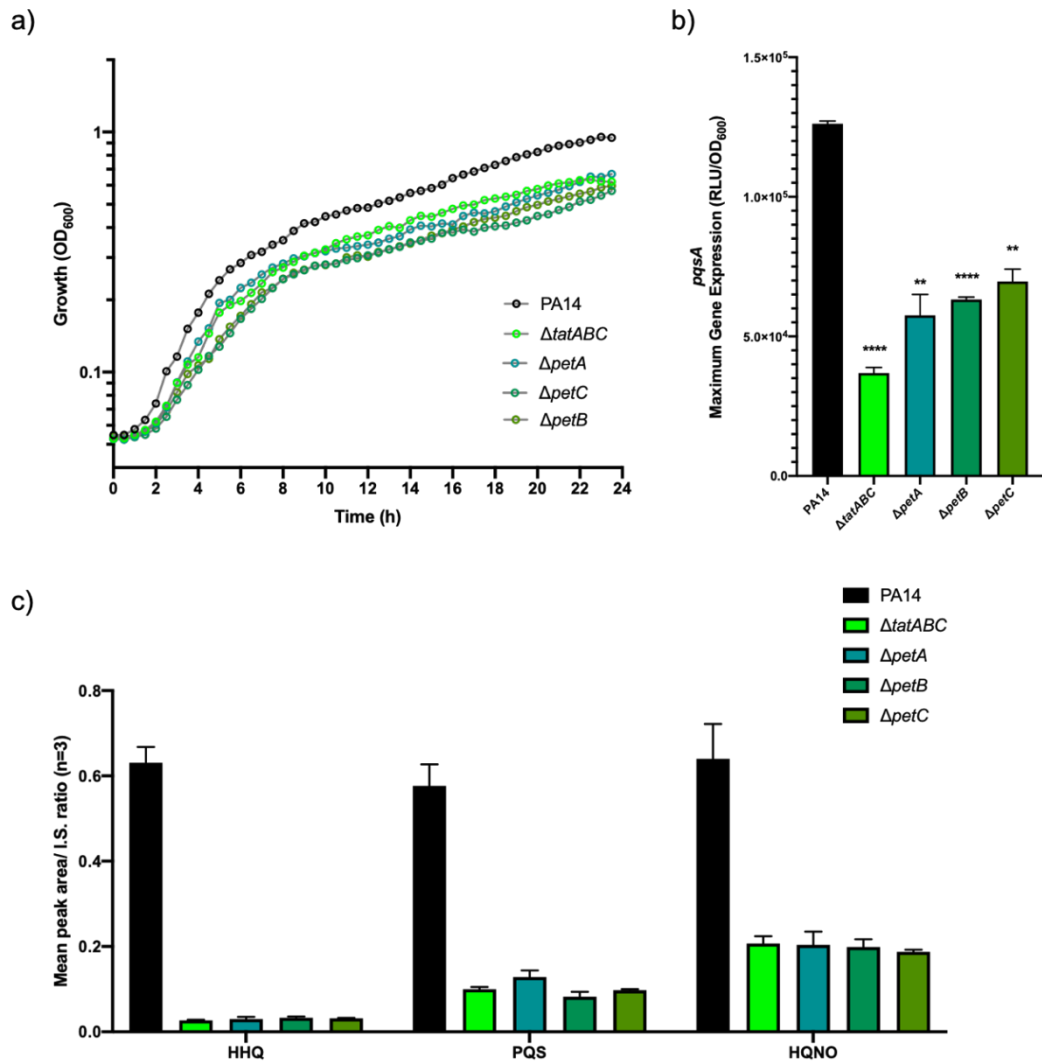


Figure 4.13. Growth (a), *pqsA* expression (b), and semi-quantification of AQs (c) in PA14, $\Delta tatABC$ and $\Delta petA$, $\Delta petB$ and $\Delta petC$ mutants. Deletion of each subunit of the cytochrome *bc*₁ complex yields the same growth defect as the *tat* mutant, as well as down-regulated *pqsA* expression and AQ production, measured using LC-MS/MS after 8 h growth. Experiments were repeated in triplicate, mean and SDs are displayed.

Section Summary

Deletion of *petA* from PA14 results in similar pleiotropic effects to those of a *tat* mutant, which can be mostly restored through complementation using a mini-CTX::*petA* vector. Therefore, it is likely that PetA, the Rieske subunit of the cytochrome *bc*₁ complex, is primarily responsible for the link between *tat* mutation and disruption of PQS-dependent quorum sensing.

4.2.3. Biofilm formation by the $\Delta petA$ mutant in comparison with wild-type and $\Delta tatABC$ mutant

In *P. aeruginosa* the formation and maturation of biofilms is tightly controlled by QS systems, including PQS dependent QS. PQS regulates the release of extracellular DNA to promote biofilm formation (Allesen-Holm *et al.*, 2006; Yang *et al.*, 2007; Haussler and Becker, 2008). During biofilm development small amounts of eDNA are present at the beginning which is then followed by a large release of extracellular DNA at a later stage (Tolker-Nielsen, 2015). Extracellular DNA is a key component of biofilms as it provides structural integrity, promotes cell-cell adhesion and acts as a nutrient source during starvation (Allesen-Holm *et al.*, 2006; Mulcahy *et al.*, 2008). It is the most abundant polymer within the matrix - in PAO1 biofilms for example, there are 500 mg for every 100 mg of protein (Matsukawa and Greenberg, 2004).

Due to the disruption of PQS biosynthesis in the *tat* and $\Delta petA$ mutants, the impact on biofilm formation was investigated. It has already been established that eDNA is decreased in a *tatA* mutant, and that subsequent biofilms are thin and flat when grown under microfluidic conditions (Soh *et al.*, 2021). Here, biofilm growth was studied under static conditions and the impact of the $\Delta petA$ deletion was investigated.

***P. aeruginosa* PAO1-DK and $\Delta tatABC$ mutants have distinct biofilm morphologies**

Biofilms were grown in 8-well glass bottom chambers under static conditions using M9 minimal medium supplemented with succinate as the sole carbon source. After 48 h spent medium was removed before staining with the

green fluorescent YOYO-1 and red fluorescent cell mask deep read (CMDR). YOYO-1 is a double-stranded DNA stain and cannot penetrate through the cell envelope to stain intracellular DNA, making it an ideal tool to visualise eDNA. CMDR is a plasma membrane stain and both dyes were added 30 min before imaging. **Figure 4.14** shows a set of images of PAO1-DK and PAO1-DK $\Delta tatABC$ mutant. Each image is representative of the strain which was grown in triplicate. Images show relative localisation of eDNA and cells in the field of view, and 3D images with each fluorescent channel overlaid are also included.

Visual analysis of the biofilms clearly shows significantly less eDNA in the *tat* mutant than in the wild-type, and it was distributed evenly through the biofilm – whereas eDNA could be seen in a concentrated layer on top of the wild-type PAO1-DK biofilm. In addition, cell density appeared to be far lower and the overall biofilm thickness was also reduced in the *tat* mutant. Quantitative analysis with COMSTAT2 software confirmed this. The maximum wild-type thickness was $\sim 60\mu\text{m}$ but only $\sim 15\mu\text{m}$ upon deletion of *tat*.

There was significantly greater biomass of both eDNA and cell membranes in wild-type PAO1-DK compared with PAO1-DK $\Delta tatABC$ mutant biofilms. The PAO1-DK wild-type had an average cell membrane biomass of $11.4\mu\text{m}^3/\mu\text{m}^2$ whereas the *tat* mutant had less than half of that at $4.1\mu\text{m}^3/\mu\text{m}^2$. The greatest difference, however, was in extracellular DNA release. PAO1-DK biofilms had more eDNA than cell membrane biomass, at $16.3\mu\text{m}^3/\mu\text{m}^2$. In contrast PAO1-DK *tat* mutants had only $0.7\mu\text{m}^3/\mu\text{m}^2$ eDNA. This is a ~ 23 fold reduction in eDNA production, and its distribution was identical to cell membrane and eDNA surface area, suggesting the PAO1-DK *tat* mutant did not make a biofilm under these conditions.

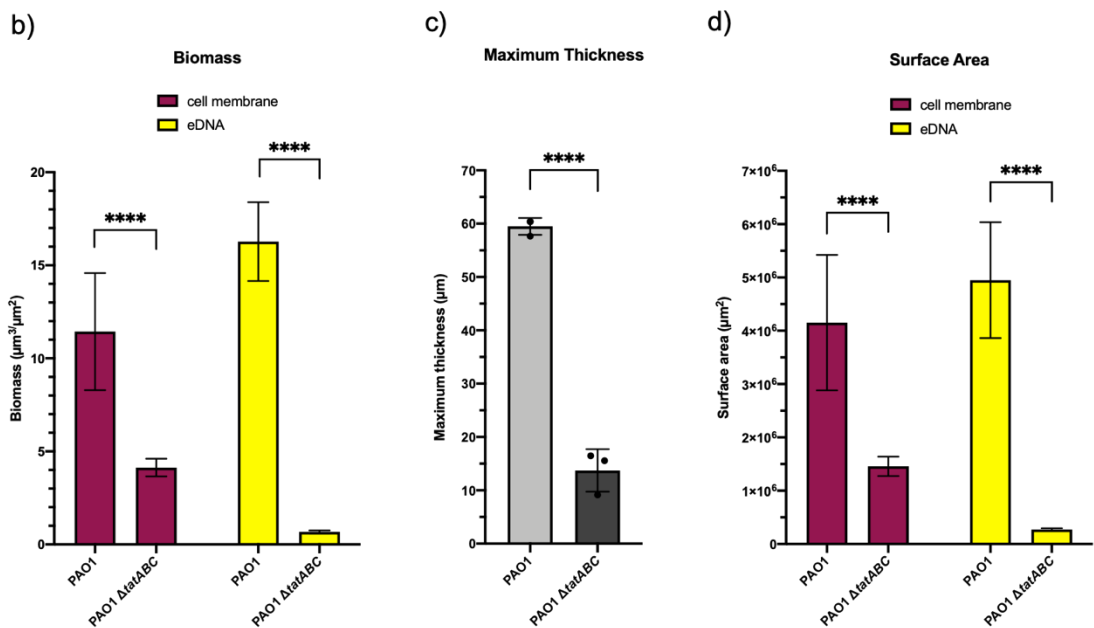
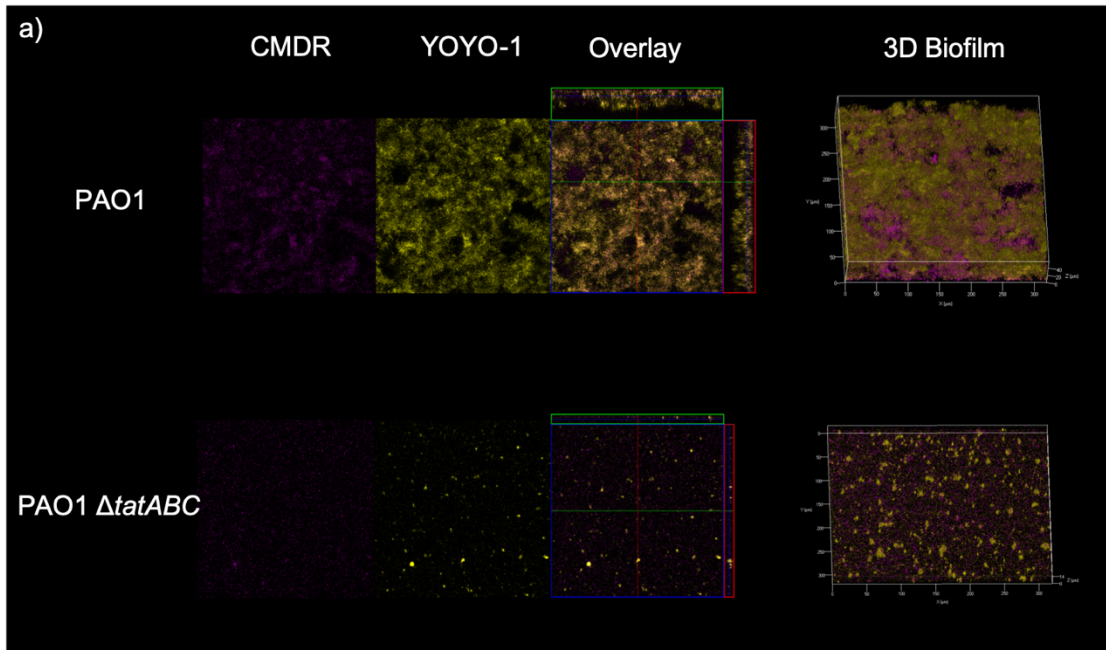


Figure 4.14. Representative images of PAO1 and PAO1 Δ tatABC biofilms following 48 h static growth (a). Biofilms were stained with CDMR (cell membranes) and YOYO-1 (extracellular DNA) to visualise specific aspects. COMSTAT2 analysis with ImageJ shows significant differences of biomass (b), maximum biofilm thickness (c) and surface area (d) between PAO1 and PAO1 Δ tatABC biofilms determined by t-tests.

4.2.4.1. PA14 Δ *petA* mutant biofilms

PA14 and PAO1-DK both readily formed biofilms under static growth conditions. Each strain has distinct biofilm formation pathways, during reversible attachment stage PAO1 cells were shown to attach to surfaces much faster than PA14, they favoured c-di-GMP mediated EPS production which assisted nearby cells in their own attachment (Lee *et al.*, 2020). Lee *et al.* also showed that PA14 displayed an alternative colonisation strategy, cAMP was used to control motility and progeny were adapted for surface attachment (Lee *et al.*, 2020). Once attached, more PAO1 progeny remained on the surface compared with PA14 (Lee *et al.*, 2020).

Due to similarities in *tat* mutant phenotypes established earlier in this study, it was considered likely that the PA14 *tat* mutant would form biofilms with similar defective architecture as that observed for PAO1-DK Δ *tatABC*. Disruption to PQS QS severely impacts extracellular DNA release – a prominent step in biofilm formation (Allesen-Holm *et al.*, 2006). As PQS production and *pqsA* expression are both severely reduced in the PA14 Δ *tatABC* and Δ *petA* mutants, it was thought they would also present similarly defective biofilms.

When grown in liquid broth, a PAO1 Δ *petA* mutant had slower growth and did not undergo autolysis (Hazan *et al.*, 2016). Orthologous mutants in other bacteria such as *Shewanella oneidensis* also had reported aerobic growth defects (Luo *et al.*, 2013). Following 48 h growth, biofilms were stained once again with YOYO-1 and CMDR and analysed with confocal laser scanning microscopy (CLSM). **Figure 4.15** shows images of PA14 and *tat* mutant, *tat* substrate mutant (*petA*), and *petA* complemented biofilms. PA14 Δ *petA* was complemented with the wild-type gene under the control of its own promoter on a miniCTX vector integrated into the chromosome. Each biofilm is shown in 3D with separate fluorescent channels and an overlay.

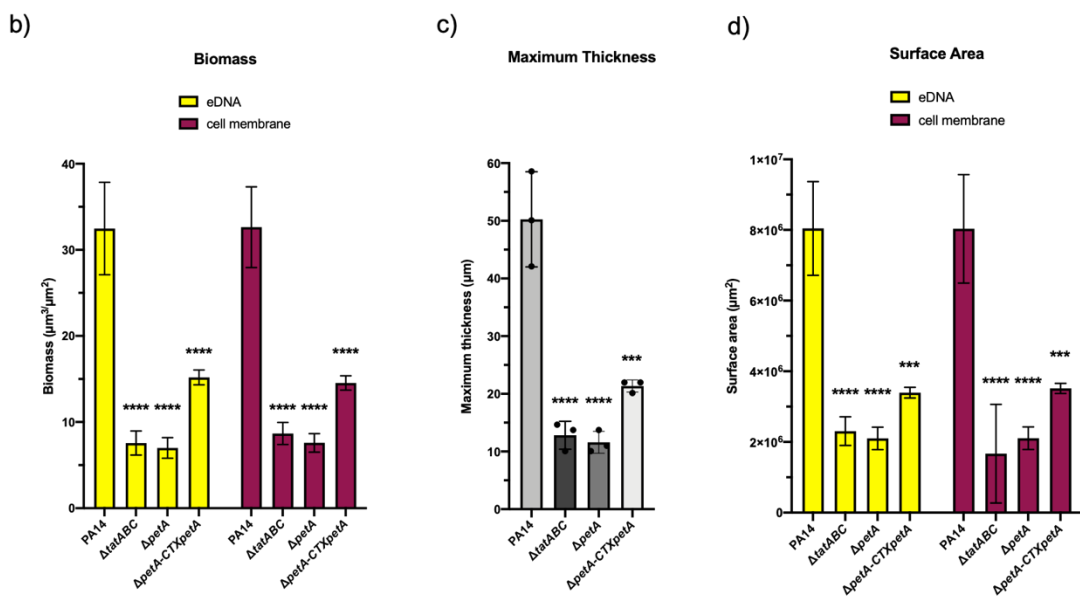
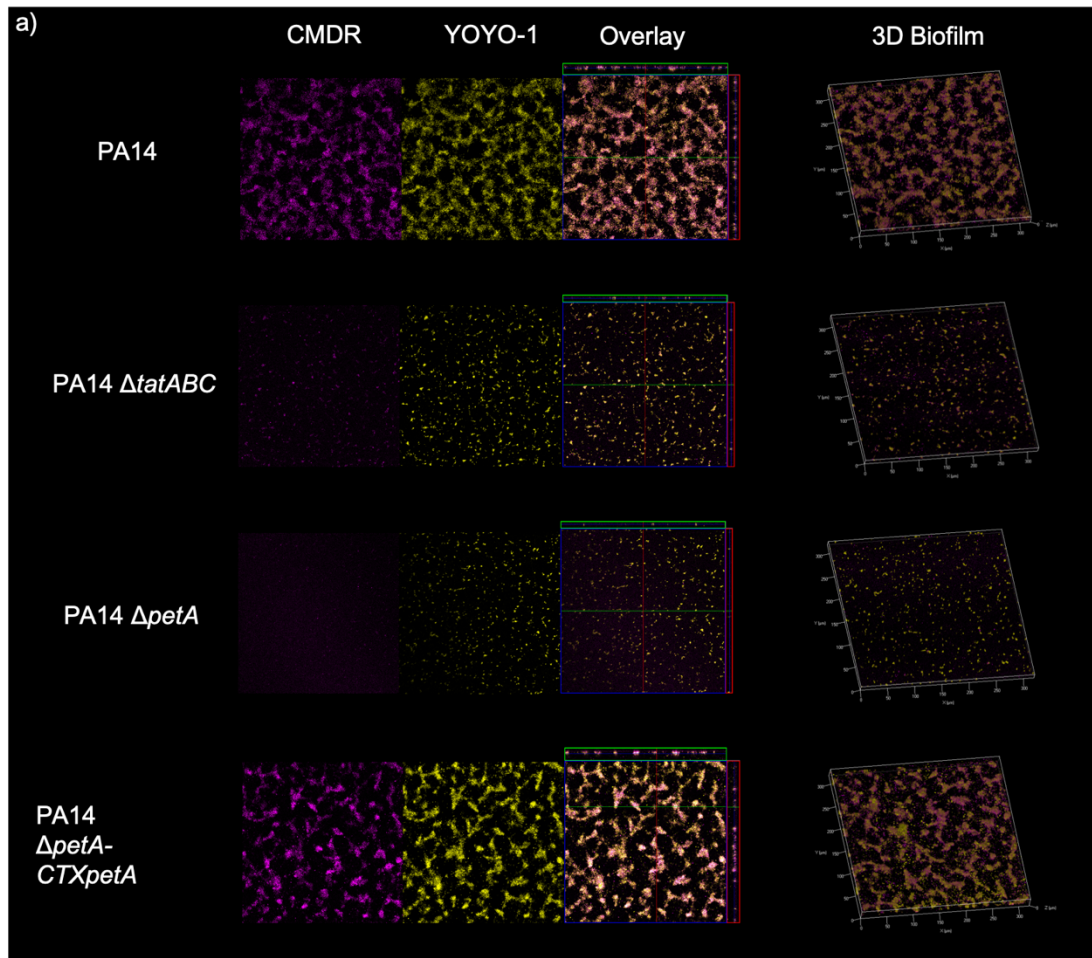


Figure 4.15. Static biofilms of PA14, a $\Delta tatABC$ mutant, $\Delta petA$ mutant and complemented $\Delta petA$ mutant (a) following 48 h growth. CMDR (cell membrane) and YOYO-1 (eDNA) stains were added prior to imaging. Quantitative analysis of eDNA and cell membrane biomass (b), surface area (d) and maximum biofilm thickness (c) was carried out with COMSTAT2 software and ImageJ.

Qualitative analysis revealed thick, eDNA-rich biofilms were formed by PA14 wild-type and the $\Delta petA$ complement. In contrast the *tat* mutant and $\Delta petA$ mutant had very similar biofilm architectures - sparse and thin with far less eDNA and cells. Unlike PAO1-DK $\Delta tatABC$ however, PA14 $\Delta tatABC$ did form a biofilm albeit a very thin and sparse one, as indicated by the raised eDNA biomass.

Each biofilm was analysed with COMSTAT2 software to quantify biomass, surface area and thickness. **Figure 4.15b,c,d** shows the results of this analysis along with representative images of each biofilm. Biomass of cell membranes and eDNA was found in relatively equal proportions in every strain. Noticeably, the eDNA and cell membrane biomass each decreased by ~ 5 fold in the $\Delta tatABC$ mutant as well as in the $\Delta petA$ mutant. This was found to be statistically significant with a *p* value of less than 0.0001.

Complementation of the *petA* deletion resulted in an increase of cells and eDNA but this was still significantly less than wild-type levels. Qualitative analysis of the PA14 $\Delta petA$ -CTX*petA* biofilms showed that the increase in eDNA and cells results in formation of typical wild-type biofilm structures compared with the sparse biofilms of the mutants. This observation is reflected in the measurements for maximum thickness. Wild-type biofilms formed around 50 μm thick, whereas the *tat* mutant and *tat* substrate mutant biofilms only reached an average thickness of 12.81 μm and 11.59 μm respectively. When the *petA* mutation was complemented, biofilms were on average 21.35 μm thick, however this is not significantly different from the mutant.

The same pattern was seen for biofilm surface area. Wild-type had a surface area of around $8 \times 10^6 \mu\text{m}^2$ for both eDNA and cell membranes. The *tat* mutant and *tat* substrate mutant surface areas were around $2 \times 10^6 \mu\text{m}^2$ for eDNA and cell membranes, and the complement had only a partially restored phenotype to $4 \times 10^6 \mu\text{m}^2$. It is worth noting that wild-type biofilms showed far more variability in all 3 variables than mutant and complement biofilms.

To further investigate eDNA production in the $\Delta petA$ mutant, DNA release in planktonic cultures was investigated. Extracellular DNA was precipitated out of filter-sterilised supernatants and quantified using a nanodrop spectrophotometer. The results were compared for PA14 wild type, $\Delta tatABC$ mutant and the $petA$ complemented strain. **Figure 4.16** shows that eDNA production was ~ 3 fold lower in both the tat and $\Delta petA$ mutants when cells were harvested at 8 h. This significant reduction in eDNA is similar to growth under static biofilm conditions but not as pronounced. It appears there was less eDNA in the wild-type culture at 16 h than at 8 h, likely due to continued degradation by the extracellular DNases EddB and EndA (Mulcahy *et al.*, 2010; Cherny and Sauer, 2019). Complementation of $\Delta petA$ gave a slight increase in eDNA and t-test determined this was not significant from $\Delta petA$ at 8 h, but eDNA levels were restored upon $petA$ complementation at 16 h.

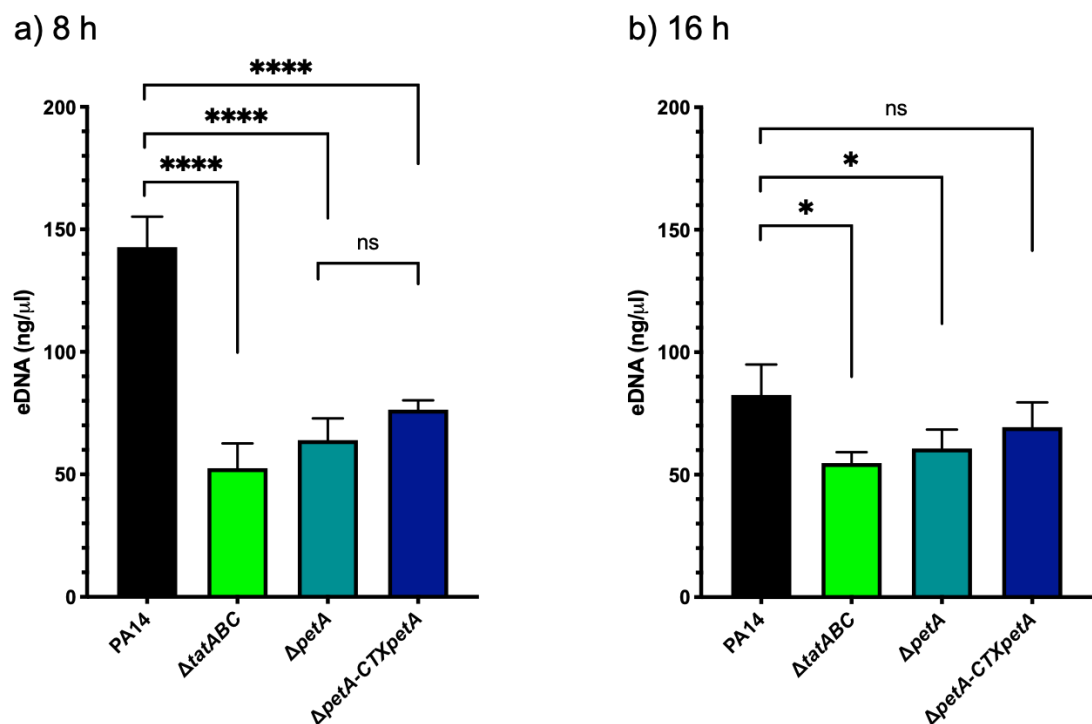


Figure 4.16. Extracellular DNA quantified from planktonic cultures after (a) 8 h growth and (b) 16 h. PA14, PA14 $\Delta tatABC$, PA14 $\Delta petA$ and a strain carrying the complemented $\Delta petA$ mutation were grown in LB broth and harvested at two timepoints. Extracellular DNA was measured in triplicate, mean and SD are shown.

Section Summary

Biofilms are surface-attached communities of cells embedded in a matrix made up of extracellular material. The matrix often dominates biofilms, in some cases only 10% of the biofilm dry weight consists of cells (Flemming and Wingender, 2010). The *P. aeruginosa* matrix contains extracellular polymeric substances (EPS) including polysaccharides and eDNA that provides a scaffold for biofilm architecture, rhamnolipids, outer membrane vesicles (OMVs) and proteins. Work during this study has shown major differences in static biofilm architecture between wild-type *P. aeruginosa* biofilms and their subsequent *tat* and *petA* mutant biofilms. The latter were thin, flat and sparse, with fewer cells and reduced eDNA.

4.3 Discussion

It was hypothesised that failure to export one of the 34 known Tat substrates caused perturbed PQS biosynthesis and induced anthranilate degradation. To explore this hypothesis, a library of deletion mutants for each Tat substrate was screened for reduced expression of *pqsA* and induced *antA*, as well as their ability to produce pyocyanin.

Screens of Tat substrate deletion mutants revealed that deletion of *petA*, also known as *PA14_57570* in PA14 and *PA4431* in PAO1-DK, resulted in very similar pleiotropic phenotypes to the *tatABC* mutant. Expression of *pqsA*, *rhlA* and pyocyanin biosynthesis were all significantly reduced, alongside characteristic *antA* overexpression. After 8 h growth, anthranilate present in Δ *petA* culture supernatants was significantly higher than wild-type PA14 which corresponds with the peak in *pqsA* expression that was absent in the *tat* mutant (**Figure 4.5**). After 16 h growth, anthranilate in culture supernatants was significantly lower in the *tat* mutant and almost non-existent in the *petA* mutant as *antA* overexpression is well underway.

There was partial restoration of phenotype when the Δ *petA* deletion was complemented with *petA* under the control of its native promoter, located in the upstream 500 bp region, on a miniCTX vector. At 16 h LC-MS/MS quantification of anthranilate showed full restoration of phenotype. Results suggest that *petA* is primarily responsible for the dysregulation of PQS-dependent QS and anthranilate degradation.

PetA is the Rieske subunit of the cytochrome *bc*₁ complex and is the only subunit exported via the Tat system. The cytochrome *bc*₁ complex is an integral part of the respiratory chain contributing to the generation of electrochemical potential across the membrane through proton translocation (Xia *et al.*, 2013). Briefly, the cytochrome *bc*₁ complex oxidases quinols and reduces metalloprotein electron carriers. In *P. aeruginosa* this is a c-type cytochrome (Thöny-Meyer,

1997). It is a homodimer, each unit consisting of 3 subunits – cytochrome *b*, cytochrome *c*₁, and an iron-sulphur protein called the Rieske subunit. The latter is a substrate of the Tat pathway, it retains the Tat signal peptide following translocation and this is used as a membrane anchor. The Rieske subunit coordinates a cluster of 2Fe-2S ions with conserved histidine and cysteine residues.

P. aeruginosa has a highly branched electron transport chain, and 15 of the 17 dehydrogenases produced take electrons from various substrates and transfer them to ubiquinone, which in turn is oxidised by Cyt *bc*₁. The remaining 2 dehydrogenases either directly reduce cytochrome *c* or reduce nitrate reductases. Electrons are transferred from Cyt *bc*₁ to cytochrome *c* before reduction of terminal oxidases (Liang *et al.*, 2020). There are five total terminal oxidases, cytochrome *c* is oxidised by either aa₃ oxidase, *cbb*₃ oxidase 1 or *cbb*₃ oxidase 2 (Arai, 2011). The ubiquinol pool can be directly oxidised by CYO (cytochrome *bo*₃ quinol oxidase) or CIO (cyanide-insensitive oxidase).

Despite the availability of cytochromes CYO and CIO that enable bypassing cyt *bc*₁, this study has shown that deletion of each of the cytochrome *bc*₁ subunits results in a phenotype similar to the *tat* mutant (**Figure 4.13**). PA14 *petA*, *petB* and *petC* deletion mutants all had slower growth, down-regulated *pqsA* expression and significantly reduced levels of HHQ, PQS and HQNO. Reliance on only 2 of 5 total terminal oxidases to oxidise quinol and maintain the electron transport chain may explain why a Δ PA4431 mutant can still grow, albeit at a much slower rate. RNAseq analysis reported in Chapter 3 shows upregulation of subunits *cyoA* and *cyoC* by 2.12 and 2.45 fold respectively. In addition, genes encoding both subunits of CIO are up-regulated 2.44 fold (*cioA*) and 2.70 fold (*cioB*), perhaps to compensate for an ineffective Cyt *bc*₁ complex.

Growth defects in *cytbc*₁ subunit mutants has previously been reported in *P. aeruginosa* and *S. oneidensis* (Luo *et al.*, 2013; Hazan *et al.*, 2016). HQNO has long been established as an inhibitor of cytochrome *bc*₁, acting at the Q_i site of cytochrome *b*, the location of quinol reduction (**Figure 4.4**). Inhibition of the Q_i

site generates reactive oxygen species by disrupting the flow of electrons and causing electron leakage. HQNO-cyt *b* inhibition is so severe that it is able to cause programmed cell death and cell lysis in *P. aeruginosa*, dependent upon a fully functioning Q_o site (Hazan *et al.*, 2016). Cell lysis releases eDNA and promotes biofilm formation. Deletion of *petA* or cytochrome *b* not only results in reduced growth, as observed in this study, but also insensitivity to exogenous HQNO and reduced cell lysis (Hazan *et al.*, 2016).

The *tat*, *petA*, *petB* and *petC* mutants produce far fewer quantities of AQs, including HQNO (See **Figure 4.6**, **Figure 4.7**, **Figure 4.13**). Thus, these mutants lack the ability to induce HQNO-mediated autolysis as they can neither produce enough inhibitor nor the complete cytochrome *bc*₁ complex required. As such, a major mechanism for eDNA release is missing from the mutants.

Given the previously established reduction in eDNA release and formation of thin, flat biofilms of *tat* mutants under microfluidic growth conditions (Soh *et al.*, 2021), this study sought to understand the role of *petA* in biofilm production. Quantification of biomass, surface area and maximum thickness of static biofilms shows *petA* mutant biofilms are eDNA deficient, sparse and flat. Formation of mature biofilm was partially restored by complementation. Microfluidic biofilm growth and subsequent treatment with tobramycin showed antibiotic sensitivity as a result of *tat* mutation, this is also likely to be the case for Δ *petA* mutation as tolerance to aminoglycoside antibiotics is in part mediated by binding with eDNA (Soh *et al.*, 2021). Indeed, deletion of *petA*, *petB*, and *petC* resulted in increased MICs to the aminoglycosides kanamycin, gentamicin, tobramycin and amikacin in planktonic growth in LB (Shen *et al.*, 2021).

Currently there are no published findings measuring anthranilate degradation in cytochrome mutants, or any data to suggest a link between the two. Here, this study has shown that anthranilate degradation is up-regulated in mutants of the rieske subunit of the cytochrome *bc*₁ complex during later stages of growth, likely due to perturbed biosynthesis of PQS and other AQs.

Conclusion

The current hypothesis is that disruption to the electron transport chain at the Cyt *bc*₁ complex causes *P. aeruginosa* to try to conserve energy for primary metabolism and growth, by shutting down processes such as secondary metabolite and virulence factor production. PAO1 Δ *petA*, PAO1 Δ *petB* and PAO1 Δ *petC* strains have lowered ATP compared with wild-type, which supports this hypothesis (Shen *et al.*, 2021). Shutting down secondary metabolite and virulence factor production can be achieved through prevention of *pqsA* autoinduction as the PQS regulatory network controls genes in multiple secondary metabolite biosynthetic pathways and over 50 AQS, which use anthranilate and tryptophan as precursors (Dézziel *et al.*, 2004; Rampioni *et al.*, 2016; Soh *et al.*, 2021). As a result of accumulating anthranilate, its degradation is induced. However, the regulatory mechanism involved remains unclear.

**Chapter 5: Screening analogues of the
Bay 11-7082 compound for increased
activity and structure-activity
relationship**

5.1. Introduction

P. aeruginosa utilises sophisticated hierarchical QS systems to regulate the expression of its genes in a population density-dependent manner. PQS-dependent QS regulates expression of an arsenal of virulence determinants as well as biofilm maturation. Antivirulence drugs targeting quorum sensing could be used as an alternative therapeutic strategy for difficult to treat, antibiotic resistant, *P. aeruginosa* infections as they prevent coordination of virulence factor release and progression of disease.

The Tat secretion system would be an ideal target for novel antivirulence drugs; its localisation within the cell envelope is relatively accessible, also inhibition of the Tat system would have a broad impact including failed export of Tat-targeted virulence factors, perturbed PQS QS, reduced pyocyanin and pyoverdine production, and severely reduced biofilm formation. Deletion of Tat modulates other PQS QS independent genes as outlined in **Section 3.2.3**, so the Tat system offers a broader target than the PQS system alone. In addition, virulence of a *tat* mutant is nearly entirely attenuated in a rat chronic pulmonary infection model (Urs a Ochsner *et al.*, 2002; Vasil *et al.*, 2012). The Tat secretion system is not found in animals or humans so inhibitors targeted to the Tat pathway with high specificity may cause attenuation of pathogenicity with minimal adverse side effects, providing such molecules are not cytotoxic or mutagenic (Palmer and Stansfeld, 2020). Inhibitors toxic to animals will still prove useful laboratory tools for further investigation of the Tat system. As there are currently no high-resolution structures of the Tat system or any of its subunits, *in silico* drug design and molecular modelling with lead compounds is not a possibility (Vasil *et al.*, 2012).

Three high-throughput screens for inhibitors of the Tat pathway have been published and are outlined in **Table 5.1**. Further details on each screen are given below.

Bacterial spp.	Number of compounds screened	Number of Tat inhibitors	Assays used to screen for Tat-specific inhibition	Reference
<i>P. aeruginosa</i>	>80,000	2	PLC activity Pyoverdine production Copper resistance Growth with choline as sole carbon and nitrogen source Tat titration	(Vasil <i>et al.</i> , 2012)
<i>P. aeruginosa</i>	~39,000	3	PLC activity Pyoverdine production PLC dose-response Elastase activity to rule out T2SS inhibition	(Massai <i>et al.</i> , 2019)
<i>E. coli</i>	~389,500	0	spTorA-mCherry-SsrA Tat-targeted fluorescent protein (FP) dose-response testing <i>in vitro</i> Tat transport assay oxonol VI fluorescence	(Bageshwar <i>et al.</i> , 2016)

Table 5.1. High-throughput screens for inhibitors of the Tat system found in the literature. Three screens of small molecular weight compound libraries have been published, two were carried out using *P. aeruginosa* and utilised Tat-translocated phospholipase C (PLC) activity as their main screen for Tat inhibition. One screen carried out in *E. coli* utilised a novel Tat-translocated fluorescent protein, spTorA-mCherry-SsrA.

The five published Tat-specific inhibitors are shown in **Table 5.2**.

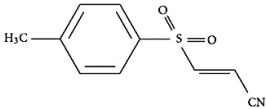
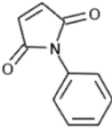
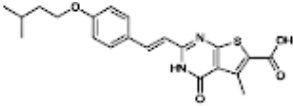
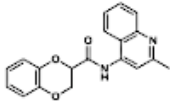
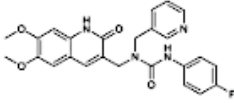
Tat inhibitor	Structure	PLC IC ₅₀ (μM)	Reference
(2E)-3-[(4-methylphenyl)sulfonyl]acrylonitrile (Also called Bay 11-7082)		-	(Vasil <i>et al.</i> , 2012)
N-phenyl-maleimide		-	(Vasil <i>et al.</i> , 2012)
TAT-3		21.7	(Massai <i>et al.</i> , 2019)
TAT-4		27.1	(Massai <i>et al.</i> , 2019)
TAT-5		29.3	(Massai <i>et al.</i> , 2019)

Table 5.2. Published Tat system inhibitors and the available structures. (2E)-3-[(4-methylphenyl)sulfonyl]acrylonitrile and N-phenyl-maleimide were discovered by Vasil *et al.* 2012. The latter three compounds were confirmed as Tat inhibitors by Massai *et al.* 2019.

Two high-throughput screens of compound libraries used phospholipase C (PLC) activity as an initial screen for hits (Vasil *et al.*, 2012; Massai *et al.*, 2019). Briefly, a colour change of the chromogenic PLC substrate *p*-nitrophenylphosphoryl choline (NPPC) only occurs when PLC is translocated across the inner membrane via the Tat system and secreted into the extracellular milieu by the general secretion pathway. As such it can be used as part of a colorimetric assay for Tat, and T2SS, inhibition.

As highlighted in **Table 5.2**, a variety of additional assays have been used to confirm Tat specificity of hit compounds following initial high-throughput screening of compound libraries. Vasil *et al.* screened >80,000 small-molecular weight compounds for potential inhibitors of the protein export pathway in *P. aeruginosa* by measuring PLC activity. A total of 122 hits were discovered, these were narrowed down to two Tat-specific inhibitors with secondary screening. *N*-Phenyl maleimide and (2E)-3-[(4-Methylphenyl)sulfonyl]acrylonitrile, more commonly known as Bay 11-7082, (**Table 5.2**) were shown to directly affect Tat function through additional assays based on pyoverdine production, copper resistance and growth using choline as the sole carbon and nitrogen source, all of which require proteins translocated by the Tat pathway (Vasil *et al.*, 2012).

While these additional assays highlighted similar phenotypes to a *tatC* mutant, a Tat titration assay of hit compounds was also carried out in parallel to eliminate false positives. Briefly, the Tat system was encoded on an arabinose-inducible plasmid and introduced to a Δ *tatABC* mutant. Overexpression of the Tat system in the presence of the hit compound revealed true Tat antagonists when the overall inhibitory effects were reduced in the up-regulated vs wild-type strain (Vasil *et al.*, 2012). A second PLC-export-based *P. aeruginosa* screen of ~39,000 compounds found 3 potential candidates for Tat inhibitors and 1 inhibitor of Type II secretion (Massai *et al.*, 2019)(**Table 2**). Tat inhibitors were verified with a fluorescence assay testing Tat-dependent export of pyoverdine maturation proteins

PvdP and PvdN, and inhibition of T2SS was ruled out using the T2SS-secreted elastase activity-based assay.

Bageshwar *et al.* (2016) developed a novel small-molecule inhibitor screen in *E. coli*. This was based around a Tat-exported fluorescent protein (FP), spTorA-mCherry-SsrA, that is rapidly degraded when Tat function is compromised. The spTorA-mCherry-SsrA FP was chosen as its fluorescence emission does not overlap with intrinsic fluorescence of LB broth, and it has an N-terminal TorA signal peptide directing it for export via the Tat secretion pathway. The C-terminal SsrA tag promotes ClpXP/ClpAP protease degradation of the pre-protein in the cytoplasm. Approximately 51,600 compounds from a local library and 337,881 compounds from National Institutes of Health (NIH) molecular libraries small molecules repository (MLSMR) were screened. None of the hits from the primary assay passed subsequent dose-response testing and additional biochemical assays (Bageshwar *et al.*, 2016). Nevertheless, this provides an excellent framework for development of a direct Tat inhibitor screen as it focuses on direct rather than indirect inhibition of the Tat system as a primary high-throughput screen, and provides a living cell assay that could be used for early assessment of Tat export inhibition in real-time.

The Bay 11-7082 compound (**Table 5.2**) was selected as the focal point for structure-activity relationship (SAR) analysis in this study as it is a small molecule inhibitor shown to target the Tat system. PAO1-DK miniCTX::*pqsA*'-lux grown in 40 μ M of Bay 11-7082 had reduced expression of *pqsA* by ~30% (Soh *et al.*, 2021). Not only does this demonstrate the potency of Bay 11-7082, it also further confirms that it targets the Tat system since a reduction in *pqsA* expression is also seen in a Tat mutant (Soh *et al.*, 2021). The aim of the work described in this chapter was to test structural analogues of the published Bay 11-7082 compound for inhibition of *pqsA* expression as a surrogate reporter for Tat inhibition in order to establish a structure-activity relationship (SAR) for Bay 11-7082 and to discover analogues with increased potency.

5.2. Results

5.2.1. Screening of Bay 11-7082 analogues for increased activity

Two key aims of this study were to develop and test novel Tat inhibitors as antivirulence drugs. Using Bay 11-7082 (**Table 5.2**) as a hit compound, structural analogues were synthesised by Alex Truman (University of Nottingham).

To develop a novel high-throughput screen that would show direct Tat inhibition, the aim was to utilise Tat-targeted export of a constitutively-expressed spTorA-mTurquoise2 fluorescent protein and measure changes in fluorescence to assess inhibition as outlined in **Figure 5.1** (Wilton *et al.*, 2018). Unfortunately, the screen was not sensitive enough for use in an automated plate reader, so *pqsA* expression was chosen as an indirect screen for Bay 11-7082 analogues and SAR analysis. Bay 11-7082 does not inhibit light output of the constitutive miniCTX::*tac'-lux* reporter fusion at 20 μ M and 40 μ M, and neither does DMSO at the concentrations used in the screen (Soh *et al.*, 2021).

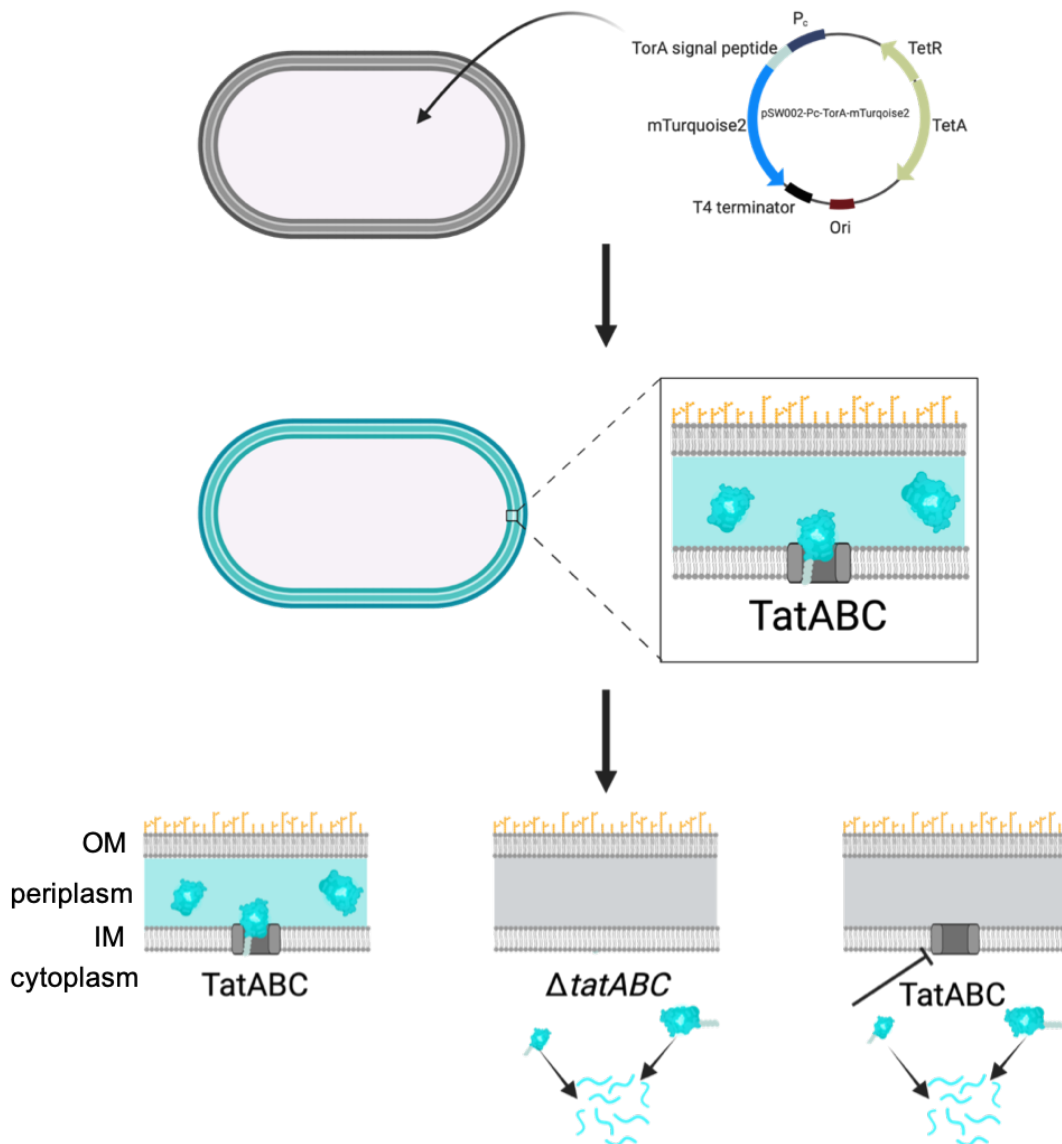


Figure 5.1 Schematic showing design of fluorescent protein screen for inhibition of the Tat system. The plasmid pSW002-Pc-TorA-mTurquoise2 is introduced to *P. aeruginosa* via conjugation (a). mTurquoise2 carrying the TorA Tat signal peptide is constitutively expressed and exported to the periplasm where it accumulates (b). Deletion or inhibition of the Tat export pathway abolishes translocation of mTurquoise2 and the protein is degraded in the cytoplasm (c). Created with BioRender.com.

Soh *et al.* showed that addition of the Bay 11-7082 compound at concentrations of 20 μM and 40 μM reduced *pqsA* expression by $\sim 30\%$ compared with the control (Soh *et al.*, 2021). This reduction in expression was accompanied by a delay in peak expression of approximately 3 h (Ye-Chen Soh, Thesis, University of Nottingham). Continuing on from this work, the response of the *antA*

operon to increasing concentrations of the Bay 11-7082 (TI1) compound synthesised by Alex Truman was also investigated. **Figure 5.2** shows downregulation of *pqsA* with an IC_{50} of 27.41 μM (a) and upregulation in *antA* expression with an EC_{50} of 20.46 μM (b). Both *pqsA* expression and *antA* expression were chosen for screening of the TI1 analogues as their respective downregulation and upregulation can be seen in a *tat* mutant so this provides an indirect preliminary screen.

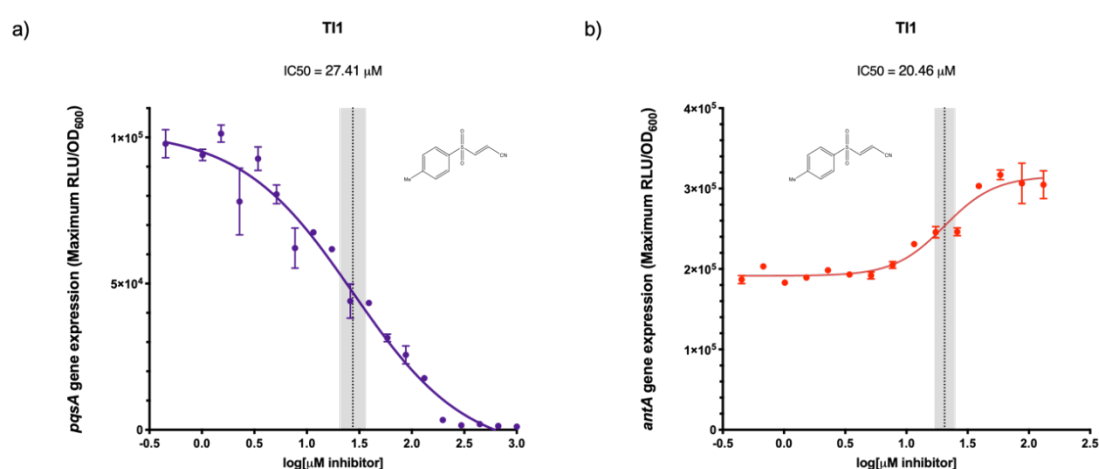


Figure 5.2. Activity of Bay 11-7082 (TI1) against *antA* (EC_{50} 20.46) and *pqsA* expression (IC_{50} 27.41). Screens were carried out in triplicate and the concentration at which there is 50% effective (EC_{50}) or inhibitory activity (IC_{50}) was calculated. These are indicated by a dotted grey line on the x-axis, and their 95% confidence limits are also shown by grey boxes either side.

Figure 5.3 shows the structure of Bay 11-7082 (2E)-3-[(4-methylphenyl)sulfonyl]acrylonitrile (4-Me-PHSAN) and highlights the two sites that were modified to create new analogues. Position 3 and/or 4 of the phenyl ring were variably substituted with methyl, bromine, fluorine, chlorine, and acetamido groups, to generate new variants. Another set of analogues were synthesised where the nitrile functional group of TI1 was modified with CONH_2 (amide), COOEt (ethoxycarbonyl), CONMe_2 (N,N-dimethylcarboxamide), COMe (acetyl), a pyridine ring, and a phenyl ring with fluorine, chlorine and nitrile substituents. In total 30 analogues were synthesised by Alex Truman (University of Nottingham) for SAR

studies and the first 16 including TI1 were screened for both their IC_{50} s for *pqsA* inhibition and their EC_{50} s for *antA* expression (**Table 5.3**). Compounds 17-30 were tested for their activity against *pqsA* and *antA* expression at 20 μ M and 40 μ M, then selected Bay 11-7082 analogues were screened for their ability to inhibit pyoverdine (PVD) production.

Analogues of TI1 with new modifications or substitutions were screened with the aim to identify new structure with increased activity as well as for SAR studies. All the new analogues and their structures are listed in **Table 5.3**.

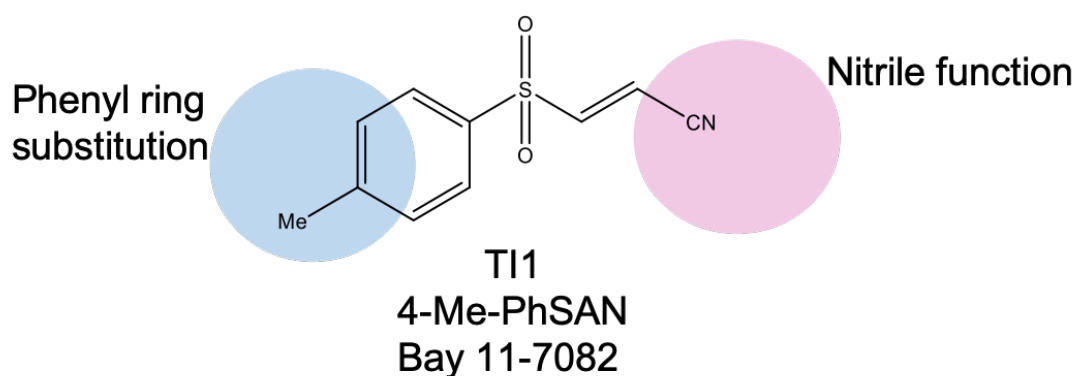
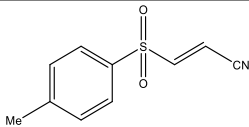
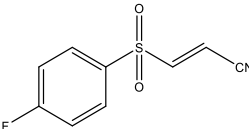
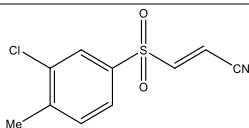
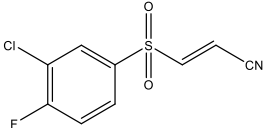
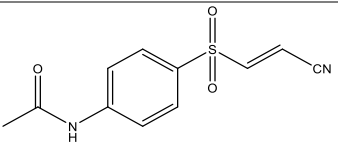
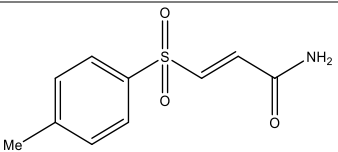
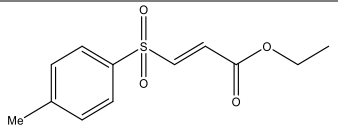
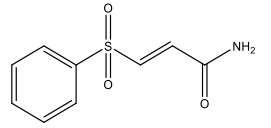
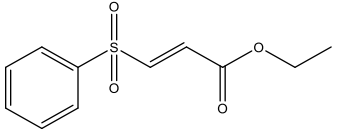
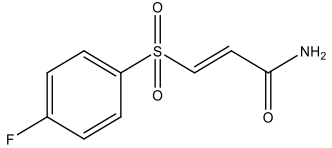
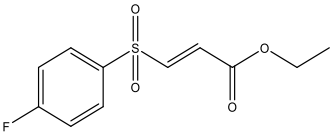
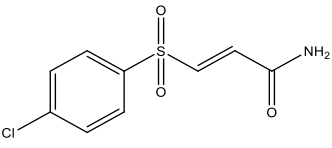
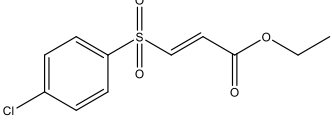
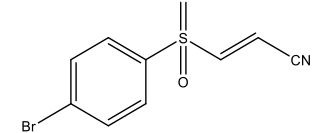
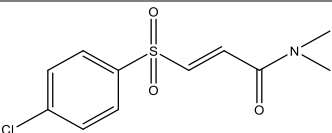


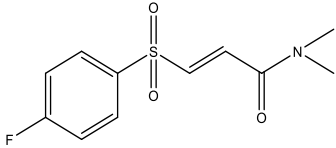
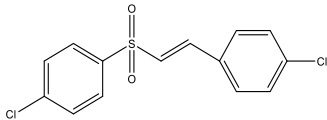
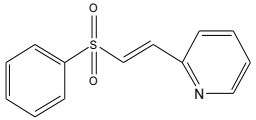
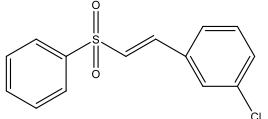
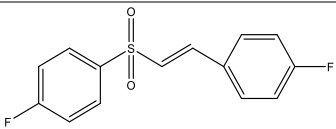
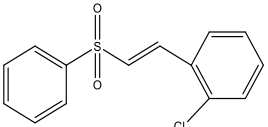
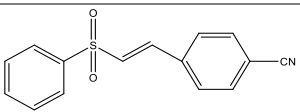
Figure 5.3. Inhibitors screened using *pqsA* expression to determine IC_{50} . Bay 11-7082 structure was modified either at positions 3 and/or 4 of the phenyl ring (within blue circle) or at the nitrile site (within pink circle). The Bay 11-7082 compound will be referred to as Tat inhibitor 1 (TI1) or 4-Me-PhSAN which is an abbreviation of (2E)-3-[(4-Methylphenyl)sulfonyl]acrylonitrile.

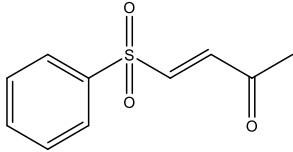
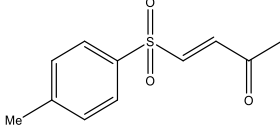
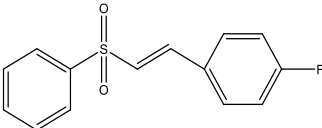
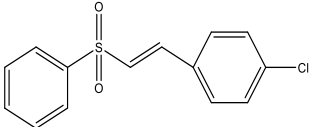
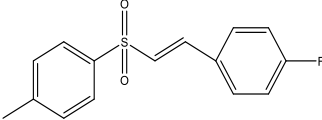
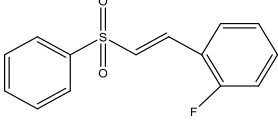
Table 5.3. Structural Analogues of the Tat inhibitor compound TI1. Compounds were synthesised by Alex Truman. IC₅₀ is the concentration at which there was 50% reduction in *pqsA* expression between the upper and lower limits of the dose-response curve, and EC₅₀, the concentration at which there was a 50% increase in *antA* expression. PVD fluorescence was measured at excitation wavelength 405 nm and emission wavelength 460 nm. Growth was measured at OD₆₀₀. Columns titled "% *pqsA* expression" and "% PVD fluorescence" at 20 μM/ 40 μM list the maximum values calculated at 20 μM (left sub-column) and 40 μM (right sub-column) on a normalised dose-response curve with 100% defined as the mean value for PAO1-DK miniCTX::*pqsA*'-lux + DMSO, and PAO1-DK + DMSO respectively.

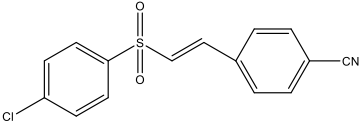
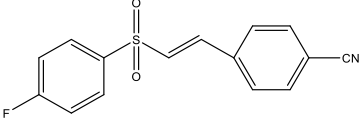
Tat inhibitor analogue (TI) number	Compound	Molecular weight	Structure	IC ₅₀ <i>pqsA</i> (μM)	EC ₅₀ <i>antA</i> (μM)	% <i>pqsA</i> expression at		% PVD fluorescence at	
						20 μM/ 40 μM	20 μM/ 40 μM		
TI1	Bay 11-7082 4-Me-PhSAN	207		27.4	20.5	74.5	52.3	58.6	10.9
TI2	4-F-PhSAN	211		30.3	23.2	66.0	54.4	-	-
TI3	3-Cl,4-Me-PhSAN	241.7		50.7	50.03	69.8	66.1	-	-

T14	3-Cl,4-F-PhSAN	245.7		5.8	19.0	38.8	30.7	68.4	20.7
T15	4-AcNH-PhSAN	250.3		38.2	68.4	73.8	56.8	-	-
T16	4-Me-PhSACONH ₂	225.3		4.8	31.6	45.5	40.01	56.4	37.6
T17	4-Me-PhSACOOEt	254		107.9	NA	68.9	60.5	77.1	77.8
T18	PhSACONH ₂	211		5.6	2.9	44.5	27.5	52.0	34.8
T19	PhSACOOEt	240.3		102.5	45.5	89.3	72.7	92.5	80.7

TI10	4-F-PhSACONH ₂	229.2		15.8	8.1	50.6	33.7	-	-
TI11	4-F-PhSACOOEt	258		NA	55.4	79.8	57.4	-	-
TI12	4-Cl-PhSACONH ₂	245.7		11.2	5.4	56.5	38.3	-	-
TI13	4-Cl-PhSACOOEt	274.7		NA	27.0	91.4	90.9	-	-
TI14	4-Br-PhSAN	272		28.0	21.8	44.9	40.2	-	-
TI15	4-Cl-PhSACONMe ₂	273.3		56.4	NA	92.1	76.0	86.2	72.9

TI16	4-F- PhSACONMe ₂	257		83.5	NA	100	81.4	86.2	77.1
TI17	4-Cl-PhSC6H4- 4-Cl	313.2		-	-	62.7	42.3	-	-
TI18	PhS-2-Py	245.3		-	-	47.1	38.5	-	-
TI19	PhSC6H4-3-Cl	278.8		-	-	58.0	43.8	-	-
TI20	4-F-PhSC6H4- 4-F	280		-	-	65.6	51.3	-	-
TI21	PhSC6H4-2-Cl	278.85		-	-	66.5	47.0	-	-
TI22	PhSC6H4-4-CN	269		-	-	72.9	45.0	-	-

TI23	PhSCOMe	210		-	-	54.5	34.4	-	-
TI24	4-Me-PhSCOMe	224		-	-	61.6	35.7	-	-
TI25	PhSC6H4-4-F	262		-	-	58.7	32.8	-	-
TI26	PhSC6H4-4-Cl	278.8		-	-	56.2	41.8	-	-
TI27	4-Me-PhSC6H4-4-F	276.3		-	-	64.3	43.6	-	-
TI28	PhSC6H4-2-F	262		-	-	75.5	46.3	-	-

TI29	4-Cl-PhSC6H4- 4-CN	303.8		-	-	66.7	49.3	-	-
TI30	4-F-PhSC6H4- 4-CN	287		-	-	76.1	53.1	-	-

5.2.2. Growth is inhibited at high concentrations of TI1

TI1 was added to LB to create a set of 20 different concentrations spanning a 1000-fold range. As PAO1-DK grew at each concentration, OD₆₀₀ and *pqsA* expression was followed and is displayed in **Figure 5.4** and **Figure 5.2** respectively.

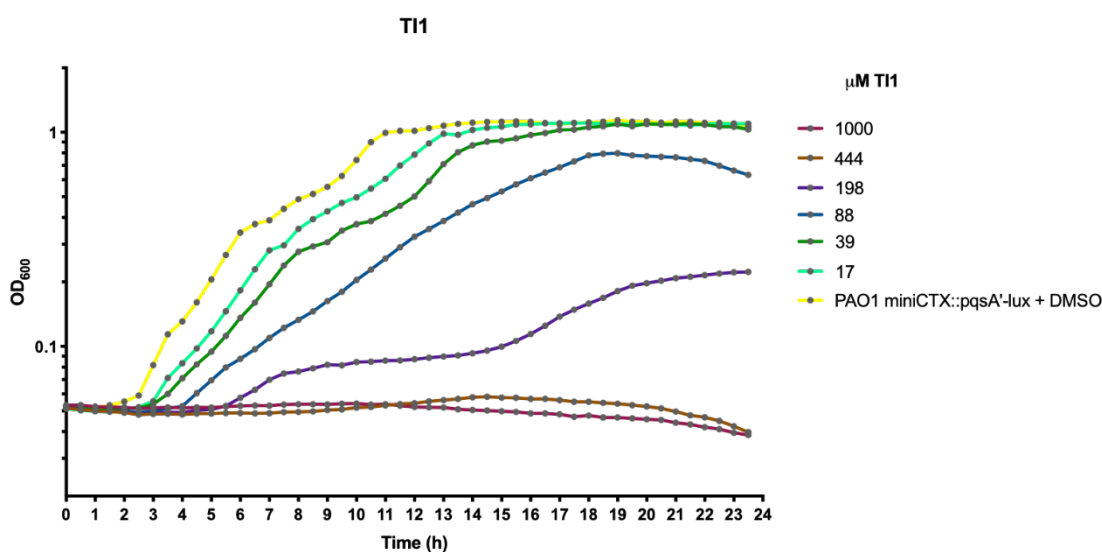


Figure 5.4. Growth in LB of PAO1 miniCTX::pqsA'-lux in 17 μM, 39 μM, 88 μM, 198 μM, 444 μM and 1000 μM TI1. Each coloured line represents a different concentration of TI1 from 1000 μM to 17 μM, and a no-TI1 control consisting of PAO1 miniCTX::pqsA'-lux + DMSO. Each time point is indicated by a grey dot.

As shown in **Figure 5.4**, increasing TI1 concentrations from 0 μM to 39 μM caused a delay in growth but the same OD₆₀₀ was reached. The final OD₆₀₀ of the DMSO control was not reached at higher concentrations of TI1, such as 88 μM and 198 μM. At concentrations 444 μM and 1000 μM there was no growth. As noted in earlier chapters, deletion of the Tat system caused a growth defect due to failed translocation of PetA. Therefore, slower growth can be expected when Tat is inhibited. However, at concentrations higher than 39 μM the growth defect becomes far more pronounced than seen in a *ΔtatABC* mutant (**Figure 3.19**) and may be due to secondary targets of the TI1 within the cell. This could be

investigated further by quantifying the growth of a *tat* mutant at a range of TI1 concentrations.

5.2.3. Growth inhibition at high concentrations of Bay 11-7082 analogues TI1-TI14

Similarly to TI1, Bay 11-7082 analogues TI2 – TI14 reduced growth with increasing concentrations and this is shown in **Figure 5.5** and **Figure 5.6**. Growth of PAO1-DK in TI1-TI6 is shown in **Figure 5.5**, all analogues displayed some level of growth inhibition with increased concentration. 3-Cl,4-Me-PhSAN (TI3) and 4-AcNH-PhSAN (TI4) were the least active against growth, as PAO1-DK reached the same final OD₆₀₀ as the PAO1-DK + DMSO control when grown in 640 µM TI13. **Figure 5.6** shows growth inhibition of PAO1-DK when grown in TI7-TI14. Replacement of the methyl group at position 4 of TI1 with a halogen (fluorine or chlorine) and of the nitrile function with an ethoxycarbonyl (COOEt) group lowered the growth inhibitory properties of the Bay 11-7082 analogues TI11 (**Figure 5.6e**) and TI13 (**Figure 5.6g**).

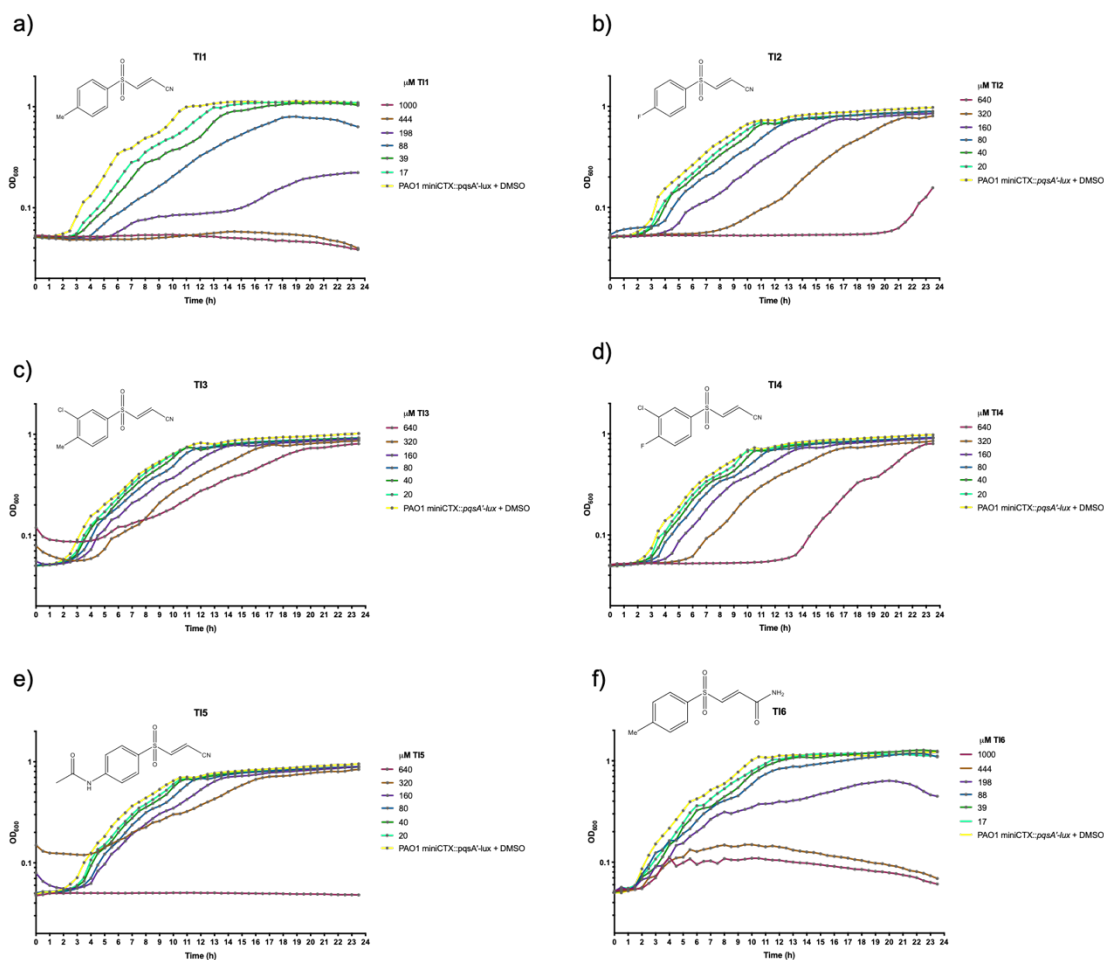


Figure 5.5. Growth in LB of PAO1 miniCTX::pqsa'-lux in a range of concentrations of a) TI1, b) TI2, c) TI3, d) TI4, e) TI5, and f) TI6. Growth in 1000 μM , 444 μM , 198 μM , 88 μM , 39 μM , 17 μM and 0 μM (DMSO only) of TI1 and TI6 is shown. Growth in 640 μM , 320 μM , 160 μM , 80 μM , 40 μM , 20 μM and 0 μM (DMSO only) of TI2-TI5 is shown. Grey circles indicate timepoints when OD_{600} was measured. The chemical structure for each compound is displayed in the top left corner of each graph.

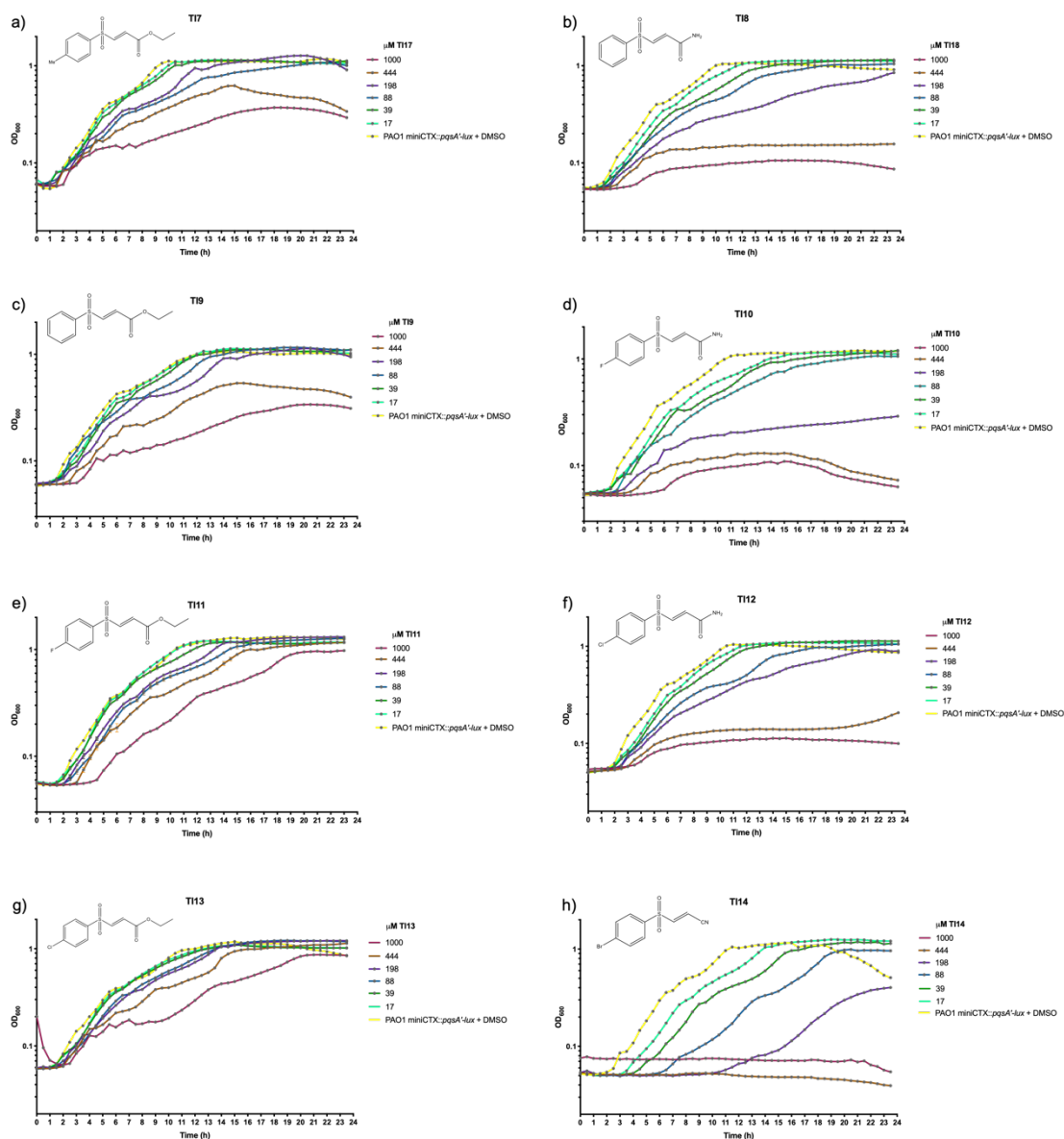


Figure 5.6. Growth in LB of PAO1 miniCTX::pqsA'-lux in a range of concentrations of a)TI7, b)TI8, c)TI9, d)TI10, e) TI11, and f) TI12, g)TI13 and h) TI14. Growth in 1000 μM, 444 μM, 198 μM, 88 μM, 39 μM, 17 μM and 0 μM (DMSO only) of TI7-TI14 is shown. Grey circles indicate timepoints when OD₆₀₀ was measured. The chemical structure for each compound is displayed in the top left corner of each graph.

5.2.4. Reduced growth inhibition is observed using Bay 11-7082 analogues bearing a CONMe₂ functional group

Bay 11-7082 analogues TI15 (4-F-PhSACONMe₂) and TI16 (4-Cl-PhSACONMe₂) did not exhibit severe growth inhibition. **Figure 5.7** shows growth curves for PAO1-DK miniCTX::*pqsA'*-*lux* in the presence of TI15 (a) and TI16 (b) at 39 μ M, 17 μ M and 1 mM.

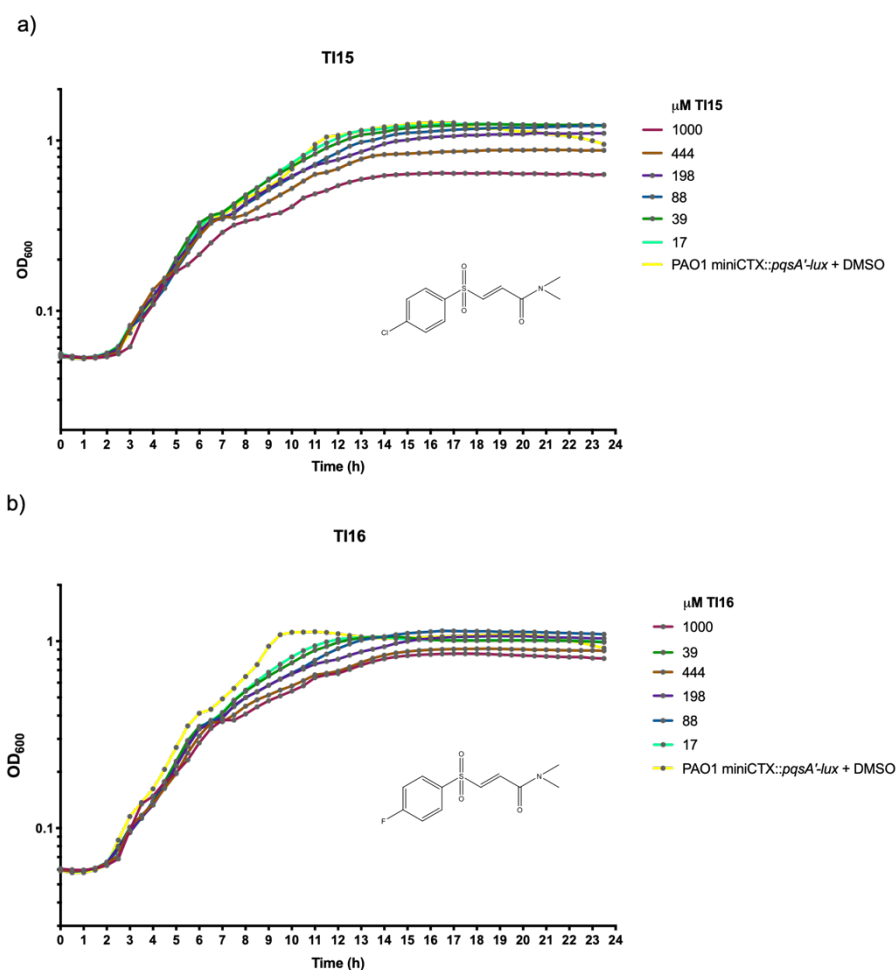


Figure 5.7. Growth in LB of PAO1 miniCTX::*pqsA'*-*lux* is not severely reduced by Tat inhibitor 15 (a) and Tat inhibitor 16 (b). Concentrations of 1 mM, 39 μ M and 17 μ M were selected to demonstrate a lack of growth inhibition that can be seen in Tat inhibitors 1-14. Experiments were repeated in triplicate and a DMSO control was included.

At the highest concentration of TI15 tested, 1 mM, growth of PAO1-DK reached an OD₆₀₀ of 0.63. compared with no growth at 1 mM TI1. TI16 had no effect on growth at any of the concentrations tested. The lack of growth inhibition suggests that these compounds directly inhibit *pqsA* expression instead of the Tat system, as deletion of the *tatABC* operon causes a noticeable growth defect. This could be through competitive inhibition of PqsR, the *pqsA* regulator. **Table 5.3** lists the IC₅₀s for inhibition of *pqsA* expression as 56.3 and 83.5 uM respectively, which is higher than TI1. It appears that addition of a CONMe₂ function reduced the potency of the compound, whether as an inhibitor of the Tat system or as an inhibitor of *pqsA* expression. TI16 was the least active compound tested.

5.2.5. Potency of TI1 was increased by 3-Cl, 4-F phenyl ring substituents and reduced by 3-Cl,4-Me or 4-AcNH substitutions

Chemical modifications at the positions 3 and/or 4 of the phenyl ring of TI1 were tested for their effect on compound activity against *pqsA* expression. **Figure 5.8** shows the results of the IC₅₀ screens and IC₅₀s are listed in **Table 5.3**. The concentration range of *pqsA*'-lux inhibitor analogues used in the assay was enough to cover lack of activity to complete inhibition. Intervals between dilutions provided sufficient measurements to obtain dose response curves.

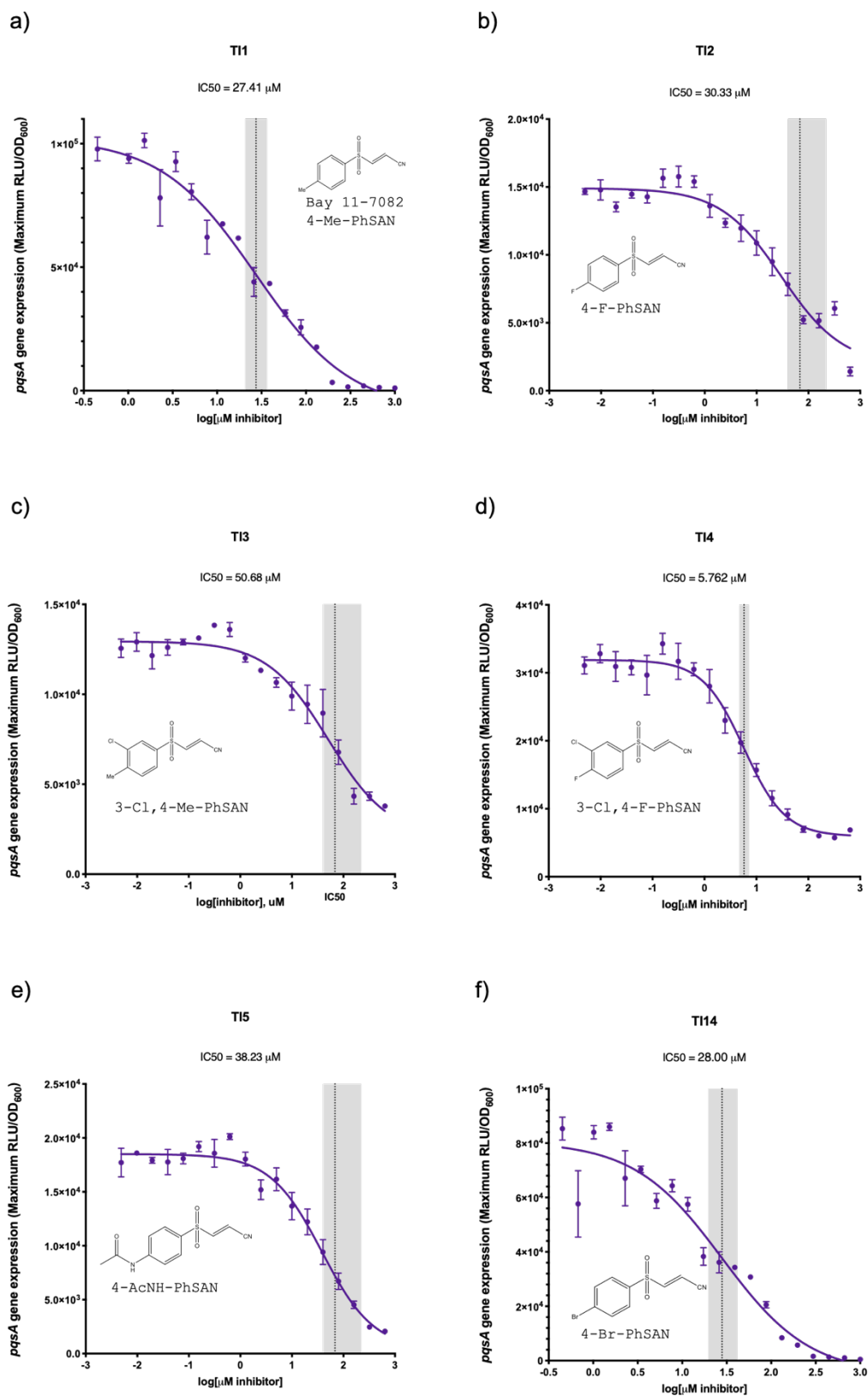


Figure 5.8. Dose response curves for TI1 and analogues TI2-5 and TI14 bearing different phenyl ring substituent groups. All compounds used have the same CN function, only substituent groups of the phenyl ring varied. Concentrations of TIs ranging from 1 mM to 0.45 μ M were tested for their activity against *pqsA* expression. Dotted line represents the IC₅₀ and grey area either side the 95% confidence limits. IC₅₀ is written above each graph.

Each IC_{50} determined for TI1 analogues with chemical modifications at the positions 3 and/or 4 of the phenyl ring (TI1-5 and TI15) are presented in **Figure 5.9**. Multiple comparisons with TI1 using a one-way Anova test showed lower activity for TI3 (3-Cl,4-Me-PhSAN) and TI5 (4-AcNH-PhSAN) compared with TI1. However, inhibitory activity was increased ~6-fold in TI4 (3-Cl,4-F-PhSAN) by replacing the methyl group at position 4 with fluorine and introducing a chlorine substituent at position 3 of the phenyl ring.

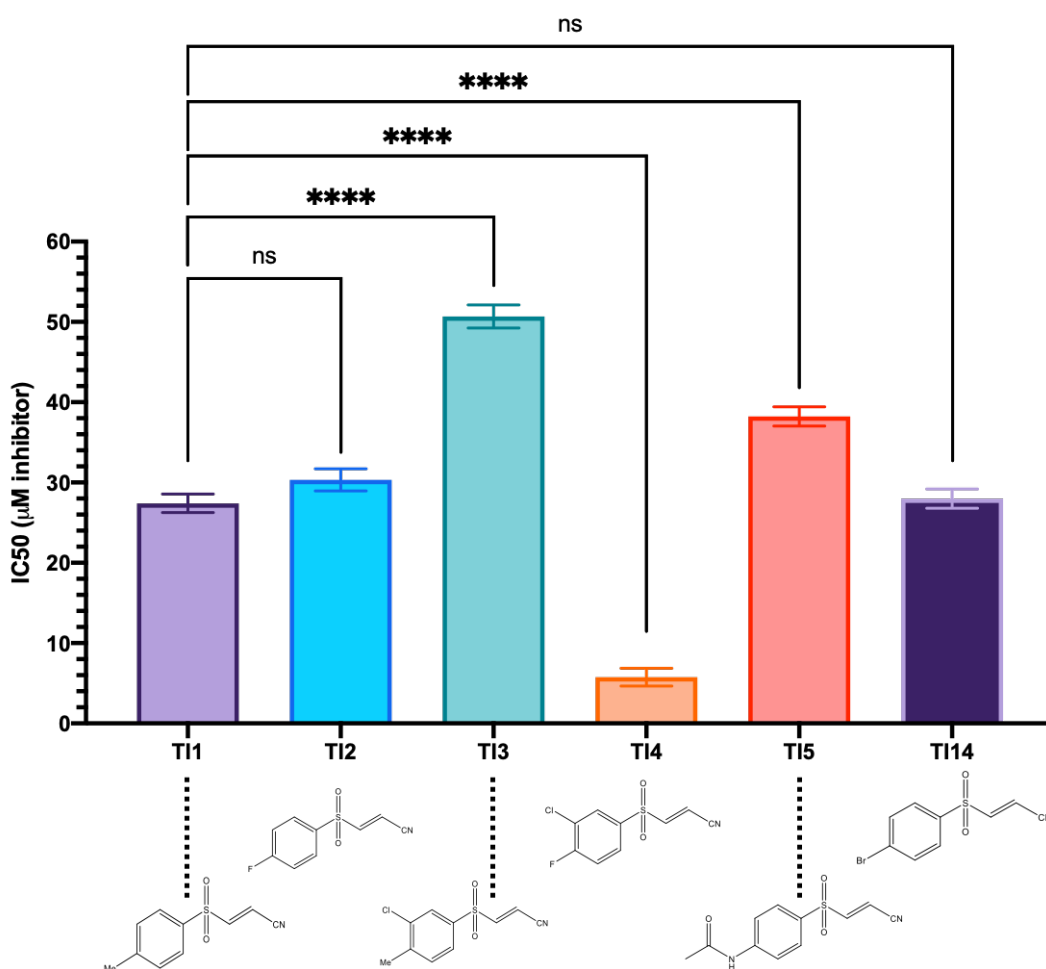


Figure 5.9. Inhibition of *pqsA* expression is influenced by phenyl ring substituents. PAO1 miniCTX::*pqsA'*-*lux* was grown in a broad concentration range of TI1 analogues TI2-5 and TI14. The IC_{50} for each is plotted with standard deviation indicated by error bars. Significance determined by one-way Anova test is indicated by ns=not significant ($p > 0.05$), ****=significant with $p \leq 0.0001$. Chemical structures are shown below each Tat inhibitor to illustrate how altering the ring substituents affects *pqsA* inhibitory activity.

5.2.6. Evaluation of nitrile group variants and their effect on activity

Having evaluated analogues with different substituent groups of the phenyl ring with respect to changes in activity, the focus was shifted to modifications of the nitrile function (**Figure 5.10**). Each Bay 11-7082 analogue was screened against *pqsA* expression to calculate an IC_{50} and these are plotted by functional group type in **Figure 5.10**. This illustrates clear differences in activity with respect to nitrile group variants.

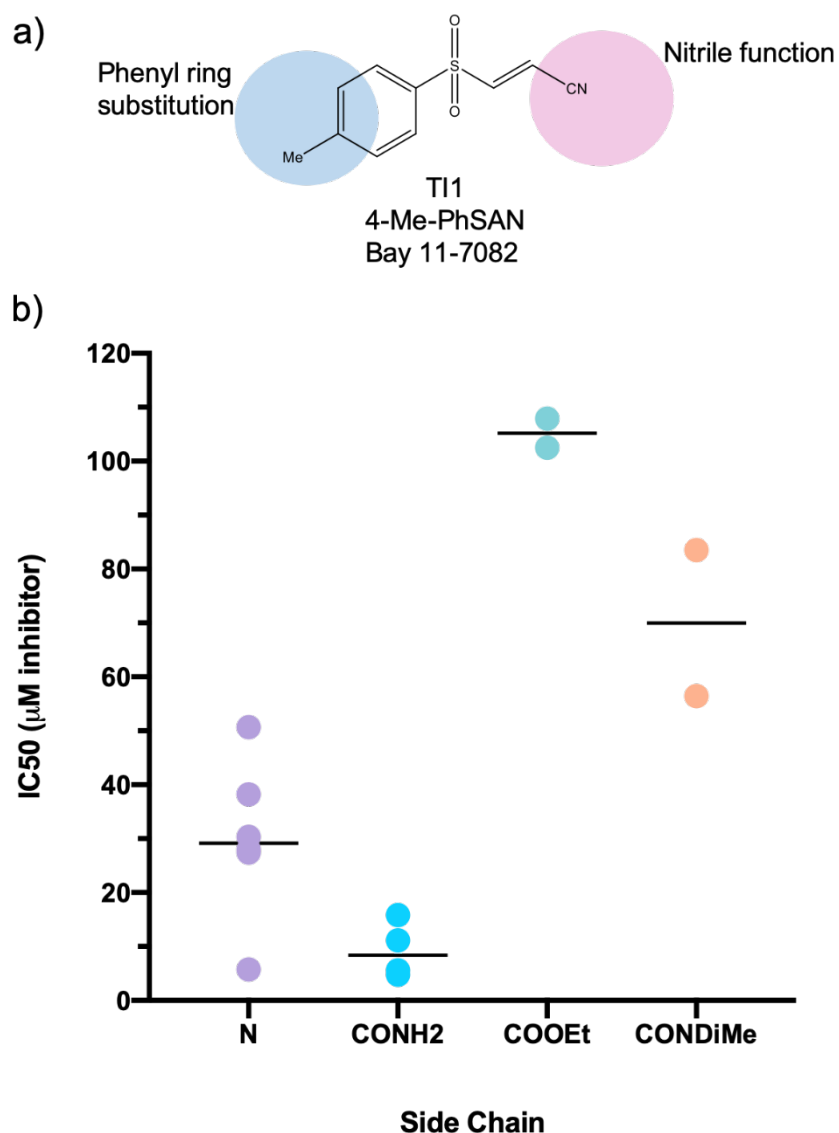


Figure 5.10. Comparison of IC_{50} for inhibition of *pqsA'*-*lux* expression by T11-TI16. (a) T11 structure with highlighted modification sites and (b) IC_{50} s categorised according to nitrile variants. CONDiMe is also referred to as CONH₂. Horizontal line indicates the median IC_{50} for each analogue class.

Figure 5.10 shows that Bay 11-7082 analogues with a CONH₂ (amide) functional group improved the potency *pqsA* inhibition for all analogues tested (TI6, TI8, TI10, TI12), irrespective of additional phenyl ring substitution. **Figure 5.11** shows dose-response curves for each of the CONH₂-containing compounds. TI6 and TI8 had IC₅₀ concentrations at around 5 μM and ~6-fold higher potency than TI1.

TI10 and TI12 contain a fluorine (TI10) and chlorine (TI12) substitution at position 4 on the phenyl ring in addition to an amide functional group. The IC₅₀ concentrations for TI10 and TI12 were 15.84 μM and 11.16 μM respectively, and therefore a ~2-3 fold higher potency than TI1. While an amide functional group greatly improved activity against *pqsA* expression, addition of a halogen at position 4 on the phenyl ring (TI10, TI12) had the opposite effect and reduced the activity of the TI1 analogues with a CONH₂ functional group.

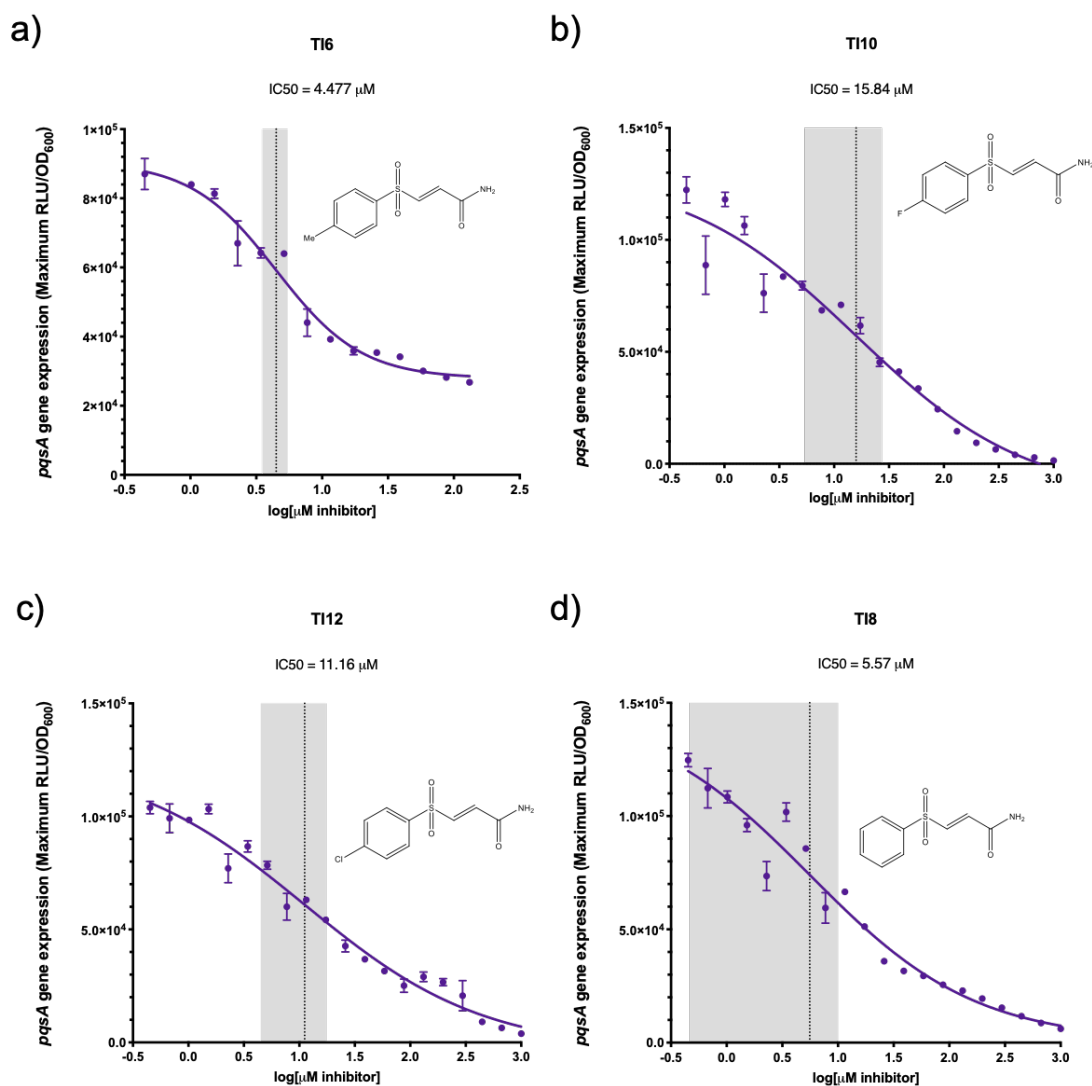


Figure 5.11. Dose-response curves of TI1 analogues TI6, TI10, TI12 and TI8 incorporating a CONH₂ functional group together with different phenyl ring substituent groups. PAO1 miniCTX::*pqsA*-*lux* was grown in concentrations of each compound ranging from 0.45 μM to 1000 μM and *pqsA* expression was measured. Maximum *pqsA* expression at each concentration is plotted ±SD from three technical repeats. Dotted line indicates the IC₅₀ concentration and the grey box indicates 95% confidence limits.

Addition of a COOEt group to the TI1 in place of the nitrile group in combination with altered phenyl ring substitution gave the analogues TI7, TI9, TI11, and TI13. The COOEt functionality reduced the *pqsA* inhibitory activity, as seen by the increased IC₅₀s displayed in **Figure 5.12**. IC₅₀s could only be

determined for TI7 and TI9 with the *pqsA* screen. These were 107.9 μM and 102.5 μM respectively, approximately 3-fold higher than that of TI1. TI11 and TI13 did not reach a plateau within the range of concentrations tested, so their IC_{50} s could be determined.

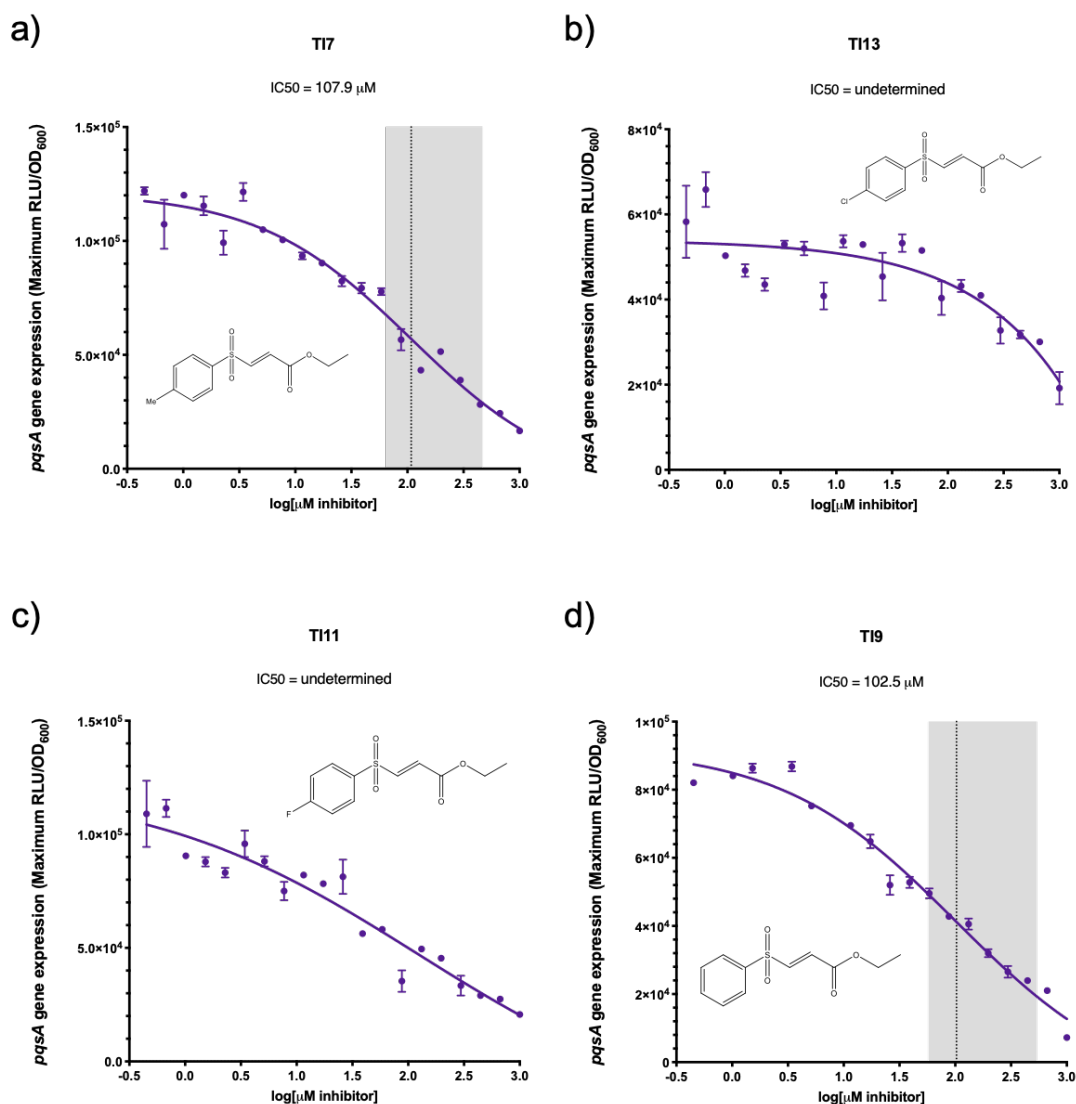


Figure 5.12. Replacement of the CN functionality with COOEt to generate analogues TI7, TI9, TI11 and TI13, increased IC_{50} for *pqsA* expression. PAO1 miniCTX::*pqsA'*-*lux* was grown in concentrations of each compound ranging from 0.45 μM to 1000 μM and *pqsA* expression was measured. Each screen was carried out in triplicate and data are plotted as mean maximum *pqsA* expression \pm SD after 24 h growth at each concentration of Tat inhibitor. Chemical structures of each compound are included. IC_{50} s are indicated by a dotted line and 95% confidence limits, by a grey shaded area.

There were significant delays in peak *pqsA* expression as inhibitor concentrations increased. **Figure 5.13a** shows a representative graph where PAO1-DK miniCTX::*pqsA'-lux* was grown in LB containing the Bay 11-7082 analogue, TI9. A peak shift to the right of the graph could in part be due to growth inhibition, either due to Tat inhibition or through inhibition of other pathways. However, it is unlikely slower growth is the sole reason for such a severe peak shift as there is an ~3 h delay *pqsA* expression at 39 μ M TI9 but growth was unaffected at this concentration of TI9 (**Figure 5.13b**). In contrast, TI1 analogues TI15 and TI16 incorporate a CONMe₂ function in place of the nitrile group, and substitution of a chlorine (TI15) or fluorine (TI16) group at position 4 on the phenyl ring. Analogues with a CONMe₂ group did not cause a delay in peak *pqsA* expression (**Figure 5.14**) or inhibit growth (**Figure 5.7**). Dose-response curves are shown in **Figure 5.15**. TI15 and TI16 have very little effect on growth, they may directly inhibit *pqsA* expression instead of inhibiting the Tat system, as a growth defect is expected upon Tat inhibition due to failure to export the Rieske subunit. However, TI15 and TI16 could be true Tat inhibitors but with such a weak activity it may be enough for the Rieske subunit to be secreted enough to maintain growth.

Figure 5.14 shows despite inhibitor concentrations of 1000 μ M, the maximal expression of *pqsA* occurred at the same timepoint, ~7 h. Therefore, it follows that the peak delay of TI1 analogues TI1-TI14 is either caused by direct inhibition of processes associated with cell growth or by altered transport of the Rieske subunit, PetA, that then results in a delay in growth.

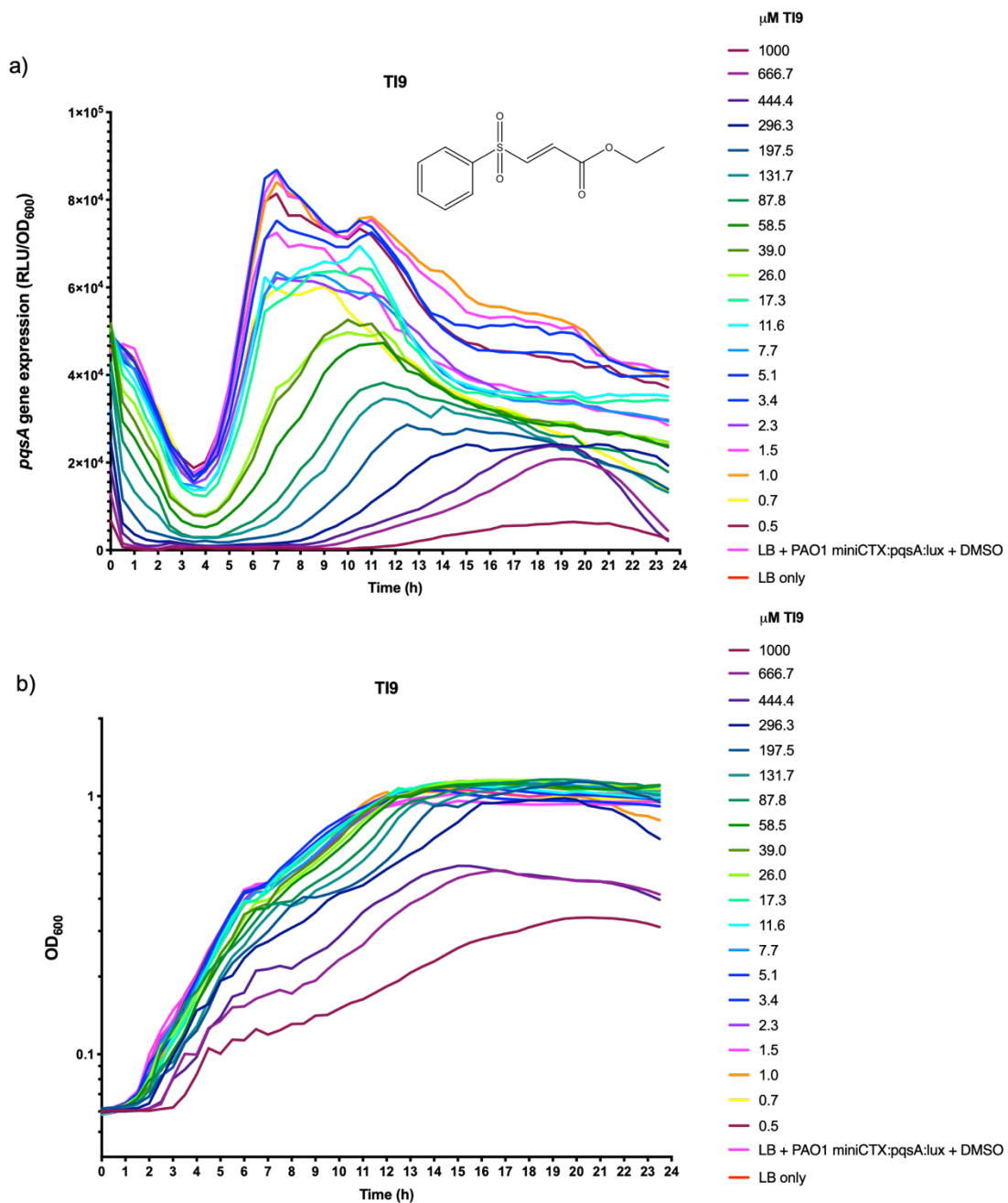


Figure 5.13. Effect of T19 on *pqsA* expression at concentrations ranging from 0.5 μM to 1000 μM. PAO1 miniCTX::*pqsA*'-lux was grown in LB + T19 at a range of concentrations and *pqsA* expression measured every 30 min over 24 h is plotted above. Experiment was carried out in triplicate. In (a) maximal expression can be seen to shift towards the right of the graph as concentration increases, indicating a delay.

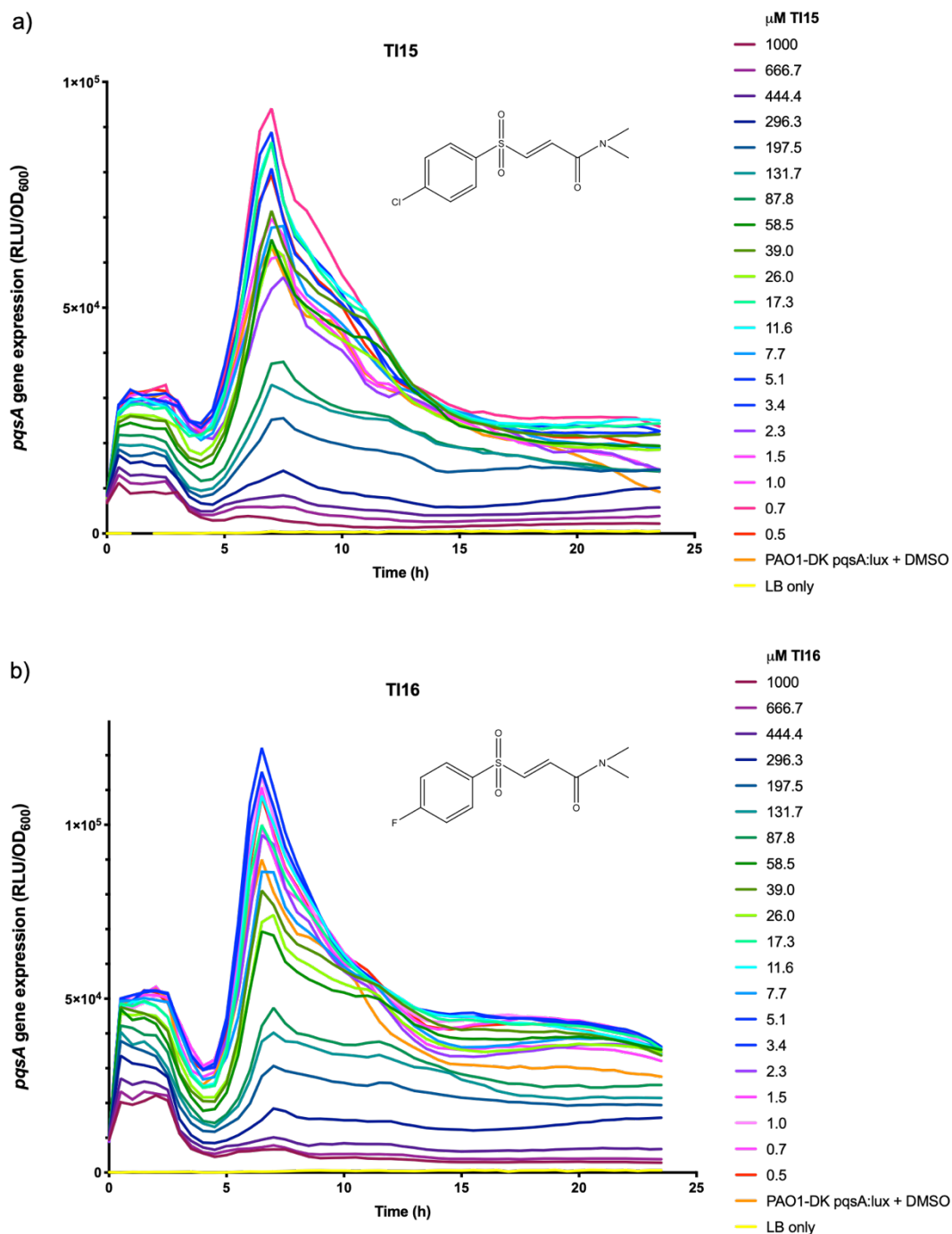


Figure 5.14. Peak expression of *pqsA* is unaltered when grown in the presence of TI15 and TI16, analogues with a CONMe₂ functional group. TI15 and TI16 have similar *pqsA* expression profiles at concentrations ranging from 0.45-1000 μM. The measurements were taken every 30 min and peak expression occurs at ~7 h and then steeply declines to ~14 h where it plateaus. Experiment was carried out in triplicate.

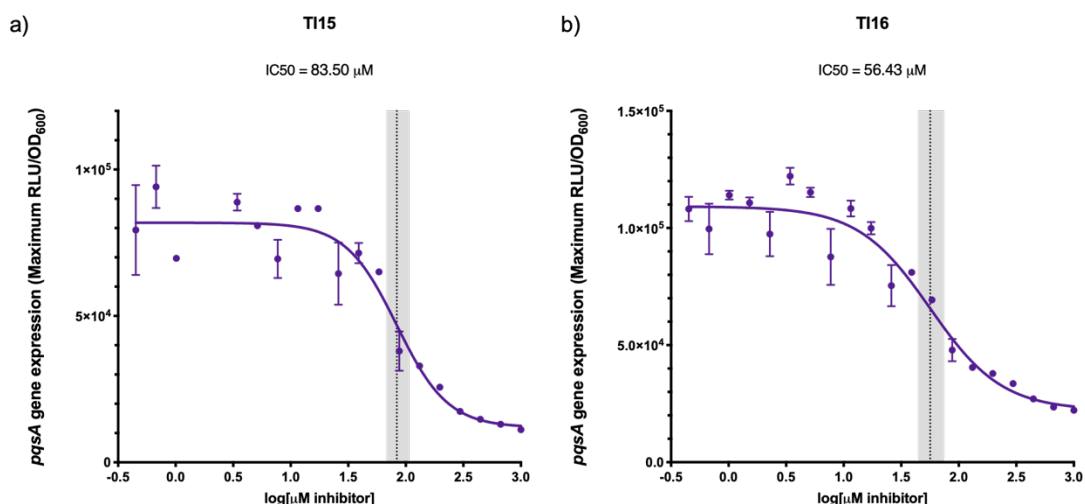


Figure 5.15. Dose-response curves for TI15 and TI16 which have a CONMe₂ functional group. PAO1 miniCTX::*pqsA'*-*lux* was grown in LB containing TI15 (a) and TI16 (b) at concentrations ranging from 0.45 μM to 1000 μM and maximum expression of three technical repeats was recorded. The mean value is shown ±theSD. The vertical dotted line represents the IC₅₀ and grey shading, the 95% confidence interval.

5.2.7. *pqsA* inhibitory activity of analogues TI17-TI30 at 20 μM and 40 μM

The IC₅₀s for TI2-TI16 were determined via inhibition of a *pqsA* expression as outlined above and listed in **Table 5.3**. In addition, the TI1 analogues TI17-TI30 were also synthesized by Alex Truman (University of Nottingham) and tested with a high-throughput screen at concentrations of 20 μM and 40 μM for their inhibitory activity against *pqsA* expression to gain further insights into the SAR (**Table 5.3**). Results were normalised for PAO1-DK miniCTX::*pqsA'*-*lux* expression (**Figure 5.16**).

All inhibitors caused a reduction in *pqsA* expression at 20 μM and 40 μM and TI18, TI23, TI24 and TI25 appeared to be more potent (**Figure 5.16**). The % *pqsA* expression was 47.1% at 20 μM and 38.5% at 40 μM for TI18, which had an unsubstituted phenyl ring and a pyridine ring functional group substituent. TI1 % *pqsA* expression was 74.5% at 20 μM and 52.3% at 40 μM. By comparison, TI4 had the lowest % *pqsA* expression at 20 μM and 40 μM of TI1-TI30, at 38.8% and

30.7% respectively. TI23 and TI24 both have an acetyl in place of the nitrile function, and TI23 had unsubstituted phenyl ring while TI24 has the 4-Me substituent as in TI1. The % *pqsA* expression was 54.5% at 20 μ M and 34.4% at 40 μ M of TI23, and 61.6% at 20 μ M and 35.7% at 40 μ M of TI24. The derivative TI25 had a phenyl ring with a fluorine substitution at position 4 and this increased the activity compared to TI1 as evidenced from *pqsA* expression which was 58.7% at 20 μ M and 32.8% at 40 μ M compared with TI1. Derivatives TI18, TI23, TI24 and TI25 where the nitrile group is replaced with a pyridine ring, acetyl group, and 4-F substituted phenyl ring increased the activity compared with TI1, however, none of these replacements made the compound as potent at *pqsA* inhibition as the amide analogues: TI6, TI8, TI10 and TI12 (**Figure 5.11** and **Table 5.3**).

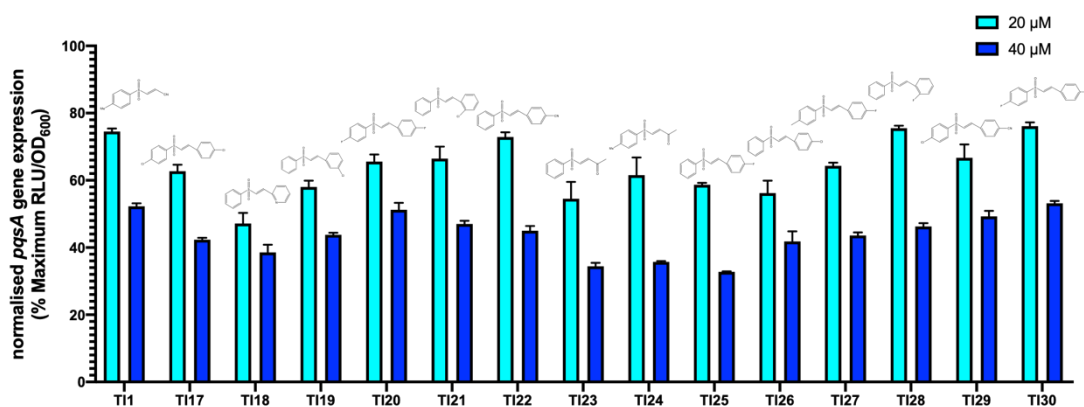


Figure 5.16. Normalised *pqsA* expression for PAO1 miniCTX::*pqsA'*-lux in response to analogues TI17-TI22 at 20 μ M or 40 μ M . TI1 (Bay 11-7082) is included for comparison. All compounds showed similar *pqsA'*-lux inhibitory activity. Experiments were carried out in triplicate and means plotted with error bars indicating standard deviation. Chemical structures are shown above each analogue.

5.2.8. Upregulation of *antA* expression in response to TI1 and analogues

As noted in the previous chapters, inhibition or deletion of the Tat system or *pqsA* resulted in upregulation of *antA* expression. Therefore, TI1 analogues were also tested for their ability to up-regulate *antA*, and EC₅₀s were calculated where possible. In this case, the EC₅₀ is the effective concentration that results in 50% increase in *antA* expression. **Figure 5.17** shows the comparison of *pqsA* screen IC₅₀s and *antA* screen EC₅₀s.

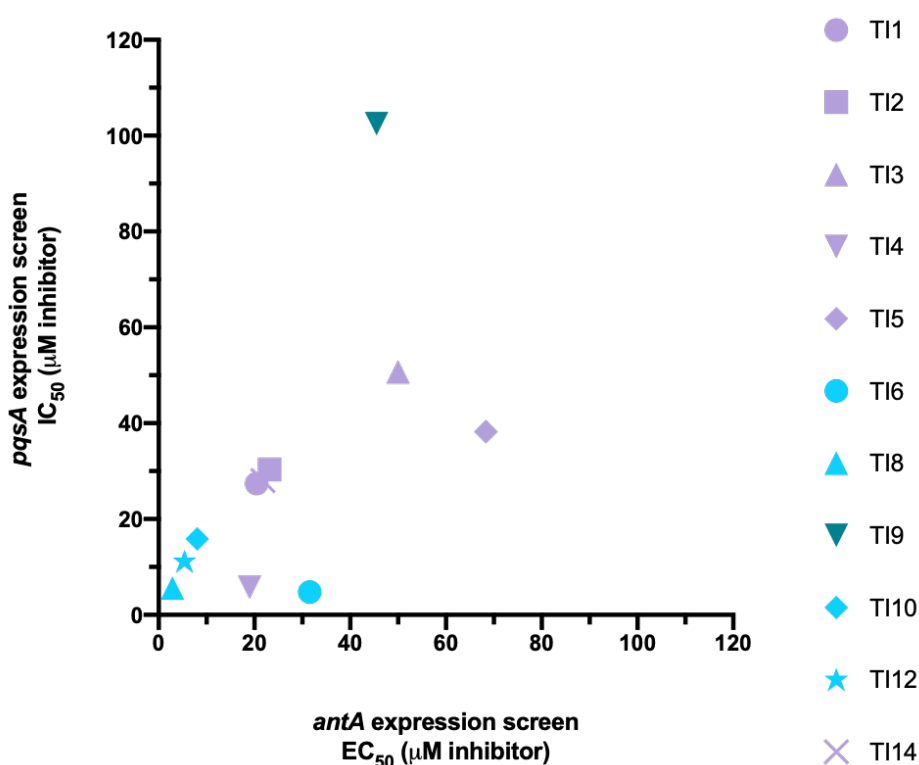


Figure 5.17. Comparison of IC₅₀ and EC₅₀ concentrations for TI1-6, TI8-TI10, TI12 and TI14. Individual dose-response curves plotting maximum *pqsA* expression versus maximum *antA* expression at 0.45 µM to 1000 µM. Analogues TI7, TI15, and TI16 are not displayed as an E₅₀ could not be derived from the available data. TI11 and TI13 are not displayed as they did not generate an IC₅₀ value for inhibition of *pqsA* expression. Purple symbols are compounds with a CN group, light blue indicates a CONH₂ group, and TI9, which has a COOEt functionality, is coloured teal.

For the most part, IC_{50} concentrations were very similar to EC_{50} concentrations. TI1 analogues are coloured by functional group in **Figure 5.17**, and it is clear that incorporation of an amide group increased activity in both *pqsA* and *antA* screens. The most potent compounds included TI8, TI12, and TI10 – all of which had an amide group. TI4 was also more active than TI1 in both screens, it had a nitrile function and two halogens, chlorine at position 3 and fluorine at position 4 on the phenyl ring. In comparison, TI5, TI3 and TI9 are far less potent.

Figure 5.18 shows representative examples of *antA* EC_{50} dose-response curves using the results for TI4 and TI5, two compounds with higher (a) and lower (b) activity than TI1 which has an EC_{50} of 20.46 μ M (**Figure 5.2**).

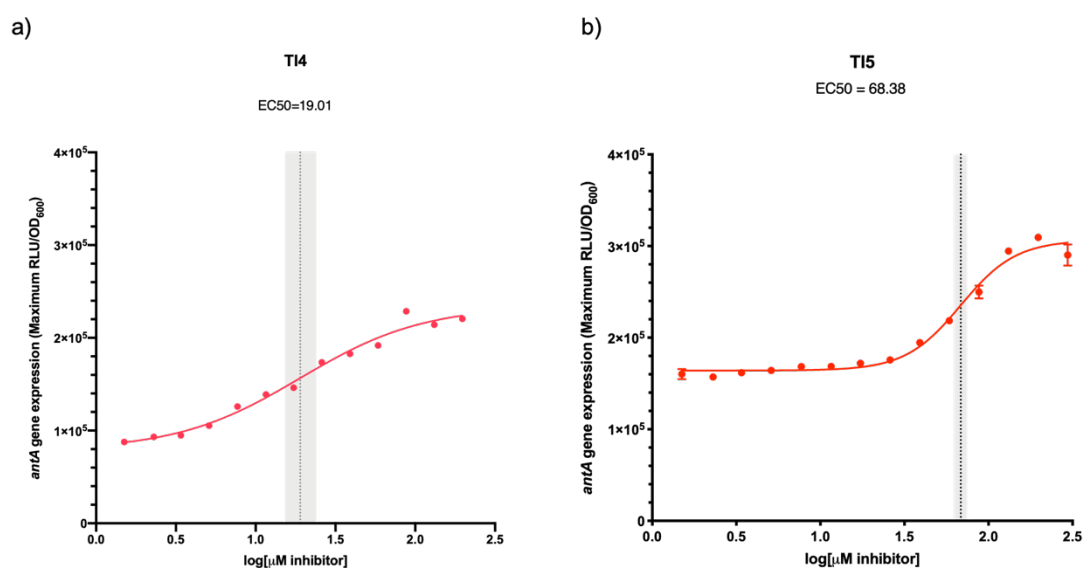


Figure 5.18. Dose-response curve for activation of *antA* following growth in response to TI4 (a) and TI5 (b). EC_{50} values were calculated (dotted line) and 95% confidence limits are shown as a shaded grey area.

5.2.9. Exploiting pyoverdine (PVD) production as a screen for TI compound inhibitory activity

Pyoverdine is a siderophore synthesised in the cytoplasm and matured to contain a green-fluorescent chromophore in the periplasm before it is released externally (Hannauer *et al.*, 2012). There are many steps to pyoverdine production, some of the final reactions involve the pyoverdine maturation proteins PvdP and PvdN which are exported via the Tat system. Complete inhibition or deletion of the Tat system abolishes mature pyoverdine production and with it, the intense green fluorescence in the culture supernatant (Ball *et al.*, 2016). This provides a simple fluorescence-based assay for assessment of Tat system inhibition.

However, PVD production is also under the control of *pqs* QS, so this screen cannot distinguish between Tat inhibition and *pqsA* inhibition. **Figure 5.19** shows fluorescence of pyoverdine in wild-type cultures grown in M9 minimal medium + succinate compared with that of a *pqsA* mutant and pyoverdine-deficient *tatABC* mutants. PVD biosynthesis was completely abolished in the *tat* mutant and reduced by ~60% upon perturbation of PQS biosynthesis. Nevertheless, measurement of PVD production in the TI1 analogues was still useful for SAR analysis as some were more active against PVD production than others as listed in **Table 5.3** and shown in **Figure 5.20**.

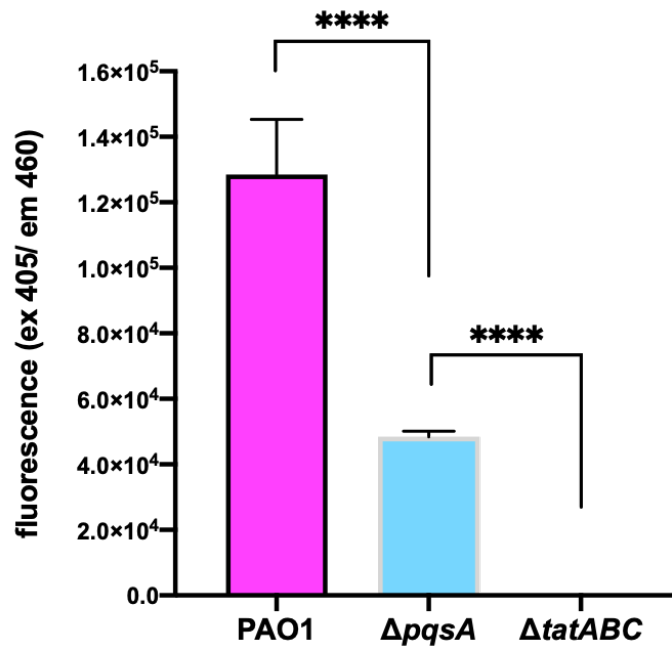


Figure 5.19. PVD production in PAO1, PAO1 $\Delta pqsA$ and PAO1 $\Delta tatABC$ mutant. Maximum fluorescence of PAO1, PAO1 $\Delta pqsA$ and PAO1 $\Delta tatABC$ mutant cultures at wavelengths of 405 nm (excitation) and 460 nm (emission). Data show mean values and error bars indicates standard deviation.

Selected compounds were chosen for the PVD assay; TI4, TI6, and TI8 for their increased potency against *pqsA* expression, TI7 and TI9 for their largely reduced activity against *pqsA* expression, and TI15 and TI16 for their lack of growth inhibitory properties as well as weak *pqsA* inhibition. Concentrations were tested at 20 μM and 40 μM and compared with TI1. The results are shown in **Figure 5.20**. Each value was normalised to the % of PAO1-DK fluorescence (ex. 405 nm/ em. 460 nm) as an indirect measurement of pyoverdine concentration.

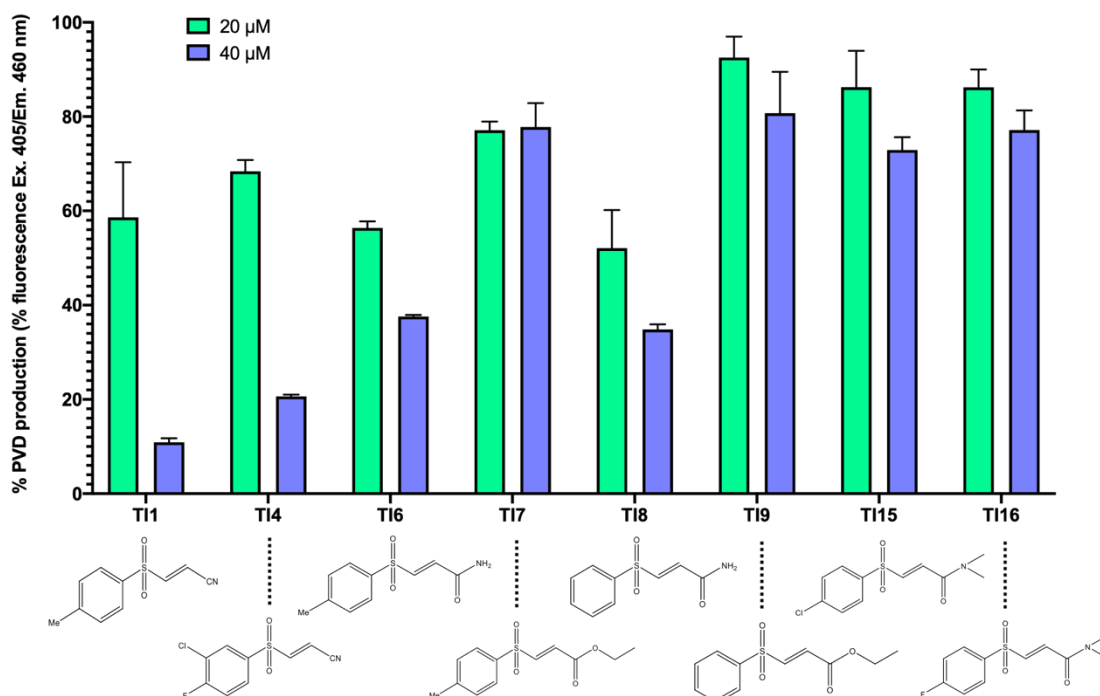


Figure 5.20. Normalised PVD production of PAO1 grown in iron-limited M9 + succinate medium containing 20 μM or 40 μM and TI1, TI4, TI6, TI7, TI8, TI9, TI15 or TI16. Fluorescence (ex. 405 nm/em. 460 nm λ) of the PAO1 + DMSO control was used to determine 100% PVD production and fluorescence values for the Bay 11-7082 analogues at 20 μM (green) and 40 μM (blue) were normalised to this number. Chemical structures are shown below each Bay 11-7082 analogue. Experiment was carried out in triplicate and the mean is plotted with SD indicated by a bar.

All compounds inhibited pyoverdine fluorescence to some degree, but TI1 was the most active. Aside from TI1, reduction in pyoverdine production was greater for compounds TI4, TI6 and TI8 – which have an amide group. Despite a greater ability to decrease *pqsA* expression and increase *antA* expression, TI4, TI6 and TI8 were not more active than TI1 with respect to inhibition of PVD production. This may suggest they target *pqsA* expression rather than the Tat system. TI7, TI9, TI15 and TI16 were very weak inhibitors of PVD production, and they have high IC_{50} and EC_{50} values against *pqsA* and *antA* expression as shown in **Table 5.3**. Additional assays measuring factors that are not regulated via *pqs* QS are needed

to measure Tat inhibition in order to distinguish between compounds that are Tat rather than *pqsA* inhibitors.

5.2.10 Jurkat T cell viability in the presence of TI1 and TI6

TI1 has been reported as being both immunomodulatory and cytotoxic (Massai *et al.*, 2019). If a compound is to be used as an antivirulence agent, it must have very low toxicity in mammalian cells. The TI1 analogue with the greatest activity, TI6 (4-Me-PhSACONH₂), was chosen for eukaryotic cell cytotoxicity assessment.

AlamarBlue is a non-toxic indigo-coloured compound that turns red when in a reducing environment, such as that of metabolically active cells. Once reduced the compound is highly fluorescent with an excitation wavelength (λ) of 560 nm and emission at 590 nm. Following overnight incubation of Jurkat T cells with TI1 and TI6, fluorescence was quantified (**Figure 5.21**). TI1 killed the positive control at a concentration of $\sim 7.8 \mu\text{M}$, whereas at this concentration, TI6 there was an 80% reduction in cell viability suggesting that TI6 it was marginally less cytotoxic. This indicates that use of an amide functional group reduced cell toxicity in addition to increasing potency.

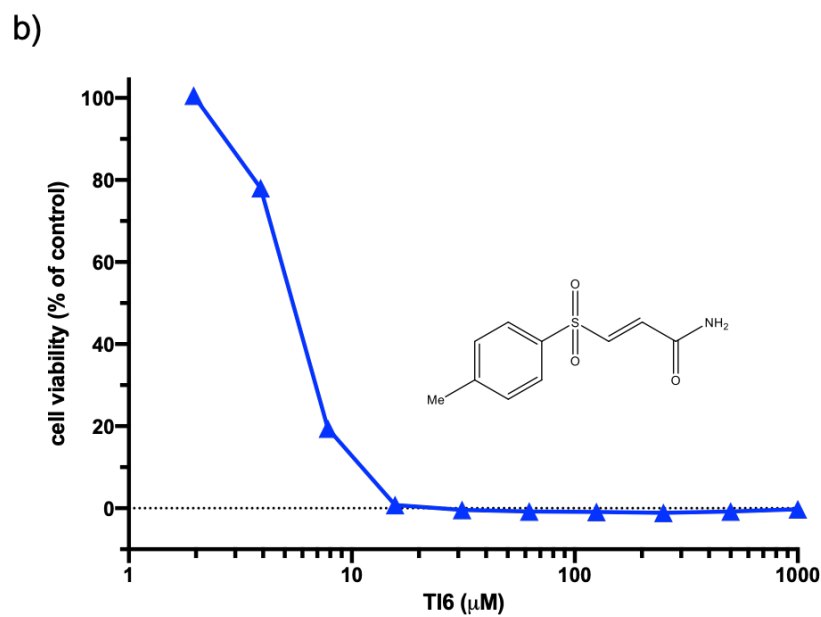
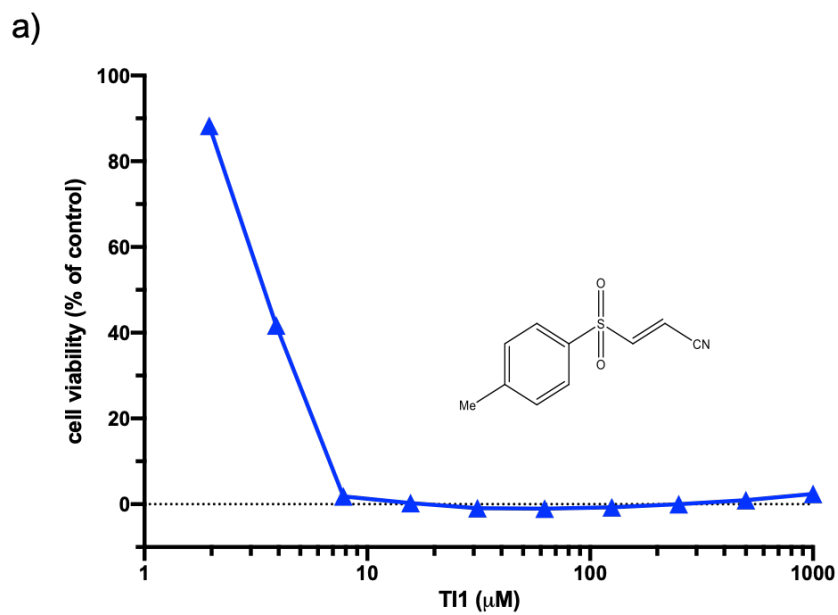


Figure 5.21. Alamar blue cell viability assay with Jurkat T cells. Experiment was carried out in triplicate with four technical repeats. Graph is a typical result showing cell viability of Jurkat T cells following 24 h incubation with TI1 (a) and TI6 (b). Cell viability falls to zero at 7.8 μM of TI1 and 15.6 μM TI6.

5.3. Discussion

In this study TI1, which was discovered as an inhibitor of the Tat system, was selected as a hit compound for SAR analysis - a key process in lead drug compound development (Vasil *et al.*, 2012). To identify the potent pharmacophores (a medicinal chemistry approach), a small library of analogues were synthesised by Alex Truman (University of Nottingham) and their comparative activity was assayed by measuring *pqsA* expression, *antA* expression and PVD production. Ideally, high compound potency would be reached through low nanomolar concentrations.

The current hypothesis for the TI1 mode of action is thought to be covalent reaction of the nitrile group with Cys23 of TatC, as it is known to react with cysteine and there is only one such residue in the TatABC machinery (Massai *et al.*, 2019). However, this cysteine is buried within the protein so it is unclear whether TI1 is able to reach its target. Moreover, TI1 does not inhibit the *E. coli* Tat pathway and it was thought this was due to absence of the uncoupled cysteine residue (Bageshwar *et al.*, 2016; Massai *et al.*, 2019). SAR analysis following inhibition of *pqsA* expression showed that the potency of TI1 can be increased up to 6-fold by replacing the reactive nitrile group with an amide. This demonstrates that TI1 is unlikely to inhibit Tat via covalent modification of a cysteine in TatC.

Of the 30 compounds tested, 5 had an IC₅₀ lower than TI1 for *pqsA* expression inhibition. Mono phenyl ring substitutions did not increase the potency of TI1 analogues, but di- substitution with chlorine and fluorine at positions 3 and 4 of the phenyl ring reduced the IC₅₀ by ~6-fold. Replacement of the nitrile function of TI1 (4-Me-PhSAN) with an amide to give TI6 (4-Me-CONH₂) increased potency with a far more active IC₅₀ of 4.8 µM compared with 27.4 µM for TI1 with respect to the inhibition of *pqsA* expression. However, PVD fluorescence at 40 µM was

higher for 4-Me-CONH₂ than 4-Me-PhSAN, suggesting 4-Me-CONH₂ is a better *pqsA* inhibitor than TI1 but less antagonistic towards PVD production. As such, 4-Me-CONH₂ may target *pqsA* and not the Tat system. All analogues with an amide functional group in place of the nitrile functional group were more active against *pqsA* expression than 4-Me-PhSAN, but not more active against PVD production.

Replacement of the amide functional group with an N,N-dimethylcarboxamide (CONMe₂) functional group converted TI10 (4-F-CONH₂) and TI12 (4-Cl-CONH₂) to TI15 (4-Cl-CONMe₂) and TI16 (4-F-CONMe₂), significantly reducing their activity as inhibitors of *pqsA* expression. To illustrate the point, the IC₅₀ of 4-F-CONH₂ increased from 11.2 μM to 83.5 μM for 4-F-CONMe₂. However, compounds with a CONMe₂ group did not inhibit growth of PAO1-DK and therefore may not be true Tat inhibitors, alternatively they may very weakly inhibit the Tat pathway so that enough Rieske subunit is translocated to maintain growth. Replacement of the nitrile group with ethoxycarbonyl (COOEt) created the least active compound series with regards to *pqsA* inhibition and PVD production. Probably, the ester group withdraws electrons away from the phenyl ring and is larger than CN and CONH₂ which may affect binding to its target.

In general, replacement of the nitrile group with a phenyl ring halogenated at position 4 with either chlorine (C₆H₄-4-Cl) or fluorine (C₆H₄-4-F) increased activity against *pqsA* expression, as seen in **Table 5.3**. Conversely, replacing the nitrile group with C₆H₄-4-CN had very little effect on *pqsA* expression at 20 μM and 40 μM. Compounds with a pyridyl or an acetyl group instead of the nitrile displayed greater increases in inhibitory activity against *pqsA* expression.

One key finding was that inhibition of *pqsA* expression mirrored inhibition of growth. This may be due to Tat inhibition, as a *ΔtatABC* deletion mutant has a growth defect (**Figure 3.19**). To distinguish between growth inhibition due to Tat inhibition and growth inhibition due to inhibition of other essential processes, a PAO1-DK *ΔtatABC* mutant should be grown in a range of concentrations of the TI1

analogue library and OD₆₀₀ measured. If further growth inhibition is seen in addition to the growth defect of a *tat* mutant then the Bay 11-7082 analogue is likely to have other targets within the cell.

TI1 has strong cytotoxic and immunomodulatory effects and it has been suggested that it has multiple targets within eukaryotic cells (Lee *et al.*, 2012; Massai *et al.*, 2019). As only inhibition of *pqsA* expression and *pqs* QS-controlled PVD production by the TI1 analogues was investigated they may have alternative targets to the Tat system such as PqsR, the transcriptional activator for *pqsA*, which would then reduce expression of the PQS biosynthetic operon. TI1 analogues may be competitive inhibitors of the native ligands, PQS and HHQ for the ligand binding site of PqsR.

This should be assessed further by quantifying *pqsA* expression while adding increasing concentrations of exogenous PQS to a culture of PAO1-DK $\Delta pqsA$ miniCTX::*pqsA'-lux* at a fixed concentration of TI1 or a TI1 analogue. If it is a competitive inhibitor of PqsR, then a reduction in *pqsA* inhibition should be seen and the dose-response curve should shift to the right when compared with the dose-response curve in the absence of a TI1 analogue. In addition, *in silico* docking of compounds with the PqsR ligand binding site should give a calculated docking score – this would be useful to predict possible PqsR binding.

Additional secondary assays are essential to determine whether TI1 analogues inhibit the Tat pathway or have alternative targets. As TI1 has been established as an inhibitor of the *P. aeruginosa* Tat system, analogues may also inhibit the same Tat secretion machinery as they are structurally similar. However, due to time restraints only *pqsA* expression, *antA* expression which has a reciprocal relationship with *pqsA*, and PQS-controlled PVD production was investigated during this PhD (Vasil *et al.*, 2012). Therefore, it is imperative that screens utilising non-*pqs* QS controlled Tat substrates are carried out to show Tat, not *pqsA*, inhibition by Bay 11-7082 analogues.

The colorimetric assay that follows hydrolysis of the chromogenic PLC substrate *p*-nitrophenylphosphorylcholine (NPPC) is well established as an indirect Tat inhibitor screen in *P. aeruginosa* (**Table 5.1**) and should be used in future screens of TI1 analogues. These analogues could also be screened by measuring growth with choline as the sole carbon and nitrogen source – this is perturbed upon deletion or inhibition of the Tat system, likely due to failed translocation of the choline oxidase (Vasil *et al.*, 2012). Transcriptomic analysis published by Rampioni *et al.* showed that PA2124, haemolytic phospholipase C (PlcH), and non-haemolytic phospholipase C (PlcN) are not under the transcriptional control of *pqs* QS so these assays should help confirm whether or not Tat system is targeted by the TI1 analogues (Rampioni *et al.*, 2010).

Translocation of the Tat substrate does not utilise energy from ATP hydrolysis, instead recruitment of TatA monomers upon substrate binding to TatBC requires membrane potential across the cytoplasmic membrane ($\Delta\psi$) and removal of the PMF causes dissociation of TatA oligomers (Alcock *et al.*, 2013). Inhibition of $\Delta\psi$ by TI1 analogues would indirectly inhibit Tat transport of PVD, PA2124, PlcH and PlcN used in other secondary assays. Therefore, an additional screen could be carried out to rule out $\Delta\psi$ inhibition. BacLight™ Bacterial Membrane Potential Kit (ThermoFisher Scientific) can be used to test PMF, it utilises a green fluorescent dye DiOC₂(3) that accumulates in the cytoplasm of cells with a greater $\Delta\psi$, and self-associates causing a fluorescence shift to red (Maiden and Waters, 2020). This provides a measurable fluorescence-based assay for $\Delta\psi$ inhibition, and could be used in combination with TI1 analogues to eliminate any compounds that indirectly cause Tat inhibition by $\Delta\psi$ inhibition.

This chapter has provided SAR data for TI1 analogues and shown that the mode of action of TI1 is unlikely to be through covalent reaction with Cys23 of TatC, as previously thought. Further screens are needed to ascertain direct Tat inhibition by the TI1 analogues, and mode-of-action.

Chapter 6: Conclusions and Outlook

Antimicrobial resistance (AMR) is a rapidly accelerating global threat and MDR, XDR and PDR hospital-acquired infections are on the rise. AMR reduces the efficacy of clinical treatment, resulting in longer hospital stays, reduced quality of life and increased mortality. Resistance arises through evolution under a selective pressure and has far-reaching consequences - AMR is estimated to cause 10 million deaths by 2050 across the globe (O'Neill, 2016). *P. aeruginosa* is one of the global leading causes of antibiotic-resistant nosocomial infections. Development of novel bactericidal and bacteriostatic antibiotics has slowed in recent years, in contrast to antibiotic resistance which is rapidly rising. The latest new class of antibiotics was discovered in the 1980s, nearly thirty years ago (World Health Organisation, 2014). There is a strong need for novel therapeutic strategies that do not have the severe consequences brought about by resistance.

Targeting virulence is a promising alternative to conventional antibiotic therapy, selective pressure is weaker than common bactericidal/bacteriostatic antibiotics. Antivirulence drugs could be used in conjunction with common antibiotics to resensitise bacteria (Rezzoagli *et al.*, 2020). *pqs* QS plays an important role in *P. aeruginosa* pathogenicity as it co-ordinates release of many virulence determinants and the formation of biofilm at a population level, thereby making it an excellent target for novel antivirulence drugs. The Tat protein export pathway has recently been a target for novel antivirulence drug development in *E. coli* and *P. aeruginosa* due to its importance in pathogenicity, *tat* mutants exhibit slower growth and reduced virulence.

Tat system mutants of *P. aeruginosa* exhibited decreased eDNA release, rhamnolipid, and microvesicle production and would not respond to exogenous PQS (Soh *et al.*, 2021). Further investigation revealed that PQS-dependent quorum sensing was perturbed in *tat* mutants and this was mediated through down-regulated *pqsA* expression. Perturbation of *pqs* QS was linked to failed export of one of the substrates of the Tat system, PetA. A deletion mutant of *petA* displayed

reduced PQS biosynthesis and induced *antA* expression, both of which are seen in a *tat* mutant.

PetA is one of three subunits of the cytochrome *bc₁* complex, and harbours a 2Fe-2S "Rieske" cluster that transfers electrons from cyt *b* to cyt *c₁* (Xia *et al.*, 2013). *petA* mutants in *P. aeruginosa* displayed impeded growth and insensitivity to inhibitors of the cyt *bc₁* complex such as HQNO, which has been implicated in a mechanism for self-poisoning and eDNA release (Hazan *et al.*, 2016). Similar defects in PQS signalling are seen in *cytB* and *cytC₁* mutants (Soh *et al.*, 2021). LC-MS/MS semi-quantification of HQNO revealed lower production in *tat* mutants, therefore it is likely that reduced eDNA release is due to a missing or severely reduced mechanism for autolysis within the population.

In Chapter 3 the impact of Tat deletion upon the transcriptome was explored. RNAseq data showed the greatest upregulation was within genes involved in aromatic amino acid catabolism – in particular, *antABC* and *catBCA*, the first operons in the anthranilate degradation pathway. Anthranilate is degraded and fed into the TCA cycle for energy production. Therefore, perhaps anthranilate within the cell is diverted from PQS biosynthesis (thus secondary metabolite and virulence factor production) and towards primary metabolism in a *petA*-deficient strain in order to conserve energy. Key findings are outlined in **Figure 6.1**.

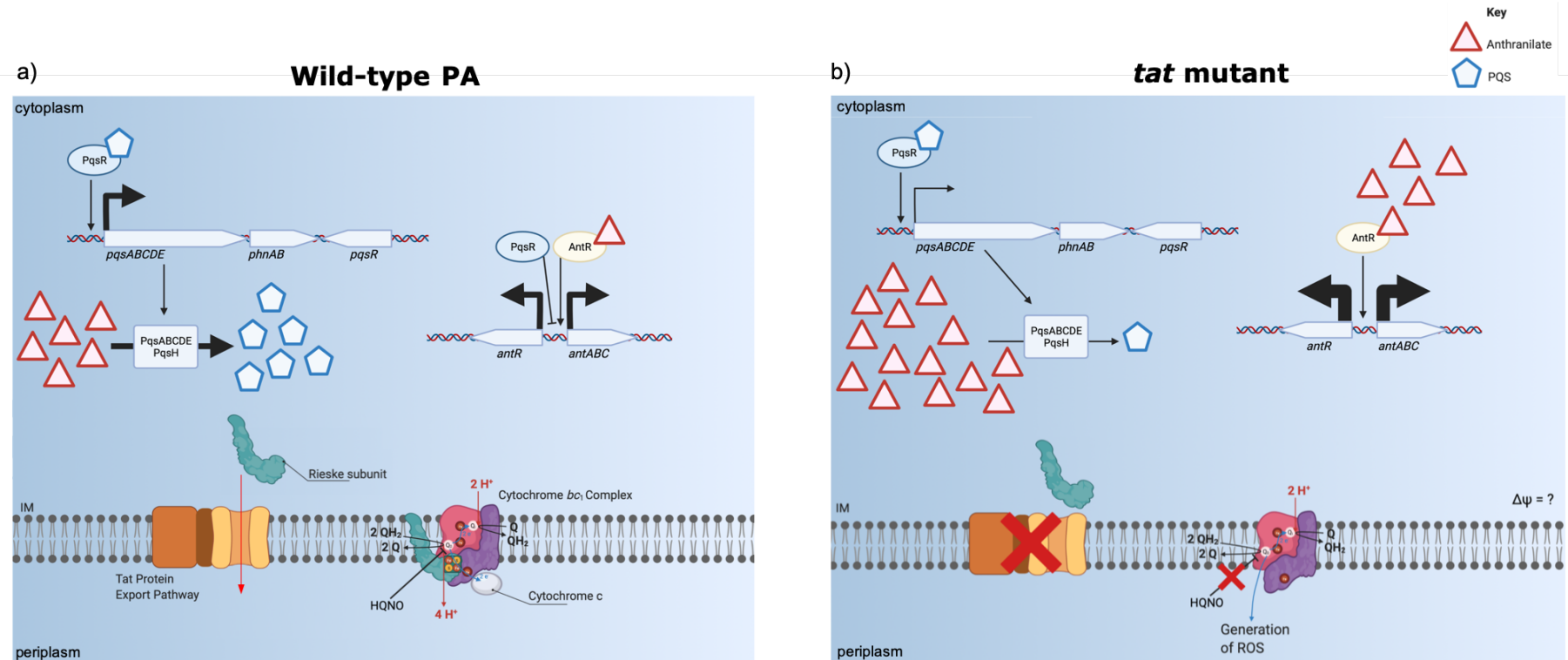


Figure 6.1. Schematic diagram showing key changes within a *tat* mutant (b) compared with wild-type *P. aeruginosa* (a) uncovered during this PhD. It is still unclear what mechanistic link connects failure to export the PetA subunit with PqsR-controlled *pqsA* expression, however it was shown that upon *tat* mutation *pqsA* expression was severely down-regulated and unable to respond to exogenous PQS (Soh *et al.*, 2021). Likely in response to rising anthranilate concentration, AntR-mediated upregulation of *antABC* and *catBCA* occurred, thus anthranilate was used for energy production via the TCA cycle and not *pqs* QS-controlled expression of genes involved in secondary metabolite production such as phenazine biosynthesis. ROS generation occurs in *petA* mutants and membrane potential ($\Delta\psi$) may be reduced as a result of an interrupted electron transport chain (Hazan *et al.*, 2016). Other virulence factors such as phospholipases, and effectors involved in motility, biofilm formation, iron acquisition, response to osmotic stress and anaerobic respiration and are no longer exported upon deletion of the *tat* system and this may also have wide-reaching effects on the cell.

The *antA* gene is regulated by *rhl* and *pqs* quorum sensing systems, as well as at a post-transcriptional level by the small regulatory RNAs PrrF1 and PrrF2 which are involved in iron homeostasis (**Figure 3.37**). MpaR, a GntR-family regulator that modulates carbon metabolism, and *rhl* QS, indirectly controls *antA* expression through PqsR (Wang *et al.*, 2020). Further studies should investigate the apparent restored growth phenotype in a $\Delta tatABC \Delta antA$ double mutant, as this would suggest that growth is reduced when *antA* is overexpressed in a Tat mutant. In addition, the regulation of *antA* and *pqsA* needs investigation and site-directed mutagenesis of upstream regions, or deletions of global regulators, may help determine which regulators are driving the change in expression seen in a *tat* and *petA* mutant. This should highlight which regulators are causing perturbed PQS biosynthesis and suggest another level of control between carbon metabolism for energy production and quorum sensing. It would be interesting to see if the TCA cycle components and their substrates have altered levels upon *tat* mutation, RNAseq data showed that TCA cycle enzymes were not expressed differently so it is likely that the components are able to cope with any increased substrate.

Autoinducers PQS and HHQ may be unable to access PqsR in a *tat* mutant and therefore unable to up-regulate *pqsA* expression. The bacterial membrane in *E. coli* is altered upon mutation of *tat* due to failed export of the N-acetylmuramoyl-L-alanine amidases AmiA and AmiC, this causes chains of cells to form as well as generates sensitivity to SDS (Gimenez *et al.*, 2018). While neither of these phenotypes occur in *P. aeruginosa* *tat* mutants, there may be a subtler effect upon the membrane due to failed export of its substrates that prevents proper distribution of PQS within the cell envelope. PQS intercalates with the outer membrane to create OMVs which are important in trafficking of said QS signal molecules (Florez *et al.*, 2017). To investigate if PQS localisation requires a functional the Tat system, PQS distribution across the inner and outer membrane leaflets should be determined in PAO1-DK, PA14, and their respective *tat* mutants.

The *petA* mutants could also be investigated. Firstly, the inner and outer membrane of *P. aeruginosa* should be separated by ultracentrifugation in a sucrose density gradient, as described recently (Florez et al., 2017). PQS should be extracted from samples taken across the gradient using acidified ethyl acetate and quantified using high resolution LC-MS/MS. A difference in PQS distribution between the outer and inner membranes of wild-type and *tat* mutants will highlight if there is a change to cell membrane distribution that might account for the loss of PQS autoinduction as a result of the *tat* mutation.

Microcolonies of Tat mutants grown in a flow cell had increased sensitivity to tobramycin, thought to be due to the inability to form thick, eDNA-rich, mature biofilms (Soh et al., 2021). This highlights the Tat system again as a promising target for novel inhibitors, as biofilms are implicated in long-term chronic AMR infections (Moses et al., 2000; Hall and Mah, 2017). In theory, administration of a Tat inhibitor as an antibiofilm drug may resensitize chronic infections to common antibiotics, thus reducing morbidity and mortality in those with long-term infections such as CF patients.

Notable examples of antibiofilm compounds in recent research include ajoene, which can be extracted from garlic and is a potent QS inhibitor (Martin et al., 2021). Ajoene prevented rhamnolipid production, one of the most important virulence factors required for maintenance of biofilms, and in a mouse pulmonary infection model challenged with a clinical *P. aeruginosa* isolate ajoene increased bacterial clearance compared to the untreated placebo group (Jakobsen et al., 2012). Furanones are able to inhibit QS and reduce biofilm formation, they were also shown to increase bacterial clearance in a murine pulmonary infection model (Wu et al., 2004). Recently, both gallium and furanone C-30 were shown to act as adjuvants by increasing the sensitivity of *P. aeruginosa* to colistin, ciprofloxacin, meropenem and tobramycin (Rezzoagli et al., 2020; Martin et al., 2021).

Abolishing virulence and slowing, but not arresting, growth are key aims when searching for alternative strategies to combat AMR crisis. The *P. aeruginosa* Tat system inhibitor Bay11-7082 was discovered in one high-throughput screen, but was later reported as immunomodulatory and cytotoxic (Vasil *et al.*, 2012; Massai *et al.*, 2019). Nevertheless, structure-activity relationship determination is a beneficial endeavour as it may lead to a more active compound that generates less of an immunogenic response. Indeed, replacement of a nitrile functional group with CONH₂ increases activity of the compound by ~6 fold. Continued SAR testing may provide combinations of functional groups and substituents of the phenyl ring that increase activity further, or decrease the activity significantly, which could be used to inform future decisions on which analogues to synthesise for increased activity.

Based on the available data it is currently unclear whether Bay 11-7082 analogues directly inhibit the Tat system or if they target *pqsA* expression through direct interaction with PqsR, so future screens should be carried out to distinguish between the two. For example, an assay following the colour change of NPPC upon hydrolysis by Tat-exported PLC will show Tat inhibition compared with *pqsA* inhibition, as the generation of a bright yellow colour only occurs upon PLC export, and PLC production is not under the control of *pqs* QS (Rampioni *et al.*, 2010). Further screens to show Tat inhibition could include growth on agar containing the Bay 11-7082 analogue and choline as the sole carbon and nitrogen source, as ChoA is required for this and is Tat-exported. Copper is a cofactor in many enzymes but can be toxic at high concentrations by oxidisation of proteins and generation of ROS, as a result *P. aeruginosa* exports CopA, the copper resistance protein. Copper resistance is a sign of a functional Tat system and therefore can be used as an additional screen to confirm Tat inhibition by Bay 11-7082 analogues. *In silico* docking of TI1-TI30 chemical structures can be carried out using the known structure of PqsR, focusing on the active site, to show likelihood of competitive

inhibition of the PqsR regulator in case the analogues are active against PqsR as well as/instead of the Tat system.

The Tat system is well studied in *E. coli* and many structures have been determined through x-ray crystallography at various stages of the Tat protein export cycle (Alcock *et al.*, 2013; Alcock *et al.*, 2016; Palmer and Stansfeld, 2020). However, no structure has ever been determined for translocation. If the Bay 11-7082 analogues are cytotoxic, they may still be useful biochemical probes for *in vitro* studies and may even help with structure determination. In summary, the Tat system is now an even more important target for development of novel antivirulence adjuvants as it is linked with PQS signalling, which controls biofilm and virulence at a population-wide level. This work aimed to further understand the mechanistic link between Tat system deletion and perturbation of PQS-dependent signalling, and for the first time has shown that this is through failed export of a subunit of cytochrome *bc₁* in the electron transport chain (Soh *et al.*, 2021).

Key Findings

1. 189 up-regulated genes and 166 down-regulated genes upon mutation of *tat*. Greatest upregulation was within aromatic amino acid degradation, namely *antABC* and *catBCA* operons.
2. *antA* and *catB* were induced by exogenous anthranilate, suggesting *tat* mutants have increased intracellular anthranilate concentration due to perturbed *pqs* QS and reduced AQ production.
3. Failed export of the PetA component of Cytochrome *bc₁* is likely the primary cause of *pqsA* and *antA* dysregulation and of the growth defect seen in *tat* mutants.
4. SAR of Bay 11-7082 showed mode-of-action is unlikely to be through covalent reaction of the nitrile group with a cysteine residue in TatC, and compound activity can be increased by replacement of CN with CONH₂.

Reference List

- Aedekerck, S., Diggle, S.P., Song, Z., Høiby, N., Cornelis, P., Williams, P., and Cámara, M. (2005) The MexGHI-OpmD multidrug efflux pump controls growth, antibiotic susceptibility and virulence in *Pseudomonas aeruginosa* via 4-quinolone-dependent cell-to-cell communication. *Microbiology* **151**: 1113–1125.
- Alcock, F., Baker, M.A.B., Greene, N.P., Palmer, T., Wallace, M.I., and Berks, B.C. (2013) Live cell imaging shows reversible assembly of the TatA component of the twin-arginine protein transport system. *Proc Natl Acad Sci* **110**: E3650–E3659
<http://www.pnas.org/cgi/doi/10.1073/pnas.1306738110>.
- Alcock, F., Stansfeld, P.J., Basit, H., Habersetzer, J., Baker, M.A., Palmer, T., *et al.* (2016) Assembling the Tat protein translocase. *Elife* **5**: 1–28.
- Alikhan, N.F., Petty, N.K., Zakour, N.L. Ben, and Beatson, S.A. (2011) BLAST Ring Image Generator (BRIG): Simple prokaryote genome comparisons. *BMC Genomics* **12**.
- Allesen-Holm, M., Barken, K.B., Yang, L., Klausen, M., Webb, J.S., Kjelleberg, S., *et al.* (2006) A characterization of DNA release in *Pseudomonas aeruginosa* cultures and biofilms. *Mol Microbiol* **59**: 1114–1128.
- Arai, H. (2011) Regulation and function of versatile aerobic and anaerobic respiratory metabolism in *Pseudomonas aeruginosa*. *Front Microbiol* **2**: 1–13.
- Ashkenazy, H., Abadi, S., Martz, E., Chay, O., Mayrose, I., Pupko, T., and Ben-Tal, N. (2016) ConSurf 2016: an improved methodology to estimate and visualize evolutionary conservation in macromolecules. *Nucleic Acids Res* **44**: W344–W350.
- Ashkenazy, H., Erez, E., Martz, E., Pupko, T., and Ben-Tal, N. (2010) ConSurf 2010: Calculating evolutionary conservation in sequence and structure of proteins and nucleic acids. *Nucleic Acids Res* **38**: 529–533.
- Azam, M.W., and Khan, A.U. (2019) Updates on the pathogenicity status of *Pseudomonas aeruginosa*. *Drug Discov Today* **24**: 350–359
<https://doi.org/10.1016/j.drudis.2018.07.003>.
- Bageshwar, U.K., VerPlank, L., Baker, D., Dong, W., Hamsanathan, S., Whitaker, N., *et al.* (2016) High throughput screen for *Escherichia coli* twin arginine translocation (Tat) inhibitors. *PLoS One* **11**: 1–25.
- Ball, G., Antelmann, H., Roger, P., Imbert, C., Gimenez, M.R., and Ize, B. (2016) Contribution of the Twin Arginine Translocation system to the exoproteome of *Pseudomonas aeruginosa*. *Sci Rep* **6** <http://dx.doi.org/10.1038/srep27675>.
- Bally, M., Ball, G., Badere, A., and Lazdunski, A. (1991) Protein secretion in *Pseudomonas aeruginosa*: The xcpA gene encodes an integral inner membrane protein homologous to *Klebsiella pneumoniae* secretion function protein PulO. *J Bacteriol* **173**: 479–486.
- Bassetti, M., Vena, A., Croxatto, A., Righi, E., and Guery, B. (2018) How to manage

Pseudomonas aeruginosa infections. *Drugs Context* **7**: 1–18.

Bassler, B.L. (1999) How bacteria talk to each other: Regulation of gene expression by quorum sensing. *Curr Opin Microbiol* **2**: 582–587.

Beebout, C.J., Sominsky, L.A., Eberly, A.R., Horn, G.T. Van, and Hadjifrangiskou, M. (2021) Cytochrome bd promotes *Escherichia coli* biofilm antibiotic tolerance by regulating accumulation of noxious chemicals. *Biofilms and Microbiomes* **7**.

Berks, B.C. (2015) The Twin-Arginine Protein Translocation Pathway. *Annu Rev Biochem* **84**: 843–864 <http://www.annualreviews.org/doi/10.1146/annurev-biochem-060614-034251>.

Bever, R.A., and Iglewski, B.H. (1988) Molecular characterization and nucleotide sequence of the *Pseudomonas aeruginosa* elastase structural gene. *J Bacteriol* **170**: 4309–4314.

Blondeau, J.M. (2004) Fluoroquinolones: Mechanism of action, classification, and development of resistance. *Surv Ophthalmol* **49**: 1–6.

Bogsch, E., Brink, S., and Robinson, C. (1997) Pathway specificity for a Δ pH-dependent precursor thylakoid lumen protein is governed by a “Sec-avoidance” motif in the transfer peptide and a “Sec-incompatible” mature protein. *EMBO J* **16**: 3851–3859.

Bolger, A.M., Lohse, M., and Usadel, B. (2014) Trimmomatic: A flexible trimmer for Illumina sequence data. *Bioinformatics* **30**: 2114–2120.

Brint, J.M., and Ohman, D.E. (1995) Synthesis of multiple exoproducts in *Pseudomonas aeruginosa* is under the control of RhIR-RhII, another set of regulators in strain PAO1 with homology to the autoinducer-responsive LuxR-LuxI family. *J Bacteriol* **177**: 7155–7163.

Buscher, B.A., Conover, G.M., Miller, J.L., Vogel, S.A., Meyers, S.N., Isberg, R.R., and Vogel, J.P. (2005) The DotL protein, a member of the TraG-coupling protein family, is essential for viability of *Legionella pneumophila* strain Lp02. *J Bacteriol* **187**: 2927–2938.

Calfee, M.W., Shelton, J.G., McCubrey, J.A., Pesci, E.C., and Carolina, N. (2005) Solubility and Bioactivity of the *Pseudomonas* Quinolone Signal Are Increased by a *Pseudomonas aeruginosa* -Produced Surfactant. *Infect Immun* **73**: 878–882.

Calvo, B., Bilbao, J.R., Nanclares, G.P. de, Vázquez, J.A., and Castaño, L. (2000) Integration-Proficient *Pseudomonas aeruginosa* Vectors for Isolation of Single-Copy Chromosomal lacZ and lux Gene Fusions *BioTechniques*. *Biotechniques* **29**: 948–94.

Cao, H., Krishnan, G., Goumnerov, B., Tsongalis, J., Tompkins, R., and Rahme, L.G. (2001) A quorum sensing-associated virulence gene of *Pseudomonas aeruginosa* encodes a LysR-like transcription regulator with a unique self-regulatory mechanism. *Proc Natl Acad Sci U S A* **98**: 14613–14618.

Castric, P.A. (1975) Hydrogen cyanide, a secondary metabolite of *Pseudomonas aeruginosa*. *Can J Microbiol* **21**: 613–618.

Cavallari, J.F., Lamers, R.P., Scheurwater, E.M., Matos, A.L., and Burrows, L.L. (2013) Changes to its peptidoglycan-remodeling enzyme repertoire modulate β -lactam resistance in *Pseudomonas aeruginosa*. *Antimicrob Agents Chemother* **57**: 3078–3084.

Celniker, G., Nimrod, G., Ashkenazy, H., Glaser, F., Martz, E., Mayrose, I., *et al.* (2013) ConSurf: Using evolutionary data to raise testable hypotheses about protein function. *Isr J Chem* **53**: 199–206.

Chaudhry, S.B., Veve, M.P., and Wagner, J.L. (2019) Cephalosporins : A Focus on Side Chains and beta-lactam Cross-Reactivity. *Pharmacy* **7**: 1–16.

Cherny, K.E., and Sauer, K. (2019) *Pseudomonas aeruginosa* requires the DNA-specific endonuclease *enda* to degrade extracellular genomic DNA to disperse from the biofilm. *J Bacteriol* **201**: 1–18.

Chevalier, S., Bouffartigues, E., Bodilis, J., Maillot, O., Lesouhaitier, O., Feuilloley, M.G.J., *et al.* (2017) Structure, function and regulation of *Pseudomonas aeruginosa* porins. *FEMS Microbiol Rev* **41**: 698–722.

Chiang, W.C., Nilsson, M., Jensen, P.Ø., Høiby, N., Nielsen, T.E., Givskov, M., and Tolker-Nielsen, T. (2013) Extracellular DNA shields against aminoglycosides in *Pseudomonas aeruginosa* biofilms. *Antimicrob Agents Chemother* **57**: 2352–2361.

Choi, Y., Park, H.-Y., Park, S.J., Kim, S.-K., Ha, C., Lee, J.-H., *et al.* (2011) Growth phase-differential quorum sensing regulation of anthranilate metabolism in *Pseudomonas aeruginosa*. *Mol Cells* **32**: 57–65.

Chuanchuen, R., Karkhoff-Schweizer, R.A.R., and Schweizer, H.P. (2003) High-level triclosan resistance in *Pseudomonas aeruginosa* is solely a result of efflux. *Am J Infect Control* **31**: 124–127.

Chugani, S., and Greenberg, E.P. (2010) LuxR homolog-independent gene regulation by acyl-homoserine lactones in *Pseudomonas aeruginosa*. *Proc Natl Acad Sci* **107**: 10673–10678 <http://www.pnas.org/cgi/doi/10.1073/pnas.1005909107>.

Chugani, S.A., Whiteley, M., Lee, K.M., D'Argenio, D., Manoil, C., and Greenberg, E.P. (2001) QscR, a modulator of quorum-sensing signal synthesis and virulence in *Pseudomonas aeruginosa*. *Proc Natl Acad Sci U S A* **98**: 2752–2757.

Cigana, C., Castandet, J., Sprynski, N., Melessike, M., Beyria, L., Ranucci, S., *et al.* (2021) *Pseudomonas aeruginosa* Elastase Contributes to the Establishment of Chronic Lung Colonization and Modulates the Immune Response in a Murine Model. *Front Microbiol* **11**.

Cigana, C., Ranucci, S., Rossi, A., Fino, I. De, Melessike, M., and Bragonzi, A. (2020) Antibiotic efficacy varies based on the infection model and treatment regimen for *Pseudomonas aeruginosa*. *Eur Respir J* **55** <http://dx.doi.org/10.1183/13993003.02456-2018>.

Coleman, J.P., Hudson, L.L., Mcknight, S.L., Iii, J.M.F., Calfee, M.W., Lindsey, C.A., *et al.* (2008) *Pseudomonas aeruginosa* PqsA Is an Anthranilate-Coenzyme A Ligase. *J Bacteriol* **190**: 1247–1255.

Coleman, S.R., Blimkie, T., Falsafi, T., and Hancock, R.E.W. (2020) Multidrug Adaptive Resistance of *Pseudomonas aeruginosa* Swarming Cells. *Antimicrob Agents Chemother* **64**: e01999-19.

Cornelis, P., and Dingemans, J. (2013) *Pseudomonas aeruginosa* adapts its iron uptake strategies in function of the type of infections. *Front Cell Infect Microbiol* **4**: 1–7.

Costaglioli, P., Barthe, C., Claverol, S., Brözel, V.S., Perrot, M., Crouzet, M., *et al.* (2012) Evidence for the involvement of the anthranilate degradation pathway in *Pseudomonas aeruginosa* biofilm formation. *Microbiologyopen* **1**: 326–339.

Dalbey, R.E., and Wickner, W. (1985) Leader peptidase catalyzes the release of exported proteins from the outer surface of the *Escherichia coli* plasma membrane. *J Biol Chem* **260**: 15925–15931.

Déziel, E., Gopalan, S., Tampakaki, A.P., Lépine, F., Padfield, K.E., Saucier, M., *et al.* (2005) The contribution of MvfR to *Pseudomonas aeruginosa* pathogenesis and quorum sensing circuitry regulation: Multiple quorum sensing-regulated genes are modulated without affecting IasRI, rhIRI or the production of N-acyl-L-homoserine lactones. *Mol Microbiol* **55**: 998–1014.

Déziel, E., Lépine, F., Milot, S., He, J., Mindrinos, M.N., Tompkins, R.G., and Rahme, L.G. (2004) Analysis of *Pseudomonas aeruginosa* 4-hydroxy-2-alkylquinolines (HAQs) reveals a role for 4-hydroxy-2-heptylquinoline in cell-to-cell communication. *Proc Natl Acad Sci U S A* **101**: 1339–1344.

Diggle, S.P., Matthijs, S., Wright, V.J., Fletcher, M.P., Chhabra, S.R., Lamont, I.L., *et al.* (2007) The *Pseudomonas aeruginosa* 4-Quinolone Signal Molecules HHQ and PQS Play Multifunctional Roles in Quorum Sensing and Iron Entrapment. *Chem Biol* **14**: 87–96.

Diggle, S.P., Stacey, R.E., Dodd, C., Cámara, M., Williams, P., and Winzer, K. (2006) The galactophilic lectin, LecA, contributes to biofilm development in *Pseudomonas aeruginosa*. *Environ Microbiol* **8**: 1095–1104.

Diggle, S.P., Winzer, K., Chhabra, S.R., Worrall, K.E., Cámara, M., and Williams, P. (2003) The *Pseudomonas aeruginosa* quinolone signal molecule overcomes the cell density-dependency of the quorum sensing hierarchy, regulates rhl-dependent genes at the onset of stationary phase and can be produced in the absence of LasR. *Mol Microbiol* **50**: 29–43.

Djapgne, L., Panja, S., Brewer, L.K., Gans, J.H., Kane, M.A., and Woodson, S.A. (2018) The *Pseudomonas aeruginosa* PrrF1 and PrrF2 Small Regulatory RNAs Promote 2-Alkyl-4-Quinolone Production through Redundant Regulation of the antR mRNA. *J Bacteriol* **200**: e00704-17.

Doi, Y., and Arakawa, Y. (2007) 16S ribosomal RNA methylation: Emerging resistance mechanism against aminoglycosides. *Clin Infect Dis* **45**: 88–94.

Dolan, S.K., Kohlstedt, M., Trigg, S., Ramirez, P.V., Wittmann, C., Kaminski, C.F., and Welch, M. (2019) Contextual flexibility in *Pseudomonas aeruginosa* central carbon metabolism during growth in single carbon sources. *bioRxiv* 1–20.

- Dubern, J.F., and Diggle, S.P. (2008) Quorum sensing by 2-alkyl-4-quinolones in *Pseudomonas aeruginosa* and other bacterial species. *Mol Biosyst* **4**: 882–888.
- Essar, D.W., Eberly, L., Hadero, A., and Crawford, I.P. (1990) Identification and characterization of genes for a second anthranilate synthase in *Pseudomonas aeruginosa*: Interchangeability of the two anthranilate synthase and evolutionary implications. *J Bacteriol* **172**: 884–900.
- Essar, D.W., Eberly, L., Han, C.Y., and Crawford, I.P. (1990) DNA sequences and characterization of four early genes of the tryptophan pathway in *Pseudomonas aeruginosa*. *J Bacteriol* **172**: 853–866.
- Farrow, J.M., and Pesci, E.C. (2007a) Two distinct pathways supply anthranilate as a precursor of the *Pseudomonas* quinolone signal. *J Bacteriol* **189**: 3425–3433.
- Farrow, J.M., and Pesci, E.C. (2007b) Two distinct pathways supply anthranilate as a precursor of the *Pseudomonas* quinolone signal. *J Bacteriol* **189**: 3425–3433.
- Fernández, L., Jenssen, H., Bains, M., Wiegand, I., Gooderham, W.J., and Hancock, R.E.W. (2012) The two-component system CprRS senses cationic peptides and triggers adaptive resistance in *Pseudomonas aeruginosa* independently of ParRS. *Antimicrob Agents Chemother* **56**: 6212–6222.
- Ferraro, D.J., Gakhar, L., and Ramaswamy, S. (2005) Rieseke business: Structure-function of Rieseke non-heme oxygenases. *Biochem Biophys Res Commun* **338**: 175–190.
- Filloux, A. (2004) The underlying mechanisms of type II protein secretion. *Biochim Biophys Acta - Mol Cell Res* **1694**: 163–179.
- Filloux, A. (2011) Protein secretion systems in *Pseudomonas aeruginosa*: An essay on diversity, evolution, and function. *Front Microbiol* **2**: 1–21.
- Fleming, A. (1945) Nobel Lecture: Penicillin. *Nobel Lect Physiol or Med 1942-1962* 83–93.
- Flemming, H., and Wingender, J. (2010) The biofilm matrix. *Nat Rev Microbiol* **8**: 623–33 <http://dx.doi.org/10.1038/nrmicro2415> <http://www.ncbi.nlm.nih.gov/pubmed/20676145>.
- Fletcher, M.P., Diggle, S.P., Crusz, S.A., Chhabra, S.R., Cámara, M., and Williams, P. (2007) A dual biosensor for 2-alkyl-4-quinolone quorum-sensing signal molecules. *Environ Microbiol* **9**: 2683–2693.
- Florez, C., Raab, J.E., Cooke, A.C., and Schertzer, J.W. (2017) Membrane Distribution of the *Pseudomonas* Quinolone Signal Modulates Outer Membrane Vesicle Production in *Pseudomonas aeruginosa*. *MBio* **8**: e01034-17.
- Frère, J.M. (1977) Mechanism of action of β -lactam antibiotics at the molecular level. *Biochem Pharmacol* **26**: 2203–2210.

- Fuqua, W.C., Winans, S.C., and Greenberg, E.P. (1994) Quorum sensing in bacteria: The LuxR-LuxI family of cell density- responsive transcriptional regulators. *J Bacteriol* **176**: 269–275.
- Fux, C.A., Costerton, J.W., Stewart, P.S., and Stoodley, P. (2005) Survival strategies of infectious biofilms. *Trends Microbiol* **13**: 34–40.
- Gallagher, L.A., and Manoil, C. (2001) *Pseudomonas aeruginosa* PAO1 Kills *Caenorhabditis elegans* by Cyanide Poisoning. *J Bacteriol* **183**: 6207–6214.
- Gallagher, L.A., McKnight, S.L., Kuznetsova, M.S., Pesci, E.C., and Manoil, C. (2002) Functions required for extracellular quinolone signaling by *Pseudomonas aeruginosa*. *J Bacteriol* **184**: 6472–6480.
- Galloway, D.R. (1991) *Pseudomonas aeruginosa* elastase and elastolysis revisited: recent developments. *Mol Microbiol* **5**: 2315–2321.
- Gambello, M.J., and Iglewski, B.H. (1991) Cloning and characterization of the *Pseudomonas aeruginosa* lasR gene, a transcriptional activator of elastase expression. *J Bacteriol* **173**: 3000–3009.
- Ganne, G., Brillet, K., Basta, B., Roche, B., Hoegy, F., Gasser, V., and Schalk, I.J. (2017) Iron Release from the Siderophore Pyoverdine in *Pseudomonas aeruginosa* Involves Three New Actors: FpvC, FpvG, and FpvH. *ACS Chem Biol* **12**: 1056–1065.
- Gimenez, M.R., Chandra, G., Overvelt, P. Van, Voulhoux, R., Bleves, S., and Ize, B. (2018) Genome wide identification and experimental validation of *Pseudomonas aeruginosa* Tat substrates. *Sci Rep* **8**: 1–18.
- Goli, H.R., Nahaei, M.R., Rezaee, M.A., Hasani, A., Samadi Kafil, H., Aghazadeh, M., and Sheikhalizadeh, V. (2016) Contribution of mexAB-oprM and mexXY (-oprA) efflux operons in antibiotic resistance of clinical *Pseudomonas aeruginosa* isolates in Tabriz, Iran. *Infect Genet Evol* **45**: 75–82.
- Govan, J.R.W., and Deretic, V. (1996) Microbial pathogenesis in cystic fibrosis: Mucoid *Pseudomonas aeruginosa* and *Burkholderia cepacia*. *Microbiol Rev* **60**: 539–574.
- Guragain, M., Lenaburg, D., Moore, F., Reutlinger, I., and Patrauchan, M. (2013) Calcium homeostasis in *Pseudomonas aeruginosa* requires multiple transporters and modulates swarming motility. *Cell Calcium* **54**: 350–361
<https://www.ncbi.nlm.nih.gov/pmc/articles/PMC4874515/pdf/nihms759814.pdf>.
- Hall, C.W., and Mah, T.-F. (2017) Molecular mechanisms of biofilm-based antibiotic resistance and tolerance in pathogenic bacteria. *FEMS Microbiol Rev* **41**: 276–301
<https://academic.oup.com/femsre/article-lookup/doi/10.1093/femsre/fux010>.
- Hammond, J.H., Dolben, E.F., Smith, T.J., Bhujju, S., and Hogan, D.A. (2015) Links between Anr and quorum sensing in *Pseudomonas aeruginosa* biofilms. *J Bacteriol* **197**: 2810–2820.

- Hamsanathan, S., Anthonyimuthu, T.S., Bageshwar, U.K., and Musser, S.M. (2017) A Hinged Signal Peptide Hairpin Enables Tat-Dependent Protein Translocation. *Biophys J* **113**: 2650–2668 <https://doi.org/10.1016/j.bpj.2017.09.036>.
- Hannauer, M., Schäfer, M., Hoegy, F., Gizzi, P., Wehrung, P., Mislin, G.L.A., *et al.* (2012) Biosynthesis of the pyoverdine siderophore of *Pseudomonas aeruginosa* involves precursors with a myristic or a myristoleic acid chain. *FEBS Lett* **586**: 96–101.
- Hare, N.J., Scott, N.E., Shin, E.H.H., Connolly, A.M., Larsen, M.R., Palmisano, G., and Cordwell, S.J. (2011) Proteomics of the oxidative stress response induced by hydrogen peroxide and paraquat reveals a novel AhpC-like protein in *Pseudomonas aeruginosa*. *Proteomics* **11**: 3056–3069.
- Hasegawa, N., Arai, H., and Igarashi, Y. (2003) Need for Cytochrome bc 1 Complex for Dissimilatory Nitrite Reduction of *Pseudomonas aeruginosa*. *Biosci Biotechnol Biochem* **67**: 121–126.
- Hassan, H.M., and Fridovich, I. (1980) Mechanism of the Antibiotic Action of Pyocyanine. *J Bacteriol* **141**: 156–163.
- Hauser, A.R. (2009) The type III secretion system of *Pseudomonas aeruginosa*: Infection by injection. *Nat Rev Microbiol* **7**: 654–665.
- Haussler, S., and Becker, T. (2008) The *Pseudomonas* Quinolone Signal (PQS) Balances Life and Death in *Pseudomonas aeruginosa* Populations. *PLoS Pathog* **4**.
- Hazan, R., Que, Y.A., Maura, D., Strobel, B., Majcherczyk, P.A., Hopper, L.R., *et al.* (2016) Auto Poisoning of the Respiratory Chain by a Quorum-Sensing-Regulated Molecule Favors Biofilm Formation and Antibiotic Tolerance. *Curr Biol* **26**: 195–206.
- He, J., Baldini, R.L., Déziel, E., Saucier, M., Zhang, Q., Liberati, N.T., *et al.* (2004) The broad host range pathogen *Pseudomonas aeruginosa* strain PA14 carries two pathogenicity islands harboring plant and animal virulence genes. *Proc Natl Acad Sci U S A* **101**: 2530–2535.
- Hengzhuang, W., Wu, H., Ciofu, O., Song, Z., and Høiby, N. (2011) Pharmacokinetics/pharmacodynamics of colistin and imipenem on mucoid and nonmucoid *Pseudomonas aeruginosa* biofilms. *Antimicrob Agents Chemother* **55**: 4469–4474.
- Henry, R.L., Mellis, C.M., and Petrovic, L. (1992) Mucoid *Pseudomonas aeruginosa* is a marker of poor survival in cystic fibrosis. *Pediatr Pulmonol* **12**: 158–161.
- Hentzer, M., Teitzel, G.M., Balzer, G.J., Heydorn, A., Molin, S., Givskov, M., and Parsek, M.R. (2001) Alginate overproduction affects *pseudomonas aeruginosa* biofilm structure and function. *J Bacteriol* **183**: 5395–5401.
- Heydorn, A., Nielsen, A.T., Hentzer, M., Sternberg, C., Givskov, M., Ersboll, B.K., and Molin, S. (2000) Quantification of biofilm structures by the novel computer program COMSTAT. *Microbiology* **146**: 2395–2407.

- Higgins, S., Heeb, S., Rampioni, G., Fletcher, M.P., Williams, P., and Cámara, M. (2018) Differential regulation of the phenazine biosynthetic operons by quorum sensing in *Pseudomonas aeruginosa* PAO1-N. *Front Cell Infect Microbiol* **8**: 1–13.
- Hocquet, D., Vogne, C., Garch, F. El, Vejux, A., Gotoh, N., Lee, A., *et al.* (2003) MexXy-OprM efflux pump is necessary for adaptive resistance of *Pseudomonas aeruginosa* to aminoglycosides. *Antimicrob Agents Chemother* **47**: 1371–1375.
- Hook, A.L., Flewellen, J.L., Dubern, J.-F., Carabelli, A.M., Zaid, I.M., Berry, R.M., *et al.* (2019) Simultaneous Tracking of *Pseudomonas aeruginosa* Motility in Liquid and at the Solid-Liquid Interface Reveals Differential Roles for the Flagellar Stators. *mSystems* **4**.
- Huang, H., Shao, X., Xie, Y., Wang, T., Zhang, Y., Wang, X., and Deng, X. (2019) An integrated genomic regulatory network of virulence-related transcriptional factors in *Pseudomonas aeruginosa*. *Nat Commun* **10**: 1–13 <http://dx.doi.org/10.1038/s41467-019-10778-w>.
- Jaeger, K.E., and Reetz, M.T. (1998) Microbial lipases form versatile tools for biotechnology. *Trends Biotechnol* **16**: 396–403.
- Jakobsen, T.H., Gennip, M. Van, Phipps, R.K., Shanmugham, M.S., Christensen, L.D., Alhede, M., *et al.* (2012) Ajoene, a sulfur-rich molecule from garlic, inhibits genes controlled by quorum sensing. *Antimicrob Agents Chemother* **56**: 2314–2325.
- Juan, C., Maciá, M.D., Gutiérrez, O., Vidal, C., Pérez, J.L., and Oliver, A. (2005) Molecular mechanisms of β -lactam resistance mediated by AmpC hyperproduction in *Pseudomonas aeruginosa* clinical strains. *Antimicrob Agents Chemother* **49**: 4733–4738.
- Kanehisa, M., Araki, M., Goto, S., Hattori, M., Hirakawa, M., Itoh, M., *et al.* (2008) KEGG for linking genomes to life and the environment. *Nucleic Acids Res* **36**: 480–484.
- Kearns, D.B. (2010) A field guide to bacterial swarming motility. *Nat Rev Microbiol* **8**: 634–644.
- Kerr, K.G., and Snelling, A.M. (2009) *Pseudomonas aeruginosa*: a formidable and ever-present adversary. *J Hosp Infect* **73**: 338–344 <http://dx.doi.org/10.1016/j.jhin.2009.04.020>.
- Kim, S.K., Im, S.J., Yeom, D.H., and Lee, J.H. (2012) AntR-mediated bidirectional activation of *antA* and *antR*, anthranilate degradative genes in *Pseudomonas aeruginosa*. *Gene* **505**: 146–152 <http://dx.doi.org/10.1016/j.gene.2012.05.004>.
- Kim, S.K., and Lee, J.H. (2016) Biofilm dispersion in *Pseudomonas aeruginosa*. *J Microbiol* **54**: 71–85.
- Kim, W., Tengra, F.K., Young, Z., Shong, J., Marchand, N., Chan, H.K., *et al.* (2013) Spaceflight Promotes Biofilm Formation by *Pseudomonas aeruginosa*. *PLoS One* **8**: 1–8.
- Klockgether, J., Munder, A., Neugebauer, J., Davenport, C.F., Stanke, F., Larbig, K.D., *et al.* (2010) Genome diversity of *Pseudomonas aeruginosa* PAO1 laboratory strains. *J*

Bacteriol **192**: 1113–1121.

Köhler, T., Curty, L.K., Barja, F., Delden, C. Van, and Pechère, J.-C. (2000) Swarming of *Pseudomonas aeruginosa* Is Dependent on Cell-to-Cell Signaling and Requires Flagella and Pili. *J Bacteriol* **182**: 5990–5996.

Kotra, L.P., Haddad, J., and Mobashery, S. (2000) Aminoglycosides: Perspectives on mechanisms of action and resistance and strategies to counter resistance. *Antimicrob Agents Chemother* **44**: 3249–3256.

Kühn, M.J., Talà, L., Inclan, Y.F., Patino, R., Pierrat, X., Vos, I., *et al.* (2021) Mechanotaxis directs *Pseudomonas aeruginosa* twitching motility. *Proc Natl Acad Sci U S A* **118**: 1–9.

Kukavica-Ibrulj, I., Bragonzi, A., Paroni, M., Winstanley, C., Sanschagrín, F., O'Toole, G.A., and Levesque, R.C. (2008) In vivo growth of *Pseudomonas aeruginosa* strains PAO1 and PA14 and the hypervirulent strain LESB58 in a rat model of chronic lung infection. *J Bacteriol* **190**: 2804–2813.

Kumar, C.G., and Anand, S.K. (2006) Significance of microbial biofilms in food industry: a review. *Int J Microgr Opt Technol* **24**: 4–5.

Langendonk, R.F., Neill, D.R., and Fothergill, J.L. (2021) The Building Blocks of Antimicrobial Resistance in *Pseudomonas aeruginosa*: Implications for Current Resistance-Breaking Therapies. *Front Cell Infect Microbiol* **11**: 1–22.

Langton Hewer, S.C., and Smyth, A.R. (2017) Antibiotic strategies for eradicating *Pseudomonas aeruginosa* in people with cystic fibrosis. *Cochrane Database Syst Rev* <https://doi.wiley.com/10.1002/14651858.CD004197.pub5>. Accessed September 7, 2021.

Larkin, M.A., Blackshields, G., Brown, N.P., Chenna, R., Mcgettigan, P.A., McWilliam, H., *et al.* (2007) Clustal W and Clustal X version 2.0. *Bioinformatics* **23**: 2947–2948.

Latifi, A., Winson, M.K., Foglino, M., Bycroft, B.W., Stewart, G.S.A.B., Lazdunski, A., and Williams, P. (1995) Multiple homologues of LuxR and LuxI control expression of virulence determinants and secondary metabolites through quorum sensing in *Pseudomonas aeruginosa* PAO1. *Mol Microbiol* **17**: 333–343.

Lee, C.K., Vachier, J., Anda, J. de, Zhao, K., Baker, A.E., Bennett, R.R., *et al.* (2020) Social Cooperativity of Bacteria during Reversible Surface Attachment in Young Biofilms : a Quantitative Comparison of *Pseudomonas aeruginosa* PA14 and PAO1. *MBio* **11**: e02644-19.

Lee, J., Rhee, M.H., Kim, E., and Cho, J.Y. (2012) BAY 11-7082 is a broad-spectrum inhibitor with anti-inflammatory activity against multiple targets. *Mediators Inflamm* **2012**.

Lee, J., and Zhang, L. (2014) The hierarchy quorum sensing network in *Pseudomonas aeruginosa*. *Protein Cell* **6**: 26–41.

Lee, J.K., Lee, Y.S., Park, Y.K., and Kim, B.S. (2005) Alterations in the GyrA and GyrB subunits of topoisomerase II and the ParC and ParE subunits of topoisomerase IV in

ciprofloxacin-resistant clinical isolates of *Pseudomonas aeruginosa*. *Int J Antimicrob Agents* **25**: 290–295.

Lee, P.A., Tullman-Ercek, D., and Georgiou, G. (2006) The Bacterial Twin-Arginine Translocation Pathway. *Annu Rev Microbiol* **60**: 373–395.

Lépine, F., Milot, S., Déziel, E., He, J., and Rahme, L.G. (2004) Electrospray/mass spectrometric identification and analysis of 4-hydroxy-2-alkylquinolines (HAQs) produced by *Pseudomonas aeruginosa*. *J Am Soc Mass Spectrom* **15**: 862–869.

Levy-Booth, D.J., Prescott, C.E., and Grayston, S.J. (2014) Microbial functional genes involved in nitrogen fixation, nitrification and denitrification in forest ecosystems. *Soil Biol Biochem* **75**: 11–25 <http://dx.doi.org/10.1016/j.soilbio.2014.03.021>.

Li, J., Nation, R.L., Milne, R.W., Turnidge, J.D., and Coulthard, K. (2005) Evaluation of colistin as an agent against multi-resistant Gram-negative bacteria. *Int J Antimicrob Agents* **25**: 11–25.

Li, J., Ramezanpour, M., Fong, S.A., Cooksley, C., Murphy, J., Suzuki, M., *et al.* (2019) *Pseudomonas aeruginosa* Exoprotein-Induced Barrier Disruption Correlates With Elastase Activity and Marks Chronic Rhinosinusitis Severity. *Front Cell Infect Microbiol* **9**: 1–9.

Li, X.H., Kim, S.K., and Lee, J.H. (2017) Anti-biofilm effects of anthranilate on a broad range of bacteria. *Sci Rep* **7**: 1–12 <http://dx.doi.org/10.1038/s41598-017-06540-1>.

Liang, P., Fang, X., Hu, Y., Yuan, M., Raba, D.A., Ding, J., *et al.* (2020) The aerobic respiratory chain of *Pseudomonas aeruginosa* cultured in artificial urine media: Role of NQR and terminal oxidases. *PLoS One* **15**: 1–20.

Llamas, M.A., Mooij, M.J., Sparrius, M., Vandenbroucke-Grauls, C.M.J.E., Ratledge, C., and Bitter, W. (2008) Characterization of five novel *Pseudomonas aeruginosa* cell-surface signalling systems. *Mol Microbiol* **67**: 458–472.

Lüke, I., Handford, J.I., Palmer, T., and Sargent, F. (2009) Proteolytic processing of *Escherichia coli* twin-arginine signal peptides by LepB. *Arch Microbiol* **191**: 919–925.

Lundgren, B.R., Bailey, F.J., and Moley, G. (2017) DdaR (PA1196) Regulates Expression of Dimethylarginine Dimethylaminohydrolase for the Metabolism of Methylarginines in. *J Bacteriol* **199**: 1–14.

Luo, Q., Dong, Y., Chen, H., and Gao, H. (2013) Mislocalization of Rieske Protein PetA Predominantly Accounts for the Aerobic Growth Defect of *tat* Mutants in *Shewanella oneidensis*. *PLoS One* **8**.

Maiden, M.M., and Waters, C.M. (2020) Triclosan depletes the membrane potential in *Pseudomonas aeruginosa* biofilms inhibiting aminoglycoside induced adaptive resistance. *PLoS Pathog* **16**: 1–26 <http://dx.doi.org/10.1371/journal.ppat.1008529>.

Martin, I., Waters, V., and Grasemann, H. (2021) Approaches to targeting bacterial biofilms in cystic fibrosis airways. *Int J Mol Sci* **22**: 1–15.

Martínez, L., and Baquero, F. (2002) Interactions among Strategies Associated with Bacterial Infection: Pathogenicity, Epidemicity, and Antibiotic Resistance. *Clin Microbiol Rev* **15**: 647–679.

Massai, F., Saleeb, M., Doruk, T., Elofsson, M., and Forsberg, Å. (2019) Development, Optimization, and Validation of a High Throughput Screening Assay for Identification of Tat and Type II Secretion Inhibitors of *Pseudomonas aeruginosa*. *Front Cell Infect Microbiol* **9**.

Masuda, N., Sakagawa, E., Ohya, S., Gotoh, N., Tsujimoto, H., and Nishino, T. (2000) Substrate specificities of MexAB-OprM, MexCD-OprJ, and MexXY-OprM efflux pumps in *Pseudomonas aeruginosa*. *Antimicrob Agents Chemother* **44**: 3322–3327.

Mathee, K. (2018) Forensic investigation into the origin of *pseudomonas aeruginosa* PA14 – Old but not lost. *J Med Microbiol* **67**: 1019–1021.

Matsukawa, M., and Greenberg, E.P. (2004) Putative exopolysaccharide synthesis genes influence *Pseudomonas aeruginosa* biofilm development. *J Bacteriol* **186**: 4449–4456.

Maura, D., Hazan, R., Kitao, T., Ballok, A.E., and Rahme, L.G. (2016) Evidence for direct control of virulence and defense gene circuits by the *pseudomonas aeruginosa* quorum sensing regulator, MvfR. *Sci Rep* **6**: 1–14 <http://dx.doi.org/10.1038/srep34083>.

Mavrodi, D. V., Bonsall, R.F., Delaney, S.M., Soule, M.J., Phillips, G., and Thomashow, L.S. (2001) Functional analysis of genes for biosynthesis of pyocyanin and phenazine-1-carboxamide from *Pseudomonas aeruginosa* PAO1. *J Bacteriol* **183**: 6454–6465.

Mayer-Hamblett, N., Rosenfeld, M., Gibson, R.L., Ramsey, B.W., Kulasekara, H.D., Retsch-Bogart, G.Z., *et al.* (2014) *Pseudomonas aeruginosa* in vitro phenotypes distinguish cystic fibrosis infection stages and outcomes. *Am J Respir Crit Care Med* **190**: 289–297.

McElroy, K.E., Hui, J.G.K., Woo, J.K.K., Luk, A.W.S., Webb, J.S., Kjelleberg, S., *et al.* (2014) Strain-specific parallel evolution drives short-term diversification during *Pseudomonas aeruginosa* biofilm formation. *Proc Natl Acad Sci U S A* **111**: E1419–27 <http://www.pnas.org/content/111/14/E1419.full>.

McKnight, S.L., Iglewski, B.H., and Pesci, E.C. (2000) The *Pseudomonas* quinolone signal regulates rhl quorum sensing in *Pseudomonas aeruginosa*. *J Bacteriol* **182**: 2702–2708.

Meighen, E.A. (1991) Molecular Biology of Bacterial Bioluminescence. *Microbiol Rev* **55**: 123–142.

Meyers, B.R., Hirschman, S.Z., Strougo, L., and Srulovitch, E. (1980) Comparative study of piperacillin, ticarcillin, and carbenicillin pharmacokinetics. *Antimicrob Agents Chemother* **17**: 608–611.

Michael K. Winson, Simon Swift, Philip J. Hill, Catriona M. Sims, Gottfried Griesmayr, Barrie W. Bycroft, *et al.* (1998) Engineering the luxCDABE genes from *Photobacterium luminescens* to provide a bioluminescent reporter for constitutive and promoter probe plasmids and mini-Tn5 constructs. *FEMS Microbiol Lett* **163**: 193–202.

Michel, G.P.F., Aguzzi, A., Ball, G., Soscia, C., Bleves, S., and Voulhoux, R. (2011) Role of fimV in type II secretion system-dependent protein secretion of pseudomonas aeruginosa on solid medium. *Microbiology* **157**: 1945–1954.

Mikkelsen, H., Sivaneson, M., and Filloux, A. (2011) Key two-component regulatory systems that control biofilm formation in Pseudomonas aeruginosa. *Environ Microbiol* **13**: 1666–1681.

Montaseri, H., and Forbes, P.B.C. (2016) A review of monitoring methods for triclosan and its occurrence in aquatic environments. *TrAC - Trends Anal Chem* **85**: 221–231
<http://dx.doi.org/10.1016/j.trac.2016.09.010>.

Moradali, M.F., Ghods, S., and Rehm, B.H.A. (2017) Pseudomonas aeruginosa Lifestyle: A Paradigm for Adaptation, Survival, and Persistence. *Front Cell Infect Microbiol* **7**
<http://journal.frontiersin.org/article/10.3389/fcimb.2017.00039/full>.

Morris, C.E., Sands, D.C., Vinatzer, B.A., Glaux, C., Guilbaud, C., Buffière, A., et al. (2008) The life history of the plant pathogen Pseudomonas syringae is linked to the water cycle. *ISME J* **2**: 321–334.

Moscoso, J.A., Mikkelsen, H., Heeb, S., Williams, P., and Filloux, A. (2011) The Pseudomonas aeruginosa sensor RetS switches Type III and Type VI secretion via c-di-GMP signalling. *Environ Microbiol* **13**: 3128–3138.

Moses, M., Singh, P.K., Schaefer, A.L., Parsek, M.R., Moninger, T.O., Welsh, M.J., and Greenberg, E.P. (2000) Quorum-sensing signals indicate that cystic fibrosis lungs are infected with bacterial biofilms. *Nature* **407**: 762–764.

Mulcahy, H., Charron-Mazenod, L., and Lewenza, S. (2008) Extracellular DNA chelates cations and induces antibiotic resistance in Pseudomonas aeruginosa biofilms. *PLoS Pathog* **4**.

Mulcahy, H., Charron-Mazenod, L., and Lewenza, S. (2010) Pseudomonas aeruginosa produces an extracellular deoxyribonuclease that is required for utilization of DNA as a nutrient source. *Environ Microbiol* **12**: 1621–1629.

Muthukumarasamy, U., Preusse, M., Kordes, A., Koska, M., Schniederjans, M., Khaledi, A., and Häussler, S. (2020) Single-nucleotide polymorphism-based genetic diversity analysis of clinical Pseudomonas aeruginosa isolates. *Genome Biol Evol* **12**: 396–406.

Niederman, M.S. (2006) Use of broad-spectrum antimicrobials for the treatment of pneumonia in seriously ill patients: Maximizing clinical outcomes and minimizing selection of resistant organisms. *Clin Infect Dis* **42**: 0–9.

Noller, H.F. (1991) Ribosomal RNA and translation. *Annu Rev Biochem* **60**: 191–227.

Normark, B.H., and Normark, S. (2002) Evolution and spread of antibiotic resistance. *J Int Med* **252**: 91–106.

Nunn, D.N., and Lory, S. (1991) Product of the Pseudomonas aeruginosa gene pilD is a

prepilin leader peptidase. *Proc Natl Acad Sci U S A* **88**: 3281–3285.

O'Neill, J. (2016) TACKLING DRUG-RESISTANT INFECTIONS GLOBALLY: FINAL REPORT AND RECOMMENDATIONS. .

O'Toole, G.A., and Kolter, R. (1998) Flagellar and twitching motility are necessary for *Pseudomonas aeruginosa* biofilm development. *Mol Microbiol* **30**: 295–304.

Ochsner, Snyder, A., Vasil, A.I., and Vasil, M.L. (2002) Effects of the twin-arginine translocase on secretion of virulence factors, stress response, and pathogenesis. *Proc Natl Acad Sci U S A* **99**: 8312–8317.

Ochsner, Urs a, Snyder, A., Vasil, A.I., and Vasil, M.L. (2002) Effects of the twin-arginine translocase on secretion of virulence factors, stress response, and pathogenesis. *Proc Natl Acad Sci U S A* **99**: 8312–8317.

Ochsner, U., and Reiser, J. (1995) Autoinducer-mediated regulation of rhamnolipid biosurfactant synthesis in *Pseudomonas aeruginosa*. *J Bacteriol* **92**: 6424–6428.

Oglesby, A.G., Farrow, J.M., Lee, J.H., Tomaras, A.P., Greenberg, E.P., Pesci, E.C., and Vasil, M.L. (2008) The influence of iron on *Pseudomonas aeruginosa* physiology: A regulatory link between iron and quorum sensing. *J Biol Chem* **283**: 15558–15567.

Olsen, I. (2015) Biofilm-specific antibiotic tolerance and resistance. *Eur J Clin Microbiol Infect Dis* **34**: 877–886.

Özen, A.I., and Ussery, D.W. (2012) Defining the *Pseudomonas* Genus: Where Do We Draw the Line with *Azotobacter*? *Microb Ecol* **63**: 239–248.

Palmer, G.C., Jorth, P.A., and Whiteley, M. (2013) The role of two *Pseudomonas aeruginosa* anthranilate synthases in tryptophan and quorum signal production. *Microbiol (United Kingdom)* **159**: 959–969.

Palmer, T., and Berks, B.C. (2012) The twin-arginine translocation (Tat) protein export pathway. *Nat Rev Microbiol* **10**: 483–496
<http://www.nature.com/doi/10.1038/nrmicro2814>.

Palmer, T., and Stansfeld, P.J. (2020) Targeting of proteins to the twin-arginine translocation pathway. *Mol Microbiol* 861–871.

Pang, Z., Raudonis, R., Glick, B.R., Lin, T.J., and Cheng, Z. (2019) Antibiotic resistance in *Pseudomonas aeruginosa*: mechanisms and alternative therapeutic strategies. *Biotechnol Adv* **37**: 177–192 <https://doi.org/10.1016/j.biotechadv.2018.11.013>.

Papp-Wallace, K.M., Endimiani, A., Taracila, M.A., and Bonomo, R.A. (2011) Carbapenems: Past, present, and future. *Antimicrob Agents Chemother* **55**: 4943–4960.

Park, A.J., Murphy, K., Surette, M.D., Bandoro, C., Krieger, J.R., Taylor, P., and Khursigara, C.M. (2015) Tracking the dynamic relationship between cellular systems and

- extracellular subproteomes in *Pseudomonas aeruginosa* biofilms. *J Proteome Res* **14**: 4524–4537.
- Parsek, M.R., Shinabarger, D.L., Rothmel, R.K., and Chakrabarty, A.M. (1992) Roles of CatR and cis,cis-muconate in activation of the catBC operon, which is involved in benzoate degradation in *Pseudomonas putida*. *J Bacteriol* **174**: 7798–7806.
- Pearson, J.P., Gray, K.M., Passador, L., Tucker, K.D., Eberhard, A., Iglewski, B.H., and Greenberg, E.P. (1994) Structure of the autoinducer required for expression of *Pseudomonas aeruginosa* virulence genes. *Proc Natl Acad Sci U S A* **91**: 197–201.
- Pechère, J.C., and Köhler, T. (1999) Patterns and modes of β -lactam resistance in *Pseudomonas aeruginosa*. *Clin Microbiol Infect* **5**: 15–18.
- Pesci, E.C., Milbank, J.B.J., Pearson, J.P., Mcknight, S., Kende, A.S., Greenberg, E.P., and Iglewski, B.H. (1999) Quinolone signaling in the cell-to-cell communication system of *Pseudomonas aeruginosa*. *Proc Natl Acad Sci U S A* **96**: 11229–11234.
- Pessi, G., and Haas, D. (2000) Transcriptional control of the hydrogen cyanide biosynthetic genes hcnABC by the anaerobic regulator ANR and the quorum-sensing regulators LasR and RhIR in *Pseudomonas aeruginosa*. *J Bacteriol* **182**: 6940–6949.
- Rada, B., Ledstrom, K., Damian, S., Dupuy, C., and Leto, T.L. (2008) The *Pseudomonas* toxin pryocyanin inhibits the Dual oxidase-based antimicrobial system as it imposes oxidative stress on airway epithelial cells. *Bone* **181**: 4883–4893.
- Ramasamy, S., Abrol, R., Suloway, C.J.M., and Clemons Jr, W.M. (2013) The glove-like structure of the conserved membrane protein TatC provides insight into signal sequence recognition in twin-arginine translocation. *Structure* **21**: 777–788
<https://www.ncbi.nlm.nih.gov/pmc/articles/PMC3624763/pdf/nihms412728.pdf>.
- Rampioni, G., Falcone, M., Heeb, S., Frangipani, E., Fletcher, M.P., Dubern, J.F., *et al.* (2016) Unravelling the Genome-Wide Contributions of Specific 2-Alkyl-4-Quinolones and PqsE to Quorum Sensing in *Pseudomonas aeruginosa*. *PLoS Pathog* **12**: 1–25.
- Rampioni, G., Pustelny, C., Fletcher, M.P., Wright, V.J., Bruce, M., Rumbaugh, K.P., *et al.* (2010) Transcriptomic analysis reveals a global alkyl-quinolone-independent regulatory role for PqsE in facilitating the environmental adaptation of *Pseudomonas aeruginosa* to plant and animal hosts. *Environ Microbiol* **12**: 1659–1673.
- Recinos, D.A., Sekedat, M.D., Hernandez, A., Cohen, T.S., Sakhtah, H., Prince, A.S., *et al.* (2012) Redundant phenazine operons in *Pseudomonas aeruginosa* exhibit environment-dependent expression and differential roles in pathogenicity. *Proc Natl Acad Sci U S A* **109**: 19420–19425.
- Reimann, C., Beyeler, M., Latifi, A., Winteler, H., Foglino, M., Lazdunski, A., and Haas, D. (1997) The global activator GacA of *Pseudomonas aeruginosa* PAO positively controls the production of the autoinducer N-butryryl-homoserine lactone and the formation of the virulence factors pryocyanin, cyanide, and lipase. *Mol Microbiol* **24**: 309–319.
- Reszka, K.J., O'Malley, Y., McCormick, M.L., Denning, G.M., and Britigan, B.E. (2004)

Oxidation of pyocyanin, a cytotoxic product from *Pseudomonas aeruginosa*, by microperoxidase 11 and hydrogen peroxide. *Free Radic Biol Med* **36**: 1448–1459.

Rezzoagli, C., Archetti, M., Mignot, I., Baumgartner, M., and Kümmerli, R. (2020) Combining antibiotics with antivirulence compounds can have synergistic effects and reverse selection for antibiotic resistance in *Pseudomonas aeruginosa*. *PLoS Biol* **18**: 1–27.

Richmond, M.H. (1978) Factors influencing the antibacterial action of β -lactam antibiotics. *J Antimicrob Chemother* **4**: 1–14.

Rodrigue, A., Quentin, Y., Lazdunski, A., Méjean, V., and Foglino, M. (2000) Two-component systems in *Pseudomonas aeruginosa*: Why so many? *Trends Microbiol* **8**: 498–504.

Rodriguez, F., Rouse, S.L., Tait, C.E., Harmer, J., Riso, A. De, Timmel, C.R., *et al.* (2013) Structural model for the protein-translocating element of the twin-arginine transport system. *Proc Natl Acad Sci U S A* **110**.

Rollauer, S.E., Tarry, M.J., Graham, J.E., Jääskeläinen, M., Jäger, F., Johnson, S., *et al.* (2012) Structure of the TatC core of the twin-arginine protein transport system. *Nature* **492**: 210–214.

Roy, A., Kucukural, A., and Zhang, Y. (2010) I-TASSER: A unified platform for automated protein structure and function prediction. *Nat Protoc* **5**: 725–738.

Ryder, C., Byrd, M., and Wozniak, D.J. (2007) Role of polysaccharides in *Pseudomonas aeruginosa* biofilm development. *Curr Opin Microbiol* **10**: 644–648.

Sadok, I., Gamian, A., and Staniszewska, M.M. (2017) Chromatographic analysis of tryptophan metabolites. *J Sep Sci* **40**: 3020–3045.

Saint-Criq, V., Villeret, B., Bastaert, F., Kheir, S., Hatton, A., Cazes, A., *et al.* (2018) *Pseudomonas aeruginosa* LasB protease impairs innate immunity in mice and humans by targeting a lung epithelial cystic fibrosis transmembrane regulator-IL-6-antimicrobial-repair pathway. *Thorax* **73**: 49–61.

Sargent, F., Stanley, N.R., Berks, B.C., and Palmer, T. (1999) Sec-independent protein translocation in *Escherichia coli*. A distinct and pivotal role for the TatB protein. *J Biol Chem* **274**: 36073–36082 <http://dx.doi.org/10.1074/jbc.274.51.36073>.

Schalk, I.J., and Guillon, L. (2013) Pyoverdine biosynthesis and secretion in *Pseudomonas aeruginosa*: Implications for metal homeostasis. *Environ Microbiol* **15**: 1661–1673.

Schultz, F., Anywar, G., Tang, H., Chassagne, F., Lyles, J.T., Garbe, L.A., and Quave, C.L. (2020) Targeting ESKAPE pathogens with anti-infective medicinal plants from the Greater Mpigi region in Uganda. *Sci Rep* **10**: 1–19 <https://doi.org/10.1038/s41598-020-67572-8>.

Sengupta, S., Chattopadhyay, M.K., and Grossart, H.P. (2013) The multifaceted roles of antibiotics and antibiotic resistance in nature. *Front Microbiol* **4**: 1–13.

- Shen, L., Gao, L., Yang, M., Zhang, J., Wang, Y., Feng, Y., *et al.* (2021) Deletion of the pa4427-pa4431 operon of pseudomonas aeruginosa pao1 increased antibiotics resistance and reduced virulence and pathogenicity by affecting quorum sensing and iron uptake. *Microorganisms* **9**: 1–19.
- Silva Filho, L.V.R.F. Da, Ferreira, F. de A., Reis, F.J.C., Britto, M.C.A. De, Levy, C.E., Clark, O., and Ribeiro, J.D. (2013) Pseudomonas aeruginosa infection in patients with cystic fibrosis: Scientific evidence regarding clinical impact, diagnosis, and treatment. *J Bras Pneumol* **39**: 495–512.
- Simon, R., Priefer, U., and Pühler, A. (1983) A Broad Host Range Mobilization System for In Vivo Genetic Engineering: Transposon Mutagenesis in Gram Negative Bacteria. *Nat Biotechnol* **1**: 784–791.
- Skerker, J.M., and Berg, H.C. (2001) Direct observation of extension and retraction of type IV pili. *Proc Natl Acad Sci U S A* **98**: 6901–6904.
- Soh, E.Y.-C., Smith, F., Gimenez, M.R., Yang, L., Vejborg, R.M., Fletcher, M., *et al.* (2021) Disruption of the Pseudomonas aeruginosa Tat system perturbs PQS-dependent quorum sensing and biofilm maturation through lack of the Rieske cytochrome bc1 sub-unit. *PLOS Pathog* **17**: e1009425.
- Stanley, N.R., Findlay, K., Berks, B.C., Findlay, K.I.M., and Berks, B.E.N.C. (2001) Escherichia coli Strains Blocked in Tat-Dependent Protein Export Exhibit Pleiotropic Defects in the Cell Envelope. *J Bacteriol* **183**: 139–144.
- Stover, C.K., Pham, X.Q., Erwin, A.L., Mizoguchi, S.D., Warrener, P., Hickey, M.J., *et al.* (2000) Complete genome sequence of Pseudomonas aeruginosa PAO1, an opportunistic pathogen. *Nature* **406**: 959–964.
- Sun, E., Gill, E.E., Falsafi, R., Yeung, A., Liu, S., and Hancock, R.E.W. (2018) Broad-spectrum adaptive antibiotic resistance associated with pseudomonas aeruginosa mucin-dependent surfing motility. *Antimicrob Agents Chemother* **62**: 1–12.
- Thompson, J.D., Higgins, D.G., and Gibson, T.J. (1994) CLUSTAL W: Improving the sensitivity of progressive multiple sequence alignment through sequence weighting, position-specific gap penalties and weight matrix choice. *Nucleic Acids Res* **22**: 4673–4680.
- Thöny-Meyer, L. (1997) Biogenesis of respiratory cytochromes in bacteria. *Microbiol Mol Biol Rev* **61**: 337–376.
- Tolker-Nielsen, T. (2015) Biofilm Development. *Microbiol Spectr* **3**: 1–12.
- Trias, J., Dufresne, J., Levesque, R.C., and Nikaido, H. (1989) Decreased outer membrane permeability in imipenem-resistant mutants of Pseudomonas aeruginosa. *Antimicrob Agents Chemother* **33**: 1201–1206.
- Turnbull, L., Toyofuku, M., Hynen, A.L., Kurosawa, M., Pessi, G., Petty, N.K., *et al.* (2016) Explosive cell lysis as a mechanism for the biogenesis of bacterial membrane vesicles and biofilms. *Nat Commun* **7**: 11220

<http://www.nature.com/doi/10.1038/ncomms11220>.

Valentini, M., and Filloux, A. (2016) Biofilms and Cyclic di-GMP (c-di-GMP) signaling: Lessons from *Pseudomonas aeruginosa* and other bacteria. *J Biol Chem* **291**: 12547–12555.

Valentini, M., Storelli, N., and Lapouge, K. (2011) Identification of C 4-dicarboxylate transport systems in *Pseudomonas aeruginosa* PAO1. *J Bacteriol* **193**: 4307–4316.

Vasil, M.L., Tomaras, A.P., and Pritchard, A.E. (2012) Identification and evaluation of twin-arginine translocase inhibitors. *Antimicrob Agents Chemother* **56**: 6223–6234.

Venturi, V. (2006) Regulation of quorum sensing in *Pseudomonas*. *FEMS Microbiol Rev* **30**: 274–291.

Voulhoux, R., Ball, G., Ize, B., Vasil, M.L., Lazdunski, A., Wu, L.-F., and Filloux, A. (2001) Involvement of the twin-arginine translocation system in protein secretion via the type II pathway. *EMBO J* **20**: 6735–6741.

Wade, D.S., Calfee, M.W., Rocha, E.R., Ling, a, Engstrom, E., Coleman, J.P., *et al.* (2005) Regulation of *Pseudomonas* quinolone signal synthesis in *Pseudomonas aeruginosa*. *J Bacteriol* **187**: 4372–4380.

Walters III, M.C., Roe, F., Bugnicourt, A., Franklin, M.J., and Stewart, P.S. (2003) Contributions of Antibiotic Penetration, Oxygen Limitation. *Antimicrob Agents Chemother* **47**: 317–323.

Wang, T., Qi, Y., Wang, Z., Zhao, J., Ji, L., Li, J., *et al.* (2020) Coordinated regulation of anthranilate metabolism and bacterial virulence by the GntR family regulator MpaR in *Pseudomonas aeruginosa*. *Mol Microbiol* **114**: 857–869.

Wang, Y., Wilks, J.C., Danhorn, T., Ramos, I., Croal, L., and Newman, D.K. (2011) Phenazine-1-carboxylic acid promotes bacterial biofilm development via ferrous iron acquisition. *J Bacteriol* **193**: 3606–3617.

Williams, P., and Cámara, M. (2009) Quorum sensing and environmental adaptation in *Pseudomonas aeruginosa*: a tale of regulatory networks and multifunctional signal molecules. *Curr Opin Microbiol* **12**: 182–191.

Wilton, R., Ahrendt, A.J., Shinde, S., Sholto-Douglas, D.J., Johnson, J.L., Brennan, M.B., and Kemner, K.M. (2018) A New Suite of Plasmid Vectors for Fluorescence-Based Imaging of Root Colonizing *Pseudomonads*. *Front Plant Sci* **8**: 1–15
<http://journal.frontiersin.org/article/10.3389/fpls.2017.02242/full>.

Winson, M.K., Miguel, C., Latifi, A., Foglino, M., Chhabra, S.R. a M., Daykin, M., *et al.* (1995) Multiple N-acyl-L-homoserine lactone signal molecules regulate production of virulence determinants and secondary metabolites in *Pseudomonas aeruginosa*. *Microbiology* **92**: 9427–9431 <http://www.pnas.org/content/92/20/9427.abstract>.

World Health Organisation (2014) Antimicrobial resistance Global Report on Surveillance. .

- Wu, H., Song, Z., Hentzer, M., Andersen, J.B., Molin, S., Givskov, M., and Høiby, N. (2004) Synthetic furanones inhibit quorum-sensing and enhance bacterial clearance in *Pseudomonas aeruginosa* lung infection in mice. *J Antimicrob Chemother* **53**: 1054–1061.
- Xia, D., Esser, L., Tang, W.-K., Zhou, F., Zhou, Y., Yu, L., and Yu, C.-A. (2013) Structural Analysis of Cytochrome bc₁ Complexes: Implications to the Mechanism of Function. *Biochim Biophys Acta - Bioenerg* **1827**: 1278–1294
<https://www.ncbi.nlm.nih.gov/pmc/articles/PMC3624763/pdf/nihms412728.pdf>.
- Xiao, G., Déziel, E., He, J., Lépine, F., Lesic, B., Castonguay, M.H., *et al.* (2006) MvfR, a key *Pseudomonas aeruginosa* pathogenicity LTTR-class regulatory protein, has dual ligands. *Mol Microbiol* **62**: 1689–1699.
- Xiao, G., He, J., and Rahme, L.G. (2006) Mutation analysis of the *Pseudomonas aeruginosa* mvfR and pqsABCDE gene promoters demonstrates complex quorum-sensing circuitry. *Microbiology* **152**: 1679–1686.
- Yang, J., Yan, R., Roy, A., Xu, D., Poisson, J., and Zhang, Y. (2014) The I-TASSER suite: Protein structure and function prediction. *Nat Methods* **12**: 7–8
<http://dx.doi.org/10.1038/nmeth.3213>.
- Yang, J., and Zhang, Y. (2015) I-TASSER server: New development for protein structure and function predictions. *Nucleic Acids Res* **43**: W174–W181.
- Yang, J., and Zhang, Y. (2016) Protein Structure and Function Using I-TASSER. *Curr Protoc Bioinforma* **52**.
- Yang, L., Barken, K.B., Skindersoe, M.E., Christensen, A.B., Givskov, M., and Tolker-Nielsen, T. (2007) Effects of iron on DNA release and biofilm development by *Pseudomonas aeruginosa*. *Microbiology* **153**: 1318–1328.
- Yuson, C., Kumar, K., Le, A., Ahmadie, A., Banovic, T., Heddle, R., *et al.* (2019) Immediate cephalosporin allergy. *Intern Med J* **49**: 985–993.
- Zhang, Y., Wang, L., Hu, Y., and Jin, C. (2014) Solution structure of the TatB component of the twin-arginine translocation system. *Biochim Biophys Acta - Biomembr* **1838**: 1881–1888
<http://dx.doi.org/10.1016/j.bbamem.2014.03.015>.
- Zwick, F., Lale, R., and Valla, S. (2013) Regulation of the expression level of transcription factor XylS reveals new functional insight into its induction mechanism at the Pm promoter. *BMC Microbiol* **13**.

Appendix

ORF	Gene name	Normalised Expression Values				Fold change
		WT 1	WT 2	Tat 1	Tat 2	
PA0041a		10.25	21.25	37.5	52.5	2.69
PA0044	<i>exoT</i>	1003.75	688.25	3572.5	4296.25	5.01
PA0046		2.75	2.25	8.75	17.25	4.52
PA0154	<i>pcaG</i>	41.25	46.75	86.75	97	2.04
PA0200		475.25	849	1407.75	2510	3.08
PA0226		26.25	18.75	1184.75	1055	51.36
PA0227		16	28.75	879.25	920.5	39.15
PA0228	<i>pcaF</i>	43.25	52.5	1920.25	1647.5	37.34
PA0229	<i>pcaT</i>	65.5	56.25	823.25	609.25	11.77
PA0230	<i>pcaB</i>	85.75	71.5	741.25	506.25	7.87
PA0231	<i>pcaD</i>	50.75	41.75	407.5	301.5	7.73
PA0232	<i>pcaC</i>	70.25	67.75	637	602.5	8.85
PA0233		61.25	50.75	135	101.5	2.07
PA0235	<i>pcaK</i>	10	13.25	64.75	64	5.37
PA0242		21.5	27	49	63.75	2.22
PA0244		14.75	7.5	33.25	24.75	2.56
PA0245	<i>aroQ2</i>	12.25	10	30	29.25	2.55
PA0247	<i>pobA</i>	25.75	22.75	174.5	141.5	6.44
PA0679	<i>hxcP</i>	9.5	8.5	20.75	19.5	2.20
PA0713		127.25	134	368.5	380	2.88
PA0714		33.25	29.75	59.25	73.5	2.06
PA0887	<i>acsA</i>	841.25	850.25	2611	2650.25	3.31
PA0895	<i>aruC</i>	432.5	396.25	1019.5	944	2.45
PA0896	<i>aruF</i>	153	170	412.25	430.25	2.59

PA0897	<i>aruG</i>	146.25	182.25	532	531	3.14
PA0898	<i>aruD</i>	115.25	124.5	496.25	459.25	3.91
PA0899	<i>aruB</i>	355.5	407.5	1045	983	2.71
PA0918		91.75	96.75	276.25	269	2.80
PA1172	<i>napC</i>	312	214.25	905.5	791.5	3.31
PA1173	<i>napB</i>	131.5	93	359.75	327.75	3.05
PA1174	<i>napA</i>	2310.25	1831	4559.75	4741	2.49
PA1183	<i>dctA</i>	24.5	31.5	61.25	57.75	2.04
PA1196	<i>ddaR</i>	126	148.25	334.5	378	2.60
PA1212		55.5	55.75	117.75	124	2.13
PA1214		106	91	185	262.25	2.22
PA1215		102.75	91	192.5	211.75	2.06
PA1216		207	212.25	527.75	556	2.53
PA1218		182.25	188	428.25	490.5	2.45
PA1317	<i>cyoA</i>	72.75	63.75	158	141	2.12
PA1319	<i>cyoC</i>	24.25	36.5	70.75	84.25	2.45
PA1414		4852	5271.25	10089	10334.25	2.35
PA1429		503	483	1384.25	1424	2.90
PA1435		34	45	108	119.25	2.78
PA1546	<i>hemN</i>	2475.75	2355.75	5003.75	5003.75	2.33
PA1551		1812	1592.5	3268.75	3060.75	2.00
PA1557	<i>ccoN2</i>	889	897.75	1897	1753	2.12
PA1604		238.25	223.5	513.75	579.5	2.32
PA1673		484	459.25	1638.75	1525.5	3.42
PA1690	<i>pscU</i>	34.5	22.75	80.5	88.25	2.89
PA1691	<i>pscT</i>	24	16.5	55.75	58.25	2.83
PA1692		12.75	10.5	76.75	67.5	6.03
PA1693	<i>pscR</i>	46.25	46.75	134	199.75	3.55

PA1694	<i>pscQ</i>	98.75	60.25	385.25	342.25	4.65
PA1695	<i>pscP</i>	131	68.75	436.25	315	3.76
PA1696	<i>pscO</i>	25.75	13.25	75	79.25	4.06
PA1697		149.75	104	413.5	419.25	3.30
PA1698	<i>popN</i>	126.25	65.75	249	294.25	2.81
PA1699	<i>pcr1</i>	45.5	27.25	93.25	132.5	3.05
PA1700	<i>pcr2</i>	23.75	7.5	35.5	42.75	2.55
PA1701	<i>pcr3</i>	25	17.25	78.75	75.5	3.63
PA1702	<i>pcr4</i>	5.75	4.25	14.75	16.5	3.19
PA1703	<i>pcrD</i>	219.75	170.5	506.25	488.25	2.53
PA1705	<i>pcrG</i>	58.5	39.75	252	296	5.56
PA1706	<i>pcrV</i>	632.5	435.75	2114.25	2267.5	4.28
PA1707	<i>pcrH</i>	215.25	201.5	949.75	1401.5	5.74
PA1708	<i>popB</i>	1369.2 5	935	5566.75	6533	5.67
PA1709	<i>popD</i>	785	493	3361.5	3840.75	6.11
PA1710	<i>exsC</i>	732	589.75	1685.75	1993.5	2.89
PA1711	<i>exsE</i>	127.75	83.75	444.25	376.5	3.89
PA1712	<i>exsB</i>	152.25	108.25	535.25	541	4.07
PA1713	<i>exsA</i>	159.75	173.75	412.25	489.75	2.68
PA1714	<i>exsD</i>	627.5	425.25	1996.75	2175.5	4.09
PA1715	<i>pscB</i>	46.25	26.75	264.25	197.25	6.30
PA1716	<i>pscC</i>	194.25	142.75	606	603.5	3.60
PA1717	<i>pscD</i>	65.5	40	178.25	224.25	3.76
PA1718	<i>pscE</i>	43.25	34.25	157.5	229.75	5.01
PA1719	<i>pscF</i>	42.25	40	252.25	286.5	6.50
PA1720	<i>pscG</i>	16.75	15.5	77.25	88.25	5.07
PA1721	<i>pscH</i>	26.5	18.25	75	97.75	3.89
PA1722	<i>pscI</i>	18.75	19	96.75	108.75	5.37
PA1723	<i>pscJ</i>	22	29.25	101.5	104.5	3.88

PA1724	<i>pscK</i>	6.75	5.5	11.75	20.25	2.66
PA1725	<i>pscl</i>	30.5	19	73.75	66	2.79
PA1789		1307	1256	3556.5	3489.5	2.99
PA2111		20.5	29	79	52.75	2.53
PA2119		616.5	612.75	1367.5	1277.5	2.20
PA2136		10.75	13	25	25.5	2.07
PA2169		68	40.5	116.25	108	2.03
PA2170		6.75	2.75	19	16.5	3.99
PA2171		187.75	194.25	732	656.25	3.64
PA2172		159	158.75	356.25	406.75	2.40
PA2173		54.5	56.75	146.25	110	2.25
PA2173a		16.5	27.25	52.5	39.75	2.02
PA2191	<i>exoY</i>	187.25	112.75	511.75	505.25	3.35
PA2378		778.25	601	1602	1656	2.46
PA2379		186.5	165.5	464.5	395.75	2.44
PA2422		11.75	9.5	27.25	21.75	2.25
PA2445	<i>gcvP2</i>	108	127.25	497.75	520.25	4.27
PA2446	<i>gcvH2</i>	12.25	19.25	50.75	71.25	3.60
PA2490		9.75	13	26	25	2.15
PA2501		102.75	117.25	224.75	247.75	2.07
PA2505	<i>opdT</i>	13.75	15	47.75	44.5	3.06
PA2506		5.75	6.75	97.75	99.5	15.28
PA2507	<i>catA</i>	21.25	16	4495	4341	247.89
PA2508	<i>catC</i>	6.75	5.75	1382.25	1523.75	231.89
PA2509	<i>catB</i>	9.5	10	1274.5	1198	122.95
PA2510	<i>catR</i>	35.75	23.25	180	155.5	5.50
PA2511	<i>antR</i>	141.5	105.25	1544	1564.25	12.79
PA2512	<i>antA</i>	791.5	643.5	45223.5	45223.5	58.99
PA2513	<i>antB</i>	163.25	127.25	7830.5	7231.75	56.85

PA2514	<i>antC</i>	216.5	182.25	8777	9429.25	50.74
PA2515	<i>xyiL</i>	90.75	65.75	4741	4448.5	61.94
PA2516	<i>xyiZ</i>	34.5	20.75	1149.75	1172.5	43.60
PA2517	<i>xyiY</i>	6.75	8.75	237	221	28.67
PA2518	<i>xyiX</i>	33.5	30	385.5	396.25	12.41
PA2519	<i>xyiS</i>	53	40.75	595.75	532.5	12.06
PA2682		107	97.75	1819	1816.5	17.80
PA2683		60.25	62.5	423.25	439.75	6.95
PA2729		26.5	17.5	54.5	43.75	2.27
PA2753		98.75	88	601	610.75	6.41
PA2759		121.25	90	455.75	412.25	4.13
PA2762		89.25	70.5	208	183.25	2.39
PA2867		1019.5	848	2026.75	1692.5	2.07
PA3032	<i>snr1</i>	442.75	460.5	1256	1372.25	2.96
PA3126	<i>ibpA</i>	2130.2 5	2199.25	4102.75	3772	2.02
PA3233		78.75	78	246.75	251	3.04
PA3234		282.75	298.5	666	665	2.31
PA3236	<i>betX</i>	118.25	141.25	296	324.25	2.39
PA3278		89.25	90	180.75	239.75	2.27
PA3305. 1	<i>phrS</i>	9211	11931.7 5	20170	25927.7 5	2.61
PA3309		6110.2 5	5605.75	14938.7 5	14675.5	2.90
PA3337	<i>rfaD</i>	350.25	436	1078.75	1477.25	3.34
PA3432		3.5	6.75	22.75	16.5	3.59
PA3531	<i>bfrB</i>	188.75	144	2225.25	2390.25	14.35
PA3572		709.75	810.5	1967.25	2091.25	2.77
PA3613		1427.5	1250.25	2829.75	2927.25	2.32
PA3840		109.25	91	337.5	368.5	3.55

PA3841	<i>exoS</i>	1713.2 5	1147.75	6533	7515.75	5.62
PA3842	<i>spcS</i>	165.5	93.25	550.5	508.5	4.03
PA3877	<i>narkI</i>	27.5	39.5	105.25	140.25	3.54
PA3928		279.5	348.75	684.75	905.5	2.57
PA3929	<i>cioB</i>	551.75	574	1393.25	1595	2.70
PA3930	<i>cioA</i>	1260.5	1343.25	2876.5	3117.5	2.44
PA4067	<i>oprG</i>	12208. 5	12504.2 5	25927.7 5	23364.7 5	2.49
PA4236	<i>katA</i>	7231.7 5	6110.25	12504.2 5	13408.2 5	2.28
PA4289		103.5	96.5	223.25	210.25	2.12
PA4290		185	222.5	601.25	612	2.89
PA4328		459.5	411.75	914.75	846.25	2.08
PA4366	<i>sodB</i>	7719	6533	14675.5	13002.7 5	2.30
PA4542	<i>clpB</i>	4656.2 5	4852	9779.5	9211	2.26
PA4571		312.5	291.25	841.25	827	2.84
PA4587	<i>ccpR</i>	733.5	648.25	3454	3572.5	5.54
PA4610		84.25	73	225.75	205	2.66
PA4761	<i>dnaK</i>	8874.2 5	9121	15904.2 5	16423.5	2.07
PA4809	<i>fdhE</i>	59	50.75	121.25	133.25	2.28
PA4810	<i>fdnI</i>	80.5	72.5	297.25	302.5	3.86
PA4811	<i>fdnH</i>	420.5	351	1403.75	1260.5	3.56
PA4812	<i>fdnG</i>	1855	1648.75	5029	5029	3.17
PA4880		338.25	295.25	1654.5	1369.25	4.90
PA4898	<i>opdK</i>	11.25	8.25	20	25.5	2.25
PA4899		64.25	68.75	457.75	546.75	7.43
PA4900		11	19	92.5	93	5.89
PA4921	<i>choE</i>	127.25	92.5	237	220.25	2.03

PA5027		1577.5	1340.25	3140.5	2876.5	2.25
PA5054	<i>hslU</i>	826.25	892.25	1933.75	1920.25	2.35
PA5071		22	20.75	214.25	225.75	10.19
PA5083	<i>dguB</i>	9.25	9.75	24	19.25	2.26
PA5170	<i>arcD</i>	2199.25	2151	6770.25	7830.5	3.67
PA5180		120	136	584.75	513.75	4.22
PA5181		1017.25	1046.5	6192.25	6110.25	6.51
PA5181.1		20.75	27.5	64.5	71	2.69
PA5232		609.25	535.25	1262.75	1282	2.27
PA5381		30.5	25.5	80.5	61.5	2.46
PA5391		1.25	2	16	10	8.06
PA5396		180	195.25	541	503.75	2.70
PA5397		28.25	31.25	72.75	76.75	2.44
PA5398	<i>dgcA</i>	204.5	225.5	532.5	515.75	2.36
PA5399	<i>dgcB</i>	78	64.5	157.25	165.25	2.19
PA5400		30.5	30	67	63	2.07
PA5401		17.5	14	29.75	39	2.18
PA5410	<i>gbcA</i>	168.75	171.25	428.25	399.75	2.42
PA5415	<i>glyA1</i>	112.25	87.75	274.5	249	2.56
PA5416	<i>soxB</i>	92.25	83.5	222	208	2.40
PA5417	<i>soxD</i>	15.5	12.25	30.75	36	2.42
PA5418	<i>soxA</i>	235.75	219	525.5	516	2.24
PA5419	<i>soxG</i>	34.5	18.25	64.75	60.5	2.36
PA5421	<i>fdhA</i>	333.75	301.5	615	665	2.05
PA5460		55.75	60.25	147.25	131.75	2.34
PA5475		1651.5	1595	3867.25	3473	2.47

Table 7.1. Up-regulated genes in PA01-DK Δ tatA mutant.

ORF	Gene name	Normalised Expression Values				Fold change
		WT 1	WT 2	Tat 1	Tat 2	
PA0149		36.5	57.75	10.75	11.75	-4.16
PA0209	<i>mdcB</i>	194.5	224.75	68.75	63.75	-3.32
PA0210	<i>mdcC</i>	53.25	67.25	12	24.75	-3.29
PA0211	<i>mdcD</i>	368.25	488.75	142.5	159	-2.89
PA0212	<i>mdcE</i>	427.75	403	133.25	121.25	-3.25
PA0213		137.75	124	50.75	47.25	-2.70
PA0214		270	317	106.5	130.25	-2.51
PA0215	<i>madL</i>	157	138	62.5	49.5	-2.67
PA0216	<i>madM</i>	127.75	139.25	52	43.25	-2.84
PA0280	<i>cysA</i>	143.25	180	59.25	53.5	-2.96
PA0281	<i>cysW</i>	86.5	127.25	51.75	49.5	-2.15
PA0282	<i>cysT</i>	46.75	55.5	18.75	26.25	-2.28
PA0283	<i>sbp</i>	126.25	178	53.5	68	-2.59
PA0284		23.5	34.5	10.75	9.5	-2.83
PA0435		22.5	25	10.75	10.5	-2.23
PA0470	<i>fiuA</i>	376	442.5	124.25	112.25	-3.46
PA0471	<i>fiuR</i>	513	555.5	42	34.25	-14.14
PA0472	<i>fiuI</i>	422.25	498	20.75	23.75	-20.55
PA0517	<i>nirC</i>	19	17	6.75	5	-2.89
PA0519	<i>nirS</i>	629.75	568.75	181.5	192.25	-3.22
PA0523	<i>norC</i>	630.75	620.75	4.25	3.5	-145.07
PA0524	<i>norB</i>	257.25	332.5	17.5	18.25	-16.19
PA0525	<i>norD</i>	62.25	46.75	19	22.75	-2.62
PA0526		29.75	18	4.5	3.5	-5.58
PA0672	<i>hemO</i>	676	934.25	16.25	17.25	-46.14
PA0707	<i>toxR</i>	43.25	27.5	13.75	19.25	-2.17
PA0800		27	36.5	6.75	9.5	-3.82

PA0801		219.5	200.25	107	94.25	-2.13
PA0802		29.75	31.75	8	10.75	-3.31
PA0929	<i>pirR</i>	238.25	255	37.5	46.75	-5.96
PA0930	<i>pirS</i>	153.5	172.75	57.75	73.5	-2.54
PA1035		303.75	280.75	136	119.25	-2.31
PA1134		20	24.25	9	10.75	-2.32
PA1178	<i>oprH</i>	25927.7 5	25927.7 5	10193.7 5	8874.2 5	-2.18
PA1245	<i>aprX</i>	3197.25	3886.5	1330	1183	-2.61
PA1299	<i>ygcN</i>	50.25	74.25	12.25	9.5	-5.78
PA1300		178	270.5	4.5	3.5	-53.53
PA1301		312.5	468.75	11	9.5	-37.41
PA1363		55.5	72.75	32.25	32.5	-2.03
PA1364		40.5	31.75	15.5	17.5	-2.17
PA1365		235.25	261.75	102.75	112.75	-2.39
PA1837		178	232.75	82.25	89	-2.50
PA1838	<i>cysI</i>	511	659.5	263.5	287.75	-2.13
PA1909		27	22.75	18	5.75	-2.17
PA1911	<i>femR</i>	194.5	193	23.25	12.75	-11.01
PA1912	<i>femI</i>	190.25	238.25	4	14.75	-22.01
PA1913		110.25	126.25	55.75	52.5	-2.23
PA2033		923	1278.75	53.25	68.75	-17.90
PA2034		221.75	262	36.5	22.75	-8.40
PA2204		129	160.5	49.5	54.5	-2.87
PA2274		662	564	126	91.75	-5.71
PA2327		321.5	311	136.75	141.25	-2.27
PA2328		476	591	196.25	200.75	-2.72
PA2329		452.75	540	181.5	200	-2.64
PA2330		939.25	1017.25	312.5	332	-2.97
PA2331		1418.5	1654.5	459.25	517.5	-3.07

PA2384		244.5	203.25	8.25	11	-23.81
PA2385	<i>pvdQ</i>	414	364.5	33.75	34.75	-11.31
PA2386	<i>pvdA</i>	1638.75	1200.75	66	49.25	-24.44
PA2387	<i>fpvI</i>	125	124.75	57.75	52.5	-2.30
PA2389	<i>pvdR</i>	132	94.25	29.75	25.25	-4.27
PA2390	<i>pvdT</i>	189.75	122.25	40.5	57.5	-3.23
PA2391	<i>opmQ</i>	101.25	80	26.5	21.5	-3.80
PA2392	<i>pvdP</i>	388.25	290.25	43.75	30	-9.29
PA2393	<i>pvdM</i>	242.5	218	33.25	30.75	-7.30
PA2394	<i>pvdN</i>	311	317.75	25	22.25	-13.53
PA2395	<i>pvdO</i>	173.25	143.75	12.75	14.5	-12.11
PA2396	<i>pvdF</i>	370	366	87	93.75	-4.07
PA2397	<i>pvdE</i>	266	284.25	87	110.25	-2.84
PA2398	<i>fpvA</i>	1041.5	1102.5	236.5	246.75	-4.46
PA2399	<i>pvdD</i>	3008.25	2611	422.25	422.5	-6.34
PA2400	<i>pvdJ</i>	1809	1672.75	241.5	252.25	-6.94
PA2402		4921	4185	376	414.5	-10.68
PA2403	<i>fpvG</i>	411	326.5	81.5	70.5	-4.92
PA2404	<i>fpvH</i>	186.5	140.75	14.75	13.75	-11.58
PA2405	<i>fpvJ</i>	100.75	79.5	11.25	11.25	-8.20
PA2406	<i>fpvK</i>	60.25	44	14.75	11.75	-3.99
PA2407	<i>fpvC</i>	85.25	94.25	20.25	21.75	-4.39
PA2408	<i>fpvD</i>	55.75	50.75	6.75	1	-14.21
PA2409	<i>fpvE</i>	64	70.25	13.75	13	-5.24
PA2410	<i>fpvF</i>	156.25	155	32.5	47.75	-3.91
PA2411		468.5	366.5	21.5	21.75	-19.19
PA2412		254	195.25	5.75	9.75	-28.57
PA2413	<i>pvdH</i>	443.75	339	58.75	53.25	-7.06
PA2424	<i>pvdL</i>	4142.5	3104.5	162	161.25	-21.16

PA2425	<i>pvdG</i>	97	86.5	5.25	8.25	-14.49
PA2426	<i>pvdS</i>	997.5	1078.75	40.5	22.5	-33.55
PA2427		150	147.75	2.5	8.5	-25.65
PA2466	<i>foxA</i>	208.5	233	111	81.25	-2.40
PA2467	<i>foxR</i>	236	296	36.5	43.25	-6.68
PA2468	<i>foxI</i>	691.25	1008.5	69.75	83.25	-11.24
PA2531		49.5	34.75	15.5	20.75	-2.28
PA2686	<i>pfeR</i>	378.25	475.25	33.75	66.75	-8.62
PA2687	<i>pfeS</i>	128.25	146.25	43.5	53.25	-2.89
PA2881		25.5	22	6.75	12	-2.50
PA3094		280.75	245.5	141.25	127.75	-2.00
PA3391	<i>nosR</i>	141.25	108.25	24.5	30.5	-4.57
PA3407	<i>hasAp</i>	216.75	276	98.5	87	-2.74
PA3409	<i>hasS</i>	39.75	42.25	7	13.25	-4.15
PA3410	<i>hasI</i>	13.75	26.5	9.5	4.75	-3.05
PA3411		3.5	11.25	1.5	0	-12.00
PA3525	<i>argG</i>	722	705.5	284.75	295.25	-2.42
PA3530	<i>bfd</i>	942.75	912.75	66.75	55.75	-15.14
PA3553	<i>arnC</i>	76.25	67.25	25.25	44.25	-2.08
PA3558	<i>arnF</i>	17	16.75	3	5	-3.63
PA3718		133	141.5	65.5	59.5	-2.28
PA3719	<i>armR</i>	42.75	40.25	7.75	10.5	-4.43
PA3720		163	181.75	51	44	-3.72
PA3721	<i>nalC</i>	333	326.25	164.5	152	-2.09
PA3768		529.25	551.75	178	172.75	-3.14
PA3814	<i>iscS</i>	3754.75	4039.5	1794.25	1660.25	-2.05
					5	
PA3815	<i>iscR</i>	872.75	896.25	253	241.25	-3.56
PA3899	<i>fecI</i>	117.25	196.75	7.25	11.25	-17.83
PA3900	<i>fecR</i>	59.25	60	11.75	6.75	-6.77

PA4141		13002.7 5	14938.7 5	5271.25	5938.5	-2.15
PA4158	<i>fepC</i>	37	48.5	13	18.25	-2.72
PA4159	<i>fepB</i>	37	55.5	4.25	12.75	-5.34
PA4205	<i>mexG</i>	2611	2744.5	671.5	672.25	-3.73
PA4206	<i>mexH</i>	3454	2813.75	1005	823.25	-3.14
PA4207	<i>mexI</i>	3180.25	2735.25	886.5	805.5	-3.21
PA4208	<i>opmD</i>	1301.25	1130.5	391.75	385.25	-3.02
PA4218	<i>ampP</i>	1340.25	1634.5	205.75	187.75	-7.54
PA4219	<i>ampO</i>	842.5	1058.5	115	111.75	-8.33
PA4220	<i>fptB</i>	437.75	599.25	68.25	61.5	-8.23
PA4221	<i>fptA</i>	10334.2 5	13002.7 5	871.75	867.5	-11.86
PA4222	<i>pchI</i>	1825.5	1865.25	210.75	176.75	-9.45
PA4223	<i>pchH</i>	2296.75	2780.25	260	248.5	-9.62
PA4224	<i>pchG</i>	2427.25	3039.25	226.5	229	-11.49
PA4225	<i>pchF</i>	18575.2 5	23364.7 5	1611.5	1485.5	-11.95
PA4226	<i>pchE</i>	14020.2 5	16865	895	889	-15.94
PA4227	<i>pchR</i>	463.5	479.5	75	77	-6.39
PA4228	<i>pchD</i>	6953	8300	518.25	447	-14.81
PA4229	<i>pchC</i>	1493	1811	145.5	148.25	-11.28
PA4230	<i>pchB</i>	1660.25	2105.5	194.5	158.75	-10.63
PA4231	<i>pchA</i>	9078.75	10334.2 5	944	939.25	-9.26
PA4356	<i>xenB</i>	328	367.25	156	189.5	-2.00
PA4357	<i>yhgG</i>	118.75	116.25	61.5	49	-2.17
PA4370	<i>icmP</i>	3249.25	3690.5	925.5	1011.5	-3.29
PA4371		181.5	205.5	75.75	65.5	-2.86
PA4443	<i>cysD</i>	496.25	532	225.75	250	-2.21

PA4467		459.5	542.25	41.5	39.75	-12.55
PA4468	<i>sodM</i>	980.5	1208	43.75	54.25	-22.12
PA4469		373.5	447	11.75	12.25	-35.32
PA4470	<i>fumC1</i>	2151	2566	107.5	101.5	-22.00
PA4471	<i>fagA</i>	367.25	656.5	17.25	21.25	-27.09
PA4513	<i>piuB</i>	129.25	141.5	63	74.25	-2.04
PA4514	<i>piuA</i>	599.25	711	233.5	214.25	-2.97
PA4515	<i>piuC</i>	207.5	239	58.5	45.25	-4.49
PA4516		157.5	188	40.5	55.5	-3.70
PA4570		1005	1512.5	48.5	27	-33.66
PA4675	<i>chtA</i>	255	232.75	99.25	97.75	-2.55
PA4704. 1	<i>prfF1</i>	103.5	65.25	18.5	17	-4.87
PA4704. 3	<i>prfF2</i>	104.25	29.25	6	2.25	-17.67
PA4707		98	110.25	43.25	57	-2.11
PA4708	<i>phuT</i>	658	763.25	116.5	90	-6.95
PA4709	<i>phuU</i>	490	552	29.75	29	-18.21
PA4710	<i>phuR</i>	636.25	918.5	122.75	100.5	-7.00
PA4895		47.25	57	3.75	4.75	-12.34
PA4896		105.25	160.75	12.75	7	-14.23
PA5068	<i>tatA</i>	445	464.25	0.5	0.5	-3640.53
PA5069	<i>tatB</i>	133.25	192.5	0.5	0.5	-1332.74
PA5070	<i>tatC</i>	88.25	105.75	0.5	0.75	-790.93
PA5217		849	854.75	238.25	212.25	-3.77
PA5507		34.5	33.25	11.75	14.5	-2.68
PA5530		56.75	70.75	27.5	30	-2.30
PA5531	<i>tonB1</i>	674.75	701.5	128.75	110.25	-5.76

Table 7.2. Down-regulated genes in PAO1-DK Δ tatA mutant.

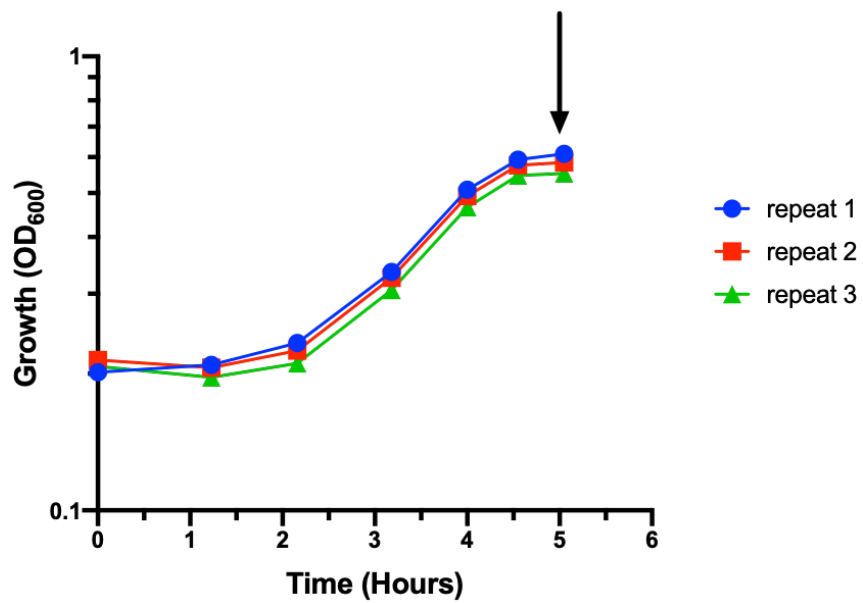


Figure 7.1. Example of cell harvest for RNAseq. Typical growth curve and sampling point of *P. aeruginosa* isolates. Grown in 24 well plate with LB miller media until early stationary phase (black arrow indicates typical sampling point). Then cultures were harvested for RNA extraction.

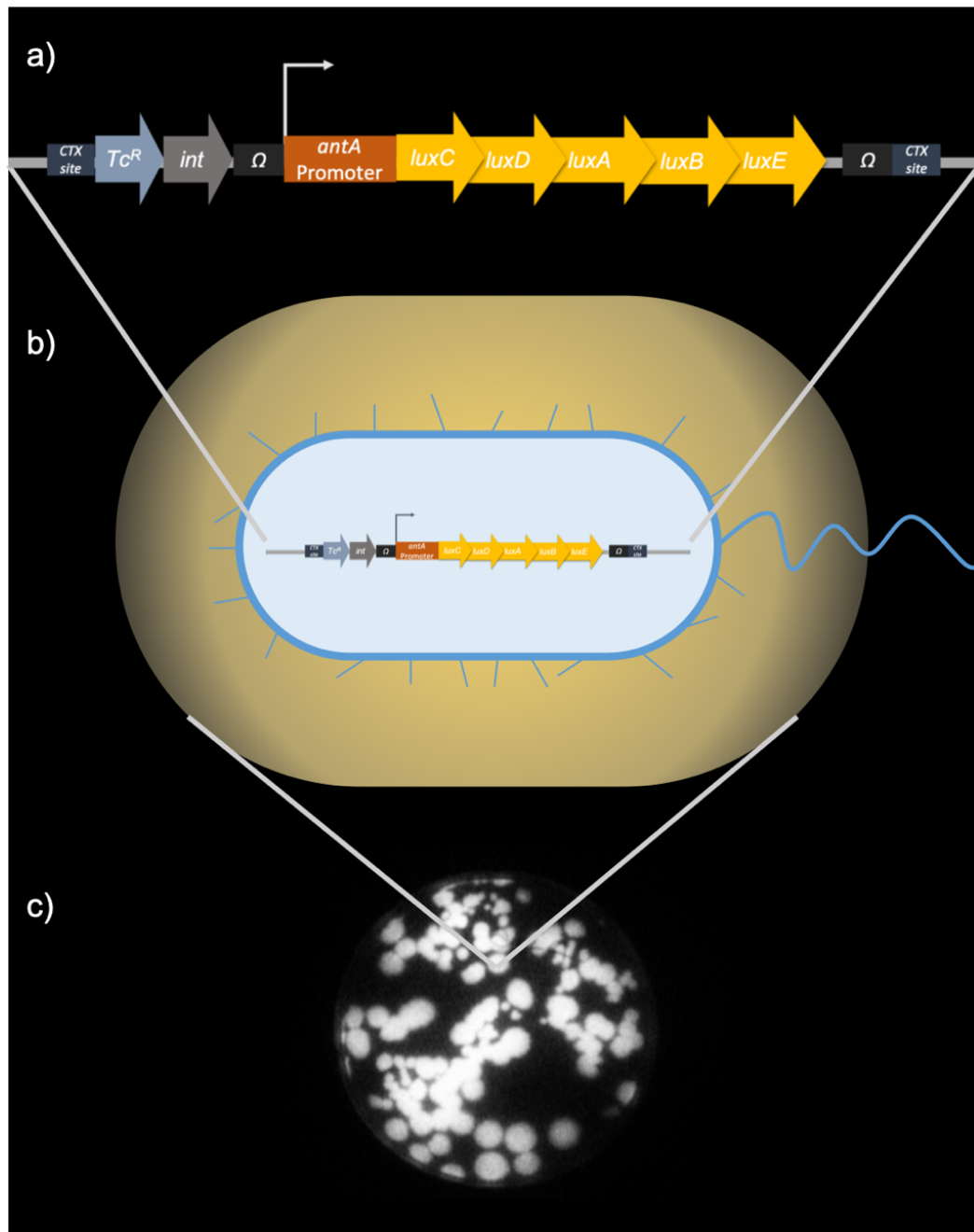


Figure 7.2. Bioluminescent transcriptional reporter in *P. aeruginosa* carrying an *antA'*::*lux* promoter fusion. a) schematic representation of miniCTX::*antA'*-*lux* on the bacterial chromosome, b) transcription from the promoter of interest creates bacterial luciferase (LuxAB) and fatty acid reductase (LuxCDE) and cells emit light c) bioluminescent clones growing on an LB + Tc 125 µg/mL plate, 37°C, 16 h.

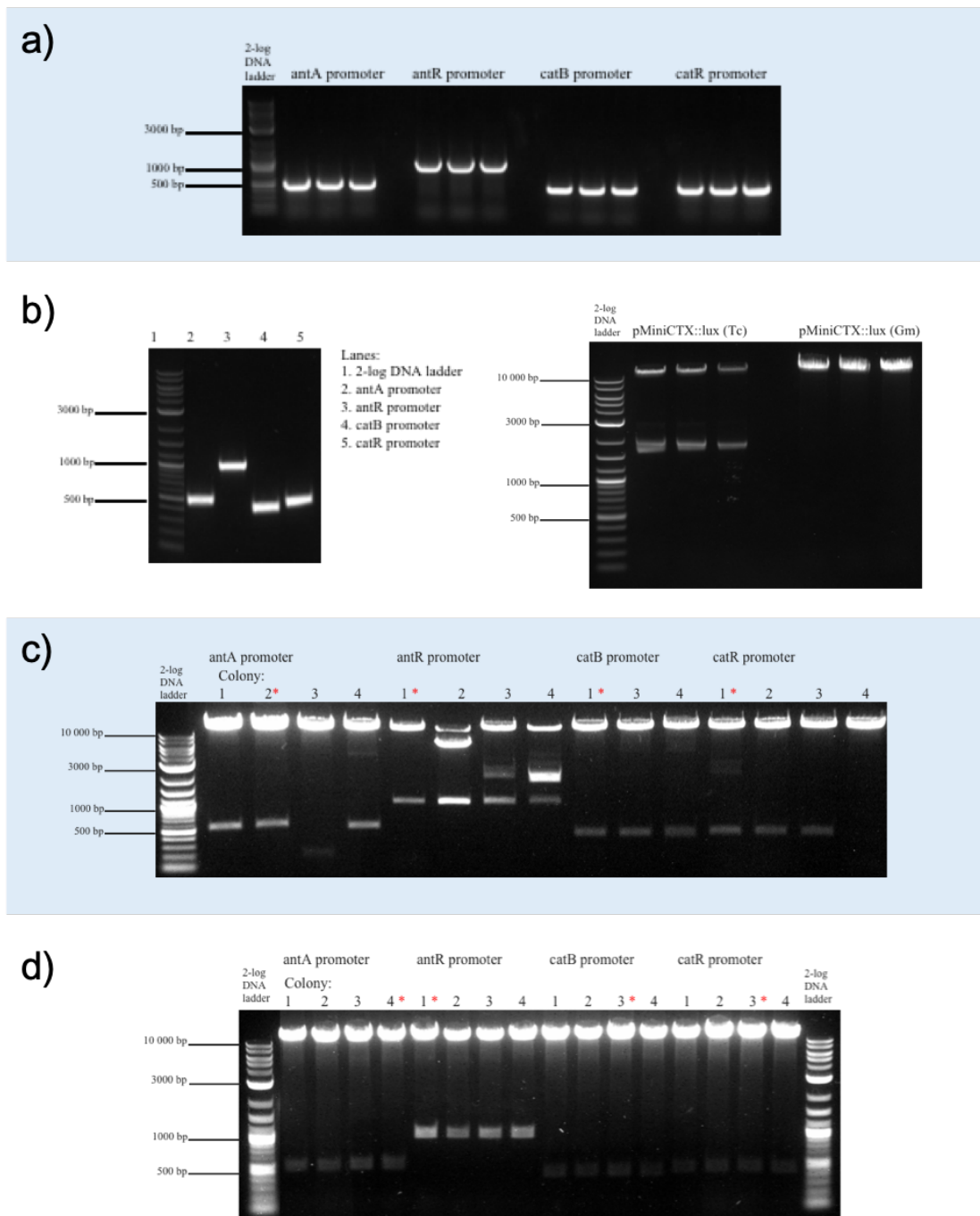


Figure 7.3. Construction of transcriptional reporters to measure anthranilate degradation pathway expression. DNA fragments separated on a 1% agarose gel by electrophoresis following a) PCR amplification of the *antA*, *antR*, *catB* and *catR* promoter regions, b) digestion of the promoter regions and miniCTX::lux vectors with *Bam*HI and *Hin*DIII, c) digestion of tetracycline-resistant vector miniCTX::*antA*'-lux, miniCTX::*antR*'-lux, miniCTX::*catB*'-lux, miniCTX::*catR*'-lux and d) gentamycin resistant miniCTX::*antA*'-lux, miniCTX::*antR*-lux, miniCTX::*catB*'-lux, miniCTX::*catR*'-lux. The red asterisk indicates clones carrying the bioreporters selected for conjugation into *P. aeruginosa*.

Statistics without reference	31330_PAO1DK	31331_PAO1DKantA	31332_PAO1DKtatABCantA	31333_PAO1DKpqsAantA
# contigs	21	29	21	29
# contigs (>= 0 bp)	40	56	37	54
# contigs (>= 1000 bp)	20	24	20	26
# contigs (>= 5000 bp)	18	20	18	23
# contigs (>= 10000 bp)	16	18	16	21
# contigs (>= 25000 bp)	15	17	15	20
# contigs (>= 50000 bp)	15	16	15	18
Largest contig	1 344 647	1 245 466	1 344 702	913 031
Total length	6 246 938	6 244 555	6 244 652	6 240 050
Total length (>= 0 bp)	6 251 490	6 251 891	6 248 351	6 246 815
Total length (>= 1000 bp)	6 246 125	6 241 306	6 243 839	6 238 015
Total length (>= 5000 bp)	6 243 716	6 230 771	6 241 430	6 234 285
Total length (>= 10000 bp)	6 233 323	6 220 110	6 230 769	6 223 624
Total length (>= 25000 bp)	6 219 106	6 205 893	6 216 552	6 209 407
Total length (>= 50000 bp)	6 219 106	6 172 808	6 216 552	6 152 318
N50	642 864	642 864	642 864	456 894
N75	480 098	480 098	480 098	261 908
L50	4	4	4	5
L75	7	7	7	9
GC (%)	66.57	66.57	66.57	66.57
Mismatches				
# N's	0	0	0	0
# N's per 100 kbp	0	0	0	0

Table 7.3. Quality assessment of genome assemblies. QUASt by centre for algorithmic biotechnology (CAB) was used to assess the quality of genome assemblies created by MicrobesNG. Full coverage was achieved of every genome and there were zero mismatches.

***In silico* analysis of PetA**

There is currently no crystal structure for the *Pseudomonas aeruginosa* PetA protein. A search of the protein data bank (PDB: <https://www.rcsb.org>) revealed no structures for *Pseudomonas aeruginosa* cytochrome *bc*₁ complex or its constituent subunits. In bovine and chicken cytochrome *bc*₁, the position of the iron-sulphur cluster region is not fixed (Xia *et al.*, 2013). The extrinsic domain of the rieske subunit has been captured in refined crystal structures in distinctly different loci, perhaps its flexibility allows it to bridge the gap to cytochrome *c*. Domain mobility is necessary for electron-shuttling as mutation of residues attempting to immobilise the domain inactivated it (Xia *et al.*, 2013). Due to the strong sequence similarity between prokaryotic and mitochondrial cytochrome *bc*₁ complexes, it is likely this is the case for the Rieske subunit of *P. aeruginosa*. Computer-based structure predictions are fast becoming accurate and reliable. As such, *in silico* analysis of PetA from *P. aeruginosa* PA14 was carried out to better understand its structure and function (Yang and Zhang, 2016).

To better understand the Rieske subunit, a predicted 3D model was created with the amino acid sequence of PA14_57570 and functional estimations based on its structure and the position of specific amino acid residues were made.

The model was generated using the Iterative Threading Assembly Refinement (I-TASSER) program. I-TASSER predicts protein structure by starting with a suitable structural template found from the protein data bank (PDB) and repeating fragment assembly simulations until a full length atomic model is generated (Roy *et al.*, 2010; Yang *et al.*, 2014; Yang and Zhang, 2015). Biological functions are then predicted by threading the predicted 3D model through the database BioLIP. Of the experimentally determined X-ray crystal structures stored in the PDB, the best template alignments were sections of the *Rhodobacter capsulatus* cytochrome *bc*₁ complex, *bovine* cytochrome *bc*₁, and the cytochrome *bc*₁ complex of the soil bacterium *Paracoccus denitrificans*.

The most likely predicted model can be seen in **Figure 7.4a**. PA14_57570 is a relatively small protein with the molecular weight calculated as 20.83 kDa (www.bioinformatics.org). Only the Tat signal peptide (pink) is predicted to be as membrane associated; the conserved twin arginine motif (based on S/TRRxFLK) is shown in red (Gimenez *et al.*, 2018). C-score rates the confidence of the model between -5 and 2 and is used to assess quality. The predicted model for PA14_57570 has a C-score of -1.32. The Tm score is a standard for measuring the structural similarity between two structures and is 0.55 ± 0.15 where 0 is no structural similarity and 1 is a perfect match. The predicted functional ligand binding domain is highlighted in **Figure 7.4b** and a list of predicted residues can be seen in **Figure 7.4c** and it suggests that the Rieske cluster is located on the interface of PetA, rather than buried within the structure.

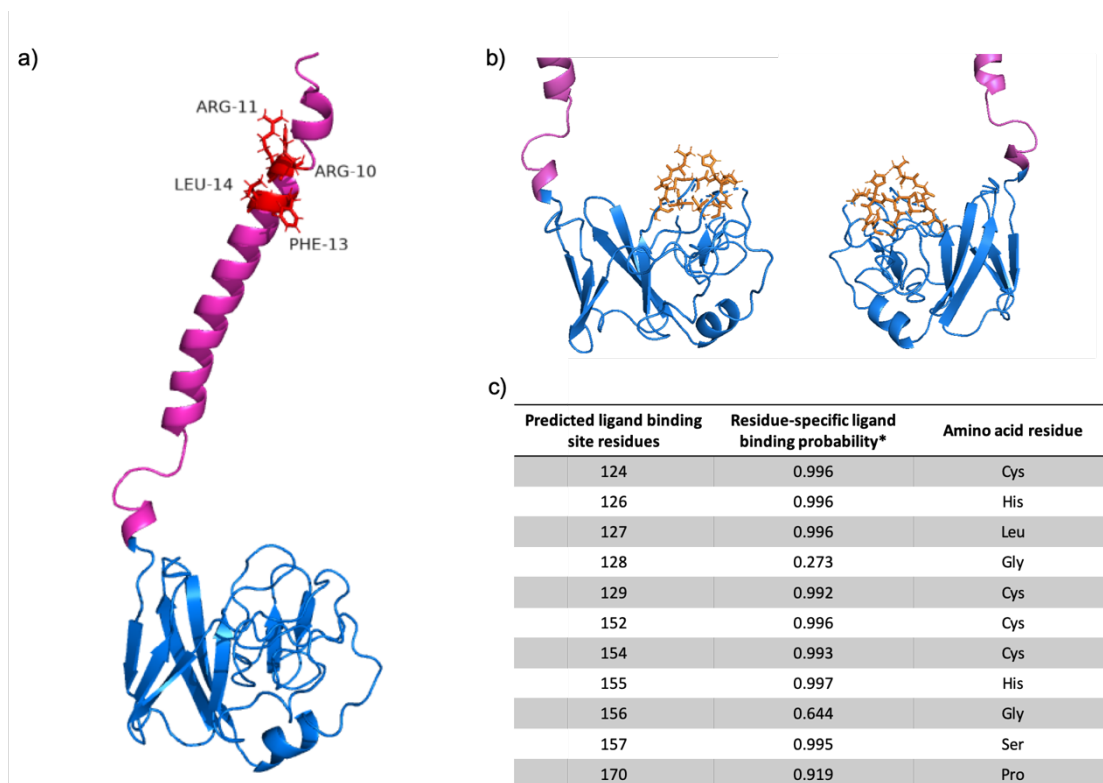


Figure 7.4. Predicted model and ligand-binding domain of PA14_57570. A 3D model was generated using ITASSER and visualised in PyMol as a ribbon (a) showing the location of the Tat signal peptide (pink) and published conserved residues of the signal peptide in greater detail (red, labelled). The predicted ligand is a 2Fe2S cluster and visualisation of predicted ligand-binding domain (b) shows two Cys and two His residues in more detail (orange) as literature states such residues coordinate the ligand. Residues predicted to be involved in ligand binding (c) by COACH and COFACTOR are listed in (c).

Following generation of a putative 3D structure, this study sought to identify the level of conservation within the PA14_57570 protein, as well as specific residues that are conserved between orthologs. Evolutionary conservation of specific residues indicates an important structural or functional role within the protein. This analysis aimed to highlight potential ligand binding domains and residues important for proper electron transfer. Conserved regions may also include those areas needed for coordination with other subunits in the cytochrome bc_1 complex.

Conserved residues were identified by carrying out a multiple sequence alignments and each position given a conservation score. The results were visualised using PyMOL. The process can be seen in **Figure 7.5**. Briefly, a search of the database www.pseudomonas.com gave 534 sequences for orthologs of PA14_57570. These were saved as a .fasta file and edited manually to remove duplicate entries. The remaining number of orthologs was 512. The multiple sequences were then assessed with CLUSTALW for their alignment to the PA14_57570 sequence and to detect homology within the sequence family (Thompson *et al.*, 1994; Larkin *et al.*, 2007).

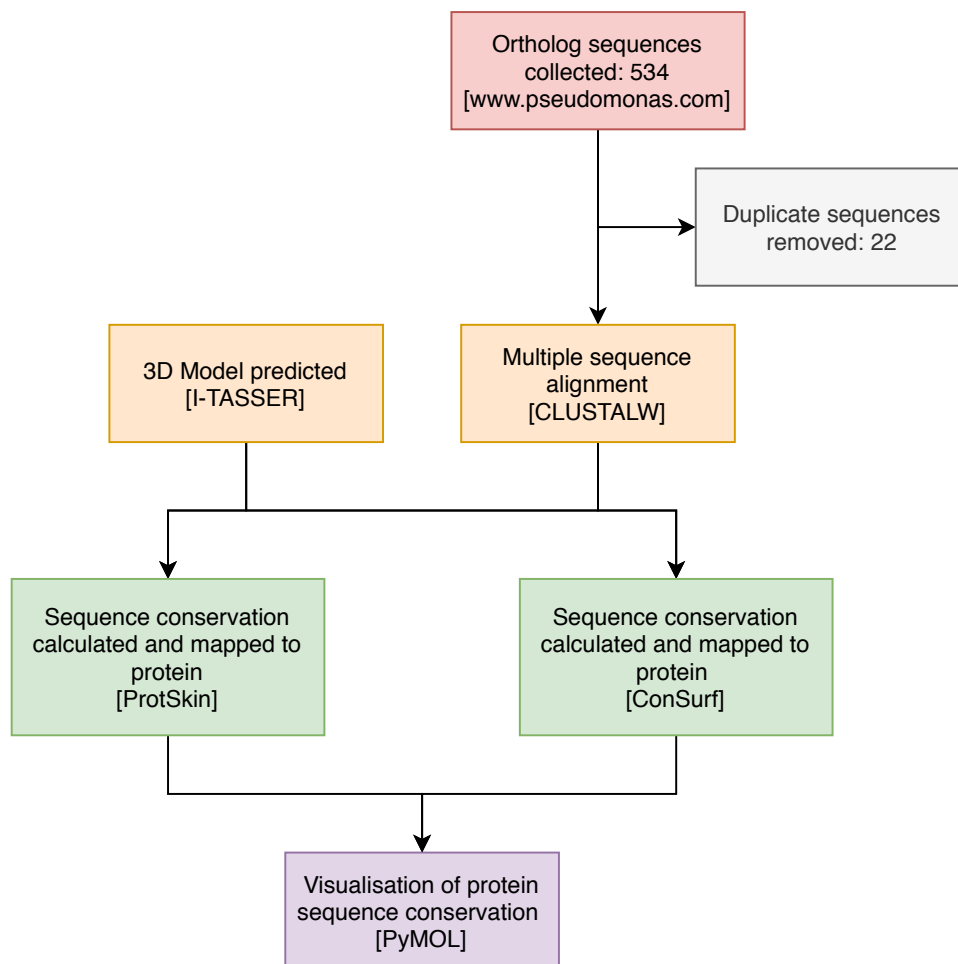


Figure 7.5. Flow chart showing process of mapping sequence conservation to 3D structure of PetA. *In silico* analysis began by collecting ortholog peptide sequences of PetA from PA14. Duplicate sequences were removed and multiple sequence alignment was carried out with CLUSTALW. A 3D model was generated with I-TASSER and sequence conservation was determined with both ProtSkin and ConSurf. In both cases the conservation was mapped to the 3D structure and visualised with PyMOL.

The evolutionary conservation of the sequence was estimated with ConSurf using the multiple sequence alignment and PA14_57570 amino acid sequence (Ashkenazy *et al.*, 2010; Celniker *et al.*, 2013; Ashkenazy *et al.*, 2016). As seen in The evolutionary conservation of the sequence was estimated with ConSurf using the multiple sequence alignment and PA14_57570 amino acid sequence (Ashkenazy *et al.*, 2010; Celniker *et al.*, 2013; Ashkenazy *et al.*, 2016). As seen in **Figure 7.6**, the query sequence is coloured according to the generated conservation scores.

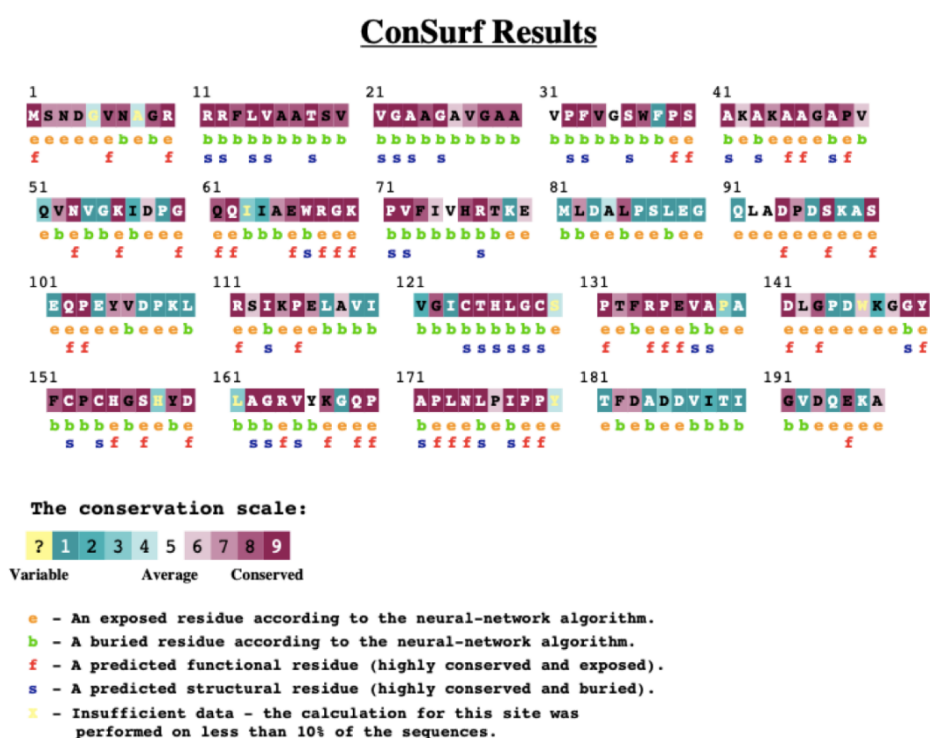


Figure 7.6. Conservation of residues within the PetA sequence as determined by ConSurf. Phylogeny of the sequence family was determined with ConSurf and each residue of the query sequence was given a score to represent conservation within the *P. aeruginosa* homologs. Exposed/buried residues were also predicted, as were functional and structural residues.

ConSurf predicted different functional residues to I-TASSER with the exception of residue His155, Ser157 and Pro170. In fact, the I-TASSER-predicted

ligand-binding residues are considered structural by the ConSurf neural-network algorithm due to their location within the 3D structure.

Visualisation of conserved residues was achieved using PyMOL to map onto the 3D structure generated by I-TASSER. **Figure 7.7** shows the highest level of conservation is grouped at the predicted ligand-binding domain, and the remaining peptide has considerable variance across the orthologue group. The Tat signal peptide is also conserved.

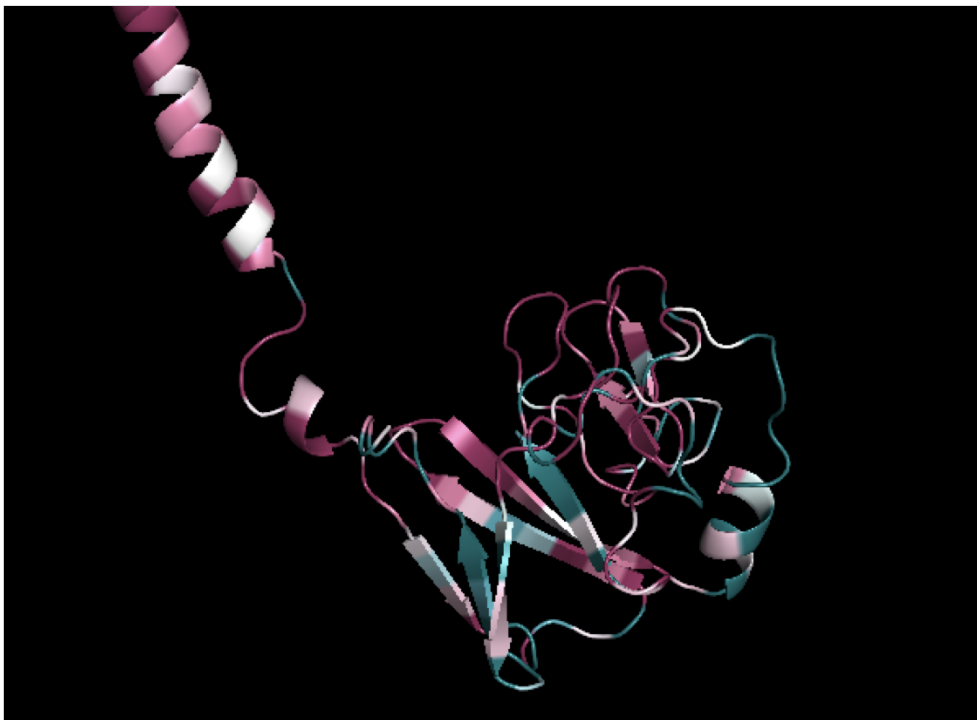


Figure 7.7. 3D model of PetA (PA14_57570) visualised with PyMol. Conservation of each residue within the *Pseudomonas* ortholog group is visualised as a dark pink to blue colour scale: highly conserved (dark pink), average (white) and phylogenetically variable (blue).

Disruption of the *Pseudomonas aeruginosa* Tat system perturbs PQS-dependent quorum sensing and biofilm maturation through lack of the Rieske cytochrome *bc₁* sub-unit

*Eliza Ye-Chen Soh¹, *Frances Smith¹, Maxime Rémi Gimenez⁶, Liang Yang^{2†}, Rebecca Munk Vejborg³, Matthew Fletcher¹, Nigel Halliday¹, Sophie Bleves⁴, Stephan Heeb¹, Miguel Camara¹, Michael Givskov^{2,3}, Kim R. Hardie¹, Tim Tolker-Nielsen³, Bérengère Ize⁴ and Paul Williams¹

¹Biodiscovery Institute, National Biofilms Innovation Centre and School of Life Sciences, University of Nottingham, Nottingham, U.K

²Singapore Centre for Environmental Life Sciences Engineering, Nanyang Technological University, 60 Nanyang Drive, Singapore 637551

³Costerton Biofilm Center, Department of Immunology and Microbiology, Faculty of Health Sciences, University of Copenhagen, 2200 Copenhagen N, Denmark.

⁴Laboratoire d'Ingénierie des Systèmes Macromoléculaires (LISM-UMR7255), Institut de Microbiologie de la Méditerranée, CNRS and Aix-Marseille Univ. 31 Chemin Joseph Aiguier, CS 70071, 13402 Marseille cedex 09, France.

*joint first authors

†Present Address: School of Medicine, Southern University of Science and Technology, Shenzhen 518055, Guangdong, China

Supporting Information

Table S1. Strains and plasmids used in this study.

Strains/Plasmids	Relevant Characteristics	Source/Reference
<i>E. coli</i>		
S17-1 λ pir	Conjugative strain for suicide plasmids	[1]
<i>P. aeruginosa</i>		
PAO1	Wild-type <i>P. aeruginosa</i> strain	Copenhagen collection

PAO1 CTX:: <i>pqsA'</i> - <i>lux</i>	PAO1 with a chromosomal miniCTX:: <i>pqsA'</i> - <i>luxCDABE</i> fusion	[2]
PAO1 CTX:: <i>rhlA'</i> - <i>lux</i>	PAO1 with a chromosomal miniCTX:: <i>rhlA'</i> - <i>luxCDABE</i> fusion	This study
PAO1 CTX:: <i>phzA1'</i> - <i>lux</i>	PAO1 with a chromosomal miniCTX:: <i>phzA1'</i> - <i>luxCDABE</i> fusion integrated into the chromosomal CTX attachment site	[3]
PAO1 CTX:: <i>phzA2'</i> - <i>lux</i>	PAO1 with a chromosomal miniCTX:: <i>phzA2'</i> - <i>luxCDABE</i> fusion	[3]
PAO1 CTX:: <i>pqsR'</i> - <i>lux</i>	PAO1 with a chromosomal miniCTX:: <i>pqsR'</i> - <i>luxCDABE</i> fusion	This study
PAO1 CTX:: <i>tac</i> - <i>lux</i>	PAO1 with a chromosomal miniCTX:: <i>tac'</i> - <i>luxCDABE</i> fusion	This study
PAO1 $\Delta pqsA$	<i>pqsA</i> in-frame deletion mutant; AQ-negative	[2]
PAO1 $\Delta pqsA$ CTX:: <i>pqsA'</i> - <i>lux</i>	PAO1 $\Delta pqsA$ with a chromosomal miniCTX:: <i>pqsA'</i> - <i>luxCDABE</i> fusion	[2]
PAO1 $\Delta pqsA$ CTX:: <i>rhlA'</i> - <i>lux</i>	PAO1 $\Delta pqsA$ with a chromosomal miniCTX:: <i>rhlA'</i> - <i>luxCDABE</i> fusion	This study
PAO1 <i>tatA</i>	<i>tatA</i> Himar 1 <i>mariner</i> transposon insertion mutant	This study
PAO1 $\Delta tatABC$	<i>tatABC</i> in-frame deletion mutant	This study
PAO1 $\Delta petA$	<i>petA</i> in-frame deletion mutant	This study
PAO1 <i>tatA</i> $\Delta pqsA$	PAO1 <i>tatA</i> with a <i>pqsA</i> in-frame deletion	This study
PAO1 <i>tatA</i> CTX:: <i>pqsA'</i> - <i>lux</i>	PAO1 <i>tatA</i> with a chromosomal miniCTX:: <i>pqsA'</i> - <i>luxCDABE</i> fusion	This study
PAO1 <i>tatA</i> CTX:: <i>rhlA'</i> - <i>lux</i>	PAO1 <i>tatA</i> with a chromosomal miniCTX:: <i>rhlA'</i> - <i>luxCDABE</i> fusion	This study
PAO1 <i>tatA</i> CTX:: <i>phzA1'</i> - <i>lux</i>	PAO1 <i>tatA</i> with a chromosomal miniCTX:: <i>phzA1'</i> - <i>luxCDABE</i> fusion	This study
PAO1 <i>tatA</i> CTX:: <i>phzA2'</i> - <i>lux</i>	PAO1 <i>tatA</i> with a chromosomal miniCTX:: <i>phzA2'</i> - <i>luxCDABE</i> fusion	This study
PAO1 <i>tatA</i> $\Delta pqsA$ CTX:: <i>pqsA'</i> - <i>lux</i>	PAO1 <i>tatA</i> $\Delta pqsA$ with a chromosomal miniCTX:: <i>pqsA'</i> - <i>luxCDABE</i> fusion	This study
PA14	Wild-type <i>P. aeruginosa</i> strain	This study
PA14 $\Delta petA$	<i>petA</i> in-frame deletion mutant	This study
PA14 $\Delta petA$::(CTX1:: <i>petA</i>)	<i>petA</i> with a chromosomal miniCTX1:: <i>petA</i> insertion, Tc ^R	This study
PA14 $\Delta cytB$	<i>cytB</i> in-frame deletion mutant	This study
PA14 $\Delta cytC_1$	<i>cytC₁</i> in-frame deletion mutant	This study

Plasmids

pBBR1MCS-5	Broad host range vector, Gm ^R	[4]
pBBR1MCS-5:: <i>pqsABCD</i>	pBBR1MCS-5 carrying the <i>pqsABCD</i> operon	[5]

pBT20	<i>Himar I mariner</i> mini-transposon delivery vector	[6]
pKNG101	Suicide vector, Sm ^R , <i>oriR6K</i> , <i>oriTRK2</i> , <i>mobRK2</i> , <i>sacBR</i> ⁺	[7]
pKNGΔ <i>cytB</i>	Suicide plasmid for <i>cytB</i> deletion, Sm ^R	This study
pKNGΔ <i>cytC₁</i>	Suicide plasmid for <i>cytC₁</i> deletion, Sm ^R	This study
pKNGΔ <i>petA</i>	Suicide plasmid for <i>petA</i> deletion, Sm	This study
pME3087	ColE1 suicide vector for allelic replacements, Tc ^R	[8]
pME3087:: <i>tatABC</i>	Suicide plasmid for <i>tatABC</i> deletion, Tc ^R	This study
pME6032:: <i>pqsR6H</i>	pME6032 carrying a functional, hexahistidine C-terminally tagged <i>pqsR</i> gene	[9]
pmini-CTX1	mini-CTX delivery vector for integration of constructs at the <i>attB</i> site of <i>P. aeruginosa</i> chromosome; Tc ^R	[10]
Pmini-CTX1- <i>petA</i>	<i>petA</i> under the control of its own promoter in mini-CTX1	This study
pminiCTX- <i>lux</i>	Promoter probe vector containing <i>luxCDABE</i> , Tc ^R	[11]
pminiCTX:: <i>phzA1'</i> - <i>lux</i>	<i>phzA1</i> promoter region fused to <i>luxCDABE</i> in pminiCTX- <i>lux</i>	[3]
pminiCTX:: <i>phzA2'</i> - <i>lux</i>	<i>phzA2</i> promoter region fused to <i>luxCDABE</i> in pminiCTX- <i>lux</i>	[3]
pminiCTX:: <i>pqsA'</i> - <i>lux</i>	<i>pqsA</i> promoter region fused to <i>luxCDABE</i> in pminiCTX- <i>lux</i>	[2]
pminiCTX:: <i>pqsR'</i> - <i>lux</i>	<i>pqsR</i> promoter region fused to <i>luxCDABE</i> in pminiCTX- <i>lux</i>	This study
pminiCTX:: <i>rhlA'</i> - <i>lux</i>	<i>rhlA</i> promoter region fused to <i>luxCDABE</i> in pminiCTX- <i>lux</i>	This study
pminiCTX:: <i>tac</i> - <i>lux</i>	<i>tac</i> promoter fused to <i>luxCDABE</i> in pminiCTX- <i>lux</i>	This study
pRK2013	Conjugative helper plasmid, ColE1 origin, Tra ⁺ , mob ⁺ , Km ^R	[12]
pTatA	pUCP22 carrying <i>tatA</i> ; Ap ^R	This study
pUCP22	<i>E.coli</i> - <i>Pseudomonas</i> shuttle vector	[13]
pUCP <i>pqsE</i>	pUCP18 containing <i>pqsE</i> ; Ap ^R	[14]

References for Table S1

1. Simon R, Priefer U, Puhler A. A broad host range mobilization system for *in vivo* genetic engineering: transposon mutagenesis in Gram-negative bacteria. *Nature Biotechnology*. 1983; 1:784-91.
2. Diggle SP, Matthijs S, Wright VJ, Fletcher MP, Chhabra SR, Lamont IL, Kong X, Hider RC, Cornelis P, Cámara M, Williams P. The *Pseudomonas aeruginosa* 4-quinolone signal molecules HHQ and PQS play multifunctional roles in quorum sensing and iron entrapment. *Chem Biol*. 2007; 14:87-96.

3. Higgins S, Heeb S, Rampioni G, Fletcher MP, Williams P, Cámara M. Differential Regulation of the Phenazine Biosynthetic Operons by Quorum Sensing in *Pseudomonas aeruginosa* PAO1-N. *Front Cell Infect Microbiol*. 2018; 8:252.
4. Kovach ME, Elzer PH, Hill DS, Robertson GT, Farris MA, Roop RM 2nd, Peterson KM. Four new derivatives of the broad-host-range cloning vector pBBR1MCS, carrying different antibiotic-resistance cassettes. *Gene*. 1995; 166:175-176
5. Niewerth H, Bergander K, Chhabra SR, Williams P, Fetzner S. Synthesis and biotransformation of 2-alkyl-4(1H)-quinolones by recombinant *Pseudomonas putida* KT2440. *Appl Microbiol Biotechnol*. 2011; 91:1399-408.
6. Kulasekara HD, Ventre I, Kulasekara BR, Lazdunski A, Filloux A, Lory S. A novel two-component system controls the expression of *Pseudomonas aeruginosa* fimbrial cup genes. *Mol Microbiol*. 2005; 55:368-80.
7. Kaniga K., Delor I., Cornelis G. R. A wide-host-range suicide vector for improving reverse genetics in gram-negative bacteria: inactivation of the *blaA* gene of *Yersinia enterocolitica*. *Gene*. 1991; **109**:137-41.
8. Schnider-Keel U, Lejbølle KB, Baehler E, Haas D, Keel C. The sigma factor AlgU (AlgT) controls exopolysaccharide production and tolerance towards desiccation and osmotic stress in the biocontrol agent *Pseudomonas fluorescens* CHA0. *Appl Environ Microbiol*. 2001; 67:5683-93.
9. Ilangovan A, Fletcher M, Rampioni G, Pustelny C, Rumbaugh K, Heeb S, Cámara M, Truman A, Chhabra SR, Emsley J, Williams P. Structural basis for native agonist and synthetic inhibitor recognition by the *Pseudomonas aeruginosa* quorum sensing regulator PqsR (MvfR). *PLoS Pathog*. 2013; 9:e1003508.
10. Hoang T. T., Kutchma A. J., Becher A., Schweizer H. P. Integration-proficient plasmids for *Pseudomonas aeruginosa*: site-specific integration and use for engineering of reporter and expression strains. *Plasmid*. 2000; **43**:59-72.
11. Becher A, Schweizer HP. Integration proficient *Pseudomonas aeruginosa* vectors for isolation of single copy chromosomal *lacZ* and *lux* gene fusions. *Biotechniques*. 2000; 29:948-50.
12. Figurski D. H., Helinski D. R. Replication of an origin-containing derivative of plasmid RK2 dependent on a plasmid function provided in trans. *Proc Natl Acad Sci U S A*. 1979; **76**:1648-52.
13. West SE, Schweizer HP, Dall C, Sample AK, Runyen-Janecky LJ. Construction of improved *Escherichia-Pseudomonas* shuttle vectors derived from pUC18/19 and sequence of the region required for their replication in *Pseudomonas aeruginosa*. *Gene*. 1994; 148:81-6.
14. Rampioni G, Pustelny C, Fletcher MP, Wright VJ, Bruce M, Rumbaugh KP, Heeb S, Cámara M, Williams P. Transcriptomic analysis reveals a global alkyl-quinolone-independent regulatory role for PqsE in facilitating the environmental adaptation of *Pseudomonas aeruginosa* to plant and animal hosts. *Environ Microbiol*. 2010; 12:1659-73.

Table S2. Oligonucleotide primers used in this study

Name	Sequence (5'-3', restriction sites underlined)
TnM1	GTGAGCGGATAACAATTTACACAG
TnM2	ACAGGAAACAGGACTCTAGAGG
TnMseq	CACCCAGCTTTCTTGTACAC
<i>FtatA</i>	<u>GGAAT</u> TCCCCTGAACCTACACATTGCCA
<i>RtatA</i>	<u>GGGTAC</u> CCCATTCGGAACATCGATGGCTA
Tat3D-UF	TAT <u>GAAT</u> TCAATCTATTGGTCGCGTTC
Tat3D-UR	TAT <u>GGAT</u> CCAAAAATGCCCATGTTCGTA
Tat3D-DF	TAT <u>GGAT</u> CCACCCGCCAGTGAACCTGC
Tat3D-DR	TAT <u>TCTAG</u> ACGCGCAGCTTGTTCGACCT
S.PA4431UF	CAGGTCGACGGATCCCCGGGGTACTGGCAAGATTTCCAT
S.PA4431DR	TATGCATCCGCGGGCCCCGGGGAGATCAGGAAGTCACCGC
S.PA4431DF	GACTGAATGTGATCGGCGTGGACCAGGAG
S.PA4431UR	CGCCGATCACATTCAGTCGTCTCCCATCA
S-4431CTXFor	TCCCCGGGCTGCAGGAATTCTTCGACGCTTGTGAAAA
S-4431CTXRev	GATAAGCTTGATATCGAATTCTCAGGCTTTCTCCTGGTC
S.PA4430UF	CAGGTCGACGGATCCCCGGGCCGTTTCGTAGGGTCATGGTT
S.PA4430DR	TATGCATCCGCGGGCCCCGGGACCACCTGTACCTGCTTGCA
S.PA4430DF	GAGAAAGCCTGATGAAAAAGCAATTCGCT
S.PA4430UR	TTGCTTTTTTCATCAGGCTTTCTCCTGGTC
S.PA4429UF	CAGGTCGACGGATCCCCGGGATCGCGTTCCATCCGTACTA
S.PA4429DR	TATGCATCCGCGGGCCCCGGGTCGCTGAGGAAATATGCCTT
S.PA4429DF	TGGCTGATGTAACCCGCACGTTGGTCTTC
S.PA4429UR	TGCGGGTTACATCAGCCAGTCACCCTTTC
<i>rhIA</i> CTX UF	TATA <u>AAGCT</u> TTGCCAAAAGCCTGAC
<i>rhIA</i> CTX DR	TAT <u>GGAT</u> CCTTGCAAACCGATACC
<i>pqsR</i> CTX UF	TCCAGC <u>GAAT</u> TCGATACGCAACCGCCG
<i>pqsR</i> CTX DR	GATGAC <u>CTGCAG</u> GAACATGTTACAGTG
<i>tac</i> CTX UF	AAACTCCTCGAGCATCAAATGAAACTG
<i>tac</i> CTX DR	GAGCTC <u>GAAT</u> CTGTTTCTGTGTGAA

Table S3. *P. aeruginosa* PA14 Tat substrate mutants used in this study

Mutant Number	PA Number/Name	Function
1	PA0144	Nucleoside 2-deoxyribosyltransferase
2	PA0365	Hypothetical protein
3	PA0735	Hypothetical protein
4	PA0844	Hemolytic phospholipase C (PlcH)
5	PA1174	Nitrate reductase catalytic subunit (NapA)
6	PA1601	Aldehyde dehydrogenase
7	PA1880	Oxidoreductase
8	PA2065	Copper resistance protein (CopA)
9	PA2124	Dehydrogenase
10	PA2264	Hypothetical protein
11	PA2328	Hypothetical protein
12	PA2378	Aldehyde dehydrogenase
13	PA2389	Hypothetical protein (PvdR)
14	PA2392	Tyrosinase (PvdP)
15	PA2394	Aminotransferase (PvdN)
16	PA2531	Aminotransferase
17	PA2635	Hypothetical protein
18	PA2699	Hydrolase
19	PA3222	Permease
20	PA3319	Non-hemolytic phospholipase C (PlcN)
21	PA3392	Nitrous-oxide reductase (NosZ)
22	PA3713	Spermidine dehydrogenase (SpdH)
23	PA3768	Metallo-oxidoreductase
24	PA3910	Phosphodiesterase/alkaline phosphatase (EddA)
25	PA4140	Cholesterol oxidase (ChoA)
26	PA4159	Iron-enterobactin transporter periplasmic binding protein (FepB)
27	PA4431	Cytochrome <i>bc</i> ₁ Rieske subunit (PetA)
28	PA4621	Oxidoreductase
29	PA4692	Sulphite oxidase subunit (YedY)
30	PA4812	Formate dehydrogenase-O, major subunit (FdnG)
31	PA4858	Hypothetical protein
32	PA5327	Oxidoreductase (SphC)

33	PA5538	N-acetylmuramoyl-L-alanine amidase AmiC*
34	PA14_48450	Peptidyl-arginine deiminase (Agu2A)**

Annotations are based on predictions from the website www.pseudomonas.com or are inferred from sequence homology. Functional predictions by Gimenez *et al.* (2018) Scientific Reports 11950. doi: 10.1038/s41598-018-30393-x.

*Annotated as AmiA on *Pseudomonas* PA14 genome but sequence is closer to that of AmiC.

**No conserved gene found in PAO1, so retains the PA14 annotation.

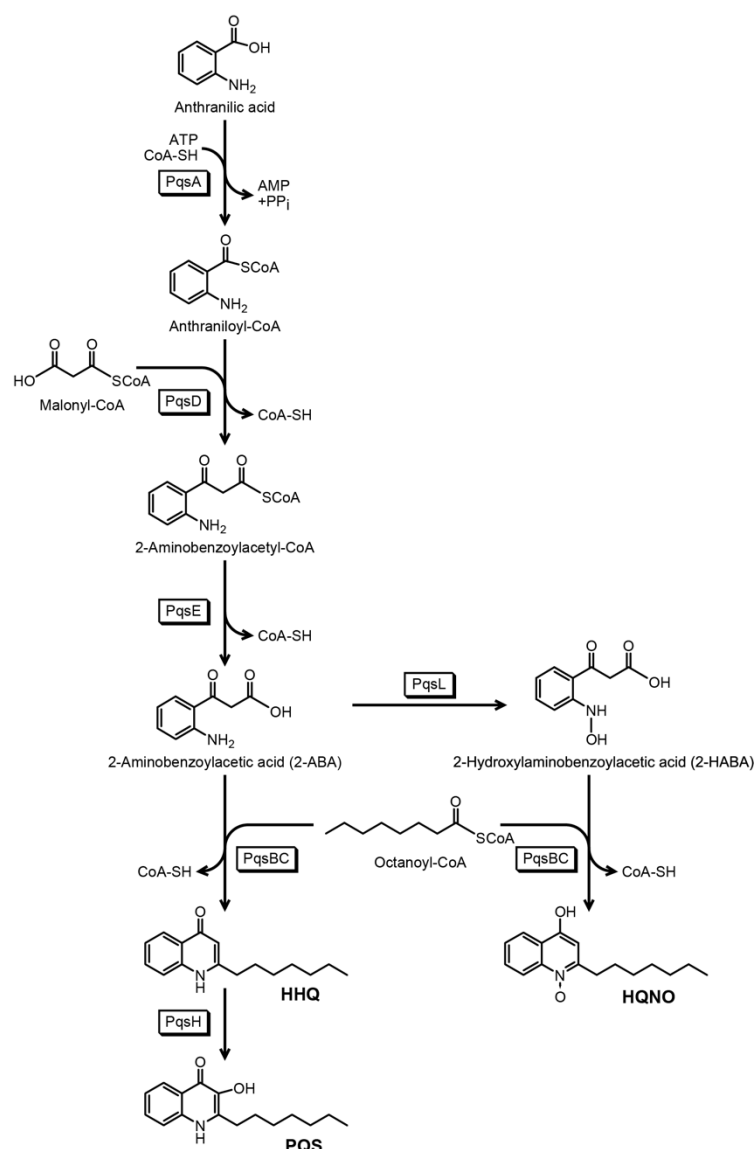


Fig. S1 Biochemical basis of AQ biosynthesis. PqsA catalyses the formation of anthraniloyl-CoA that is condensed with malonyl-CoA by PqsD to form 2-aminobenzoylacetyl-CoA (2-ABA-CoA). The latter is converted to 2-aminobenzoylacetate (2-ABA) via the thioesterase functionality of PqsE. The PqsBC heterodimer condenses 2-ABA with octanoyl-CoA to generate HHQ. PQS is formed through the oxidation of HHQ by PqsH. For AQ *N*-oxides such as 2-heptyl-4-hydroxyquinoline *N*-oxide (HQNO), 2-ABA is oxidized to 2-HABA by the alternative mono-oxygenase PqsL and then condensed with octanoyl-CoA by PqsBC to form HQNO. PqsBC can accept acyl-CoAs of different acyl chain lengths to generate diverse AQS and AQ *N*-oxides.

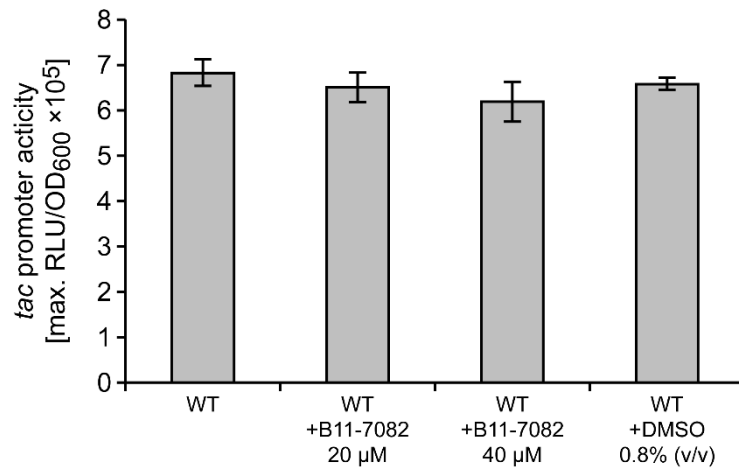


Fig. S2 The Tat inhibitor Bayer 11-7082 has no effect on light output at 20 or 40 μM from a constitutive *P. aeruginosa* CTX:*ptac*'-luxCDABE chromosomal reporter fusion. The co-solvent DMSO, had no effect at 0.8% on the *lux* reporter fusion either. Data are presented as maximal light output as a function of growth (RLU/OD₆₀₀). Experiments were repeated in triplicate at least twice.

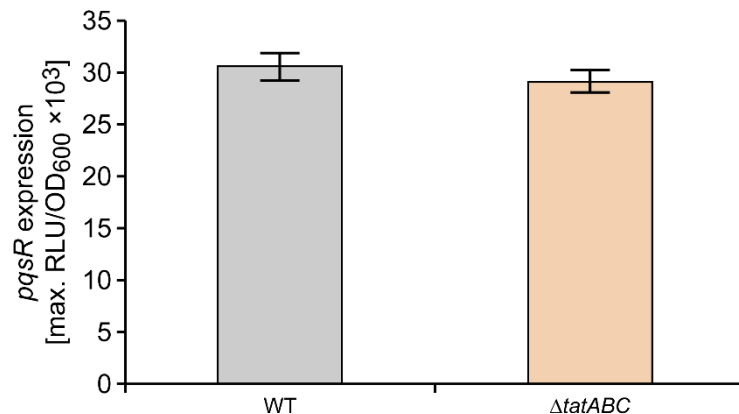


Fig. S3 Deletion of the *tatABC* genes does not influence *pqsR* expression. The data show that there are no differences in the expression of a chromosomal CTX::*pqsR*'-luxCDABE fusion in the *P. aeruginosa* wild type compared with the Δ*tatABC* mutant. Data are presented as maximal light output as a function of growth (RLU/OD₆₀₀). Experiments were repeated in triplicate at least twice.

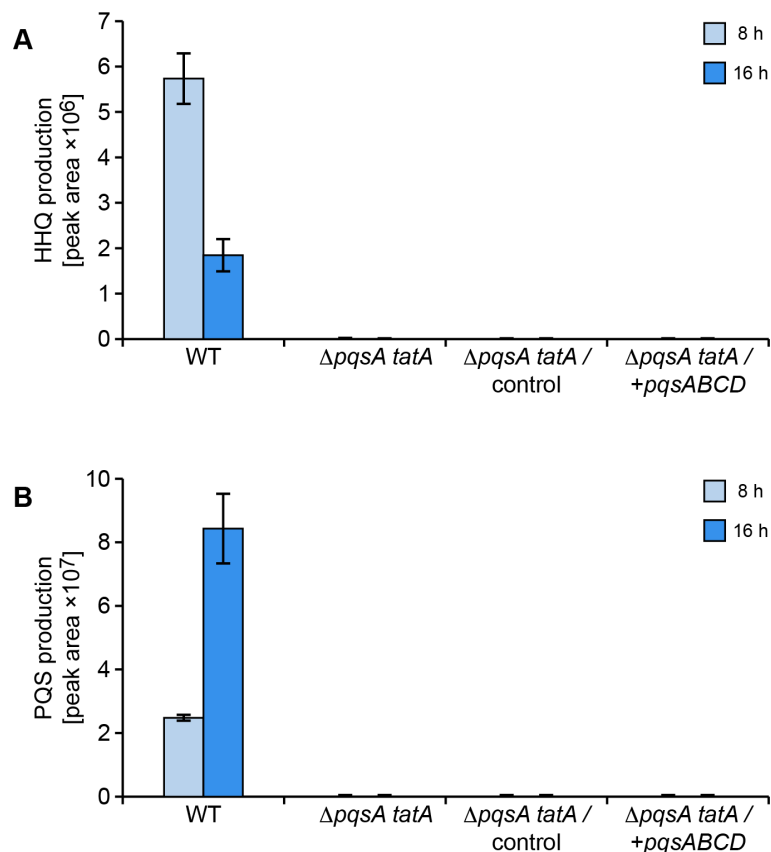


Fig. S4. HHQ and PQS do not accumulate intracellularly in a *tatA* $\Delta pqsA$ double mutant harboring the plasmid-borne *pqsABCD* genes in the absence of autoinduction. Semi-quantitative analysis by LC-MS/MS of PQS (**A**) and HHQ (**B**) extracted from whole cells of *P. aeruginosa* wild type and the *tatA* $\Delta pqsA$ mutant without (control) or with (+*pqsABCD*) the *pqsABCD* biosynthetic genes provided via pBBR1MCS-5::*pqsABCD*. Cells were harvested at 8 h and 16 h respectively. Experiments were repeated in triplicate.

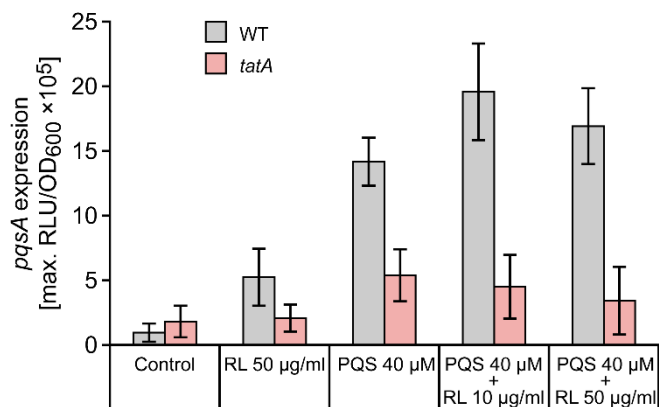


Fig. S5. Exogenous rhamnolipids do not enhance PQS-dependent expression of *pqsA* in a *tatA* $\Delta pqsA$ mutant. PQS (40 µM) was added with or without purified rhamnolipids (50 µg/mL) to a *pqsA* mutant or a *tatA* $\Delta pqsA$ mutant carrying chromosomal *pqsA*-*lux* fusions. Maximal light output as a function of growth (RLU/OD₆₀₀) is presented. Experiments were repeated in triplicate at least twice.

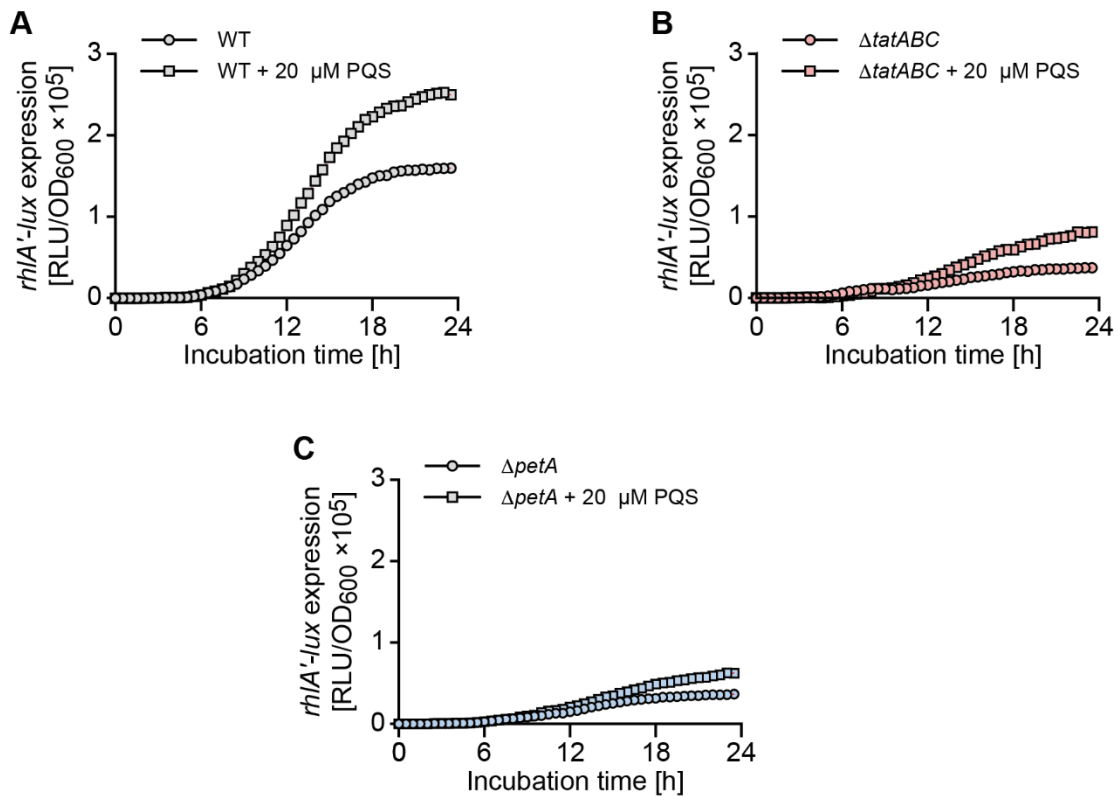


Fig. S6. Rhamnolipid biosynthesis gene *rhIA* shows altered expression profiles in *P. aeruginosa* PA14 ΔtatABC and ΔpetA mutants compared with wild type and fail to respond to exogenous PQS. Bioluminescence from a chromosomal *rhIA'*-*lux* fusion as a function of growth (RLU/OD) over time when introduced into (A) the PA14 wild type, (B) ΔtatABC and (C) ΔpetA mutants in the absence or presence of exogenous PQS (20 μM).

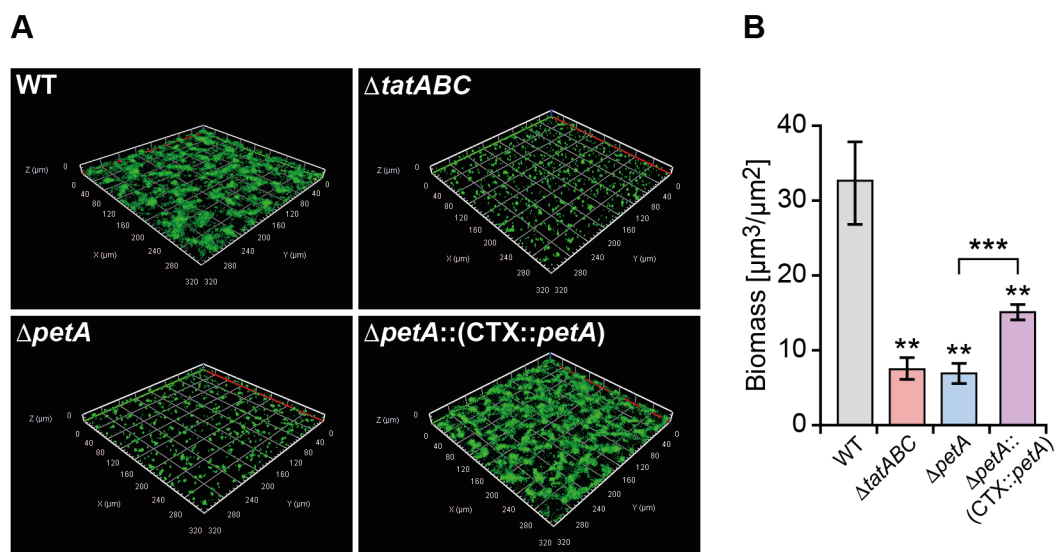


Fig. S7. Deletion of *petA* in *P. aeruginosa* PA14 results in a reduction in the eDNA content of biofilms. Biofilms of wild type PA14, the ΔtatABC and ΔpetA mutants and the genetically complemented PA14 mutant ($\Delta\text{petA}::(\text{CTX}::\text{petA})$) were

grown cultured statically and stained for eDNA with YOYO-1. **(A)** Confocal fluorescence microscopy images and **(B)** eDNA quantification. Experiments were repeated in triplicate at least twice. *** $p < 0.001$, ** $p < 0.01$.

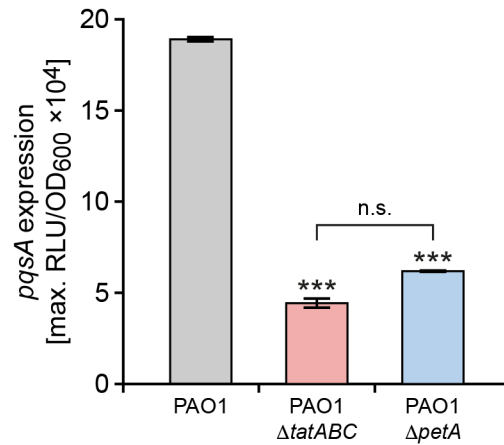


Fig. S8 Comparison of *pqsA* expression in *P. aeruginosa* PAO1 wild type, Δ *tatABC* and Δ *petA* mutants. Experiments were repeated in triplicate at least twice. *** $p < 0.001$, ** $p < 0.01$, and * $p < 0.05$; n.s. not significant.

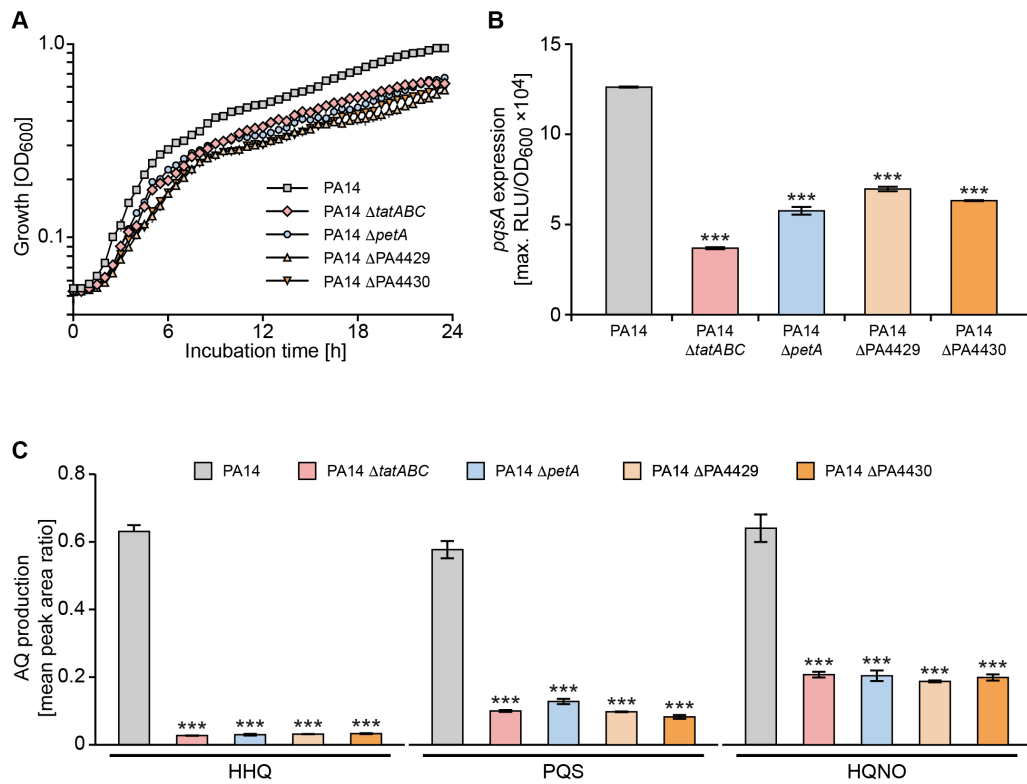


Fig. S9. Growth, *pqsA* expression and AQ production in wild type *P. aeruginosa* PA14 compared with Δ *cytB* (PA4429) and Δ *cytC1* (PA4430), Δ *petA* and Δ *tatABC* mutants. ***p < 0.001, **p < 0.01, and *p < 0.05; n.s. not significant.

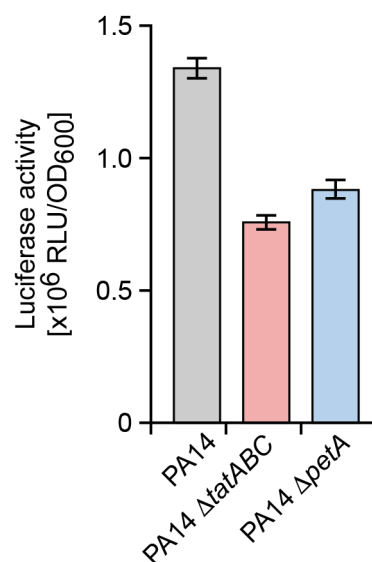


Fig. S10. Comparison of cellular ATP levels in *P. aeruginosa* PA14 wild type, Δ *tatABC*, and Δ *petA*. Experiments were repeated in triplicate at least twice.

RESEARCH ARTICLE

Disruption of the *Pseudomonas aeruginosa* Tat system perturbs PQS-dependent quorum sensing and biofilm maturation through lack of the Rieske cytochrome *bc₁* sub-unit

Eliza Ye-Chen Soh^{1†}, Frances Smith^{1‡}, Maxime Rémi Gimenez², Liang Yang^{3‡}, Rebecca Munk Vejborg⁴, Matthew Fletcher¹, Nigel Halliday¹, Sophie Bleves², Stephan Heeb¹, Miguel Cámara¹, Michael Givskov^{3,4}, Kim R. Hardie¹, Tim Tolker-Nielsen^{4*}, Bérengère Ize^{2*}, Paul Williams^{1*}

1 Biodiscovery Institute, National Biofilms Innovation Centre and School of Life Sciences, University of Nottingham, Nottingham, United Kingdom, **2** Laboratoire d'Ingénierie des Systèmes Macromoléculaires (LISM-UMR7255), Institut de Microbiologie de la Méditerranée, CNRS and Aix-Marseille University, Marseille, France, **3** Singapore Centre for Environmental Life Sciences Engineering, Nanyang Technological University, Singapore, **4** Costerton Biofilm Center, Department of Immunology and Microbiology, Faculty of Health Sciences, University of Copenhagen, Copenhagen, Denmark

‡ Current Address: School of Medicine, Southern University of Science and Technology, Guangdong, China

† These authors share first authorship on this work.

* ttn@sund.ku.dk (TT-N); bize@imsn.cnrs.fr (BI); paul.williams@nottingham.ac.uk (PW)



OPEN ACCESS

Citation: Soh EY-C, Smith F, Gimenez MR, Yang L, Vejborg RM, Fletcher M, et al. (2021) Disruption of the *Pseudomonas aeruginosa* Tat system perturbs PQS-dependent quorum sensing and biofilm maturation through lack of the Rieske cytochrome *bc₁* sub-unit. PLoS Pathog 17(8): e1009425. <https://doi.org/10.1371/journal.ppat.1009425>

Editor: Matthew Parsek, University of Washington, UNITED STATES

Received: February 23, 2021

Accepted: August 10, 2021

Published: August 30, 2021

Peer Review History: PLOS recognizes the benefits of transparency in the peer review process; therefore, we enable the publication of all of the content of peer review and author responses alongside final, published articles. The editorial history of this article is available here: <https://doi.org/10.1371/journal.ppat.1009425>

Copyright: © 2021 Soh et al. This is an open access article distributed under the terms of the [Creative Commons Attribution License](https://creativecommons.org/licenses/by/4.0/), which permits unrestricted use, distribution, and reproduction in any medium, provided the original author and source are credited.

Data Availability Statement: All relevant data are within the manuscript and its [Supporting Information](#) files.

Abstract

Extracellular DNA (eDNA) is a major constituent of the extracellular matrix of *Pseudomonas aeruginosa* biofilms and its release is regulated via pseudomonas quinolone signal (PQS) dependent quorum sensing (QS). By screening a *P. aeruginosa* transposon library to identify factors required for DNA release, mutants with insertions in the twin-arginine translocation (Tat) pathway were identified as exhibiting reduced eDNA release, and defective biofilm architecture with enhanced susceptibility to tobramycin. *P. aeruginosa* *tat* mutants showed substantial reductions in pyocyanin, rhamnolipid and membrane vesicle (MV) production consistent with perturbation of PQS-dependent QS as demonstrated by changes in *pqsA* expression and 2-alkyl-4-quinolone (AQ) production. Provision of exogenous PQS to the *tat* mutants did not return *pqsA*, *rhIA* or *phzA1* expression or pyocyanin production to wild type levels. However, transformation of the *tat* mutants with the AQ-independent *pqs* effector *pqsE* restored *phzA1* expression and pyocyanin production. Since mutation or inhibition of Tat prevented PQS-driven auto-induction, we sought to identify the Tat substrate(s) responsible. A *pqsA::lux* fusion was introduced into each of 34 validated *P. aeruginosa* Tat substrate deletion mutants. Analysis of each mutant for reduced bioluminescence revealed that the primary signalling defect was associated with the Rieske iron-sulfur subunit of the cytochrome *bc₁* complex. In common with the parent strain, a Rieske mutant exhibited defective PQS signalling, AQ production, *rhIA* expression and eDNA release that could be restored by genetic complementation. This defect was also phenocopied by deletion of *cytB* or *cytC₁*. Thus, either lack of the Rieske sub-unit or mutation of cytochrome *bc₁* genes results in the

Funding: This work was supported via grants to PW, MC and KH from the Biotechnology and Biological Sciences Research Council (BBSRC), U.K. (BB/F014392/1), BBSRC/National Biofilms Innovation Centre (BB/R012415/1), the Medical Research Council U.K. (MR/N501852/1), the Wellcome Trust (103884/Z/14/Z and 108876/Z/15/Z) and the European Union FP7 collaborative action grant (NABATIVI, 223670). BI was supported by a grant from Vaincre la Mucoviscidose and the Grégory Lemarchal associations (RF20140501138). TTN and MG were supported by grants from the Danish Strategic Research Council (9040-00023B), the Danish Council for Independent Research (09-065732), the Novo Nordisk Foundation (Biofilm2-AEEE/CPH) and the Lundbeck Foundation (2015-486), Denmark. The funders had no role in study design, data collection and analysis, decision to publish, or preparation of the manuscript.

Competing interests: No authors have competing interests

perturbation of PQS-dependent autoinduction resulting in eDNA deficient biofilms, reduced antibiotic tolerance and compromised virulence factor production.

Author summary

Pseudomonas aeruginosa is a highly adaptable human pathogen responsible for causing chronic biofilm-associated infections. Biofilms are highly refractory to host defences and antibiotics and thus difficult to eradicate. The biofilm extracellular matrix incorporates extracellular DNA (eDNA). This stabilizes biofilm architecture and helps confer tolerance to antibiotics. Since mechanisms that control eDNA release are not well understood, we screened a *P. aeruginosa* mutant bank for strains with defects in eDNA release and discovered a role for the twin-arginine translocation (Tat) pathway that exports folded proteins across the cytoplasmic membrane. Perturbation of the Tat pathway resulted in defective biofilms susceptible to antibiotic treatment as a consequence of perturbed pseudomonas quinolone (PQS) signalling. This resulted in the failure to produce or release biofilm components including eDNA, phenazines and rhamnolipids as well as microvesicles. Furthermore, we discovered that perturbation of PQS signalling was a consequence of the inability of *tat* mutants to translocate the Rieske subunit of the cytochrome *bc₁* complex involved in electron transfer and energy transduction. Given the importance of PQS signalling and the Tat system to virulence and biofilm maturation in *P. aeruginosa*, our findings underline the potential of the Tat system as a drug target for novel antimicrobial agents.

Introduction

Pseudomonas aeruginosa is an opportunistic pathogen that causes a wide range of human infections including lung, urinary tract and wound, bacteremia and infections associated with medical devices [1]. It is notorious for its tolerance to antimicrobial agents, a property that is largely a consequence of its ability to form biofilm communities [1,2]. Bacterial exoproducts including cell surface appendages, extracellular polymeric substances, biosurfactants and secondary metabolites all contribute to *P. aeruginosa* biofilm formation and maturation [3–7].

Apart from exopolysaccharides such as Psl, Pel and alginate, the extracellular polymeric matrix of *P. aeruginosa* biofilms incorporates proteins, rhamnolipids, membrane vesicles (MVs) and extracellular DNA (eDNA) [5,8–10]. Rhamnolipid biosurfactants are required during the initial stages of micro-colony formation and are involved in the migration-dependent formation of the caps of mushroom-shaped micro-colonies formed in flow-cell grown biofilms [10]. They also aid the maintenance of channels between multicellular structures within biofilms and contribute to biofilm dispersal [5]. With respect to the biofilm micro-colonies that characteristically form in flow-chambers fed with glucose minimal medium, eDNA is present at high concentrations in the outer layers of microcolonies in young biofilms. However, in mature biofilms, eDNA is primarily located in the stalks at the borders between micro-colony caps and stalks [8].

The release of eDNA occurs via the lysis of a sub-population of bacterial cells [10–14]. It is involved in attachment, aggregation and stabilization of biofilm microcolonies. eDNA can act as a nutrient source, chelate metal cations and confer tolerance to antibiotics such as the polymyxins and aminoglycosides [10,12,13]. eDNA also binds other biopolymers

(exopolysaccharides and proteins) stabilizing biofilm architecture and conferring protection against adverse chemical and physical challenges [12,13]. By intercalating with eDNA, secondary metabolites such as phenazines enhance biofilm integrity [12,15]. Pyocyanin for example can contribute to DNA release through the formation of reactive oxygen species such as hydrogen peroxide that damage cell membranes [12]. Although the mechanism(s) responsible for eDNA release has not been fully elucidated both eDNA and MVs can be generated via explosive cell lysis mediated via a cryptic prophage endolysin encoded within the R- and F-pyocin gene clusters [14].

In *P. aeruginosa*, rhamnolipids and pyocyanin production, eDNA and MV release, and hence biofilm development, are all controlled by quorum sensing (QS) [1,8,16]. Consequently, *P. aeruginosa* mutants with defects in this cell-to-cell communication system form aberrant, flat undifferentiated biofilms [10]. In *P. aeruginosa*, the QS regulatory network consists of a hierarchical cascade incorporating the overlapping Las, Rhl and PQS pathways that employ *N*-acylhomoserine lactones (AHLs) and 2-alkyl-4-quinolones (AQs) as signal molecules [1,16,17]. All three QS systems contain auto-induction loops whereby activation of a dedicated transcriptional regulator by the cognate QS signal molecule induces expression of the target synthase such that QS signal molecule production can be rapidly amplified to promote co-ordination of gene expression at the population level.

P. aeruginosa produces a diverse family of AQs and AQ *N*-oxides [18] of which 2-heptyl-3-hydroxy-4-quinolone (the *Pseudomonas* Quinolone Signal, PQS) and its immediate precursor 2-heptyl-4-hydroxyquinoline (HHQ) are most closely associated with PQS signalling [17] (Fig 1). Most of the genes required for AQ biosynthesis (*pqsABCDE*) and response (*pqsR/mvfR*) are located at the same genetic locus although *pqsH* and *pqsL* are distally located [17]. The biochemical basis for AQ and AQ *N*-oxide biosynthesis is summarized in S1 Fig. PqsA catalyses the formation of anthraniloyl-CoA that is condensed with malonyl-CoA by PqsD to form 2-aminobenzoylacetyl-CoA (2-ABA-CoA) [19,20]. The latter is converted to 2-aminobenzoylacetate (2-ABA) via the thioesterase functionality of PqsE [21]. The PqsBC heterodimer condenses 2-ABA with octanoyl-CoA to generate HHQ [22,23]. PQS is formed through the oxidation of HHQ by PqsH [24] while formation of the AQ *N*-oxides such as 2-heptyl-4-hydroxyquinoline *N*-oxide (HQNO) requires the alternative mono-oxygenase PqsL [25]. The PqsE protein has dual functions; while it is not essential for AQ biosynthesis, it is required for the AQ-independent production of several factors that contribute to biofilm maturation including pyocyanin, rhamnolipids and lectin A [26]. While activation of RhlR-dependent genes depends on PqsE [27], the AQ-independent, thioesterase-independent mechanism by which PqsE acts has not yet been elucidated [17,21].

The *pqs* system is subject to positive autoinduction, since the LysR-type transcriptional regulator PqsR (MvfR), binds to the promoter region of *pqsABCDE* (*PpqsA*) triggering transcription once activated by HHQ or PQS [28–30] (Fig 1). Therefore, by analogy with other QS systems, HHQ and PQS can both act as autoinducers by generating a positive feedback loop that accelerates their biosynthesis and co-ordinates a population-wide response. However, in contrast to HHQ which only regulates the *pqsABCDE* operon [17], PQS is a ferric iron chelator [31] that not only drives AQ biosynthesis via PqsR but also the expression of genes involved in the iron-starvation response and virulence factor production via PqsR-dependent and PqsR-independent pathways [17]. In addition, PQS can act as a cell-sensitizing pro-oxidant [32] and is required for MV production via a direct physical interaction with lipopolysaccharide (LPS) within the outer membrane [33]. The packaging of PQS within MVs also provides a means for trafficking this hydrophobic QS signal within a *P. aeruginosa* population [34].

With respect to biofilm development, PQS signalling is of particular interest because *pqsA* biosynthetic mutants fail to produce eDNA, rhamnolipids, pyocyanin and MVs, and form thin

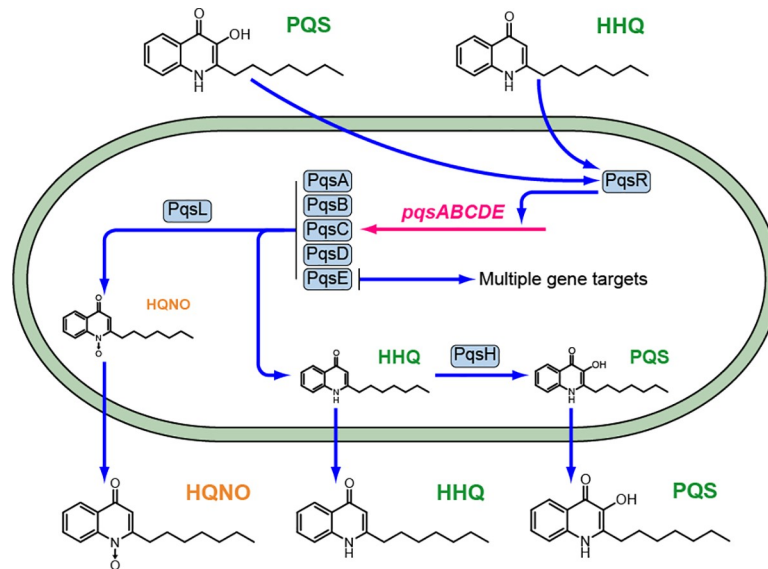


Fig 1. The PQS signalling pathway in *P. aeruginosa*. The PqsABCDE proteins synthesize HHQ, which is converted to PQS by PqsH and also HqNO in conjunction with PqsL. Both HHQ and PQS are released by the cells into the extracellular environment and are taken back up by neighboring cells. Autoinduction occurs when either HHQ or PQS binds to PqsR and amplifies expression of the *pqsABCDE* operon. The *pqsE* gene product has dual functions contributing to AQ biosynthesis as a thioesterase and also via an AQ-independent, thioesterase-independent mechanism for e.g. pyocyanin, rhamnolipid and lectin production as well as biofilm maturation. The conversion of HHQ to PQS confers additional functionalities since PQS unlike HHQ induces microvesicle formation and is a potent iron chelator.

<https://doi.org/10.1371/journal.ppat.1009425.g001>

defective biofilms containing little eDNA [8, 27,33,35]. The mechanism involved in PQS-mediated DNA-release in biofilms is not understood but has been suggested to be linked to phage induction causing cell lysis [8,36–40]. Although explosive cell lysis releases eDNA in biofilms and generates MVs through vesicularization of shattered membrane fragments, *pqsA* mutants are not defective for explosive lysis [14] and therefore this phenomenon is unlikely to account for PQS-dependent eDNA release.

In the present study we sought to identify additional factors involved in eDNA release by screening a transposon (Tn) mutant library for eDNA-release defective mutants. Apart from *pqs* biosynthetic mutants, we obtained Tn insertion mutants within the twin-arginine translocation (Tat) pathway that exhibited reduced levels of eDNA release, fail to produce rhamnolipids or pyocyanin and form defective, eDNA- poor, antibiotic susceptible biofilms. Since mutation or deletion of *tat* resulted in altered AQ production, reduced pyocyanin, rhamnolipid and MVs, and as the *tat* mutants were refractory to exogenously supplied PQS, the aberrant biofilm phenotype observed could be accounted for by perturbation of PQS autoinduction. By screening a library of *P. aeruginosa* Tat substrate mutants, we identified the Rieske sub-unit of the cytochrome *bc₁* complex as the Tat substrate required for PQS-dependent QS and hence eDNA release and biofilm maturation.

Results

Transposon mutagenesis screen for *P. aeruginosa* mutants exhibiting reduced DNA release

To identify *P. aeruginosa* genes that contribute to eDNA release, a mariner Tn mutant library was generated in strain PAO1. Approximately 10,000 mutants grown in microtitre plates were

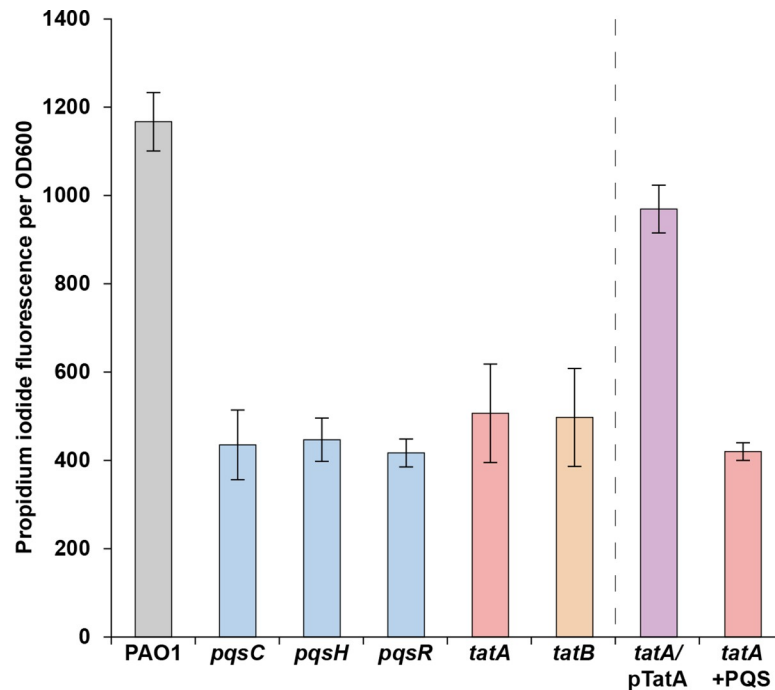


Fig 2. Transposon mutant screen for *P. aeruginosa* strains defective for eDNA release. *P. aeruginosa* wild-type and mutant strains were grown for 24 h in 96 well microtiter plates containing ABTG medium, after which the relative levels of eDNA in the cultures were determined using a PI binding assay. The means and standard deviations of eight replicates are shown.

<https://doi.org/10.1371/journal.ppat.1009425.g002>

assayed for reduced eDNA release using propidium iodide (PI) to quantify eDNA because it is unable to penetrate live bacteria and its fluorescence is enhanced 30-fold on binding DNA [41]. From the initial screen, 84 Tn insertion mutants were selected and re-screened to eliminate strains with double Tn insertions and to confirm their eDNA phenotype. For each of the remaining 34 mutants exhibiting reduced eDNA, the regions flanking each Tn insertion were sequenced and the corresponding genes identified. For most of the eDNA-release deficient mutants, the Tn insertions were located within genes required for AQ biosynthesis (*pqsC* and *pqsH*) or regulation (*pqsR*) (Fig 2). These data confirm our previous work that first uncovered a role for PQS signalling in eDNA release [8].

Apart from the *pqs* mutants, two mutants were obtained with insertions in the *tatA* and *tatB* genes respectively (Fig 2) that code for components of the twin-arginine translocation (Tat) system. Tat exports folded proteins out of the cytoplasm and across the cytoplasmic membrane in an ATP-independent manner [42]. It was originally named with respect to the presence of an Arg-Arg motif in the signal sequence of Tat-exported products (sometimes called Tat substrates) [42,43]. In *P. aeruginosa* the Tat translocase complex consists of three proteins (TatA, B and C) [43]. TatB and TatC form the receptor complex for Tat substrate precursors whereas TatA functions as the main facilitator for protein translocation across the membrane [42]. In *P. aeruginosa* diverse proteins involved in phosphate and iron metabolism, virulence and energy transduction are exported to the periplasm, or secreted via the Tat export system and *tat* mutants exhibit pleiotropic phenotypes [44,45]. Fig 2 shows that genetic complementation of the *P. aeruginosa* *tatA* mutant with a plasmid-borne copy restored eDNA release.

The Tat pathway contributes to biofilm development and tobramycin susceptibility in *P. aeruginosa*

Since eDNA makes an important contribution to biofilm development and architecture [10,12,13], biofilm formation by the *P. aeruginosa* *tatA* mutant in flow-chambers was investigated. After 4-days growth, the *P. aeruginosa* wild-type and complemented *tatA/pTatA* mutant formed biofilms with mushroom-shaped structures whereas the *tatA* mutant formed thin, flat biofilms (Fig 3A). In addition, eDNA was observed primarily in the stalks of the mushroom-shaped structures in the wild-type whereas *tatA* mutant biofilms contained no stalks and little extracellular DNA. Consistent with this flow-cell biofilm phenotype, exposure of the biofilms formed by each of the three strains to tobramycin showed that the *tatA* mutant biofilm was more sensitive to tobramycin than either the wild-type or *tatA/pTatA* mutant biofilm (Fig 3B). Since eDNA binds positively charged antibiotics and as exogenously provided DNA increases aminoglycoside tolerance by integrating into *P. aeruginosa* biofilms, the increased sensitivity to tobramycin is likely to be a consequence of the reduction in eDNA within the biofilm extracellular matrix [46,47].

P. aeruginosa *tatA* mutants are defective in the production of rhamnolipids, pyocyanin and MVs

Since rhamnolipids, pyocyanin and MVs are all important components of *P. aeruginosa* biofilms, their production was quantified in the *tatA* Tn insertion mutant and in a Δ *tatABC*

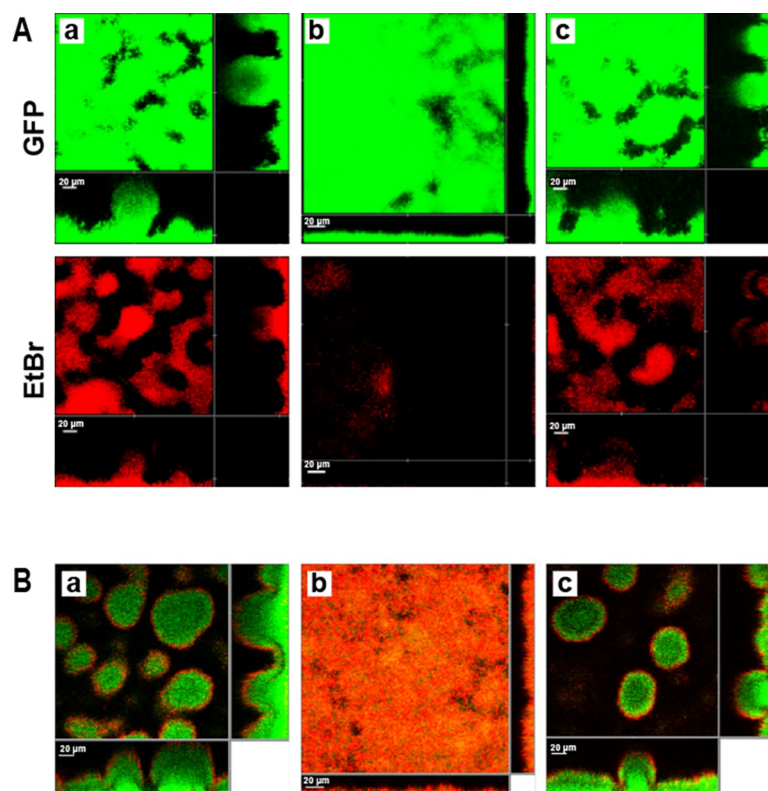


Fig 3. *P. aeruginosa* *tat* mutants form defective biofilms with increased susceptibility to tobramycin. CLSM images showing four-day-old biofilms formed in flow chambers of the *gfp*-tagged *P. aeruginosa* wild-type (a), *tatA* mutant (b) and genetically complemented *tatA* mutant (c). In (A) biofilms were stained for total biomass with Syto9 (green) and for eDNA with ethidium bromide (red). In (B) biofilms were treated with tobramycin and the medium was supplemented with propidium iodide prior to CLSM such that dead cells appear red while live cells appear green. Each panel shows one horizontal optical section two flanking vertical optical sections. Bars, 20 μm.

<https://doi.org/10.1371/journal.ppat.1009425.g003>

deletion mutant. **Fig 4A and 4B** show that *tat* mutants produce substantially less pyocyanin and rhamnolipid than the parent or *tatA* complemented strain. Furthermore, MV levels (**Fig 4C**) were reduced by ~50% in the *tatA* mutant compared with the wild type and could be restored by genetic complementation.

Inactivation of the Tat pathway by mutation or small molecule-mediated inhibition perturbs PQS signalling

The reductions in eDNA release, rhamnolipids, pyocyanin and MVs noted in the *tat* mutant as well as its biofilm phenotype are comparable with those observed for *P. aeruginosa* strains with mutations in *pqs* genes such as *pqsA*, the first gene in the AQ biosynthetic pathway (see **Figs 1 and 4** and [8, 40]). These data therefore suggested that the *tat* mutant biofilm phenotype was likely, at least in part, to be due to a defect in PQS signalling. To investigate the impact of the *tatA* mutation on the expression of *pqsA*, a CTX::*pqsA*'-lux fusion was introduced into the chromosomal CTX site of both the wild type and *tatA* mutant. **Fig 5A** shows that *pqsA* expression in the *tatA* mutant is reduced ~4 fold compared with the wild type strain and restored by genetic complementation of the mutant. In agreement with these data, the Tat inhibitor, Bayer 11-7082, identified by Vasil *et al* [48] reduced *pqsA* expression in the wild type PAO1 strain by ~4 fold consistent with the reduction noted for the CTX::*pqsA*'-lux fusion in the *tatA* mutant (**Fig 5B**). Bayer-11 7082 had no effect on growth or light output in *P. aeruginosa* expressing the *lux* genes from a derepressed *lac* promoter (**S2 Fig**). In addition, the concentration of PQS in whole culture extracts of *P. aeruginosa* after growth in LB medium as determined by LC-MS/MS was respectively ~56% lower in the *tatA* mutant compared with the wild type and complemented *tat* mutant (**Fig 5C**). Since *pqsA* expression and hence AQ production is also PqsR/MvfR-dependent, we compared the expression of *pqsR* in the Δ *tatABC* with the parent strain but found no difference (**S3 Fig**).

Exogenous PQS does not restore PQS signalling in a *P. aeruginosa* *tatA* mutant

QS systems are characteristically autoinducible such that exogenous provision of the cognate signal molecule usually induces expression of the signal synthase and hence activation of downstream target genes [49]. When the *tatA* mutant was provided with exogenous PQS, eDNA release did not increase (**Fig 2**). To investigate this finding further, either PQS or HHQ was exogenously supplied to the wild type, *tatA* mutant or the complemented *tatA* mutant strains carrying chromosomal *pqsA*'-lux fusions. The data presented in **Fig 6A** show that the response of the *tatA* mutant to PQS or HHQ respectively at 5 or 20 μ M with respect to *pqsA* expression was at least 2-fold lower than the controls. Since both wild type and *tatA* mutant still produce Aqs endogenously, the experiments were repeated in the *P. aeruginosa* Δ *pqsA* and *tatA* Δ *pqsA* mutants since no Aqs are produced in these genetic backgrounds. **Fig 6B** shows that the response to both PQS and HHQ is substantially reduced (e.g. ~3 fold at 5 μ M PQS) in the absence of *tatA* in the *P. aeruginosa* *tatA* Δ *pqsA* double mutant. This reduced response to PQS could be due either to reduced uptake or the inability to respond to the exogenous QS signal molecule.

To determine the consequences of perturbed PQS signalling on the expression of the rhamnolipid (*rhlA*) and pyocyanin biosynthetic genes (*P. aeruginosa* has two, almost identical redundant 7 gene phenazine biosynthetic operons termed *phzA1-G1* and *phzA2-G2*; [50]), the corresponding miniCTX-lux promoter fusions for *rhlA* and *phzA1* respectively were constructed and introduced onto the chromosomes of the wild type, Δ *pqsA* and *tatA* Δ *pqsA* mutants respectively. **Fig 7A** shows the expression profiles of *rhlA*'-lux as a function of time.

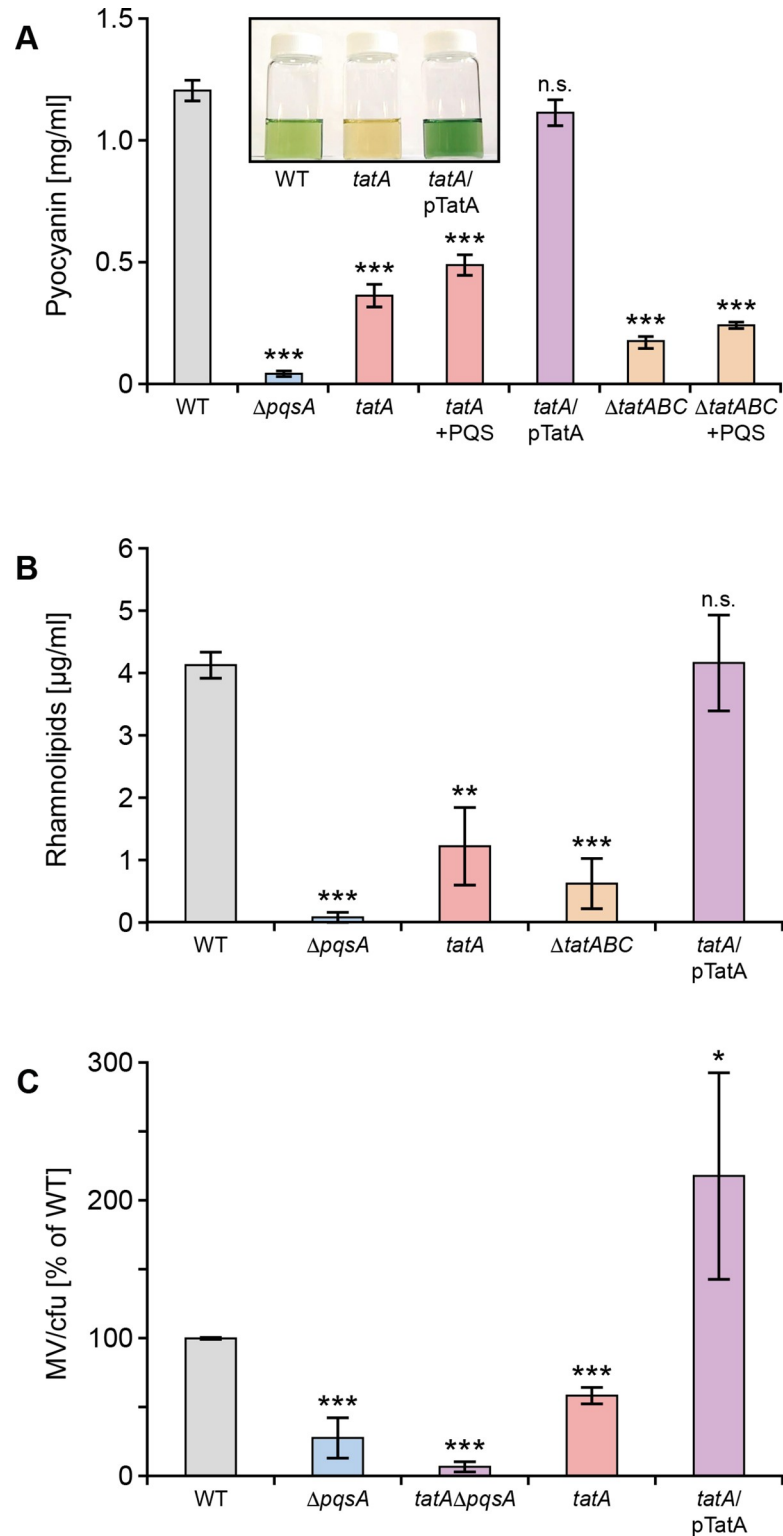


Fig 4. Production of pyocyanin (A), rhamnolipids (B) and MVs (C) are reduced in *P. aeruginosa* *tat* mutants. (A) Pyocyanin levels are shown in the *P. aeruginosa* wild type, $\Delta pqsA$, *tatA*, and *tatABC* deletion mutants and the *tatA* mutant complemented with plasmid-borne *tatA*. The impact of exogenous PQS (40 μM) on the *tatA* and $\Delta tatABC$ mutants is also shown. Insert panel shows the absence of green pigment in the *tatA* mutant compared with the wild type and complemented *tatA* mutant. (B) Rhamnolipid production in the *tatA* and $\Delta tatABC$ mutants compared with

the wild type, $\Delta pqsA$ mutant and *tatA* complemented with plasmid-borne *tatA*. (C) Comparison of MV production in the *tatA* mutant, complemented *tatA* mutant and in a double *tatA* $\Delta pqsA$ mutant compared with the wild type strain. Experiments were repeated in triplicate at least twice. *** $p < 0.001$, ** $p < 0.01$; n.s. not significant.

<https://doi.org/10.1371/journal.ppat.1009425.g004>

Both the wild type and $\Delta pqsA$ mutant show an ~2 fold increase in *rhlA* expression when supplied with exogenous PQS (20 μ M) and share similar profiles over the growth curve. In contrast, the *rhlA*'-lux fusion in the *tatA* mutant does not show the same expression profile or response to exogenous PQS as the wild type and $\Delta pqsA$ mutant strains. The *rhlA*'-lux expression profile in the *tatA* mutant supplied with exogenous PQS is however clearly restored when the mutation is complemented by pTatA (Fig 7A).

AQ-dependent QS is required for *phzA1* expression [27,50]. Exogenous PQS increased *phzA1*'-lux expression by ~4 fold in both wild type and $\Delta pqsA$ mutant backgrounds (Fig 7B). However, the *tatA* $\Delta pqsA$ double mutant responded comparatively poorly to PQS (Fig 7B).

Constitutive expression of *pqsABCD* does not restore AQ biosynthesis in a *tat* mutant

Since mutation of *tatA* resulted in reduced *pqsA* expression, it was possible that the auto-induction of PQS biosynthesis via PqsR (MvfR) is compromised. To uncouple the autoinduction of AQ production, the *pqsABCD* genes were introduced into the *P. aeruginosa* $\Delta pqsA$ and $\Delta pqsA\Delta tatA$ mutants respectively on a plasmid (pBBRMCS5::*pqsABCD*) constitutively expressing *pqsABCD* [51]. Fig 8 shows that PQS, HHQ and HQNO are present in the culture medium of the $\Delta pqsA$ mutant transformed with pBBRMCS5::*pqsABCD*. However neither the cell free supernatant (Fig 8) nor whole cells of the *tatA* $\Delta pqsA$ double mutant transformed with pBBRMCS5::*pqsABCD* contained or accumulated intracellular AQS (S4 Fig). These data suggested that in a *tat* mutant background, the lack of AQS is not a consequence of an AQ transport defect, but is due to the inability to fully activate AQ biosynthesis at the appropriate time/population density. In the absence of an auto-inducible *pqs* system in a *tat* mutant background, the defect in AQ biosynthesis and hence PQS signalling appears to be more severe.

Reduced rhamnolipid production does not account for defective PQS signalling

In *P. aeruginosa* biofilms, rhamnolipids provide protective shielding against neutrophils [52,53] and contribute to the effectiveness of PQS signalling by increasing the solubility and bioactivity of PQS [54]. In Fig 4B, we showed that rhamnolipid production was substantially reduced in the *P. aeruginosa* *tat* mutant background. To determine whether the perturbation of PQS signalling in the *tat* mutants was a consequence of reduced rhamnolipid production, we investigated the impact of exogenous rhamnolipids on *pqsA* expression. S5 Fig shows that the addition of purified rhamnolipids (10 or 50 μ g/ml) to the *tatA* $\Delta pqsA$ mutant with or without PQS (40 μ M) had little effect on PQS signalling indicating that the defect in the *tat* mutants was not simply due to the loss of rhamnolipid production and an inability to solubilize PQS.

PqsE restores pyocyanin in the *tat* mutants

Although PqsE is not essential for AQ biosynthesis, it is an effector protein required for the production of pyocyanin, rhamnolipids and biofilm maturation and its function is independent of PQS, HHQ or PqsR [27,55]. Consequently, the expression of PQS -dependent exoproducts such as pyocyanin can be restored in a *pqsA* negative (and hence AQ-negative) mutant by expressing a plasmid-borne copy of *pqsE*. In the *tatA* $\Delta pqsA$ double mutant, *phzA1*

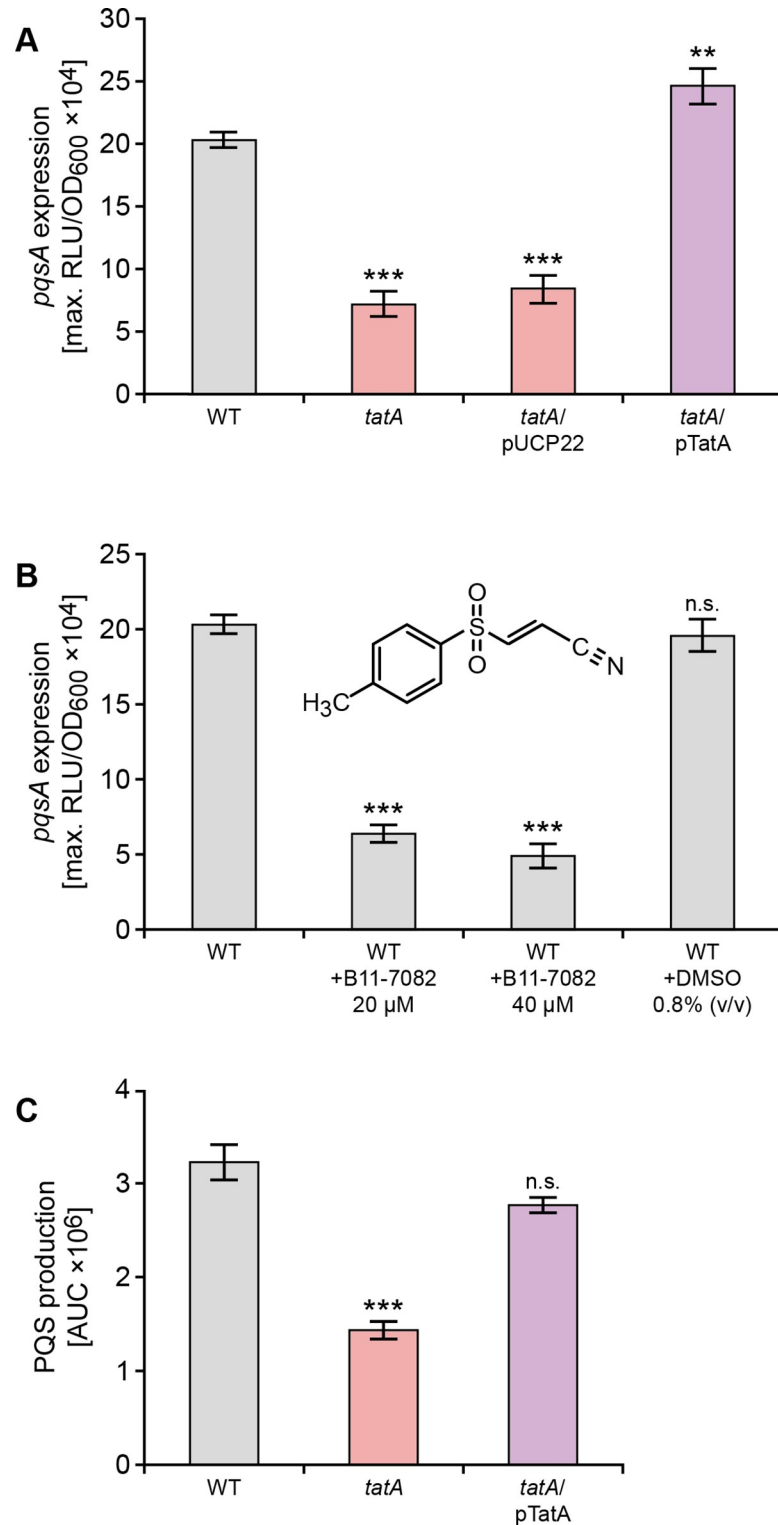


Fig 5. Mutation of *tatA* or exposure to the Tat inhibitor Bayer 11-7082 inhibits *pqsA* expression and AQ production. (A) Mutation of *tatA* or (B) treatment with Bayer 11-7082 supplied at either 20 μM or 40 μM reduces the maximal expression of a *P. aeruginosa* PAO1 chromosomal *pqsA*-*lux* promoter fusion without affecting growth. (C) LC-MS/MS analysis of PQS production by *P. aeruginosa* PAO1 wild type compared with the *tatA* mutant and complemented *tatA* mutant. Experiments were repeated in triplicate at least twice. ****p* < 0.001; n.s. not significant.

<https://doi.org/10.1371/journal.ppat.1009425.g005>

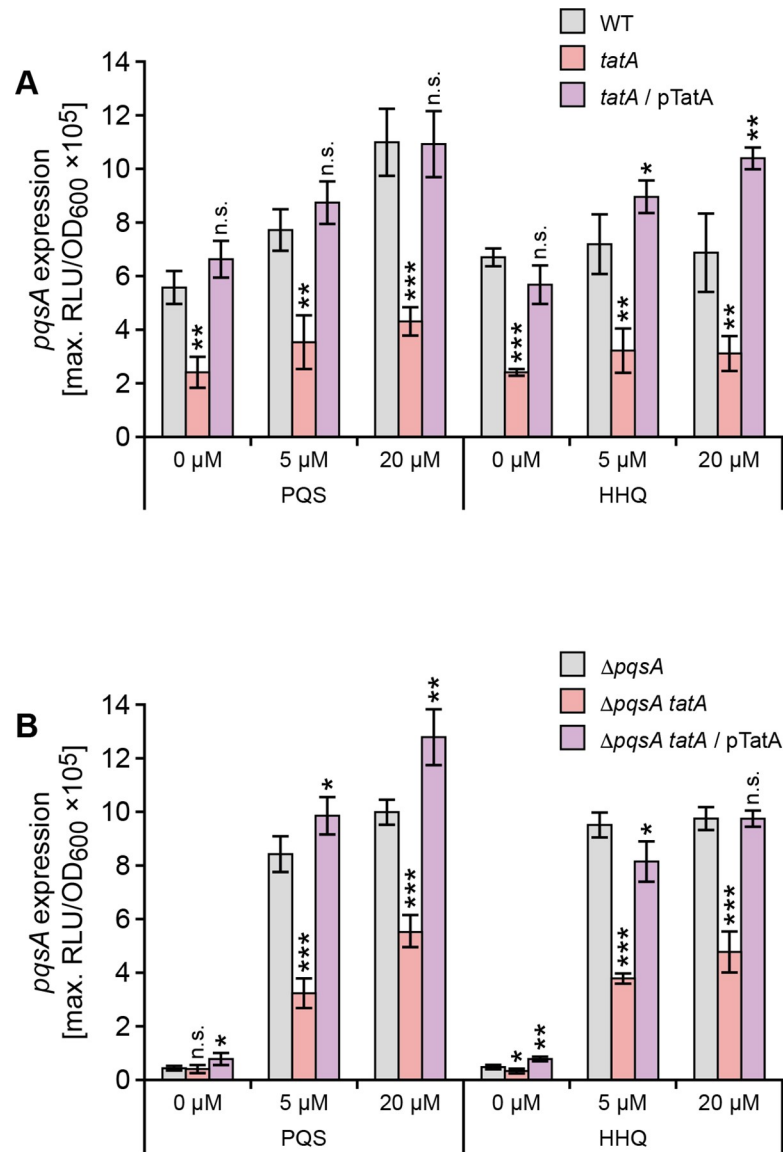


Fig 6. Exogenous AQs do not restore *pqsA* expression in *P. aeruginosa* *tatA* (A) or *tatA* $\Delta pqsA$ (B) mutants. Exogenous PQS or HHQ was added at 5 μ M or 20 μ M to (A) wild type, the *tatA* mutant and complemented *tatA* mutant or (B) $\Delta pqsA$, $\Delta pqsA$ *tatA* or *tatA* $\Delta pqsA$ mutant complemented with *tatA*. Maximal light output from the chromosomal *pqsA*-*lux* fusion was recorded as a function of growth (RLU/OD₆₀₀). Experiments were repeated in triplicate at least twice. ***p < 0.001, **p < 0.01, and *p < 0.05; n.s. not significant.

<https://doi.org/10.1371/journal.ppat.1009425.g006>

expression (Fig 7B) and pyocyanin production (Fig 9) were respectively restored by *pqsE* expression indicating that the *tat* mutation does not affect PqsE functionality.

Identification of the Tat substrate responsible for perturbation of PQS signalling

Recently Gimenez et al [45] experimentally validated the Tat-mediated export of 34 *P. aeruginosa* gene products predicted to have Tat signal peptides. To determine which of the exported Tat substrates was responsible for perturbation of PQS signalling, allelic replacement mutants were constructed in *P. aeruginosa* strain PA14 for each substrate. Before introducing the

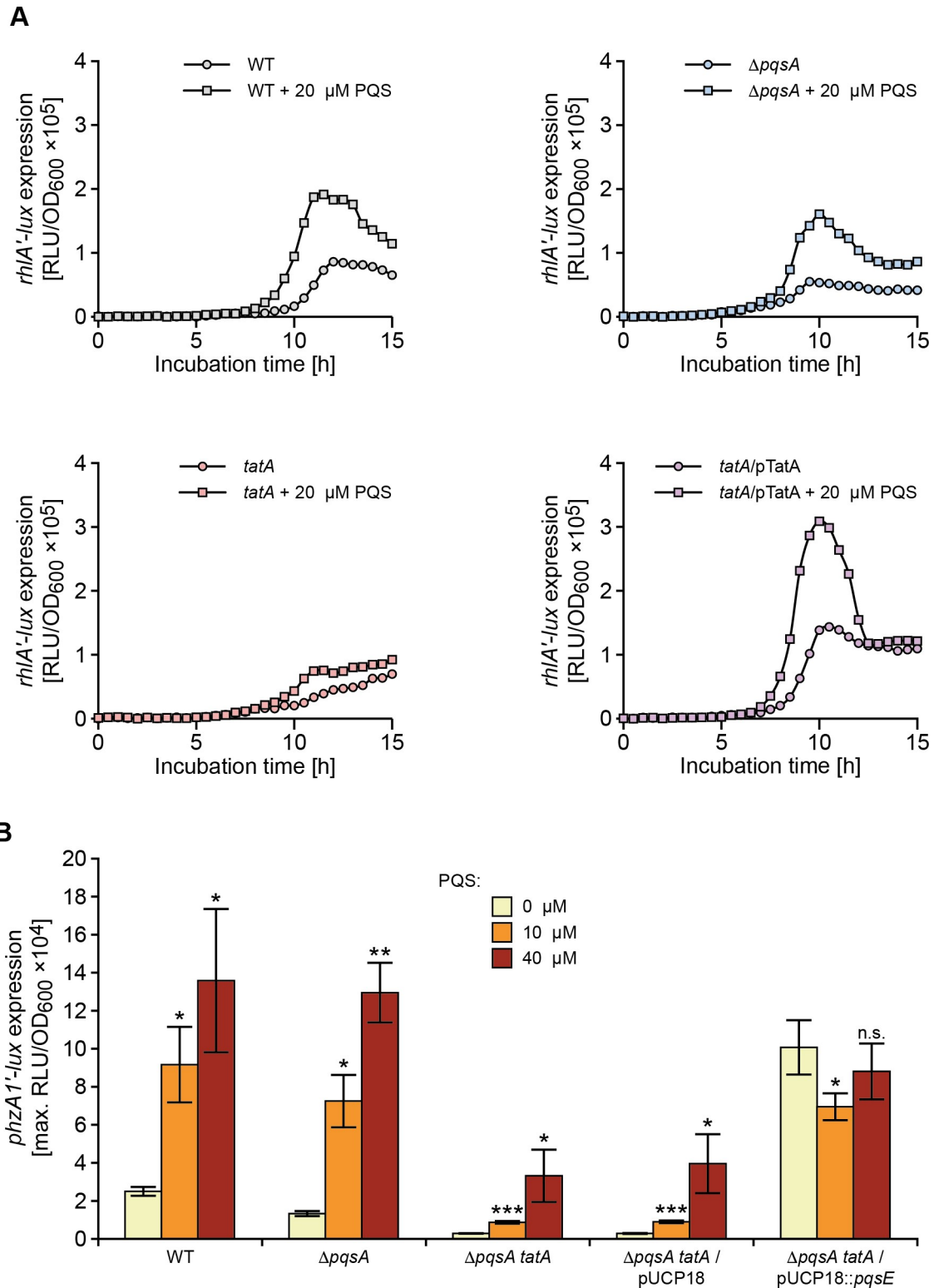


Fig 7. Rhamnolipid (*rhlA*) and pyocyanin biosynthetic (*phzA1*) genes show altered expression profiles in *P. aeruginosa* *tat* mutants and fail to respond to exogenous PQS. (A) Light output from a chromosomal *rhlA'*-*lux* fusion as a function of growth (RLU/OD) over time when introduced into the wild type, *pqsA* and *tatA* mutants or complemented *tatA* mutant in the absence or presence of exogenous PQS (20 μM). (B) Maximal light output from a chromosomal *phzA1'*-*lux* fusion as a function of growth (RLU/OD₆₀₀) when introduced into the wild type, Δ*pqsA*, or Δ*pqsA* *tatA* mutants in the absence or presence of exogenous PQS (10

or 40 μM) or plasmid-borne *pqsE* or the pUCP18 vector control. Experiments were repeated in triplicate at least twice. *** $p < 0.001$, ** $p < 0.01$, and * $p < 0.05$; n.s. not significant.

<https://doi.org/10.1371/journal.ppat.1009425.g007>

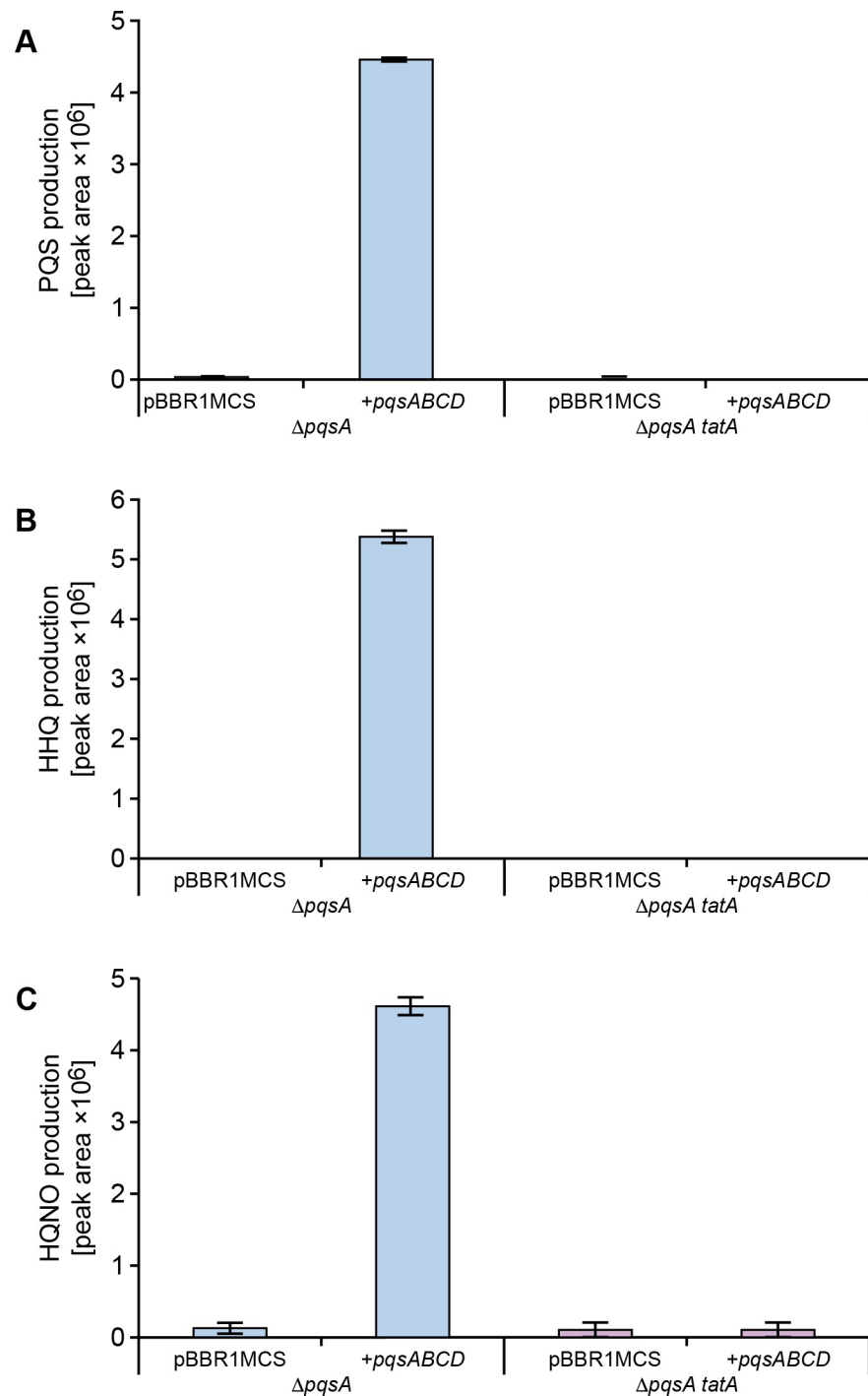


Fig 8. AQ biosynthesis is not restored in a *tatA* $\Delta pqsA$ double mutant by plasmid-borne *pqsABCD* in the absence of autoinduction. Semi-quantitative analysis by LC-MS/MS of PQS, HHQ and HQNO production by *P. aeruginosa* *pqsA* and *tatA* $\Delta pqsA$ mutants respectively without or with the *pqsABCD* biosynthetic genes provided *in trans* via pBBR1MCS-5::*pqsABCD*. Experiments were repeated in triplicate at least twice.

<https://doi.org/10.1371/journal.ppat.1009425.g008>

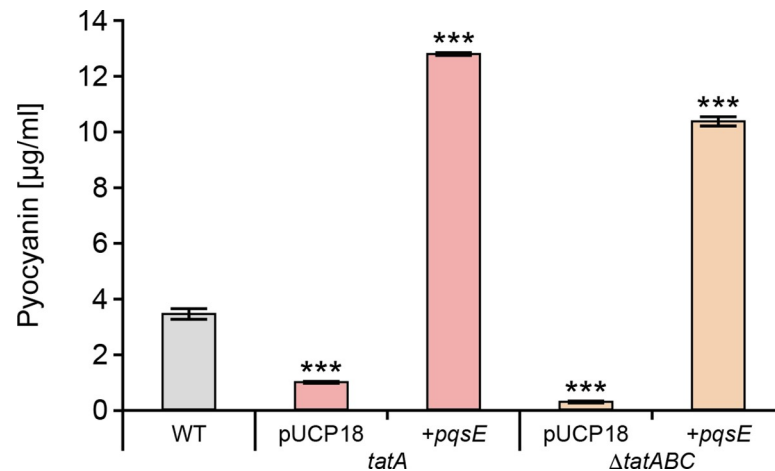


Fig 9. PqsE restores pyocyanin production in *P. aeruginosa* *tat* mutants. Production of pyocyanin by the wild type compared with the *tata* and Δ *tatABC* mutants transformed with plasmid-borne *pqsE* or the empty vector. Experiments were repeated in triplicate at least twice. ****p* < 0.001.

<https://doi.org/10.1371/journal.ppat.1009425.g009>

pqsA'-lux fusion onto the chromosomal CTX site of each Tat substrate mutant, we first confirmed that PQS signalling in a PA14 Δ *tatABC* mutant was perturbed in a similar manner to that observed for PAO1, the genetic background used so far in the study (Fig 10A). Determination of the maximum expression of *pqsA*'-lux for each of the 34 Tat substrate mutants (Fig 10A) revealed that although a number of mutants exhibited reduced light output, the greatest reduction was observed for deletion of PA14_57570 (equivalent to PA4431 in PAO1, here designated *petA* following the nomenclature of orthologues described in other species). This gene codes for the Rieske subunit of the cytochrome *bc*₁ complex that is involved in electron transfer and respiration under aerobic conditions and is also required for *P. aeruginosa* growth under anaerobic conditions in the presence of nitrite, nitric oxide or nitrous oxide [56].

To confirm that the Δ *petA* mutant in common with the *P. aeruginosa* *tat* mutants exhibited similar defects as a consequence of perturbed PQS signalling, we compared their AQ production (Fig 10B), *rhlA* expression, and eDNA release in biofilms (S6 and S7 Figs). Comparison of PQS, HHQ and HQNO production in PA14 with the Δ *petA* mutant and the strain with a *cis* complementation of the *petA* mutation at the CTX site confirmed the loss and increase in AQ production (Fig 10B). Similar results were obtained for *pqsA* expression in a PAO1 Δ *petA* mutant (S8 Fig). In *P. aeruginosa* PA14, the *rhlA* expression profiles for the parent and Δ *tatABC* deletion mutant in the absence or presence of exogenously supplied PQS were similar to those of strain PAO1 (compare S6 Fig with Fig 7A). Confocal microscopy images of biofilm formation by *P. aeruginosa* PA14 under static growth conditions shows that in common with the Δ *tatABC* mutant, Δ *petA* mutant biofilms lack the eDNA content observed in the wild type and complemented mutant (S7 Fig) demonstrating that PetA is the primary Tat substrate required for PQS-dependent eDNA release. Since PetA is one of the three electron transfer proteins that constitute the cytochrome *bc*₁ complex we also investigated whether mutation of *cytB* and *cytC*₁ genes (PA4429 and PA4430 respectively) perturbed PQS-signalling. S9 Fig shows Δ *cytB* and Δ *cytC*₁ mutants also exhibited reduced *pqsA* expression and AQ production indicating that a fully functional cytochrome *bc*₁ is essential for PQS-dependent QS. Given the importance of cytochrome *bc*₁ for energy transduction and growth, we also compared aerobic growth and ATP production in the *P. aeruginosa* wild type with that of the *tat* and *petA* mutants. S9 Fig shows that there is a similar small reduction in growth for mutants compared

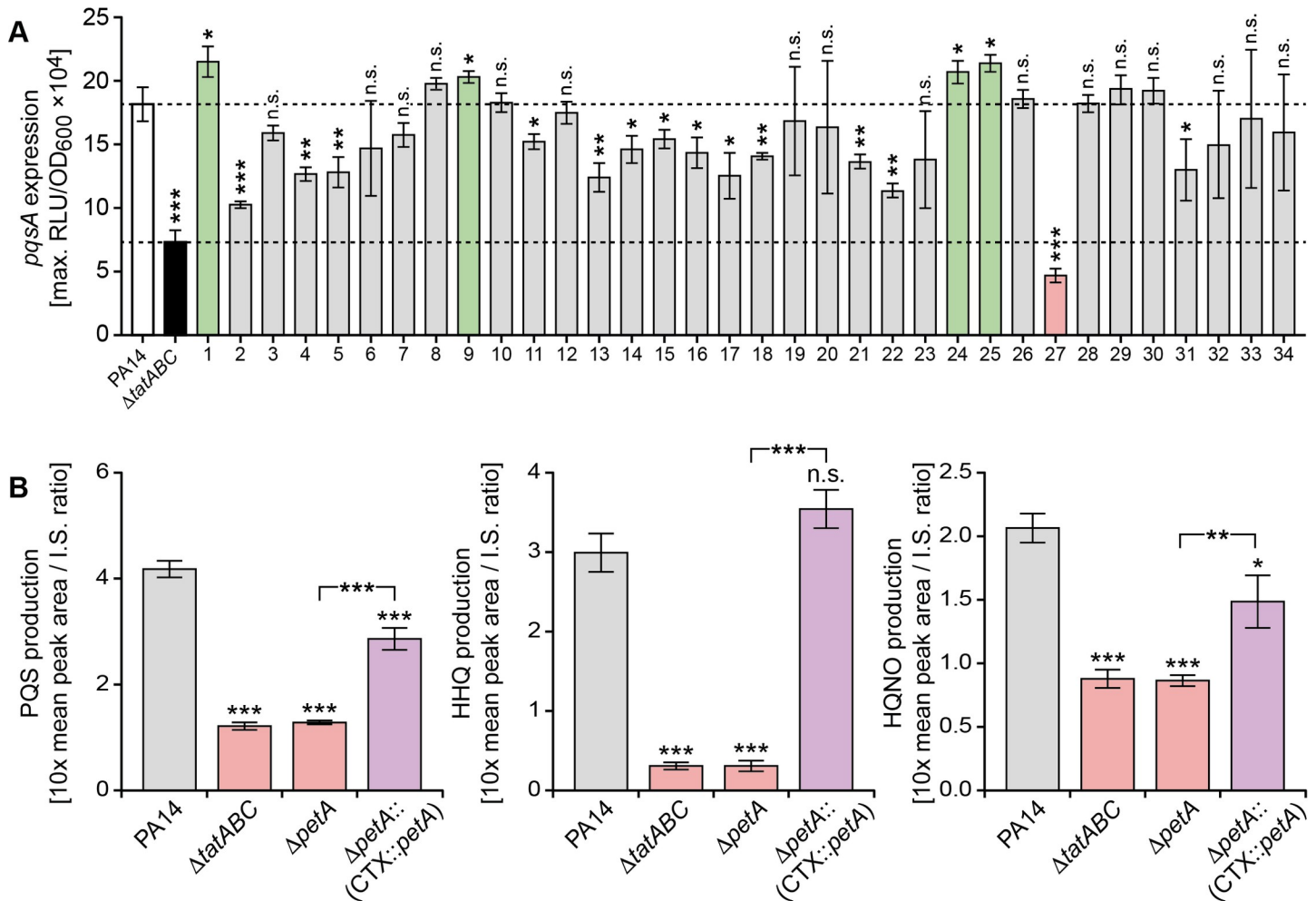


Fig 10. Tat substrate screen for *P. aeruginosa* PA14 mutants with defects in *pqs* signaling uncovers a role for the cytochrome *bc₁* Rieske sub-unit. (A) Comparison of peak *pqsA* expression in each of 34 Tat substrate mutants (S3 Table) transformed with a CTX::*pqsA*'-lux fusion compared with the PA14 wild type (white bar) and the *ΔtatABC* mutant (black bar). The bars represent mutants where *pqsA* expression is higher (green bar) or lower (grey bar) as the wild type. PA14 mutant 27 (pink bar) has the lowest *pqsA* expression and carries a deletion in PA14-57570 (*petA*), the Rieske subunit of cytochrome *bc₁*. (B) Production of PQS, HHQ and HQNO after 16 h growth by *P. aeruginosa* PA14, the *ΔtatABC* and *ΔpetA* mutants and the genetically complemented PA14 mutant (*ΔpetA*::(CTX::*petA*)). ***p < 0.001, **p < 0.01, and *p < 0.05; n.s. not significant.

<https://doi.org/10.1371/journal.ppat.1009425.g010>

with the wild type. Consistent with these observations, ATP levels were reduced by ~35% in the *Δtat* and *ΔpetA* mutants respectively compared with wild type (S10 Fig). This finding suggested that in *P. aeruginosa* strains carrying mutations in *tat* or cytochrome *bc₁* the energy required to synthesize secondary metabolites such as the AQs is diverted to maintain primary metabolism.

Discussion

To gain further insights into eDNA release, a *P. aeruginosa* Tn mutant library was screened and two groups of mutants exhibiting reduced eDNA release were identified. The first of these contained Tn insertions in *pqsC*, *pqsH* and *pqsR*. Mutations in *pqsC* or *pqsR* in common with *pqsA* both abrogate AQ biosynthesis while *pqsH* mutants are unable to produce 3-hydroxy-AQs such as PQS but maintain production of AQs and AQ N-oxides such as HHQ and HQNO respectively [17, 54]. These data suggest that eDNA release is likely to require

PQS/HHQ rather than the effector protein PqsE. This is because although *pqsE* mutants in common with *pqsA* mutants form poor biofilms, *pqsE pqsA* double mutants could not be complemented by *pqsE* alone to restore biofilm development [26]. This contrasts with pyocyanin and lectin A for example, as production of both can be restored by PqsE in the absence of AQ biosynthesis [26].

The Tn insertions in the second group of *P. aeruginosa* eDNA release mutants were in *tatA* and *tatB* [42,43]. In *P. aeruginosa*, proteins exported by the Tat system are most frequently terminally localized in the periplasm, but some (e.g. phospholipase C) can be transported across the outer membrane by the Xcp type II secretion system, thereby becoming extracellular [43]. Using prediction algorithms for Tat substrates, 44 putative *P. aeruginosa* PA14 Tat signal peptides have been identified and of these, 34 confirmed experimentally [45]. These include phospholipases, and proteins involved in pyoverdine-mediated iron-uptake, respiration, osmotic stress defence, motility, and biofilm formation [44, 45]. However, none of these are known to be involved in AQ biosynthesis, transport or PQS signal transduction.

The formation of flat, eDNA deficient, tobramycin-sensitive biofilms and the reduction in rhamnolipid, pyocyanin and MV production by the *P. aeruginosa* *tatA* mutant are consistent with the *pqsA* mutant biofilm phenotype [8] and implied the existence of a link between Tat export and PQS signalling. Since transcriptomic studies of PQS signalling in *P. aeruginosa* have not provided any evidence that the Tat export system is QS controlled [17,26], we considered it likely that mutation of the *tat* genes resulted in perturbed PQS signalling. This observation could also account, at least in part, for the reduced virulence of *P. aeruginosa* *tat* mutants in a rat pulmonary infection model [44]. For both *P. aeruginosa* PAO1 and PA14 strains *pqsA* expression and AQ production were reduced in the respective *tat* mutants while exogenous provision of either PQS or HHQ failed to fully restore *pqsA* expression in a *tatA ΔpqsA* mutant. The consequences of perturbed PQS signalling are clearly apparent in the altered expression profiles of the *rhlA*²-*lux* and *phzA1*²-*lux* fusions. Thus disruption of Tat clearly impairs the ability of *P. aeruginosa* either to fully induce PQS-dependent QS or to respond fully to exogenous PQS.

Since pyocyanin can be produced in the absence of PQS by ectopic expression of *pqsE* [26], it was possible that the *tat* phenotype was either a consequence of the inability of PQS/HHQ to activate the *pqsABCDE* operon via PqsR to generate sufficient PqsE protein or because the activity of PqsE depends on a functional Tat system. However, introduction of a plasmid-borne copy of *pqsE* into the *tat* mutants fully restored pyocyanin production suggesting that the *tat* mutant phenotype is not due to the inability of PqsE to function but rather a failure of the PQS auto-induction circuitry to produce sufficient PQS/HHQ to efficiently activate *pqsABCDE*.

To uncover a direct link between Tat and PQS signalling, we screened a bank of Tat substrate mutants for reduced *pqsA* expression and identified PetA as primarily responsible for the PQS signalling defect. As PetA is one of the three protein sub-units that constitute the cytochrome *bc*₁ complex, we also showed that a similar PQS signalling defect was apparent in *cytB* or *cytC*₁ mutants. Since growth of both the *tat* and cytochrome *bc*₁ subunit mutants was reduced compared with the wild type (S9 Fig), our working hypothesis is that shutting down secondary metabolism and virulence factor production would aid conservation of energy for primary metabolism and growth. This shutdown could be efficiently achieved by preventing PQS autoinduction since it co-ordinates the expression of multiple genes involved in secondary metabolite production [17] including the biosynthesis of over 50 different AQS [54] that are heavily-dependent on tryptophan/anthranilate and fatty acid metabolic pathways. How PQS 'shutdown' is achieved at the molecular level in the *tat* mutants is not yet apparent but given that *tat ΔpqsA* double mutants do not respond to exogenous PQS, it may involve uptake

into the cell and/or access to the response regulator PqsR(MvfR). At present there is little information on the mechanism by which PQS gains intracellular access although PQS is known to induce MV formation via a direct interaction with LPS and to be trafficked within MVs [33,34]. This is consistent with the reduction in MV production that we observed in the *tat* and *pqsA* mutants.

As shown in Figs 1 and S1, PQS biosynthesis generates a diverse series of AQs including the *N*-oxide, HQNO, a well known cytochrome *bc₁* inhibitor [57]. HQNO binds to the quinone reduction (Qi) site of the cytochrome *bc₁* complex disrupting the flow of electrons resulting in the leakage of reducing equivalents to oxygen [57]. This results in the generation of reactive oxygen species that cause *P. aeruginosa* cell death and autolysis favouring biofilm formation and antibiotic tolerance [57]. Rieske subunit and cytochrome *bc₁* mutants do not undergo autolysis and are insensitive to exogenous HQNO [57]. Similarly, *P. aeruginosa pqsL* mutants that are unable to produce HQNO also fail to undergo autolysis [57]. Our data also show that in common with the *tat* mutants, the *petA* as well as *cytB* and *cytC₁* mutants all produce lower levels of HQNO. This suggests that lack of eDNA in the *tat* mutant biofilms is because the cells do not undergo limited autolysis [57] as they lack the self-poisoning mechanism that depends on both an intact cytochrome *bc₁* and sufficient HQNO [57]. Thus, lack of the Rieske sub-unit export is primarily responsible for the Tat-mediated perturbation of PQS-dependent QS, the loss of virulence factor production, biofilm eDNA and the tobramycin tolerance of *P. aeruginosa* biofilms. Given the importance of PQS signalling and the Tat system to virulence and biofilm maturation in *P. aeruginosa*, our findings underline the potential of the Tat system as a drug target for novel antimicrobial agents.

Materials and methods

Bacterial strains and growth conditions

The *P. aeruginosa* and *E. coli* strains used are listed in S1 Table and were grown in LB or ABTG [8] at 37°C unless otherwise stated. *P. aeruginosa* biofilms were cultivated at 30°C in flow-chambers irrigated with FAB medium [58] supplemented with 0.3 mM glucose or in M9 medium with succinate (for static biofilms). Selective media were supplemented with ampicillin (Ap; 100 µg ml⁻¹), gentamicin (Gm; 60 µg ml⁻¹), or streptomycin (Sm; 100 µg ml⁻¹). PQS, HHQ and 2-heptyl-4-hydroxyquinoline *N*-oxide (HQNO) were synthesized and characterized in house as described before [30, 59] and dissolved in methanol before being added to growth media at the appropriate concentration.

Mutant construction, screening and validation

A *P. aeruginosa* PAO1 Tn mutant library was constructed using the Mariner Tn vector pBT20 as previously described [60]. Transconjugants carrying Tn insertions were picked from the selective plates and inoculated into microtiter plates containing ABTG medium [61] supplemented with propidium iodide (PI) and the level of red fluorescence quantified. Mutants producing reduced levels of eDNA were selected and the sequences flanking the Tn insertion identified by arbitrary PCR essentially as described by Friedman and Kolter [62] but using the specific primers TnM1 and TnM2 (S2 Table). DNA Sequencing was performed by Macrogen, Seoul, Korea with primer TnMseq (S2 Table). An in-frame *P. aeruginosa tatABC* deletion mutant was generated by allelic exchange using the oligonucleotide primers Tat3D-UF, Tat3D-UR, Tat3D-DF and Tat3D-DR (S2 Table) to introduce the up- and down- stream regions of the *tatABC* locus into the suicide vector pME3087 to generate pME3087::*tatABC* (S1 Table). The latter was introduced into *P. aeruginosa* via conjugation with *E. coli* S17-1 λpir followed by enrichment for tetracycline-sensitive cells as described by Ye *et al* [63]. The Δ*tatABC*

deletion in *P. aeruginosa* PAO1 was confirmed by PCR and sequence analysis. To generate the PA14 $\Delta petA$ mutant, 500 bp upstream and downstream of the gene were amplified using respectively primers S.PA4431upFor/S.PA4431upRev and S.PA4431downFor/S.PA4431downRev listed in [S2 Table](#). The PCR product was cloned in pKNG101 suicide vector by one-step sequence and ligation-independent cloning (SLIC) [64] and sequenced. The resulting plasmid, pKNG $\Delta petA$, maintained in the *E. coli* CC118 λ pir strain, was then mobilized in *P. aeruginosa* strains. The mutant, in which the double recombination events occurred, was confirmed by PCR analysis. A similar strategy was used to construct allelic replacement mutants for each of 34 validated Tat substrates as well as the *cytB* and *cytC*₁ mutants [45]. These strains are summarized in [S3 Table](#) and their validation will be described in detail elsewhere. For the generation of the *petA* cis-complemented strain, PA14 $\Delta petA::(CTX1::petA)$, the *petA* genes along with a 500 bp fragment corresponding to the putative promoter region for the *petA* gene were PCR amplified using S-4431CTXFor/S-4431CTXRev and cloned by SLIC into the mini-CTX1 vector yielding pminiCTX1-*petA*. Transfer of this plasmid in *P. aeruginosa* $\Delta petA$ strain was carried out by triparental mating using the conjugative properties of the helper plasmid pRK2013. The recombinant clones containing the mini-CTX inserted at the *attB* locus on the *P. aeruginosa* genome were selected on tetracycline-containing PIA generating PA14 $\Delta petA::(attB::petA)$.

Construction of a *tatA* complementation plasmid

The *tatA* gene was amplified by PCR using primers *FtatA* and *RtatA* ([S2 Table](#)), introduced into pUCP22 ([S1 Table](#)) and electroporated into the *P. aeruginosa* *tatA* and *tatA* $\Delta pqsA$ mutants. Transformants were selected on LB plates containing 200 $\mu\text{g ml}^{-1}$ carbenicillin.

Bioluminescent reporter assays

To investigate the impact of the *tat* mutation and Tat inhibitor Bayer 11–7082 [48] on PQS signalling, transcriptional fusions between the promoter regions of *pqsA*, *pqsR*, *rhlA*, *phzA1* and *phzA2* and the *luxCDABE* operon were constructed using the miniCTX-*lux* plasmid as previously described [17]. In addition, a constitutively bioluminescent reporter using a miniCTX::*tac-luxCDABE* promoter fusion was constructed as a control for Bayer 11–7082. Bioluminescence as a function of bacterial growth was quantified in 96 well plates using a combined luminometer- spectrometer.

Semi-quantification of cellular ATP was carried out using the BacTiter-GloTM Microbial Cell Viability Assay (Promega). Briefly, the *P. aeruginosa* PA14, $\Delta tatABC$ mutant and $\Delta petA$ mutant were grown in LB broth for 8 h, diluted 1000-fold with fresh media and mixed with equal volume of BacTiter-GloTM reagent in a 96-well plate. After a 5 min incubation period, luminescence for each well was recorded in an automated plate reader.

Cultivation of biofilms

Biofilms were grown in flow-chambers with individual channel dimensions of 1 x 4 x 40 mm as described previously [65]. One hour after inoculation, with bacteria, the growth medium flow (0.2 mm/s corresponding to laminar flow with a Reynolds number of 0.02) was started. When required, eDNA in biofilms was stained with 1 μM ethidium bromide prior to microscopy. Tobramycin (10 μM) was added to the biofilm medium after 4 days of cultivation. After 24 h of tobramycin treatment, propidium iodide (10 μM) was added to the flow cells to visualize the dead cells via confocal laser scanning microscopy. *P. aeruginosa* PA14 and *petA* mutant biofilms were grown under static conditions over 48 h at 37°C on glass slides (Ibidi)

incorporating 300 μ l chambers. After 48 h incubation, spent medium was removed and the biofilm eDNA stained with YoYo-1 (40 μ M).

Microscopy and image processing of flow cell biofilms

All images of flow-chamber-grown and static biofilms were captured with a confocal laser scanning microscope (CLSM) equipped with detectors and filter sets for monitoring green fluorescent protein, Syto9, propidium iodide, and ethidium bromide. Images were obtained using a 63x/1.4 objective or a 40x/1.3 objective. Simulated 3-D images and sections were generated using the IMARIS software package (Bitplane AG, Zürich, Switzerland).

AQ, pyocyanin, rhamnolipid and MV analysis

The AQs (PQS, HHQ and HQNO) were quantified by LC-MS/MS after extracting cell free supernatants or whole bacterial cell cultures in triplicate with acidified ethyl acetate or methanol respectively as described by Ortori *et al* [59]. Pyocyanin was extracted with chloroform and quantified spectrophotometrically [26]. Rhamnolipids were quantified indirectly using the orcinol method [35]. For PQS solubilization experiments, rhamnolipids were purified as described by Muller *et al* [66]. MVs were harvested by ultracentrifugation, the pellets resuspended in 10mM HEPES buffer and the lipid content quantified using FM4-64 essentially as described previously [67]. MV production was normalized by dividing the lipid fluorescence units by CFU values determined by dilution plating. Assays were performed in triplicate at least twice.

Statistical analysis

Significance for differences between wild type and isogenic mutants was determined by two-tailed *t*-tests where *****p* < 0.001, ****p* < 0.001, ***p* < 0.01, and **p* < 0.05 and n.s., not significant.

Supporting information

S1 Fig. Biochemical basis of AQ biosynthesis. PqsA catalyses the formation of anthraniloyl-CoA that is condensed with malonyl-CoA by PqsD to form 2-aminobenzoylacetyl-CoA (2-ABA-CoA). The latter is converted to 2-aminobenzoylacetate (2-ABA) via the thioesterase functionality of PqsE. The PqsBC heterodimer condenses 2-ABA with octanoyl-CoA to generate HHQ. PQS is formed through the oxidation of HHQ by PqsH. For AQ *N*-oxides such as 2-heptyl-4-hydroxyquinoline *N*-oxide (HQNO), 2-ABA is oxidized to 2-HABA by the alternative mono-oxygenase PqsL and then condensed with octanoyl-CoA by PqsBC to form HQNO. PqsBC can accept acyl-CoAs of different acyl chain lengths to generate diverse AQs and AQ *N*-oxides.

(TIF)

S2 Fig. The Tat inhibitor Bayer 11–7082 has no effect on light output at 20 or 40 μ M from a constitutive *P. aeruginosa* CTX::*tac*⁺-*luxCDABE* chromosomal reporter fusion. The co-solvent DMSO, had no effect at 0.4 or 0.8% on the *lux* reporter fusion. Data are presented as maximal light output as a function of growth (RLU/OD₆₀₀). Experiments were repeated in triplicate at least twice.

(TIF)

S3 Fig. Deletion of the *tatABC* genes does not influence *pqsR* expression. The data show that there are no differences in the expression of a chromosomal CTX::*pqsR*⁺-*luxCDABE* fusion

in the *P. aeruginosa* wild type compared with the $\Delta tatABC$ mutant. Data are presented as maximal light output as a function of growth (RLU/OD₆₀₀). Experiments were repeated in triplicate at least twice.

(TIF)

S4 Fig. HHQ and PQS do not accumulate intracellularly in a *tatA* $\Delta pqsA$ double mutant harboring the plasmid-borne *pqsABCD* genes in the absence of autoinduction. Semi-quantitative analysis by LC-MS/MS of PQS (A) and HHQ (B) extracted with methanol from whole cell cultures of *P. aeruginosa* wild type and the *tatA* $\Delta pqsA$ mutant without (control) or with (+*pqsABCD*) the *pqsABCD* biosynthetic genes provided via pBBR1MCS-5::*pqsABCD* and harvested at 8 h and 16 h respectively. Experiments were repeated in triplicate.

(TIF)

S5 Fig. Exogenous rhamnolipids do not enhance PQS-dependent expression of *pqsA* in a *tatA* $\Delta pqsA$ mutant. PQS (40 μ M) was added with or without purified rhamnolipids (50 μ g/ml) to a *pqsA* mutant (grey bars) or a *tatA* $\Delta pqsA$ mutant (pink bars) carrying chromosomal *pqsA*'-lux fusions. Maximal light output as a function of growth (RLU/OD₆₀₀) is presented. Experiments were repeated in triplicate at least twice.

(TIF)

S6 Fig. Rhamnolipid biosynthesis gene *rhlA* shows altered expression profiles in *P. aeruginosa* PA14 $\Delta tatABC$ and $\Delta petA$ mutants compared with wild type and fail to respond to exogenous PQS. Bioluminescence from a chromosomal *rhlA*'-lux fusion as a function of growth (RLU/OD) over time when introduced into (A) the PA14 wild type, (B) $\Delta tatABC$ and (C) $\Delta petA$ mutants in the absence or presence of exogenous PQS (20 μ M).

(TIF)

S7 Fig. Deletion of *petA* in *P. aeruginosa* PA14 results in a reduction in the eDNA content of biofilms. Biofilms of wild type PA14, the $\Delta tatABC$ and $\Delta petA$ mutants and the genetically complemented PA14 mutant ($\Delta petA$::(CTX::*petA*)) were grown cultured statically and stained for eDNA with YOYO-1. (A) confocal fluorescence microscopy images and (B) eDNA quantification. Experiments were repeated in triplicate at least twice. ***p < 0.001, **p < 0.01.

(TIF)

S8 Fig. Comparison of *pqsA* expression in *P. aeruginosa* PAO1 wild type, $\Delta tatABC$ and $\Delta petA$ mutants. Experiments were repeated in triplicate at least twice. ***p < 0.001, **p < 0.01, and *p < 0.05; n.s. not significant.

(TIF)

S9 Fig. Growth, *pqsA* expression and AQ production in wild type *P. aeruginosa* PA14 compared with $\Delta cytB$ (PA4429), $\Delta cytC_I$ (PA4430) $\Delta petA$ and $\Delta tatABC$ mutants. ***p < 0.001, **p < 0.01, and *p < 0.05; n.s. not significant.

(TIF)

S10 Fig. Comparison of cellular ATP levels in *P. aeruginosa* PA14 wild type, $\Delta tatABC$ and $\Delta petA$. Experiments were repeated in triplicate at least twice.

(TIF)

S1 Table. Strains and plasmids used in this study.

(DOCX)

S2 Table. Oligonucleotide primers used in this study.

(DOCX)

S3 Table. *P. aeruginosa* PA14 Tat substrate mutants used in this study.
(DOCX)

Acknowledgments

The authors wish to thank Alex Truman for synthesis of the AQ and AQ-N-oxide standards.

Author Contributions

Conceptualization: Liang Yang, Sophie Bleves, Miguel Cámara, Michael Givskov, Kim R. Hardie, Tim Tolker-Nielsen, Bérengère Ize, Paul Williams.

Data curation: Eliza Ye-Chen Soh, Frances Smith, Maxime Rémi Gimenez, Rebecca Munk Vejborg, Matthew Fletcher, Nigel Halliday.

Formal analysis: Eliza Ye-Chen Soh, Frances Smith, Maxime Rémi Gimenez, Liang Yang, Rebecca Munk Vejborg, Matthew Fletcher, Nigel Halliday, Stephan Heeb, Tim Tolker-Nielsen, Bérengère Ize, Paul Williams.

Funding acquisition: Sophie Bleves, Michael Givskov, Tim Tolker-Nielsen, Bérengère Ize, Paul Williams.

Investigation: Eliza Ye-Chen Soh, Frances Smith, Maxime Rémi Gimenez, Liang Yang, Rebecca Munk Vejborg, Matthew Fletcher, Nigel Halliday, Bérengère Ize.

Methodology: Eliza Ye-Chen Soh, Frances Smith, Maxime Rémi Gimenez, Matthew Fletcher, Nigel Halliday.

Project administration: Sophie Bleves, Michael Givskov, Tim Tolker-Nielsen, Bérengère Ize, Paul Williams.

Resources: Sophie Bleves.

Supervision: Sophie Bleves, Stephan Heeb, Kim R. Hardie, Tim Tolker-Nielsen, Bérengère Ize, Paul Williams.

Validation: Frances Smith.

Visualization: Stephan Heeb.

Writing – original draft: Paul Williams.

Writing – review & editing: Eliza Ye-Chen Soh, Frances Smith, Maxime Rémi Gimenez, Liang Yang, Rebecca Munk Vejborg, Matthew Fletcher, Nigel Halliday, Sophie Bleves, Stephan Heeb, Miguel Cámara, Michael Givskov, Kim R. Hardie, Tim Tolker-Nielsen, Bérengère Ize.

References

1. Moradali MF, Ghods S, Rehm BH. *Pseudomonas aeruginosa* Lifestyle: A paradigm for adaptation, survival, and persistence. *Front Cell Infect Microbiol.* 2017; 7:39–42. <https://doi.org/10.3389/fcimb.2017.00039> PMID: 28261568
2. Costerton JW, Stewart PS, Greenberg EP. Bacterial biofilms: a common cause of persistent infections. *Science.* 1999; 284:1318–22. <https://doi.org/10.1126/science.284.5418.1318> PMID: 10334980.
3. Klausen M, Aaes-Jørgensen A, Molin S, Tolker-Nielsen T. Involvement of bacterial migration in the development of complex multicellular structures in *Pseudomonas aeruginosa* biofilms. *Mol Microbiol.* 2003; 50:61–8. <https://doi.org/10.1046/j.1365-2958.2003.03677.x> PMID: 14507363.

4. Klausen M, Heydorn A, Ragas P, Lambertsen L, Aaes-Jørgensen A, Molin S, et al. Biofilm formation by *Pseudomonas aeruginosa* wild type, flagella and type IV pili mutants. *Mol Microbiol*. 2003; 48:1511–24. <https://doi.org/10.1046/j.1365-2958.2003.03525.x> PMID: 12791135.
5. Pamp SJ, Tolker-Nielsen T. Multiple roles of biosurfactants in structural biofilm development by *Pseudomonas aeruginosa*. *J Bacteriol*. 2007; 189:2531–39. <https://doi.org/10.1128/JB.01515-06> PMID: 17220224.
6. Harmsen M, Yang L, Pamp SJ, Tolker-Nielsen T. An update on *Pseudomonas aeruginosa* biofilm formation, tolerance, and dispersal. *FEMS Immunol Med Microbiol*. 2010; 59:253–68. <https://doi.org/10.1111/j.1574-695X.2010.00690.x> PMID: 20497222.
7. Yang L, Hu Y, Liu Y, Zhang J, Ulstrup J, Molin S. Distinct roles of extracellular polymeric substances in *Pseudomonas aeruginosa* biofilm development. *Environ Microbiol*. 2011; 13:1705–17. <https://doi.org/10.1111/j.1462-2920.2011.02503.x> PMID: 21605307.
8. Allesen-Holm M, Barken KB, Yang L, Klausen M, Webb JS, Kjelleberg S, et al. A characterization of DNA release in *Pseudomonas aeruginosa* cultures and biofilms. *Mol Microbiol*. 2006; 59:1114–28. <https://doi.org/10.1111/j.1365-2958.2005.05008.x> PMID: 16430688.
9. Tashiro Y, Uchiyama H, Nomura N. Multifunctional membrane vesicles in *Pseudomonas aeruginosa*. *Environ Microbiol*. 2012; 14:1349–62. <https://doi.org/10.1111/j.1462-2920.2011.02632.x> PMID: 22103313.
10. Tolker-Nielsen T. Biofilm Development. *Microbiol Spectr*. 2015 3:MB-0001–2014. <https://doi.org/10.1128/microbiolspec.MB-0001-2014> PMID: 26104692.
11. Okshevsky M, Meyer RL. The role of extracellular DNA in the establishment, maintenance and perpetuation of bacterial biofilms. *Crit Rev Microbiol*. 2015; 41:341–52. <https://doi.org/10.3109/1040841X.2013.841639> PMID: 24303798.
12. Das T, Sehar S, Manefield M. The roles of extracellular DNA in the structural integrity of extracellular polymeric substance and bacterial biofilm development. *Environ Microbiol Rep*. 2013 5:778–86. <https://doi.org/10.1111/1758-2229.12085> PMID: 24249286.
13. Wilton M, Charron-Mazenod L, Moore R, Lewenza S. Extracellular DNA acidifies biofilms and induces aminoglycoside resistance in *Pseudomonas aeruginosa*. *Antimicrob Agents Chemother*. 2015; 60:544–53. <https://doi.org/10.1128/AAC.01650-15> PMID: 26552982
14. Turnbull L, Toyofuku M, Hynen AL, Kurosawa M, Pessi G, Petty NK, et al. Explosive cell lysis as a mechanism for the biogenesis of bacterial membrane vesicles and biofilms. *Nat Commun*. 2016; 7:11220. <https://doi.org/10.1038/ncomms11220> PMID: 27075392.
15. Das T, Kutty SK, Tavallaie R, Ibugo AI, Panchompoo J, Sehar S, et al. Phenazine virulence factor binding to extracellular DNA is important for *Pseudomonas aeruginosa* biofilm formation. *Sci Rep*. 2015; 5:8398. <https://doi.org/10.1038/srep08398> PMID: 25669133.
16. Williams P, Cámara M. Quorum sensing and environmental adaptation in *Pseudomonas aeruginosa*: a tale of regulatory networks and multifunctional signal molecules. *Curr Opin Microbiol*. 2009; 12:182–91. <https://doi.org/10.1016/j.mib.2009.01.005> PMID: 19249239.
17. Rampioni G, Falcone M, Heeb S, Frangipani E, Fletcher MP, Dubern JF, et al. Unravelling the genome-wide contributions of specific 2-alkyl-4-quinolones and PqsE to quorum sensing in *Pseudomonas aeruginosa*. *PLoS Pathog*. 2016; 12:e1006029. <https://doi.org/10.1371/journal.ppat.1006029> PMID: 27851827.
18. Lépine F, Milot S, Déziel E, He J, Rahme LG. Electrospray/mass spectrometric identification and analysis of 4-hydroxy-2-alkylquinolines (HAQs) produced by *Pseudomonas aeruginosa*. *J Am Soc Mass Spectrom*. 2004; 15:862–9. <https://doi.org/10.1016/j.jasms.2004.02.012> PMID: 15144975.
19. Coleman JP, Hudson LL, McKnight SL, Farrow JM 3rd, Calfee MW, Lindsey CA, et al. *Pseudomonas aeruginosa* PqsA is an anthranilate-coenzyme A ligase. *J Bacteriol*. 2008; 190:1247–55. <https://doi.org/10.1128/JB.01140-07> PMID: 18083812
20. Zhang YM, Frank MW, Zhu K, Mayasundari A, Rock CO. PqsD is responsible for the synthesis of 2,4-dihydroxyquinoline, an extracellular metabolite produced by *Pseudomonas aeruginosa*. *J Biol Chem*. 2008; 283:28788–94. <https://doi.org/10.1074/jbc.M804555200> PMID: 18728009.
21. Drees SL, Fetzner S. PqsE of *Pseudomonas aeruginosa* acts as pathway-specific thioesterase in the biosynthesis of alkylquinolone signaling molecules. *Chem Biol*. 2015; 22:611–8. <https://doi.org/10.1016/j.chembiol.2015.04.012> PMID: 25960261.
22. Dulcey CE, Dekimpe V, Fauvelle DA, Milot S, Groleau MC, Doucet N, et al. The end of an old hypothesis: the pseudomonas signaling molecules 4-hydroxy-2-alkylquinolines derive from fatty acids, not 3-ketofatty acids. *Chem Biol*. 2013; 20:1481–91. <https://doi.org/10.1016/j.chembiol.2013.09.021> PMID: 24239007

23. Drees SL, Li C, Prasetya F, Saleem M, Dreveny I, Williams P, Hennecke U, et al. PqsBC, a condensing enzyme in the biosynthesis of the *Pseudomonas aeruginosa* quinolone signal: crystal structure, inhibition, and reaction mechanism. *J Biol Chem*. 2016; 291:6610–24. <https://doi.org/10.1074/jbc.M115.708453> PMID: 26811339;
24. Schertzer JW, Brown SA, Whiteley M. Oxygen levels rapidly modulate *Pseudomonas aeruginosa* social behaviours via substrate limitation of PqsH. *Mol Microbiol*. 2010; 77:1527–38. <https://doi.org/10.1111/j.1365-2958.2010.07303.x> Epub 2010 Aug 17. PMID: 20662781.
25. Drees SL, Ernst S, Belviso BD, Jagmann N, Hennecke U, Fetzner S. PqsL uses reduced flavin to produce 2-hydroxylaminobenzoylacetate, a preferred PqsBC substrate in alkyl quinolone biosynthesis in *Pseudomonas aeruginosa*. *J Biol Chem*. 2018; 15: 293:9345–9357. <https://doi.org/10.1074/jbc.RA117.000789> PMID: 29669807
26. Rampioni G, Pustelny C, Fletcher MP, Wright VJ, Bruce M, Rumbaugh KP, et al. Transcriptomic analysis reveals a global alkyl-quinolone-independent regulatory role for PqsE in facilitating the environmental adaptation of *Pseudomonas aeruginosa* to plant and animal hosts. *Environ Microbiol*. 2010; 12:1659–73. <https://doi.org/10.1111/j.1462-2920.2010.02214.x> PMID: 20406282.
27. Groleau MC, de Oliveira Pereira T, Dekimpe V, Déziel E. PqsE Is Essential for RhIR-Dependent Quorum Sensing Regulation in *Pseudomonas aeruginosa* *mSystems*. 2020; 5:e00194–20; <https://doi.org/10.1128/mSystems.00194-20> PMID: 32457239
28. Wade DS, Calfee MW, Rocha ER, Ling EA, Engstrom E, Coleman JP, et al. Regulation of pseudomonas quinolone signal synthesis in *Pseudomonas aeruginosa*. *J Bacteriol*. 2005; 187:4372–80. <https://doi.org/10.1128/JB.187.13.4372-4380.2005> PMID: 15968046.
29. Xiao G, Déziel E, He J, Lépine F, Lesic B, Castonguay MH, et al. MvfR, a key *Pseudomonas aeruginosa* pathogenicity LTTR-class regulatory protein, has dual ligands. *Mol Microbiol*. 2006; 62:1689–99. <https://doi.org/10.1111/j.1365-2958.2006.05462.x> PMID: 17083468.
30. Ilangovan A, Fletcher M, Rampioni G, Pustelny C, Rumbaugh K, Heeb S, et al. Structural basis for native agonist and synthetic inhibitor recognition by the *Pseudomonas aeruginosa* quorum sensing regulator PqsR (MvfR). *PLoS Pathog*. 2013; 9:e1003508. <https://doi.org/10.1371/journal.ppat.1003508> PMID: 23935486.
31. Diggle SP, Matthijs S, Wright VJ, Fletcher MP, Chhabra SR, Lamont IL, et al. The *Pseudomonas aeruginosa* 4-quinolone signal molecules HHQ and PQS play multifunctional roles in quorum sensing and iron entrapment. *Chem Biol*. 2007; 14:87–96. <https://doi.org/10.1016/j.chembiol.2006.11.014> PMID: 17254955.
32. Häussler S, Becker T. The pseudomonas quinolone signal (PQS) balances life and death in *Pseudomonas aeruginosa* populations. *PLoS Pathog*. 2008; 4:e1000166. <https://doi.org/10.1371/journal.ppat.1000166> PMID: 18818733;
33. Mashburn-Warren L, Howe J, Garidel P, Richter W, Steiniger F, Roessle M, et al. Interaction of quorum signals with outer membrane lipids: insights into prokaryotic membrane vesicle formation. *Mol Microbiol*. 2008; 69:491–502. <https://doi.org/10.1111/j.1365-2958.2008.06302.x> PMID: 18630345.
34. Mashburn LM, Whiteley M. Membrane vesicles traffic signals and facilitate group activities in a prokaryote. *Nature*. 2005; 437:422–5. <https://doi.org/10.1038/nature03925> PMID: 16163359
35. Pustelny C, Albers A, Büldt-Karentzopoulos K, Parschat K, Chhabra SR, Cámara M, et al. Dioxygenase-mediated quenching of quinolone-dependent quorum sensing in *Pseudomonas aeruginosa*. *Chem Biol*. 2009; 16:1259–67. <https://doi.org/10.1016/j.chembiol.2009.11.013> PMID: 20064436.
36. D'Argenio DA, Calfee MW, Rainey PB, Pesci EC. Autolysis and autoaggregation in *Pseudomonas aeruginosa* colony morphology mutants. *J Bacteriol*. 2002; 184:6481–9. <https://doi.org/10.1128/JB.184.23.6481-6489.2002> PMID: 12426335.
37. Webb JS, Thompson LS, James S, Charlton T, Tolker-Nielsen T, Koch B, et al. Cell death in *Pseudomonas aeruginosa* biofilm development. *J Bacteriol*. 2003; 185:4585–92. <https://doi.org/10.1128/JB.185.15.4585-4592.2003> PMID: 12867469
38. Spoering AL, Gilmore MS. Quorum sensing and DNA release in bacterial biofilms. *Curr Opin Microbiol*. 2006; 9:133–7. <https://doi.org/10.1016/j.mib.2006.02.004> PMID: 16529982.
39. Yang L, Barken KB, Skindersoe ME, Christensen AB, Givskov M, Tolker-Nielsen T. et al Effects of iron on DNA release and biofilm development by *Pseudomonas aeruginosa*. *Microbiology*. 2007; 153:1318–28. <https://doi.org/10.1099/mic.0.2006/004911-0> PMID: 17464046.
40. Yang L, Nilsson M, Gjermansen M, Givskov M, Tolker-Nielsen T. Pyoverdine and PQS mediated sub-population interactions involved in *Pseudomonas aeruginosa* biofilm formation. *Mol Microbiol*. 2009; 74:1380–92. <https://doi.org/10.1111/j.1365-2958.2009.06934.x> PMID: 19889094.
41. Suzuki T, Fujikura K, Higashiyama T, Takata K. DNA staining for fluorescence and laser confocal microscopy. *J Histochem Cytochem*. 1997; 45:49–53. <https://doi.org/10.1177/002215549704500107> PMID: 9010468.

42. Frain KM, Robinson C, van Dijl JM. Transport of folded proteins by the tat system. *Protein J*. 2019; 38:377–388. <https://doi.org/10.1007/s10930-019-09859-y> PMID: 31401776.
43. Voulhoux R, Ball G, Ize B, Vasil ML, Lazdunski A, Wu LF, et al. Involvement of the twin-arginine translocation system in protein secretion via the type II pathway. *EMBO J*. 2001; 20: 6735–6741. <https://doi.org/10.1093/emboj/20.23.6735> PMID: 11726509.
44. Ochsner UA, Snyder A, Vasil AI, Vasil ML. Effects of the twin-arginine translocase on secretion of virulence factors, stress response, and pathogenesis. *Proc Natl Acad Sci U S A*. 2002; 99:8312–8317. <https://doi.org/10.1073/pnas.082238299> PMID: 12034867.
45. Gimenez MR, Chandra G, Van Overvelt P, Voulhoux R, Ize B, Bleves S, et al. Genome wide identification and experimental validation of *Pseudomonas aeruginosa* Tat substrates. *Sci Rep* 2018; 11950. <https://doi.org/10.1038/s41598-018-30393-x> PMID: 30093651
46. Calfee MW, Shelton JG, McCubrey JA, Pesci EC. Solubility and bioactivity of the *Pseudomonas* quinolone signal are increased by a *Pseudomonas aeruginosa*-produced surfactant. *Infect Immun*. 2005; 73:878–82. <https://doi.org/10.1128/AI.73.2.878-882.2005> PMID: 15664929.
47. Chiang WC, Nilsson M, Jensen PØ, Høiby N, Nielsen TE, Givskov M, et al. Extracellular DNA shields against aminoglycosides in *Pseudomonas aeruginosa* biofilms. *Antimicrob Agents Chemother*. 2013; 57:2352–61. <https://doi.org/10.1128/AAC.00001-13> PMID: 23478967
48. Vasil ML, Tomaras AP, Pritchard AE. Identification and evaluation of twin-arginine translocase inhibitors. *Antimicrob Agents Chemother*. 2012; 56:6223–34. <https://doi.org/10.1128/AAC.01575-12> PMID: 23006747
49. Williams P, Winzer K, Chan WC, Cámara M. Look who's talking: communication and quorum sensing in the bacterial world. *Philos Trans R Soc Lond B Biol Sci*. 2007; 362:1119–34. <https://doi.org/10.1098/rstb.2007.2039> PMID: 17360280;
50. Recinos DA, Sekedat MD, Hernandez A, Cohen TS, Sakhtah H, Prince AS, et al. Redundant phenazine operons in *Pseudomonas aeruginosa* exhibit environment-dependent expression and differential roles in pathogenicity. *Proc Natl Acad Sci U S A*. 2012; 109:19420–5. <https://doi.org/10.1073/pnas.1213901109> PMID: 23129634
51. Niewerth H, Bergander K, Chhabra SR, Williams P, Fetzner S. Synthesis and biotransformation of 2-alkyl-4(1H)-quinolones by recombinant *Pseudomonas putida* KT2440. *Appl Microbiol Biotechnol*. 2011; 91:1399–408. <https://doi.org/10.1007/s00253-011-3378-0> PMID: 21670979.
52. Van Gennip M, Christensen LD, Alhede M, Phipps R, Jensen PØ, Christophersen L, et al. Inactivation of the *rhlA* gene in *Pseudomonas aeruginosa* prevents rhamnolipid production, disabling the protection against polymorphonuclear leukocytes. *APMIS*. 2009 117:537–46. <https://doi.org/10.1111/j.1600-0463.2009.02466.x> PMID: 19594494
53. Alhede M, Bjarnsholt T, Jensen PØ, Phipps RK, Moser C, Christophersen L, et al. *Pseudomonas aeruginosa* recognizes and responds aggressively to the presence of polymorphonuclear leukocytes. *Microbiology (Reading)*. 2009 155:3500–3508. <https://doi.org/10.1099/mic.0.031443-0> PMID: 19643762.
54. Déziel E, Lépine F, Milot S, He J, Mindrinos MN, Tompkins RG, et al. Analysis of *Pseudomonas aeruginosa* 4-hydroxy-2-alkylquinolines (HAQs) reveals a role for 4-hydroxy-2-heptylquinoline in cell-to-cell communication. *Proc Natl Acad Sci U S A*. 2004; 101:1339–44. <https://doi.org/10.1073/pnas.0307694100> PMID: 14739337
55. Farrow JM 3rd, Sund ZM, Ellison ML, Wade DS, Coleman JP, Pesci EC, et al. PqsE functions independently of PqsR-*Pseudomonas* quinolone signal and enhances the *rhl* quorum-sensing system. *J Bacteriol*. 2008; 190:7043–51. <https://doi.org/10.1128/JB.00753-08> PMID: 18776012
56. Williams HD, Zlosnik JE, Ryall B. Oxygen, cyanide and energy generation in the cystic fibrosis pathogen *Pseudomonas aeruginosa*. *Adv Microb Physiol*. 2007; 52:1–71. [https://doi.org/10.1016/S0065-2911\(06\)52001-6](https://doi.org/10.1016/S0065-2911(06)52001-6) PMID: 17027370.
57. Hazan R, Que YA, Maura D, Strobel B, Majcherczyk PA, Hopper LR, et al. Auto poisoning of the respiratory chain by a quorum-sensing-regulated molecule favors biofilm formation and antibiotic tolerance. *Curr Biol*. 2016; 26:195–206. <https://doi.org/10.1016/j.cub.2015.11.056> PMID: 26776731
58. Heydorn A, Nielsen AT, Hentzer M, Sternberg C, Givskov M, Ersbøll BK, et al. Quantification of biofilm structures by the novel computer program COMSTAT. *Microbiology*. 2000; 146:2395–407. <https://doi.org/10.1099/00221287-146-10-2395> PMID: 11021916.
59. Ortori CA, Dubern JF, Chhabra SR, Cámara M, Hardie K, Williams P, et al. Simultaneous quantitative profiling of *N*-acyl-L-homoserine lactone and 2-alkyl-4(1H)-quinolone families of quorum-sensing signaling molecules using LC-MS/MS. *Anal Bioanal Chem*. 2011; 399:839–50. <https://doi.org/10.1007/s00216-010-4341-0> PMID: 21046079.
60. Kulasekara HD, Ventre I, Kulasekara BR, Lazdunski A, Filloux A, Lory S, et al. A novel two-component system controls the expression of *Pseudomonas aeruginosa* fimbrial cup genes. *Mol Microbiol*. 2005 Jan; 55(2):368–80. <https://doi.org/10.1111/j.1365-2958.2004.04402.x> PMID: 15659157.

61. Chua SL, Tan SY, Rybtke MT, Chen Y, Rice SA, Kjelleberg S, et al. Bis-(3'-5')-cyclic dimeric GMP regulates antimicrobial peptide resistance in *Pseudomonas aeruginosa*. *Antimicrob Agents Chemother*. 2013; 57:2066–75. <https://doi.org/10.1128/AAC.02499-12> PMID: 23403434.
62. Friedman L, Kolter R. Genes involved in matrix formation in *Pseudomonas aeruginosa* PA14 biofilms. *Mol Microbiol*. 2004; 51:675–90. <https://doi.org/10.1046/j.1365-2958.2003.03877.x> PMID: 14731271.
63. Ye RWI, Haas D, Ka JO, Krishnapillai V, Zimmermann A, Baird C, et al. Anaerobic activation of the entire denitrification pathway in *Pseudomonas aeruginosa* requires Anr, an analog of Fnr. *J Bacteriol*. 1995; 177:3606–9. <https://doi.org/10.1128/jb.177.12.3606-3609.1995> PMID: 7768875
64. Jeong JY, Yim HS, Ryu JY, Lee HS, Lee JH, Seen DS, et al. One-step sequence- and ligation-independent cloning as a rapid and versatile cloning method for functional genomics studies. *Appl Environ Microbiol*. 2012; 78:5440–3. <https://doi.org/10.1128/AEM.00844-12> PMID: 22610439.
65. Crusz SA, Popat R, Rybtke MT, Cámara M, Givskov M, Tolker-Nielsen T, et al. Bursting the bubble on bacterial biofilms: a flow cell methodology. *Biofouling*. 2012; 28:835–42. <https://doi.org/10.1080/08927014.2012.716044> PMID: 22877233
66. Müller MM, Hörmann B, Syldatk C, Hausmann R. *Pseudomonas aeruginosa* PAO1 as a model for rhamnolipid production in bioreactor systems. *Appl Microbiol Biotechnol*. 2010; 87:167–74. <https://doi.org/10.1007/s00253-010-2513-7> PMID: 20217074.
67. McBroom AJ, Johnson AP, Vemulapalli S, Kuehn MJ. Outer membrane vesicle production by *Escherichia coli* is independent of membrane instability. *J Bacteriol*. 2006; 188:5385–92. <https://doi.org/10.1128/JB.00498-06> PMID: 16855227.